NJU NIP
NOV 9-11, 2018
Nanjing, China

a nature conference
on Nanophotonics and
Integrated Photonics 2018

NIP 2018

自然学术会议——纳米光子学和集成光子学

Poster Abstract

中国 · 南京
2018年11月9-11日

南京大学
NANJING UNIVERSITY

nature electronics
nature materials
nature nanotechnology
nature photonics

Research

NIP 2018

Poster Abstract

Poster List

For downloading poster abstracts please scan the QR code.
http://light.nju.edu.cn/nip2018/Poster_Abstract.pdf

No.	Author	Title	Poster Session
1	Hansen Zhong	12-photon entanglement and scalable scattershot boson sampling with optimal entangled photon pairs from parametric down-conversion	I
2	Huazhou Chen	Imaging the dark emission of spasers	I
3	Xiaoxiao Wu	Direct observation of valley-locked topological edge states in designer surface plasmon crystals	I
4	Zhen Shen	Non-reciprocal photonic devices based on optomechanical microresonator	I
5	Yingying Zhu	Strong localization of surface plasmon polaritons with engineered disorder	I
6	Qi Guo	Photo-patterning of chiral smectic-C liquid crystal for electrically-addressed diffractive optical elements	I
7	Kai Wang	A non-local quantum delayed-choice experiment	I
8	Jing Zhou	Visualizing Mie resonances in low-index dielectric nanoparticles	I
9	Chen Chen	Tomographic microscopy by chromatic metalens	I
10	Jiafang Li	Nano-kirigami enabled 2D-to-3D transformations of photonic functional metastructures	I
11	Tong Wu	Experimental multi-photon quantum walk on a directed graph	I
12	Kunpeng Jia	Mid-infrared $\chi^{(2)}$ frequency comb generation from a dielectric superlattice box resonator	I
13	Wenchan Dong	An integrated all-optical programmable logic array using cross gain modulation based on semiconductor optical amplifiers	I
14	Xiaohu Wu	Strong chiral response in the whole visible band	I
15	Suo Wang	Unusual scaling laws for plasmonic nanolasers beyond the diffraction limit	I
16	Wang Zhang	Evolution of orbital angular momentum in a soft quasi-periodic structure with topological defects	I
17	Chi Li	High nonlinear light-field-driven photoemission from carbon nanotubes	I
18	Huizeng Li	Au-areoles arrayed microchip for multiple trace SERS detection	I
19	Tiancheng Han	Full-parameter omnidirectional thermal meta-devices of anisotropic geometry	I
20	Mingbo He	Hybrid silicon and lithium niobate Mach–Zehnder modulators for 100 Gbits and beyond	I
21	Lemeng Leng	High-density waveguide integration and optical phased arrays	I
22	Lan Wang	THz enhanced EIT resonance based on the coupled electrical dropping effect with undulating meta-surface	I
23	Yanqing Hu	Hard evidence revealing the cause of thermally-induced luminescence enhancement in upconversion nanocrystals	I

No.	Author	Title	Poster Session
24	Xinyu Liao	Octave spanning supercontinuum generation in air cladding tantalum pentoxide based optical waveguide	I
25	Yinzhu Jiang	Rabi splitting in photoluminescence of gold nanorod–WS_2 heterostructure	I
26	Zhixia Xu	Induce surface plasmon on thin gold films using dimer-structure plasmonic metadevices	I
27	Qiuyang Jiang	High extinction ratio 2×2 thermo-optic switch in silicon	I
28	Ruxue Wang	Exciting and shaping the Bloch surface wave	I
29	Yang Li	Gradient index metamaterials for enhancing local field	I
30	Chang Li	Janus structural color from a 2D photonic crystal hybrid with a Fabry–Perot cavity	I
31	Qi Chen	Demonstration of a next generation of satellite laser ranging with superconductor single photon detector array	I
32	Hongliang Hao	Strong damping of the localized surface plasmon resonance of metal nanoparticles and its applications	I
33	Lei Tang	A near-perfect chiral single-photon interface:isolation and unidirectional emission	I
34	Xuexian Chen	Strong plasmon–exciton coupling in single Au nanohole–monolayer WS_2 hybrid nanostructures	I
35	Yineng Liu	Metasurface realization for complementary medium-type optical illusion	I
36	Pengfei Qin	Toroidal Response Based on Localized Spoof Plasmons	I
37	Hao Jing	Broadband integrated polarization rotator using three-layer metallic grating structures	I
38	Yongchao Li	Optically controllable superconducting electromechanical oscillator	I
39	Xueqiong Su	Investigation of thermal evolution in $Ge_xAs_ySe_{1-x-y}$ thin films by in-situ measurements	I
40	Yifan Xu	Plasmon enhanced optical coherence tomography imaging using nanorods of large aspect ratios	I
41	Pu Zhang	Rigorous analysis and engineering of radiation pattern of single emitters in anisotropic planar structure via coupling to nanoantenna	I
42	Jing Zhou	Suppressing ohmic loss and enhancing active material absorption in a plasmonic cavity	I
43	Yunfei Zou	Strong coupling between a quasi-single molecule and a plasmonic cavity based on molecules trapping in the blue-detuned trapping system	I
44	Bamadev Das	Strain induced Terahertz modulation in nanogap	I
45	Fangzhou Shu	Dynamic plasmonic color generation based on phase transition of vanadium dioxide	I
46	Mingzhu Li	High efficient perovskite photovoltaic devices through nanophotonic light trapping	I
47	Wei Kou	Independent linear dual-polarization Terahertz focusing at a composite multifunctional metasurface	I
48	Xinyu Chai	Green synthesis and characterization of graphene quantum dots prepared from D-xylose	I
49	Zeying Zhang	Precisely control of nanoparticles assembly and patterning for three-primary-color micro-light-emitting arrays	I

NP 2018

Poster Abstract

No.	Author	Title	Poster Session
50	Jun Xing	Dramatically enhanced photoluminescence from femtosecond laser induced micro/nano-structures on $MAPbBr_3$ single crystal surface	I
51	Wei Liu	CO_2-assisted fabrication of amorphous molybdenum oxide for enhanced plasmon resonances	I
52	Tianchi Zhou	THz ultra-high Q meta-surface based on the tip coupling enhanced FANO resonance	I
53	Xinhe Jiang	Quantum teleportation of surface plasmon polariton	II
54	Baicheng Yao	Gate-tunable Kerr combs in graphene-nitride microresonators	II
55	Xintao He	A silicon-on-insulator slab for topological valley transport	II
56	Chengzhi Qin	Frequency diffraction management through photonic gauge potentials and effective electric-field forces	II
57	Yi Xu	Six dimensional light-matter interactions	II
58	Haowen Liang	High numerical aperture crystalline silicon metalenses and applications at visible wavelengths	II
59	Zhizhou Lu	Dissipative Kerr solitons generation and switching in a thermally controlled micro-ring resonator	II
60	Yubo Xie	Integrated quantum memory based on rare-earth ion nanowire	II
61	Lantian Feng	On-chip photonic quantum sources based on silicon waveguides	II
62	Wange Song	Topologically protected edge states for robust integrated photonic devices	II
63	Xu Wang	Engineered graphene GaAs van der Waals heterostructures and InAs quantum dots for mode-locked laser	II
64	Liangliang Lu	Entangled qutrits on a silicon chip	II
65	Biye Xie	Second-order photonic topological insulator with corner states	II
66	Meng Su	Self-assembling of nanomaterials via droplet manipulation for multifunctional optoelectronics devices	II
67	Yuansong Zeng	Efficient conversion between plasmonic waves and spin optical waves enabled by nanopatch antenna array	II
68	Xinchao Lu	The study on plasmonics imaging to single nanoparticle	II
69	Jiawei Lv	Bio-inspired chiral photonic crystals	II
70	Thomas Lettner	Bright and tunable single-photon sources for quantum optics	II
71	Xueke Duan	Length-relaxed nanocavity for large spontaneous emission enabled by epsilon-near-zero substrate	II
72	Zebo Zheng	Mid-infrared biaxial hyperbolic phonon polaritons in a van der Waals crystal	II
73	Zhubing He	Hexagonal packed tungsten nanocylinder array as efficient selective solar absorber for concentrating solar thermoelectrical generator	II
74	Liang Xu	Weak-measurement-enhanced metrology in the presence of CCD noise and saturation	II
75	Shumin Xiao	Dynamic color displays using all-dielectric metasurfaces	II
76	Yuanmu Yang	High-harmonic generation in an epsilon-near-zero material	II
77	Jing Zhou	Enhancing graphene photoresponse by an optical patch antenna	II

No.	Author	Title	Poster Session
78	Kaixuan Li	Tunable whispering gallery mode lasing from the printed high-Q microdisk	II
79	Yanlin Song	Green printing technology for colloidal photonic crystals	II
80	Weiwei Zhu	Topological properties of comb-like waveguide systems	II
81	Qiang Li	On-demand generation and depth control of shallow silicon vacancy in silicon carbide	II
82	Kaimin Zheng	Deterministic phase estimation in standard quantum limit with real-time feedback control	II
83	Rui Niu	Repetition rate tuning of soliton in microrod resonators	II
84	Yanjing Zhao	Optical frequency comb generation based on high order mode in a thin micro-ring resonator	II
85	Peiyan Zhao	High speed silicon Mach-Zehnder modulator via a pilot run	II
86	Gaoneng Dong	High-contrast and low-power all-optical switch using fano resonance based on a silicon nanobeam cavity	II
87	Chao Zhuang	Plasmonic photothermoelectric generator	II
88	Aonan Zhang	Device-independent characterization of quantum measurements	II
89	Sajid Ur Rehman	Novel Cubic Tin Sulfide (π-SnS) chalcogenide as a potential candidate for optoelectronic and energy storage devices	II
90	Jianbin Liu	Scattering-immune surface-wave open resonator for arbitrary disorders	II
91	Woongkyu Park	Terahertz-induced resist polymerization in nanoantennas	II
92	Ximiao Wang	Mid-infrared edge plasmon modes of chemically-doped graphene	II
93	Junfeng Lu	Piezoelectric effect tuning on ZnO microwire WGM lasing	II
94	Xinjie Lv	Generation of optical frequency comb in a $\chi^{(2)}$ sheet micro optical parametric oscillator via cavity phase matching	II
95	Weiyang Cai	Optical focusing based on the planar metasurface reflector with application to trapping cold molecules	II
96	Fengsheng Sun	Hybridized plasmon–phonon modes supported in graphene/MoO_3 stacked hybrid structures	II
97	Shunyu Yao	Generation of visible Kerr comb and platicon via Raman assisted four wave mixing in microresonator	II
98	Stephan Steinhauer	Excitonic quantum states in Cu_2O microcrystals grown on silicon substrates	II
99	Xi Yang	Turbidimetric inhibition immunoassay revisited to enhance its sensitivity by optofluidic laser	II
100	Zhenqian Yang	High performance single crystalline perovskite thin film photodetector	II
101	Tanchao Pu	Ultra-high reflectivity all-dielectric metasurface at ultra-violet wavelength	II
102	Guangchao Zheng	A large-scale synthetic methods for tuning the morphology and chiroptical properties of discrete chiral gold nanorods	II
103	Xueqing Liu	High precision fabrication of sapphire micro-optical elements by femtosecond laser and dry etching	II

No.	Author	Title	Poster Session
104	John Ho	Radio surface plasmons on metamaterial textiles for efficient and secure body networks	II
105	Yang Sun	Electromagnetic engineered mechanical trapping potential and the conversion in optomechanical system	II
106	Suo Wang	High performance plasmonic nanolasers with external quantum efficiency exceed 10%	II
107	Ran Hao	Wideband slowlight in grating waveguide	II
108	Ziwei Liu	Low refractive index coating induced resonant Kerker effect	I
109	Siyi Min	Refractometric sensing using gradient plasmonic nanostructures: mapping spectral information to spatial patterns	I

12-photon entanglement and scalable scattershot boson sampling with optimal entangled photon pairs from parametric down-conversion

Han-Sen Zhong[1,2], Yuan Li[1,2], Wei Li[1,2], Li-Chao Peng[1,2], Zu-En Su[1,2], Yi Hu[1,2], Yu-Ming He[1,2], Xing Ding[1,2], W.-J. Zhang[3], Hao Li[3], L. Zhang[3], Z. Wang[3], L.-X. You[3], Xi-Lin Wang[1,2], Xiao Jiang[1,2], Li Li[1,2], Yu-Ao Chen[1,2], Nai-Le Liu[1,2], Chao-Yang Lu[1,2], Jian-Wei Pan[1,2]

[1] *Hefei National Laboratory for Physical Sciences at Microscale and Department of Modern Physics, University of Science and Technology of China, Hefei, Anhui, 230026, China*
[2] *CAS Centre for Excellence and Synergetic Innovation Centre in Quantum Information and Quantum Physics, University of Science and Technology of China, Hefei, Anhui 230026, China*
[3] *State Key Laboratory of Functional Materials for Informatics, Shanghai Institute of Micro system and Information Technology (SIMIT), Chinese Academy of Sciences, 865 Changning Road, Shanghai 200050, China*

Since the discovery of spontaneous parametric down-conversion (SPDC), it has been one of the most popular quantum light source. In the area of SPDC, one of our main target is to achieve near-unity purity and collection efficiency simultaneously. In previous work [], beamlike method is employed to reach a high collection efficiency. However, because of the frequency correlation, we must filter the down-conversion beam to increase the purity. This reduces the collection efficiency significantly. Here, we introduce a new entanglement photon pair source based on SPDC whose heralding efficiency is 97% and indistinguishability is 96%.

We perform a twelve-photon entanglement experiment to validate the SPDC source. Six entanglement sources are employed to produce a twelve-photon Greenberger-Horne-Zeilinger state. As shown in Fig. 1, we calculate the population of 0.732(24) and the coherence of 0.419(41), from which the fidelity of 0.576(24) is derived.

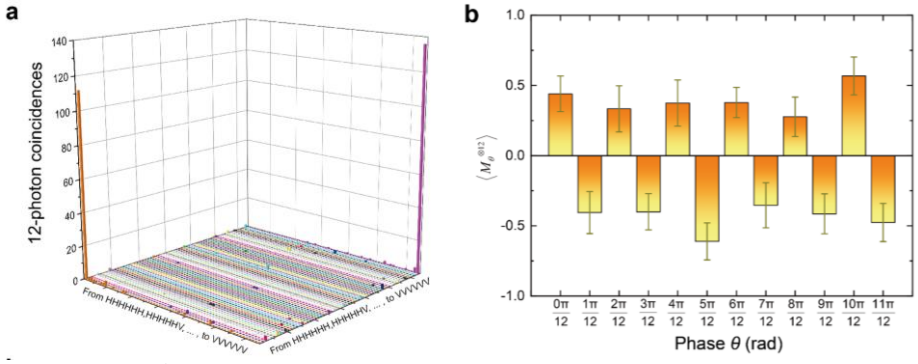

Fig. 1 Experimental results of twelve-photon entanglement. (a) The measured 12-photon events distribution in *H/V* basis. (b) Results of observables $M_\theta^{\otimes N} = (\cos\theta\sigma_x + \sin\theta\sigma_y)^{\otimes N}$.

We further perform a scattershot boson sampling. 12 SPDC sources are used to produce and to herald single photons. A 12×12 mode interferometric is used to implement a random linear transformation. The three-, four- and five-photon sampling rate is 3.9 kHz, 44 Hz and 0.3 Hz, respectively.

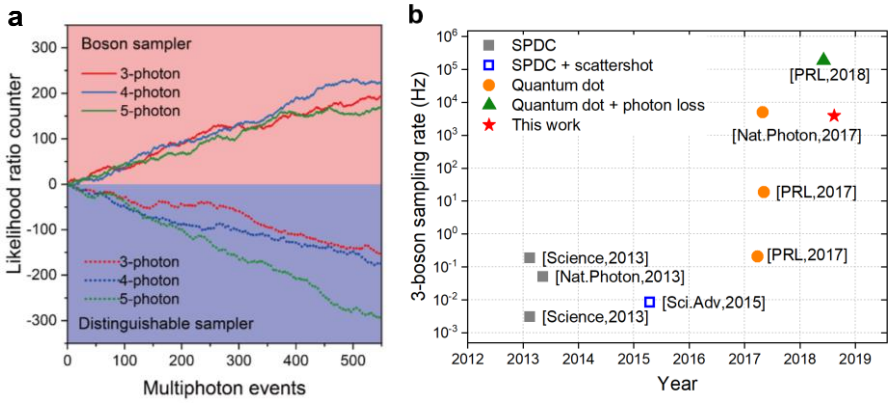

Fig. 2 (a) A validation of 3-, 4- and 5-photon boson sampling. (b) A count rate comparison of 3-photon sampling rates.

References

[1] Wang, X.-L. et al. Experimental Ten-Photon Entanglement. Phys. Rev. Lett. **117**, 210502 (2016).

Imaging the Dark Emission of Spasers

Hua-Zhou Chen[1‡], Jia-Qi Hu[1‡], Suo Wang[1‡], Bo Li[1], Xing-Yuan Wang[1], Yi-Lun Wang[1], Lun Dai[1,2], Ren-Min Ma[1,2*]

[1]State Key Lab for Mesoscopic Physics and School of Physics, Peking University, Beijing 100871, China.
[2]Collaborative Innovation Center of Quantum Matter, Beijing, China
**Corresponding Author Renmin Ma: renminma@pku.edu.cn*
‡These authors contributed equally.

The recent rapidly advancing nanoscience and technology calls for a nanoscale laser spot for various technologies, such as nanolithography, high-density data storage and uper resolution imaging. However, conventional lasers amplify photons where diffraction limit puts a forbidden barrier to scaling down its physical size and mode volume. In 2003, David J. Bergman and Mark I. Stockman proposed a new class of amplifier, named spaser, an acronym of surface plasmon amplification by stimulated emission of radiation [1]. In stark contrast to classical laser, spaser amplifies surface plasmons instead of photons providing an optical amplifier with size beyond diffraction limit, which is of major interest for various applications, ranging from all-optical computing to biomedical sensing. Because of this, numerous studies on the experimental implementation of spasers have been reported [2-3].

However, to date, spasers have only been characterized by the photons scattered to the optical far field. According to its original definition, a spaser is a surface plasmon amplifier that does not necessarily generate radiative photon output. Its intrinsic surface plasmon emission is yet unrevealed "dark" emission due to its evanescent nature. Consequently, there is a lack of direct evidence of spasing, and the intentional manipulation and utilization of spaser emission becomes difficult to achieve.

Here, for the first time, we directly image surface plasmon emission, an intrinsic but unrevealed feature of spasers in spatial, momentum and frequency spaces simultaneously [4-5]. We demonstrate that spaser can serve as a pure surface plasmon generator with the ratio of surface plasmon emission over total radiation approaching to 100% and experimentally demonstrated 74%. Our results supply an unambiguous evidence of spasing behavior, an intrinsic but unrevealed feature of this intensively studied new class of optical amplifier. Furthermore, in contrast to the scattered photons, the surface plasmon emission of spasers is the crucial element for various nanophotonic applications.

References

[1] D. J. Bergman, M. I. Stockman, Surface plasmon amplification by stimulated emission of radiation: Quantum generation of coherent surface plasmons in nanosystems. Phys. Rev. Lett. 90, 027402, 2003.
[2] Ma, R. M., Oulton, R. F., Sorger, V. J. & Zhang, X. Plasmon lasers coherent light source at molecular scales. Las. Photon. Rev. 7, 1-21 (2012)
[3] Gwo, S. & Shih, C. K. Semiconductor plasmonic nanolasers current status and perspectives. Rep. Prog. Phys. 79, 086501, 2016.
[4] H.-Z. Chen, et al. Imaging the dark emission of spasers. Science Advances 3, e1601962 (2017).
[5] H.-Z. Chen, et al. Characterization of plasmonic nanolasers in spatial, momentum and frequency spaces. IEEE Journal of Quantum Electronics, 54, 7200307 (2017).

Direct Observation of Valley-locked Topological Edge States in Designer Surface Plasmon Crystals

Xiaoxiao Wu[1,2], Yan Meng[2], Jingxuan Tian[3], Yingzhou Huang[2], Hong Xiang[2], Dezhuan Han[2], Weijia Wen[1,2]

Affiliations

[1]Department of Physics, The Hong Kong University of Science and Technology, Clear Water Bay, Kowloon, Hong Kong, China

[2]Department of Applied Physics, Chongqing University, Chongqing 401331, China

[3]Department of Mechanical Engineering, Faculty of Engineering, The University of Hong Kong, Hong Kong, China

E-mail Address: xwuan@connect.ust.hk

Abstract

The extensive researches of two-dimensional layered materials have suggested that valleys, as energy extrema in momentum space, could offer a new degree of freedom for carrying information. Based on this concept, researchers have predicted the existence of valley-Hall topological insulators which could support valley-locked edge states propagating along non-trivial domain walls. Recently, several kinds of photonic or sonic crystals have been proposed as classical counterparts of valley-Hall topological insulators. However, direct experimental observation of valley-locked edge states in classical systems is still difficult until now. Here, we demonstrate a designer surface plasmon crystal comprised of periodic metallic patterns deposited on a dielectric substrate, which can become a valley-Hall photonic topological insulator by exploiting the mirror-symmetry-breaking mechanism. Topological edge states with valley-dependent transport are directly imaged in the microwave regime. The observed edge states are confirmed to be fully valley-locked through spatial Fourier transforms. Topological protection of the edge states at sharp corners is also experimentally demonstrated.

References

[1] Wu, Xiaoxiao, et al. Nature communications 8.1 (2017): 1304.

Non-reciprocal Photonic Devices Based on Optomechanical Microresonator

Zhen Shen, Yan-Lei Zhang, Yuan Chen, Fang-Wen Sun, Chang-Ling Zou, Chun-Hua Dong
Key Lab of Quantum Inforamtion, University of Science and Technology of China, Hefei, Anhui 230026, China

Light has bidirectional transmission reciprocity in common dielectric material, and breaking this reciprocity, that is, achieving non-reciprocity in the direction of light transmission, is of great significance in classical and quantum information processing [1]. Optical isolators, circulators, directional amplifiers, etc. are typical non-reciprocal devices. The optical isolators and circulators allow light to pass in a specified direction but block it in an undesired direction, which can be used for light source protection and precise measurement. The most common optical non-reciprocal devices are based on the Faraday effects using magneto-optical materials, which are difficult to integrate on-chip [2]. Therefore, in recent years, interest has increased in realizing on-chip all-optical circulators, isolators, and directional amplifiers.

In 2016, we experimentally demonstrated non-magnetic non-reciprocity using optomechanical interactions in a whispering-gallery microresonator, as proposed by Hafezi and Rabl. We observed optomechanically induced non-reciprocal transparency (OMIT) and amplification (OMIA), and demonstrated a non-reciprocal phase shift of up to 40 degrees [3]. Here, we experimentally demonstrate a reconfigurable circulator and directional amplifier in a two tapered fibre-coupled silica microresonator. Via a simple change in the control field, the device performs as an add-drop filter and can be switched to circulator mode or directional amplifier mode [4]. The demonstrated device exhibits considerable flexibility and offers exciting opportunities for combining reconfigurability, non-reciprocity and active properties in single photonic devices. The principle demonstrated herein can also be incorporated into microwave superconducting devices as well as acoustic devices in the emerging research field of quantum phononic.

References

[1] Y. Shoji, and T. Mizumoto, "Magneto-optical nonreciprocal devices in silicon photonics," Sci. Technol. Adv. Mater. **15**, 014602 (2014).
[2] L. Bi, J. Hu, P. Jiang, D. H. Kim, G. F. Dionne, L. C. Kimerling, and C. A. Ross, "On-chip optical isolation in monolithically integrated non-reciprocal optical resonators," Nat. Photon. **5**, 758–762 (2011).
[3] Z. Shen, Y.-L. Zhang, Y. Chen, C.-L. Zou, Y.-F. Xiao, X.-B. Zou, F.-W. Sun, G.-C. Guo, and C.-H. Dong, "Experimental demonstration of optomechanically induced non-reciprocity," Nat. Photon. **10**, 657-661 (2016).
[4] Z. Shen, Y.-L. Zhang, Y. Chen, F.-W. Sun, X.-B. Zou, G.-C. Guo, C.-L. Zou, and C.-H. Dong, "Reconfigurable optomechanical circulator and directional amplifier," Nat. Commun. **9**, 1797 (2018).

Strong Localization of Surface Plasmon Polaritons with Engineered Disorder

Ying-Ying Zhu[1], Wen-Bo Shi[1], Jia-Nan Wang[1], Jie He[1], Ming-Jun Tuo[1], Ru-Wen Peng[1], and Mu Wang[1]

[1]National Laboratory of Solid State Microstructures, School of Physics, and Collaborative Innovation Center of Advanced Microstructures, Nanjing University, Nanjing 210093, China

The absence of diffusion in disordered systems is an important effect in condensed matter physics, which was initially investigated by Anderson in 1958 [1]. The absence of electron propagation was predicted because of Anderson localization in disordered systems, eventually causing conductive materials to be insulating. On the other hand, surface plasmon polaritons (SPPs) are electromagnetic excitations at the metal-dielectric interface. Due to the strong field confinement and enhancement effects, SPPs have attracted significant attention. Yet so far, only very limited examples have been shown with near field approaches in fully random systems [2]. Since Anderson localization of SPPs associates spatial-disorder-induced light localization with SPP-induced light confinement, it can be applied to achieve stronger field confinement for various applications. In this work [3], we experimentally demonstrate for the first time strong localization of surface plasmon polaritons (SPPs) at visible regime in metallic nanogratings with short-range correlated disorder. The localization of SPPs is significantly enhanced by increasing the degree of disorder, and the propagation of SPPs is suppressed. Our study enriches the family of Anderson localization and develops a way for disorder engineering to manipulate light on nanoscale, which may achieve various applications in random nanolasing, solar energy, and strong light-matter interactions.

References

[1] P. W. Anderson, "Absence of Diffusion in Certain Random Lattices." Phys. Rev. **109**, 1492 (1958).
[2] S. Grésillon, L. Aigouy, A. C. Boccara, J. C. Rivoal, X. Quelin, C. Desmarest, P. Gadenne, V. A. Shubin, A. K. Sarychev, and V. M. Shalaev, "Experimental observation of localized optical excitations in random metal-dielectric films." Phys. Rev. Lett. **82**, 4520 (1999).
[3] W. B. Shi, L. Z. Liu, R. W. Peng, D. H. Xu, K. Zhang, H. Jing, R. H. Fan, X. R. Huang, Q. J. Wang, and Mu Wang. "Strong Localization of Surface Plasmon Polaritons with Engineered Disorder." Nano Letters. **18**, 1896-1902 (2018).

Photo-patterning of Chiral Smectic-C Liquid Crystal for Electrically-addressed Diffractive Optical Elements

Qi Guo[1], **Xiaoqian Yang**[1], **Kexin Yan**[1], **Huijie Zhao**[1], **V.G. Chigrinov**[2], **H.S. Kwok**[2]

1. Beihang University, Beijing, 100191, China
2. Hong Kong University of Science and Technology, Hong Kong

Diffractive optical elements(DOEs), such as Dammann gratings, attract considerable attentions recently owing to their potential applications in optical trapping, imaging coding and optical sensing[1,2]. However, the fabrication of switchable diffractive optical elements suffers from a contradiction between the complexity of fabrication procedures and the performance of such gratings. In this letter, a fast switching circular Dammann grating(CDG) is demonstrated based on the photoalignment technology of ferroelectric liquid crystals(FLCs). By applying low electric field (V=6V) on the FLC CDG, it is switched between an eight-order diffractive state and a non-diffractive state with high diffraction efficiency of 84.5%. The fast response time of 64μs is achieved under 4.3V/μm, which is approximate two-order faster than existing nematic LC DOEs.

A binary phase FLC eight-order CDG zone plane consisting of alignment directions perpendicular to each other for odd zone and even zone was fabricated through a two-exposure photoalignment process using photo-sensitive material sulfonic Azo-dye SD1 (Dai-Nippon Ink and Chemicals DIC, Japan, formula shown in Fig. 1(d)) as the active aligning layer. When exposed with linearly polarized UV or blue light, the SD1 layer will be providing alignment along the direction perpendicular to the exposure light polarization, as shown in Fig. 1(a). Then, the alignment direction of SD1 was re-aligned by the second exposure with mask and polarization direction rotated 90 degrees to create the two orthogonal aligned domains on the same substrate, as shown in Fig. 1(b). Then a LC cell was assembled with the prepared patterned aligned substrate as one side of the cell and ITO glass substrate without alignment layer as the other side, as shown in Fig. 1(c).

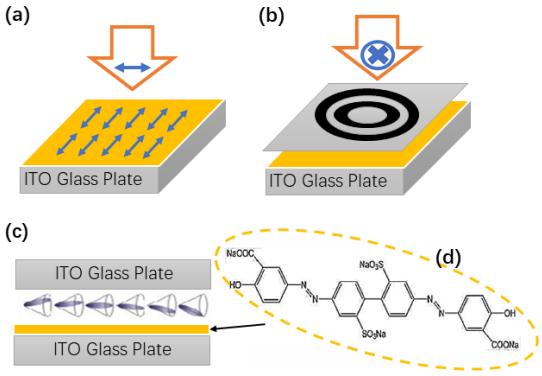

Fig. 1 The schematic of two-step exposure process for patterned alignment layer of FLC CDG. (a) The first exposure of polarized UV on the SD1 substrate; (b) Exposure of SD1substrate with mask; (c) FLC CDG cell with single-side alignment (d)Chemical structure of SD1.

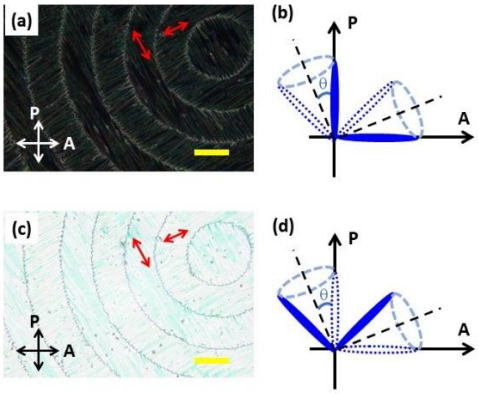

Fig. 2. (a) and (c) Microscopic photo of the FLC CDG driven by two electrical polarities under crossed polarizer and analyzer. Line scales represent 200 μm. The red arrows indicate the alignment directions; (b) and (d) Illustration of the molecule directions and the helical orientation with respect to the polarizer and analyzer in odd and even zones.

When no voltage applied on the FLC sample, the helix is aligned along the alignment direction. The helix is fully suppressed and the FLC molecules switch to either side of the position parallel to the substrates around the cone surface [Fig. 2 (a) and (c)], which are decided by the polarity of the electric field applied. The designed arrangements of FLC molecules in the odd and even zones are always oriented orthogonal to each other, endow the CDG with the polarization independence [3]. With the half-wave condition satisfied, π phase shift is achieved for the passing light between every two adjacent alignment domains. In this case, the far-field diffraction patterns exhibit equal-intensity rings.

Example References

[1] G.A. Siviloglou, J. Broky, A. Dogariu, and D.N. Christodoulides, "Observation of Accelerating Airy Beams", Phys. Rev. Lett. **99**, 213901 (2007)
[2] E. Arbabi, A. Arbabi, S.M. Kamali, Y. Horie, and A. Faraon, "Controlling the sign of chromatic dispersion in diffractive optics with dielectric metasurfaces", Optica **4**, 625 (2017).
[3] W. Hu, A.K. Srivastava, X.W. Lin, X. Liang, and Z.J. Wu, "Polarization independent liquid crystal gratings based on orthogonal photoalignments", Appl. Phys. Lett. **100**, 111116(2012).

A non-local quantum delayed-choice experiment

Kai Wang[1], **Qian Xu**[1], **Xiao-song Ma**[1]

1. School of Physics, National Laboratory of Solid-state Microstructures, Collaborative Innovation Center of Advanced Microstructures, Nanjing University, China

Quantum delayed-choice experiment was proposed to test the predictions of quantum theory versus classical hidden-variable (HV) theory. Here we realize an entanglement-assisted version of the quantum delayed-choice experiment with four photons. By harnessing the nonlocal correlations between entangled photons, we reveal the choice-dependent wave-particle superposition features of the photon under test even under the space-like separation of the underlying events. Our work provides striking distinctions between quantum and classical theories. The experiment set up is shown in Fig.1.

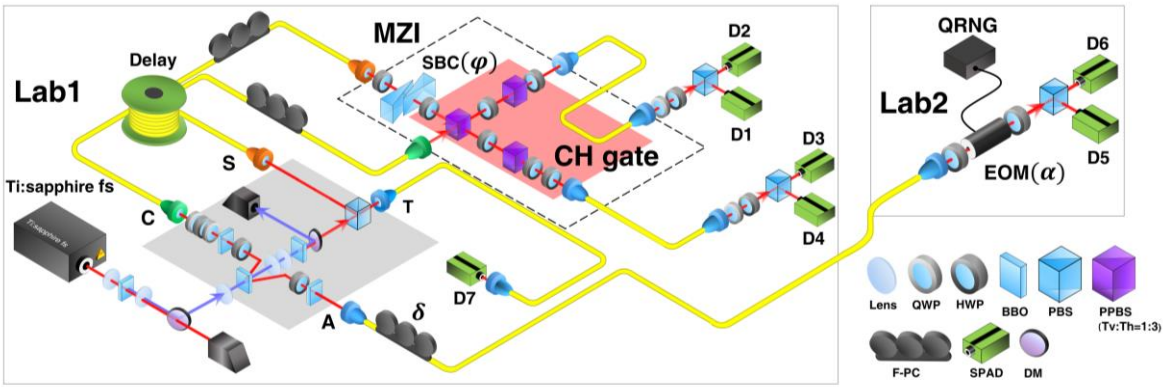

Fig. 1 Sketch of experiment. We used entangled photon pair (control photon and ancillary photon) generated in Lab1 to assist quantum delayed-choice experiment as proposed in [1]. Horizontal polarization of control photon corresponds to BS2 in and vertical polarization corresponds to BS2 out. Ancillary photon was transmitted to Lab2 and will be detected on random polarization base $|\alpha\rangle = \cos\alpha\,|H\rangle + \sin\alpha\,|V\rangle$ controlled by quantum random number to realize a space-like configuration. **A.** Aerial photo of the location of two labs. **B.** Experiment setup. **C.** Space-time diagram. (I) Interference of system and control photon in MZI. (F)Function generator signal(square,5MHz) enters into QRNG. (R)Random number signal is shaped with a discriminator and transfered to the EOM driver. (D)Detection of photon and polarization analysis.

In most of the previous delayed-choice experiments, only classical mixture of |wave⟩ and |particle⟩ states were shown[2-4]. $\rho_s = cos^2\,\alpha\,|p\rangle\langle p| + sin^2\,\alpha|w\rangle\langle w|$ gives $P_s = \frac{1}{2}cos^2\,\alpha + sin^2\,\alpha\,cos^2\frac{\varphi}{2}$ as shown in Fig.2(a). By harnessing multi-photon entanglement and remote quantum gate preparation, we obtain a coherent superposition state of system photon $|\varphi_s\rangle = cos\,\alpha\,|p\rangle + e^{i\delta}\,sin\,\alpha\,|w\rangle$ and conditional probability $P_{s|c} = \frac{1}{2}cos^2\,\alpha + sin^2\,\alpha\,cos^2\frac{\varphi}{2} + \sqrt{2}\,cos\,\alpha\,sin\,\alpha\,sin\frac{\varphi}{2}sin\left(\delta + \frac{\varphi}{2}\right)$ gives a quantum superposition of wave and particle as shown in Fig.2 (b) ($\delta = 0$) .

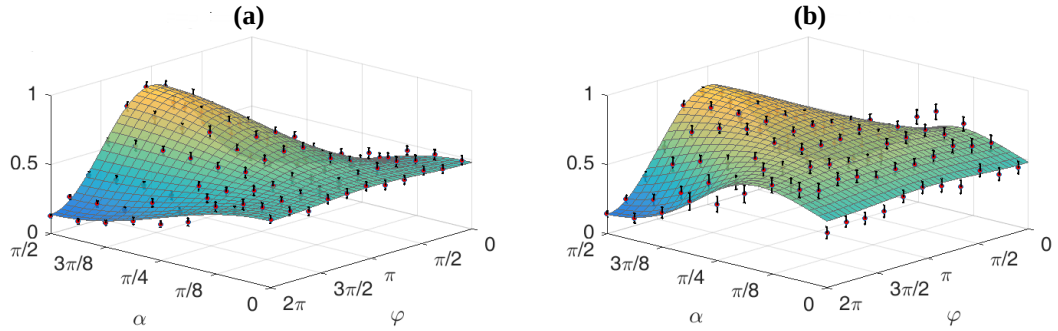

Fig. 2 Experiment Result. Z axis represent the probability of system photon on the horizontal polarization output port. (a) Classical mix of |wave⟩ and |particle⟩. As α increased from 0 to 2π, it shows the morph from particle nature to wave nature. (b) Quantum superposition of |wave⟩ and |particle⟩. It shows a difference from (a), as there is interference of |wave⟩ and |particle⟩.

References

[1] R. Ionicioiu, T. Jennewein, R. B. Mann, D. R. Terno, Nature communications 5, 3997(2014).
[2] J. A. Wheeler,W. H. Zurek, Quantum theory and measurement (Princeton University Press, 2014).
[3] V. Jacques, et al., Science 315, 966 (2007).
[4] X.-s. Ma, J. Kofler, A. Zeilinger, Rev. Mod. Phys. 88, 015005 (2016).

Visualizing Mie resonances in low-index dielectric nanoparticles

Jing Zhou[1,2], Ashwin Panday[3], Yuntao Xu[1], Xi Chen[4], Long Chen[4], Chengang Ji[1], L. Jay Guo[1,3,4]

1. Department of Electrical Engineering and Computer Science, The University of Michigan, Ann Arbor, Michigan 48109, USA
2. State Key Laboratory of Infrared Physics, Shanghai Institute of Technical Physics, Chinese Academy of Sciences, China
3. Macromolecular Science and Engineering, The University of Michigan, Ann Arbor, Michigan 48109, USA.
4. Applied Physics, The University of Michigan, Ann Arbor, Michigan 48109, USA.

Light scattering by small particles is a fundamental topic in electromagnetics and attracts much attention throughout modern history. Among all the phenomena, resonant scattering is the most outstanding behavior because it can be easily detected by spectroscopy and features a strong local field, enabling various applications of nanoparticles [1-6]. Metallic nanoparticles with localized surface plasmon resonances have been extensively studied and practically utilized in surface enhanced spectroscopy and metamaterials [7,8]. Recently, high-index dielectric nanoparticles with strong Mie resonances drew considerable interest. Efficient field localization and negligible material absorption facilitate prominent Mie resonances, leading to optical magnetic response and scattering manipulation [3-6]. For low-index dielectric nanoparticles, the Mie resonances are weak and broad due to poor light confinement caused by low reflection at particle boundaries, so that they are typically not visible in light scattering spectra. However, low-index dielectric nanoparticles, such as SiO_2 and polystyrene nanoparticles, have more applications than their high-index or even metallic counterparts. If pronounced Mie resonances can be realized, many potential applications can be envisioned. In this work, we found a simple and effective approach to drastically enhance the resonance effect of the low-index particles by partial metal dressing. Mie resonances of low-index nanoparticles can now be easily visualized by scattered light. This scattering peak depends on sphere size and has a reasonable line width. A size difference as small as 8 nm was resolved by peak shift or even by color change. The scattering peak is attributed to the enhanced TE_{11} Mie resonance of the low-index nanospheres. The metal dress not only provides high-reflection boundary, but also functions as an antenna to couple the confined light power to the far field, leading to scattering maxima in the spectra. Additionally, the enhanced TE_{11} Mie resonance in low-index nanoparticles features considerable magnetic response due to the strong circulating displacement currents induced by the intensified *E*-field instead of a high permittivity for index particles. The enhanced Mie resonances could be used to sense minute changes in size or refractive index of low-index nanoparticles and benefit a wide range of applications.

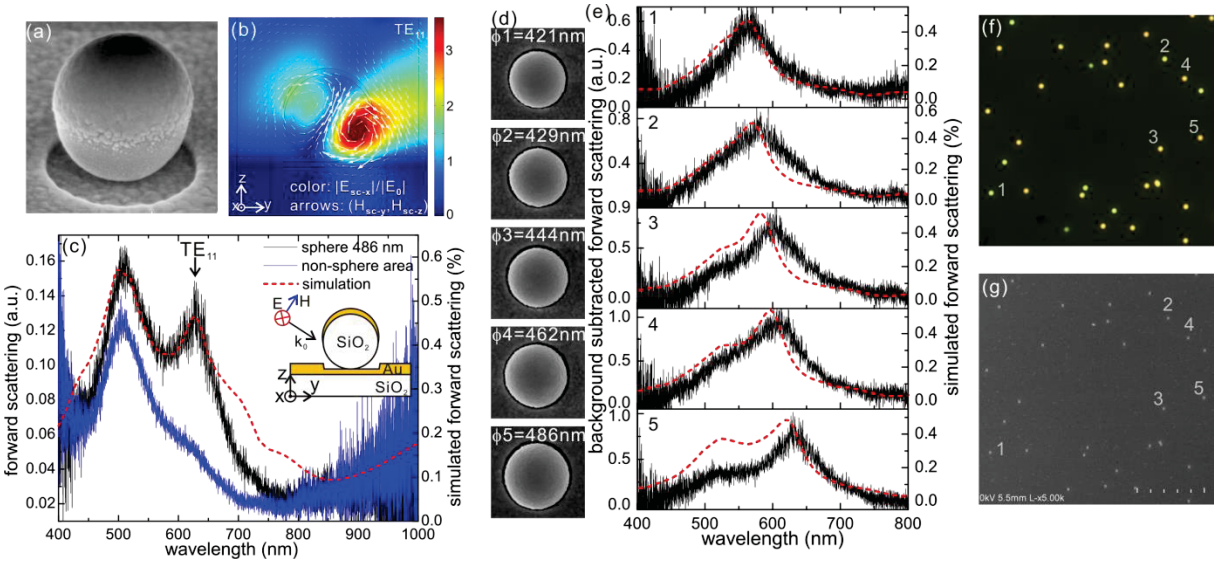

Fig. 1 (a) SEM image of a metal-dressed SiO_2 nanosphere. (b) Forward scattering spectrum and field distribution of the metal-dressed nanosphere (486 nm) at the TE_{11} resonance. (c) Measured forward scattering spectrum of a 486 nm nanosphere (black) together with simulation (red), and that at a blank area without nanospheres (blue). The simulated spectrum is normalized to the incident power. The incident *E*-field is along the *x*-axis. (d) SEM images of five selected metal-dressed SiO_2 nanospheres with different sizes. (e) Background subtracted forward scattering spectra (black lines) of the five nanospheres and the corresponding simulations (dashed red lines). (f) Photopicture in the dark field transmission view for nanospheres including the five selected ones with size dependent colors. (g) SEM image of the same nanospheres in (f) with the same scope and the same magnification.

References

[1] K. L. Kelly, et al., J. Phys. Chem. B **107**, 668–677 (2003).
[2] J. N. Anker, et al., Nat. Mater. **7**, 442-453 (2008).
[3] A. I. Kuznetsov, et al., Science **354**, aag2472 (2016).
[4] J. C. Ginn, et al., Phys. Rev. Lett. **108**, 097402 (2012).
[5] L. Shi, et al., Adv. Mater. **24**, 5934–5938 (2012).
[6] A. B. Evlyukhin, et al., Nano Lett. **12**, 3749−3755 (2012).
[7] S. Nie, et al., Science **275**, 1102 (1997).
[8] J. A. Fan, et al., Science **328**, 1135 (2010).

Tomographic microscopy by chromatic metalens

Chen Chen[1], Jia-Wern Chen[2,3], Din Ping Tsai[2,3], Shining Zhu[1] and Tao Li[1]*

1.National Laboratory of Solid State Microstructures, Key Laboratory of Intelligent Optical Sensing and Integration, Jiangsu Key Laboratory of Artificial Functional Materials, College of Engineering and Applied Sciences, Nanjing University, Nanjing, 210093, China.

2.Research Center for Applied Sciences, Academia Sinica, Taipei, Taiwan.

3.Department of Physics, National Taiwan University, Taipei, Taiwan..

**Corresponding author: taoli@nju.edu.cn*

As the most attractive flat optics, metasurfaces have shown great abilities to manipulate the amplitude, phase and polarization of the light. Among many potential applications of metasurfaces (holograms, wave plates, etc), metalens keeps catching great attention recently. Many excellent works have been reported, most focus on the performance improving, including chromatic aberration correction, efficiency improvement, and so on. It has been demonstrated that metalens based on PB phase has a dramatic negative chromatic property [1] (about an order of BK7 lens). Different from many efforts made to realize achromatic meta-devices [2-4], this work developed an aplanatic design and ingeniously utilized the large chromatic property of metalens.

Here, we fabricated a GaN metalens to work in the visible region. The crucial aplanatic design was used to extremely improve the longitudinal resolution and image quality. Due to the large chromaticity, a 1.7 fold focal length change was obtained in the micro-imaging with wavelength changing from 430 nm to 680 nm. This spectral zooming is non-mechanical and has tremendous advantages on chip integration. Based on this, a microscopic tomography was carried out, where a biological specimen was directly placed in front of the metalens with a certain distance. By changing the illumination wavelength, different layer images can be captured through the metalens with good depths of field (FOV) resolution. Figure 1 shows the tomographic images of two frog egg cells. The spectral resolved images show different FOVs of the cell membrane and nucleus, indicating their different feature sizes in longitudinal dimension.

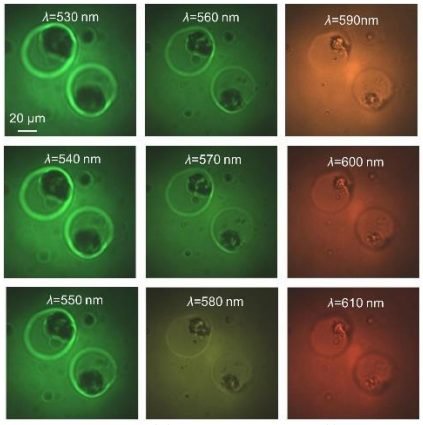

Fig. 1 Tomographic images of frog egg cells at different wavelengths

Taking an ingenious use of large chromaticity of metalens, this work proposed a new method for microscopic tomographic imaging in a totally non-motional manner. It promises great potential in detecting highly compact and stable imaging system, and possibly illuminate new revolution in optical devices and technology.

References

[1] Chen, C. et al. Spectral optical zooming and tomographic imaging by chromatic aplanatic metalens. (2018) submitted.
[2] Wang, S. et al. Broadband achromatic optical metasurface devices. Nat. Commun. 8, 187 (2017).
[3] Wang, S. et al. A broadband achromatic metalens in the visible. Nat. Nanotech. 13, 227-232 (2018).
[4] Chen, W. T. et al. A broadband achromatic metalens for focusing and imaging in the visible. Nat. Nanotech. 13, 220–226 (2018).

Nature Conference on Nanophotonics and Integrated Photonics 2018

Nano-kirigami Enabled 2D-to-3D Transformations of Photonic Functional Metastructures

Jiafang Li
Institute of Physics, Chinese Academy of Sciences, Beijing 100190, China
Email: jiafangli@aphy.iphy.ac.cn

Kirigami is one of the most traditional Chinese arts (named "paper-cuts" or "jianzhi") that has been widely used in window decorations, gift cards, festivals, ceremonies, etc. Through cutting and folding 2D/flat objects into 3D shapes, the knowledge of kirigami has recently aroused tremendous interests in both sciences and technologies, including deployable designs of solar arrays, biomedical devices, micro-/nano- electromechanical systems (MEMS/NEMS) and advanced 3D/4D fabrication techniques.

Inspired by a traditional Chinese paper-cut named "pulling flower", here we report a direct nano-kirigami method in flat films at the nanoscale [1]. This method utilized focused ion beam (FIB) instead of knives/scissors to cut a precise pattern in a free-standing gold nanofilm, and used the same FIB instead of hands to gradually "pull" the nanopattern into a complex 3D shape [2]. The "pulling" forces were induced by heterogeneous vacancies (introducing tensile stress) and the implanted ions (introducing compressive stress) within the gold nanofilm during FIB irradiation. By utilizing the topography-guided stress equilibrium within the nanofilm, versatile 3D shape transformations such as upward buckling, downward bending, complex rotation and twisting of nanostructures were precisely achieved. The resulted unprecedented 3D nanogeometries could enable exceptional and flexible functionalities in optical, mechanical, thermal, acoustic, electric, magnetic, and biological areas. As an example, photonic metastructures with giant optical chirality, polarization conversion property and phase engineering capability have been explored [1-3].

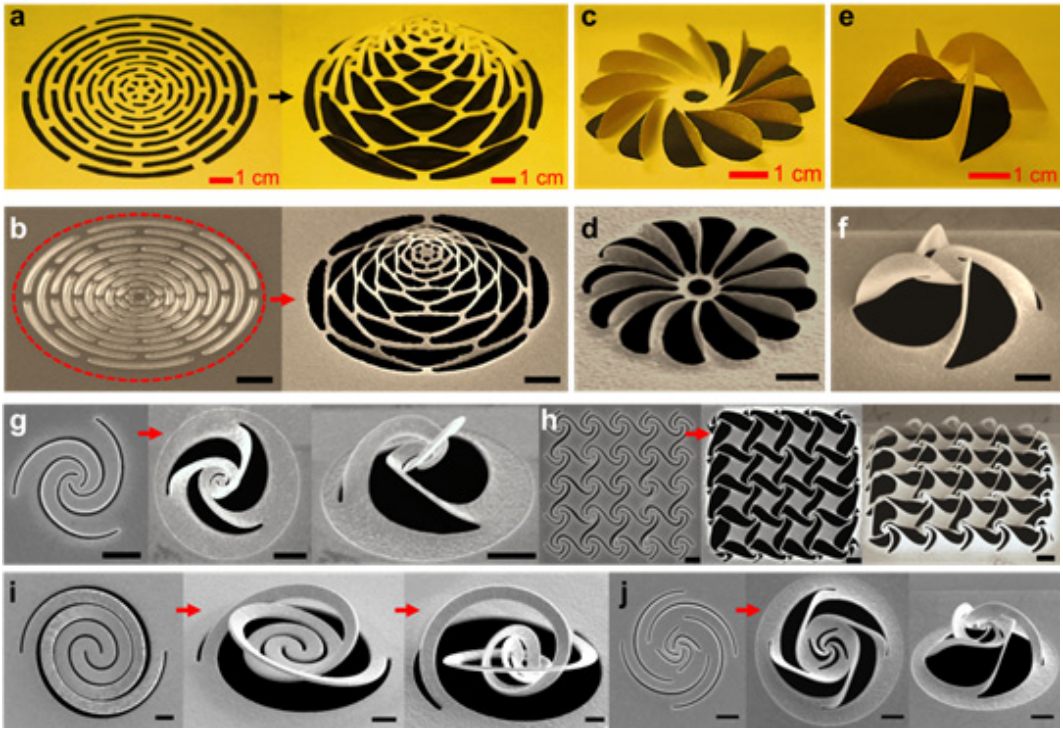

Fig. 1 (a,c,e) Paper-based macro-kirigami by hands and (b,d,f-j) nano-kirigami by FIB irradiation. Scale bars: 1 μm.

References

[1] Z. Liu, H. Du, J. Li, L. Lu, Z.-Y. Li, N. X. Fang., "Nano-kirigami with giant optical chirality", **Science Advances 4** , eaat4436 (2018).
[2] J. Li and Z. Liu, "Focused-ion-beam based nano-kirigami: from art to photonics", **Nanophotonics**, in press (2018).
[3] Z. Liu, H. Du, Z.-Y. Li, N. X. Fang, and J. Li, "Nano-kirigami metasurfaces by focused-ion-beam induced close-loop transformation", **APL Photonics 3**, 100803 (2018).

Experimental Multi-Photon Quantum Walk on a Directed Graph

Tong Wu[1], **Josh Izaac**[2], **Zixi Li**[1], **Kai Wang**[1], **Zhaozhong Chen**[1], **Jingbo Wang**[2], **Xiaosong Ma**[1]

1. School of Physics, National Laboratory of Solid-State Microstructures, Collaborative Innovation Center of Advanced Microstructures, Nanjing University, Nanjing 210093, China

2. School of Physics, The University of Western Australia, Crawley, WA 6009, Australia

Quantum walks [1] are of crucial importance in the development of quantum information processing algorithms. Recently, another potential application has been proposed, where one could efficiently perform network analysis with quantum walks, especially on vertex centrality ranking [2]. However, it is challenging to rank the centrality of a directed network via quantum walks, since it corresponds to a non-Hermitian Hamiltonian, which leads to non-unitary dynamics and thus cannot be simulated by conventional quantum walks.

Here, we solved the non-unitary challenge by introducing pseudo-Hermitian evolutions [3]. We report the first experimental realization of centrality ranking of a directed graph on a photonic platform with multi-photon parity-time-symmetric quantum walks. The experimental setup is shown in Fig. 1.

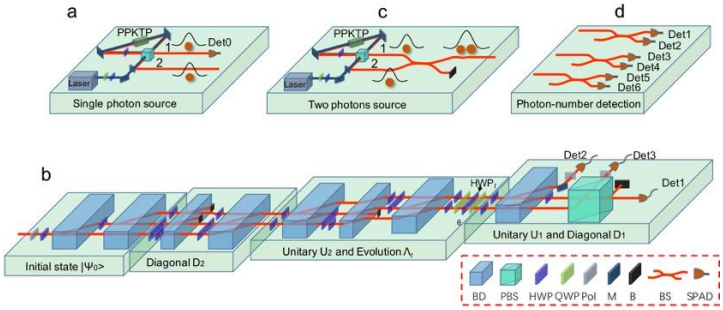

Fig. 1 Experimental setup for realizing quantum walk on directed graphs with single photons and two photons. (a) The single-photon source. (b) The optical circuitry for realizing directed quantum walk. (c) The two-photon source. (d) Non-deterministic photon-number resolving detections are realized by using three fiber BSs and six SPADs.

With single-photon and two-photon Fock states as inputs, we successfully demonstrated quantum centrality rankings on a three-vertex and a nine-vertex graph respectively as shown in Fig. 2, the experimental results agree well with theoretical predictions.

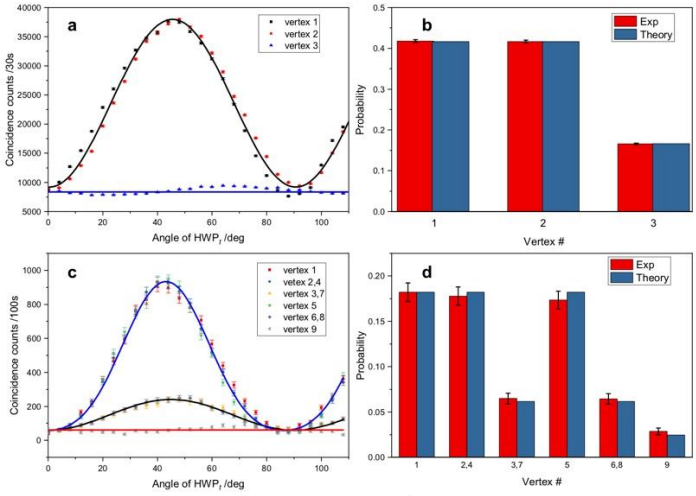

Fig. 2 Experimental data. (a) The experimental coincidence counts of the three vertices. (b) The centrality ranking of the three vertices. (c) The experimental coincidence counts of the nine vertices. (d) The centrality ranking of the nine vertices.

References

[1] Y. Aharonov, L. Davidovich, and N. Zagury, "Quantum random walks," Phys. Rev. A **48**, 1687–1690 (1993).

[2] S. D. Berry and J. B. Wang, "Quantum-walk-based search and centrality," Phys. Rev. A **82**, 042333 (2010).

[3] J. A. Izaac, J. B. Wang, P. C. Abbott and X. S. Ma, "Quantum centrality testing on directed graphs via *pt*-symmetric quantum walks," Phys. Rev. A **96**, 032305 (2017).

Mid-infrared $\chi^{(2)}$ frequency comb generation from a dielectric superlattice box resonator

Kunpeng Jia, Xiaohan Wang, Xin Ni, Liyun Hao, Jian Ning, Gang Zhao, Xinjie Lv, Zhenda Xie*, and Shining Zhu*

1.National Laboratory of Solid State Microstructures, School of Physics, College of Engineering and Applied Sciences, and School of Electronic Science and Engineering, Nanjing University, Nanjing 210093, China

*Corresponding author E-mail:xiezhenda@ nju.edu.cn, zhusn@nju.edu.cn

Optical frequency combs (OFC) are widely used in applications such as precise optical frequency metrology, optical clock, gas sensing and molecular fingerprinting. In the last decade, microresonator OFC has made considerable progress as an integrated alternate of the conventional OFC based on mode-locked lasers [1, 2], with high repetition rates from ~10GHz to over 1THz. Such Kerr comb wavelength is usually at telecom band, while mid-infrared (MIR) comb are also demonstrated with special dispersion engineering with mid-infrared pump [3, 4]. On the other hand, the recent development of the Lithium Niobate resonator makes it a good candidate of the OFC generation [4, 5, 6], because of its high non-linear efficiency and near infrared pump wavelength may be used for MIR OFC generation.

Here we report the first MIR OFC generation based on lithium niobate (PPLN) dielectric superlattice box resonator with high quality factor. Pumped by continuous wave at 1030nm, MIR OFC can be generated with a broadband spectrum over 400nm at 2060nm centre wavelength via second-order optical parametric process. The generated comb has low noise and ultrahigh power over 350mW with threshold of 0.3W and a peak conversion efficiency of 9%. Compared to existing approaches of OFC generation, this technology provides the practicality of many applications such as remote gas sensing.

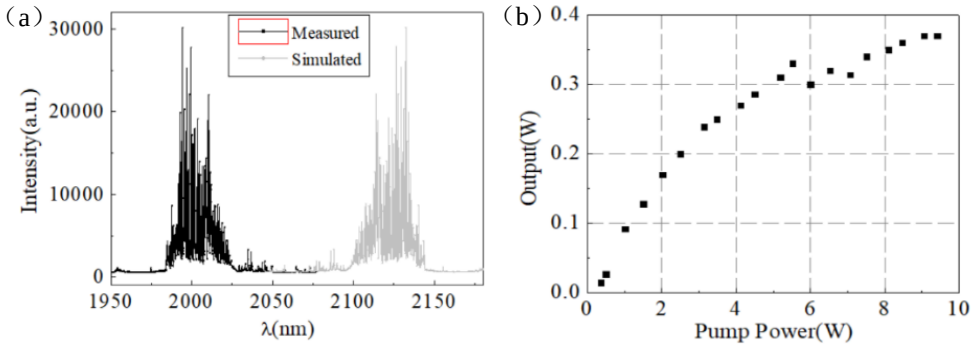

Fig. 1 (a) Optical spectrum of the output centered at 2060nm. The grey line is simulated according to energy conservation due to the limited wavelength range of grating spectrometer. (b) The output power of the 2um comb via the pump power.

References

[1] T. Herr, V. Brasch, J. D. Jost, C. Y. Wang, N. M. Kondratiev, M. L. Gorodetsky and T. J. Kippenberg, "Temporal solitons in optical microresonators," Nat. Photonics 8, 145–152 (2014).

[2] T. J. Kippenberg, R. Holzwarth, and S. Diddams, "Microresonator-based optical frequency combs," Science 332, 555–559 (2011).

[3] Austin G. Griffith, Ryan K.W. Lau, Jaime Cardenas, Yoshitomo Okawachi, Aseema Mohanty, Romy Fain, Yoon Ho Daniel Lee, Mengjie Yu, Christopher T. Phare, Carl B. Poitras, Alexander L. Gaeta and Michal Lipson, "Silicon-chip mid-infrared frequency comb generation," Nat. Communications 6, 6299 (2015).

[4] S. Mosca, M. Parisi, I. Ricciardi, F. Leo, T. Hansson, M. Erkintalo, P. Maddaloni, P. De Natale, S. Wabnitz, and M. De Rosa, "Modulation Instability Induced Frequency Comb Generation in a Continuously Pumped Optical Parametric Oscillator," Phys. Rev. Lett. 121, 093903 (2018)

[5] Mian Zhang, Brandon Buscaino, Cheng Wang, Amirhassan Shams-Ansari, Christian Reimer, Rongrong Zhu, Joseph M. Kahn, and Marko Loncar, "Broadband electro-optic frequency comb generation in an integrated microring resonator," arXiv:1809.08636v1

[6] M. Stefszky, R. Ricken, C. Eigner, V. Quiring, H. Herrmann, and C. Silberhorn, "Waveguide cavity resonator as a source of optical squeezing," Phys. Rev. A 7, 044026 (2017).

An integrated all-optical programmable logic array using cross gain modulation based on semiconductor optical amplifiers

Wenchan Dong[1], Zhuyang Huang[1], Jie Hou[1], Rui Santos[2], Xinliang Zhang[1,*]

[1]*Wuhan National Laboratory for Optoelectronics & School of Optical and Electronic Information, Huazhong University of Science and Technology, Wuhan 430074, China*

[2]*SMART Photonics, Eindhoven, the Netherlands*

Optical logic functions to be realized efficiently is a difficulty in all-optical signal processing [1]. Over the past decades, apart from the basic logic gates, such as AND, OR, NOR, optical complex logic devices, such as full adder and full subtracter, encoder, programmable logic array (PLA), have also been widely studied. In these optical complex logic devices and basic logic gates, various optical nonlinear effects and operation mechanisms were exploited, such as cross gain modulation (XGM) and cross phase modulation (XPM) in semiconductor optical amplifiers (SOAs), and four-wave mixing (FWM) in SOAs, highly nonlinear fiber (HNLF) or silicon waveguide. As for the potential of integration and reconfiguration, HNLF-based schemes are too bulky for integration on a chip, but SOA-based schemes are worthy of further investigation. Among those complex logic devices, PLA is a typical representative of reconfigurable and complex logic devices, and it can flexibly implement combinational logic functions by combining certain canonical logic units (CLUs), also known as CLUs-PLA [2].

Here, we demonstrated a fully integrated scheme for all-optical CLUs-PLA with SOAs. Based on the PLA chip, all four minterms (i.e., CLUs) for two input signals at 40 Gb/s have been demonstrated successfully, and XNOR and XOR were further realized based on these four minterms. The schematic diagram of the integrated all-optical PLA as shown in Fig. 1(a). This PLA consists of input circuit, CLUs array, and switch array. Input circuit consists of a delay interferometer (DI), which helps to pre-code the input signals by demodulating the input differential phase shift keying (DPSK) signals [3]. CLUs array includes SOA1 and SOA2. They are nonlinear mediums for generating different CLUs using XGM. Switches array consists of SOA3 and SOA4, whose role is to select out appropriate CLUs. The off-chip tunable bandpass filters (TBPFs) are used to extract and optimize the CLUs by adjusting the detuning of the TBPFs. The micrograph of the chip is shown in Fig. 1(b), the FSR of DI is about 40 GHz which is designed to match with the bitrate of input signals. The SOAs with long cavity are 1650 μm in length, which are optimized to enhance the nonlinear effect by increasing the cavity length. The SOAs with short cavity are 200 μm in length, which are operating on linear regime. The temporal waveforms of the full set of CLUs, XOR, and XNOR are illustrated in Fig. 1(c). These logic sequences are correct with clear data streams, and the logic levels of the results can be clearly identified.

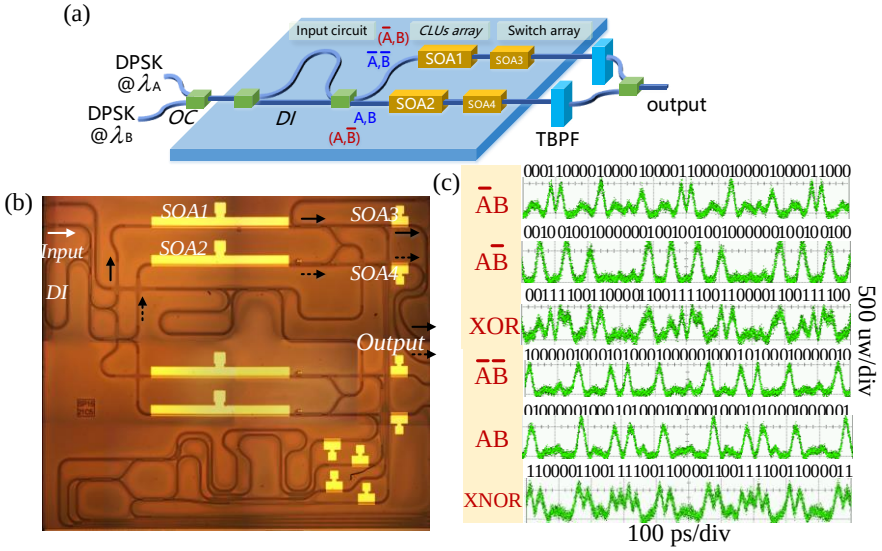

Fig. 1 (a) Schematic diagram of the integrated optical PLA. (b) Micrograph of the integrated all-optical PLA based on SOA. (c) Measured temporal waveforms of the output logic functions.

References

[1]. A. E. Willner, S. Khaleghi, M. R. Chitgarha, O. F. Yilmaz, "All-optical signal processing," J. Lightwave Technol. 32, 660-680 (2014).
[2]. Dong W., Hou J., and Zhang X. Investigation on Expanding the Computing Capacity of Optical Programmable Logic Array Based on Canonical Logic Units, Journal of Lightwave Technology, 2018, 36(18): 3949-3958.
[3]. J. Xu, X. Zhang, Y. Zhang, J. Dong, D. Liu, and D. Huang, "Reconfigurable all-optical logic gates for multi-input differential phase-shift keying signals: design and experiments," J. Lightwave Technol. **27**, 5268-5275 (2009).

Strong Chiral Response in the Whole Visible Band

Xiaohu Wu[1,2], **Ceji Fu**[1], **Zhuomin M. Zhang**[2]

1. Peking University, Yiheyuan Road 5, Beijing 100871, China
2. Georgia Institute of Technology, North Avenue, Atlanta 30332, USA

Left and right handed circularly polarized waves interact differently with structures that cannot be superimposed upon their own mirror images, which is known as chirality [1]. Circular dichroism (CD), on the other hand, is an important measurement for the difference, and it is a useful tool in chemical and biological sensor applications [2]. Various designs of structures and materials have been proposed to realize strong CD, given that natural materials have small chirality response. Among them, the twisted multilayer cascaded structures are the largest category. However, most of the proposed chiral structures commonly require sophisticated fabrication process, even though they can be employed to achieve giant chiral response. It is then desirable to design a simple structure with strong chirality. In additions, previous approaches have not so far enabled structures with an efficient chiral response at visible light frequencies. Here we propose to achieve giant chiral response in the whole visible range by combining anisotropic hexagonal boron nitride (hBN) with metallic grating.

The structure proposed in this work is shown in Fig. 1(a), which consists of one hBN slab and one silver grating sandwiched in the middle of two SiO_2 slabs. The optical axis (OA) of the hBN slab is in the x-y plane and it is tilting off the x-axis with an angle of ϕ. The hBN slab can be used to realize polarization conversion between circularly and linearly polarized waves. By adjusting the thickness and the orientation of the OA of the hBN slab, the incident right handed circularly polarized (RCP) wave can be converted into the transverse magnetic (TM) wave, while the incident left handed circularly polarized (LCP) wave can be converted into the transverse electric (TE) wave. The silver grating characterized by period Λ and filling ratio f can be used to achieve selective transmission for TE and TM waves. Such subwavelength metallic grating has been extensively investigated in published papers and the selective transmission for different linearly polarized waves can be understood with the help of the metallic waveguide theory [3]. The low transmission for TE wave is due to the large imaginary part of the propagation constant of the guided TE mode, while the high transmission for TM wave is due to the small imaginary part of the propagation constant of the guided TM mode [3]. Consequently, the RCP wave can pass the whole structure with high transmission, while the LCP wave cannot pass the whole structure. The SiO_2 slab between the hBN slab and the silver grating is used to reduce the interaction between polarization conversion and selective transmission.

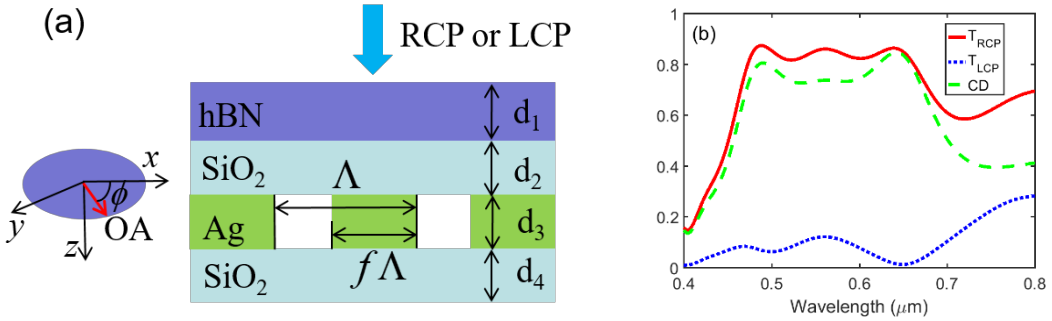

Fig. 1 (a) The schematic of the proposed structure in this work, the optical axis of the hBN slab is in the x-y plane and it tilted off the x-axis with an angle of ϕ. (b) The transmission of the RCP and LCP waves, and the circular dichroism.

When d_1=0.24 μm, d_2=0.2 μm, d_3=0.18 μm, d_4=0.1 μm, Λ=0.1 μm, f=0.5, ϕ=45°, the transmission of RCP and LCP waves are shown in Fig. 1(b). The CD is close to 0.84 at wavelength 0.64 μm, and the chiral response can occur in the whole visible band. By changing the thickness of the hBN slab, one can also achieve high transmission for LCP and low transmission for RCP. Besides, the CD parameter can be tuned by controlling the orientation of the OA of the hBN.

References

[1] Y. H. Cui, L. Kang, S. F. Lan, S. Rodrihues, and W. S. Cai, "Giant chiral optical response from a twisted-arc metamaterial," Nano Lett. 14, 1021-1025 (2014).
[2] J. T. Collins, C. Kuppe, D. C. Hooper, C. Sibilia, M. Centini, and V. K. Valev, "Chirality and chiroptical effects in metal nanostructures: fundamentals and current trends," Adv. Optical Mater. 5, 1700182 (2017).
[3] M. Xu, H. P. Urbach, D. K. G. D. Boer, and H. J. Cornelissen, "Wire-grid diffraction gratings used as polarizing beam splitter for visible light and applied in liquid crystal on silicon," Opt. Express 13(7) 2303-2320 (2005).

Unusual Scaling Laws for Plasmonic Nanolasers beyond the Diffraction Limit

Suo Wang[1], Xing-Yuan Wang[1], Bo Li[1], Hua-Zhou Chen[1], Yi-Lun Wang[1], Lun Dai [1,2], Rupert F. Oulton[3], Ren-Min Ma[1,2]

[1] State Key Lab for Mesoscopic Physics and School of Physics, Peking University, Beijing 100871, China.

[2] Collaborative Innovation Center of Quantum Matter, Beijing 100871, China

[3] The Blackett Laboratory, Department of Physics, Imperial College London, London SW7 2AZ, UK.

ABSTRACT:

Plasmonic nanolasers are a new class of amplifiers that generate coherent light well below the diffraction barrier bringing fundamentally new capabilities to biochemical sensing, superresolution imaging, and on-chip optical communication. However, a debate about whether metals can enhance the performance of lasers has persisted due to the unavoidable fact that metallic absorption intrinsically scales with field confinement. Here, we report plasmonic nanolasers with extremely low thresholds on the order of 10 kW cm^{-2} at room temperature, which are comparable to those found in modern laser diodes. More importantly, we find unusual scaling laws allowing plasmonic lasers to be more compact and faster with lower threshold and power consumption than photonic lasers when the cavity size approaches or surpasses the diffraction limit. This clarifies the long-standing debate over the viability of metal confinement and feedback strategies in laser technology and identifies situations where plasmonic lasers can have clear practical advantage.

REFERENCES:

[1] Suo Wang, Xing-Yuan Wang, Bo Li, Hua-Zhou Chen, Yi-Lun Wang, Lun Dai, Rupert F. Oulton, Ren-Min Ma. Unusual Scaling Laws for Plasmonic Nanolasers beyond the Diffraction Limit. *Nature Communications* 8: 1889 (2017)

Evolution of orbital angular momentum in a soft quasi-periodic structure with topological defects

Wang Zhang[1] , Jie Tang[1] , Peng Chen[1], Guo-xin Cui[1], Yang Ming[2], Wei Hu[1] , and Yan-qing Lu[1]

1. National Laboratory of Solid State Microstructures, College of Engineering and Applied Sciences, Nanjing University, Nanjing 210093, China

2. School of Physics and Electronic Engineering, Changshu Institute of Technology, Suzhou 215000, China

Many advances have been made in our understanding of the mechanisms of interaction for optical singularities with topologically modulated structures, both in linear [1] and nonlinear systems [2]. However, all of the studies to date have been limited to periodic structures. The evolution of orbital angular momentum (OAM) in quasi-periodic structures (QPS) with topological defects remain unknown. Compared to ordinary periodic structures, QPS are deterministic disordered structures with long-range order; they can be recognized as the intermediate state between periodic structures and completely disordered structures. The transition from periodic structure to quasi-periodic structure undergoes the breaking of translational symmetry. This means that the conversation law of OAM must inevitably change during the transition according to Noether's theorem; it is important to recognize and understand the effect of translational symmetry on diffraction characteristics. In addition, QPS have high-dimensional complexity, which may allow for OAM manipulation with multiple degrees of freedom. Therefore, there is a need to study the mechanism of the interaction between optical singularities and topologically modulated QPS, both in terms of physical meaning and practical application.

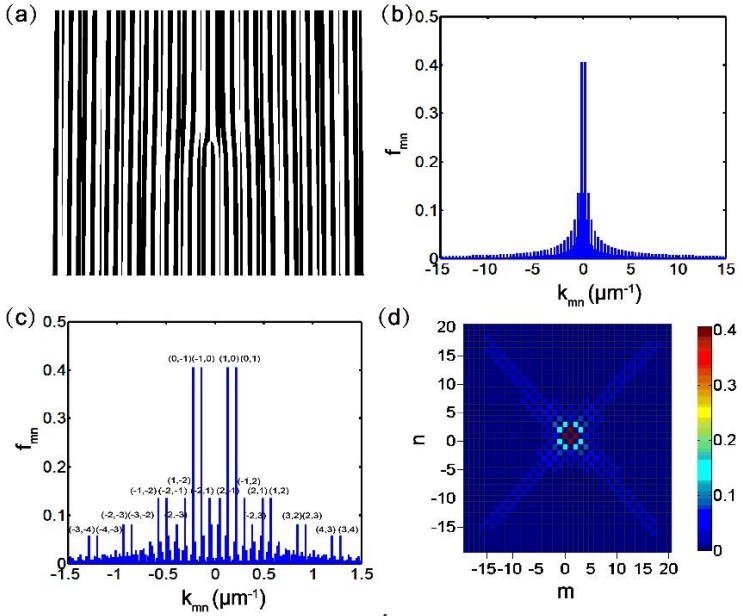

Fig. 1 Structure and Fourier spectra for QPS with $\tau = (1+\sqrt{5})/2$ and l_1 =l_2 =1. (a) Structure of the QPS. (b) Self-similar Fourier spectrum of QPS for $\max(k_{mn}) = 15\mu m^{-1}$. (c) Fourier spectrum of the low-order diffraction part, with some diffraction orders labeled. (d) Two-dimensional distribution of the Fourier spectrum; the magnitude of the Fourier coefficient is represented by a color bar.

The proposed QPS with $\tau = (1+\sqrt{5})/2$ and l_1 =l_2 =1 is shown in Fig. 1(a). The analytical expression of the corresponding Fourier spectrum is derived, which reflects the combined effects of topological structure and quasi-translational symmetry. Light-matter interaction therein brings unusual diffraction characteristics with exotic evolution of orbital angular momentum (OAM). Long-range correlation of QPS resulted in multi-fractal and pairwise distribution of optical singularities. A general conversation law of OAM was revealed. A liquid crystal photopatterning QPS is fabricated to demonstrate the above characteristics. Dynamic reconfigurable manipulation of optical singularities was achieved. Our approach offers the opportunity to manipulate OAM with multiple degrees of freedom, which has promising applications in multi-channel quantum information processing and high-dimensional quantum state generation.

References

[1] C. Peng et al., "Digitalizing Self-Assembled Chiral Superstructures for Optical Vortex Processing", *Advanced Materials* **30**, 1705865 (2018).

[2] N. V. Bloch, K. Shemer, A. Shapira, R. Shiloh, I. Juwiler, and A. Arie, "Twisting light by nonlinear photonic crystals," Phys. Rev. Lett. 108, 233902 (2012).

High nonlinear light-field-driven photoemission from carbon nanotubes

Chi Li[1†], Ke Chen[1†], Mengxue Guan[2], Xiaowei Wang[3], Xu Zhou[4], Feng Zhai[5], Jiayu Dai[3], Zhenjun Li[1], Zhipei Sun[6], Sheng Meng[2*], Kaihui Liu[4*] Qing Dai[1*]

[1]Division of Nanophotonics, CAS Center for Excellence in Nanoscience, National Center for Nanoscience and Technology, Beijing 100190, China.
[2]Beijing National Laboratory for Condensed Matter Physics and Institute of Physics, Chinese Academy of Science, Beijing, 100190, China
[3]Department of Physics, College of Science, National University of Defense Technology, Changsha 410073, China
[4]School of Physics, Academy for Advanced Interdisciplinary Studies, Collaborative Innovation Center of Quantum Matter, Peking University, Beijing 100871, China.
[5]Department of Physics, Zhejiang Normal University, Jinhua 321004, China.
[6]Department of Electronics and Nanoengineering, Aalto University, Tietotie 3, FI-02150 Espoo

*Correspondence: daiq@nanoctr.cn (Q.D.), khliu@pku.edu.cn (K.L.), smeng@iphy.ac.cn (S.M.).
†These authors contributed equally to this work.

Driving electron motion efficiently using a strong electric field of light on the attosecond (10^{-18} seconds) timescale (i.e. light-field-driven effect), lies at the heart of lightwave electronics[1]. Light-field-driven photoemission has been demonstrated in various nanostructures, which has great potential application in attosecond control and measurements. However, its practical application is hampered by its limited modulation efficiency, as the reported dependency of photoemission current on light-field strength followed power-functions with low power[2] less than 2. In this work, a record high-power (up to 40) light-field-driven photoemission is achieved by shining strong laser pluses on carbon nanotubes, as shown in Fig. 1(a). The total photoemission current shows strong dependency on the carrier-envelope phase (CEP) of the pulses and gained a modulation depth up to 95% as shown in Fig. 1(b), twice higher than conventional metal nanotips[3]. Time-dependent density functional calculations reveal that the high-power photoemission originates from quantized electronic states in the carbon nanotubes' valence band and the emission power can be further improved by tuning its bandgap. Our results provide a new design philosophy for ultra sensitive lightwave electronics with an advanced temporal precision by utilizing tunable quantized electronic states in nanomaterials.

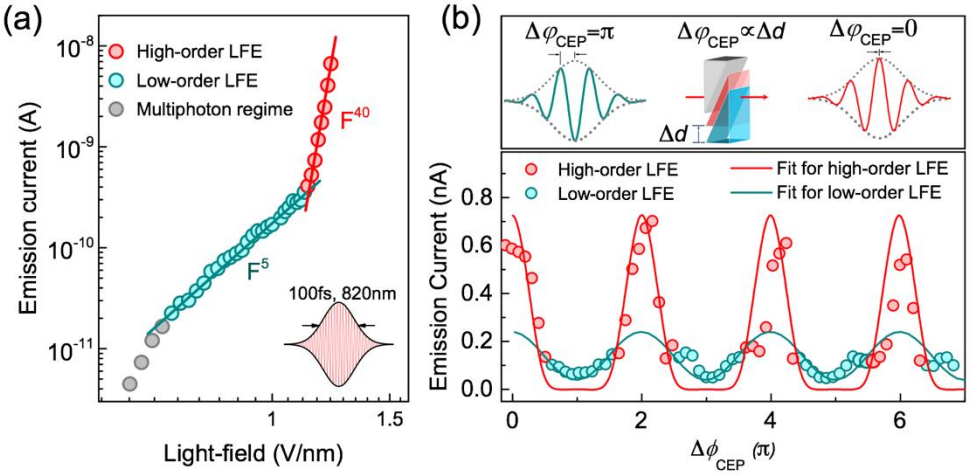

Figure 2 | Light-field and CEP dependent photoemission current. (a) Experimentally obtained log-log plot of light field (F) dependent total photoemission current for CNT emitter, driven by 100 fs laser pulses with a central wavelength of 820 nm. Three linear behaviors are observed, as shown by the different colors: grey, multi-photon photoemission regime; blue, low-power LFE, red, high-power LFE. (b) Upper panel: 7 fs laser pulses at a central wavelength of 800 nm. The CEP is tuned by two opposite glass wedges. Lower panel: Effect of CEP variation on photoemission current. Shown are pronounced periodical variation in the emission current for 6π, with sensitive CEP modulation up to 95%, evidenced light field driven regime.

Example References

[1] Goulielmakis, E. et al. Attosecond control and measurement: Lightwave electronics. Science **317**, 769-775 (2007).
[2] Putnam, W. P., Hobbs, R. G., Keathley, P. D., Berggren, K. K. & Kartner, F. X. Optical-field-controlled photoemission from plasmonic nanoparticles. Nat. Phys. **13**, 335-339 (2017).
[3] Piglosiewicz, B. et al. Carrier-envelope phase effects on the strong-field photoemission of electrons from metallic nanostructures. Nat Photonics **8**, 38-43 (2014).

Au-areoles Arrayed Microchip for Multiple Trace SERS Detection

Huizeng Li[1,2], Qiang Yang[1,2], Mingzhu Li[1], Yanlin Song[1]

1. Institute of Chemistry Chinese Academy of Sciences, Beijing 100190, China
2. University of Chinese Academy of Sciences, Beijing 100094, China

Surface enhanced Raman scattering (SERS) provides an approach for the label-free and miniaturized detection of the trace amount of analyte molecules[1-5]. A SERS microchip of Au-areoles array, mimicking the areole on the cactus, is facilely and controllably prepared through selectively electrochemical deposition on patterned superhydrophilic-superhydrophobic substrates. The Au-areoles are full of SERS hot-spots thanks to the large amounts of sharp edges, tips, and coupled branches. Meanwhile, the superhydrophilic sites on the superhydrophobic substrate can collect the target molecules into those hot-spots. The combination of the SERS enhancement of the nanostructured-Au and the collective effect of the superhydrophilic-superhydrophobic pattern endows the microchip with sample-effective, ultrasensitive, and efficient Raman detection capabilities, which are demonstrated by integrated detection of femtomol R6G and diverse bio-analytes. The chip also can be used for mutually independent multi-sample detection without interference.

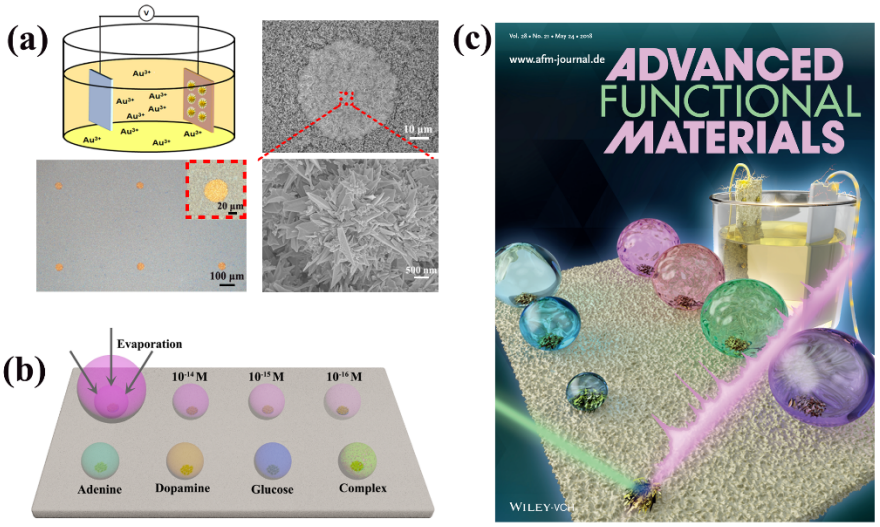

Fig. 1 (a) Schematic illustration of the selectively electrochemical deposition process on the wettability patterned substrate and the morphology/microstructure characterization of the Au-areoles. (b) Concentration effect of the analyte solution on the Au-areoles array for multiple detection. (c) Cover feature to highlight the preparation process and trace Raman detection based on a wettability regulation strategy.

References

[1] C. Ciraci, R. T. Hill, J. J. Mock, Y. Urzhumov, A. I. Fernandez-Dominguez, S. A. Maier, J. B. Pendry, A. Chilkoti and D. R. Smith, *Science*, **2012**, *337*, 1072-1074.

[2] D.-K. Lim, K.-S. Jeon, H. M. Kim, J.-M. Nam and Y. D. Suh, *Nat. Mater.*, **2010**, *9*, 60-67.

[3] S. Schlucker, *Angew. Chem. Int. Ed.*, **2014**, *53*, 4756-4795.

[4] S. Yang, X. Dai, B. B. Stogin and T.-S. Wong, P. *Natl. Acad. Sci.*, USA, **2016**, *113*, 268-273.

[5] H. Li, Q. Yang, J. Hou, Y. Li, M. Li, Y. Song, *Adv. Funct. Mater.*, 2018, 1800448.

Full-parameter Omnidirectional Thermal Meta-devices of Anisotropic Geometry

Tiancheng Han
School of Physical Science and Technology, Southwest University, Chongqing 400715, China
E-mail: tchan123@swu.edu.cn

Inspired by the pioneering theoretical works of transformation optics (TO) [1] and scattering cancelling technology [2], a plethora of unprecedented devices, especially invisibility cloaks, have been successfully demonstrated at various frequencies. The concept of invisible cloaking has attracted intensive research in various communities, e.g., optics, acoustics, and thermotics [3,4]. A truly invisibility cloak should have full-parameters instead of reduced parameters, and should be omnidirectional rather than unidirectional. However, the above two characteristics are often difficult to achieve simultaneously due to the extreme parameters (which are inhomogeneous, anisotropic, and singular). In 2014, we proposed and experimentally demonstrated a bilayer thermal cloak that is derived directly from the thermal conduction equation and is composed of only two layers of bulk materials [5]. Based on the bilayer cinfiguration, many interesting thermal devices are demonstrated, e.g., invisible sensor [6] and thermal expand [7]. However, the previously reported thermal meta-devices are limited to centrosymmetric geometry, which suffers from a limitation in practical applications. A long-held captivation is that transformation-optic metamaterials of anisotropic or non-centrosymmetric geometry (e.g., ellipsoids) commonly come along with parameter approximation or directional functions [8]. Recently, we theoretically and experimentally build a platform for the design of full-parameter omnidirectional meta-devices of anisotropic geometry [9]. The synthetic methodology could be used on objects of irregular shapes fabricated from homogeneous and isotropic bulk natural materials. More importantly, it no longer suffers from imperfect performance or the restriction of only working at one direction. We experimentally validate three proof-of-concept experiments going much beyond just cloaks: a cloaked sensor, invisibility cloak, and a super expander. The robustness of the proposed concept has also been demonstrated in time-dependent cases. Our paradigm is rigorous, exact, and robust, which may open a new avenue to manipulate the Laplacian fields and wave-dynamic fields in ways inconceivable.

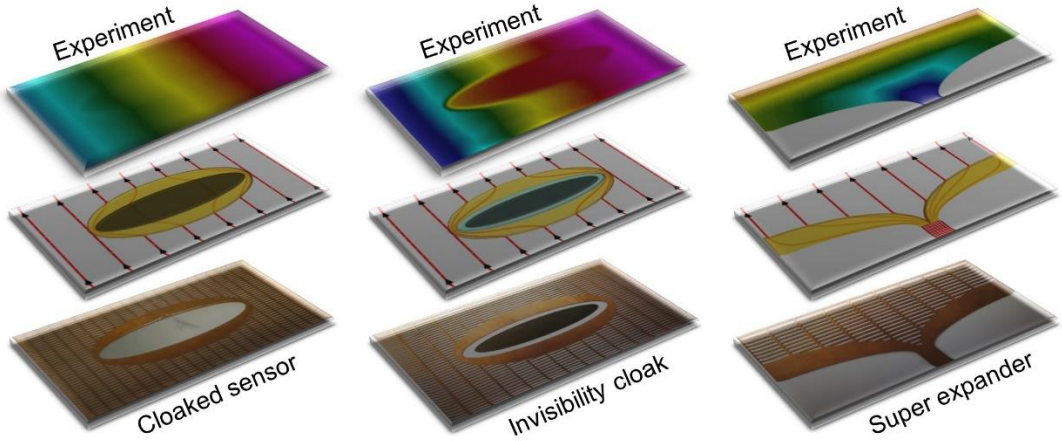

Fig. 1 Function, realization, and experiment of the three proposed thermal meta-devices with anisotropic geometry.

References

[1] J. B. Pendry, D. Schurig, and D. R. Smith, "Controlling electromagnetic fields," Science **312**, 1780-1782 (2006).
[2] A. Alù and N. Engheta, "Achieving transparency with plasmonic and metamaterial coatings," Phys. Rev. E **72**, 016623 (2005).
[3] S. Narayana and Y. Sato, "Heat flux manipulation with engineered thermal materials," Phys. Rev. Lett. **108**, 214303 (2012).
[4] R. Schittny, M. Kadic, S. Guenneau, and M. Wegener, "Experiments on transformation thermodynamics: Molding the flow of heat," Phys. Rev. Lett. **110**, 195901 (2013).
[5] T. Han, X. Bai, D. Gao, J.T.L. Thong, B. Li, and C.-W. Qiu, "Experimental demonstration of a bilayer thermal cloak," Phys. Rev. Lett. **112**, 054302 (2014).
[6] T. Yang, X. Bai, D. Gao, L.Z. Wu, B.W. Li, J.T.L. Thong, C.-W. Qiu, "Invisible sensor: Simultaneous sensing and camouflaging in multiphysical fields," Adv. Mater. **27**, 7752-7758 (2015).
[7] J. Huang, X. Shen, C. Jiang, Z. Wu, and J. Huang, "Thermal expander," Physica B **518**, 56-60 (2017).
[8] X. Yuan, G. Lin, and Y. Wang, "Design of elliptic cylindrical thermal cloak with layered structure," Int. J. Mod. Phys. B **31**, 1650244 (2017).
[9] T. Han, P. Yang, Y. Li, D. Lei, B. Li, K. Hippalgaonkar, and C.-W. Qiu, "Full-parameter omnidirectional thermal meta-devices of anisotropic geometry," Adv. Mater., accepted (2018).

Hybrid Silicon and Lithium Niobate Mach–Zehnder Modulators for 100 Gbit/s and Beyond

Mingbo He[1], **Mengyue Xu**[1], **Jian Jian**[1], **Liu Liu**[2] and **Xinlun Cai**[1]

1. State Key Laboratory of Optoelectronic Materials and Technologies and School of Physics and Engineering, Sun Yat-sen University, Guangzhou 510275, China.

2. State Key Laboratory of Optoelectronic Materials and Technologies and School of Physics and Engineering, Sun Yat-sen University, Guangzhou 510275, China.

Optical modulators are at the heart of optical communication links. Ideally, they should feature low insertion loss, low drive voltage, large modulation bandwidth, high linearity, compact footprint and low manufacturing cost. Unfortunately, these criteria have only been achieved on separate occasions. Based on a Silicon and Lithium Niobate hybrid integration platform, we demonstrate Mach–Zehnder modulators that simultaneously fulfill these criteria. The presented device exhibits an insertion-loss of 2.5 dB, half-wave voltage of less than 4 V, electro-optic bandwidth of at least 70 GHz, high linearity and modulation rates up to 112 Gbit/s. The realization of a high-performance modulator is due to seamlessly integration of high-contrast waveguide based on Lithium Niobate - the most mature modulator material - with compact, low-loss silicon circuits. The hybrid platform demonstrated here allows "best-in-breed" active and passive components to be combined and opens up new avenues for future high-speed, energy efficient and cost-effective communication networks.

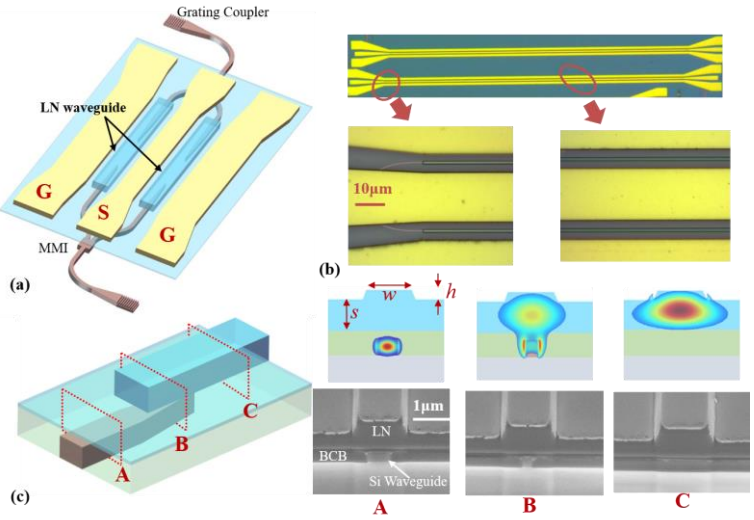

Fig. 1 Structure of the hybrid Si/LN MZM. (a) Schematic of the structure of the whole circuit. (b) Microscope image of the fabricated devices. (c) Schematic of the vertical adiabatic coupler, scanning electron microscopy images of the cross-sections of the VAC at different positions, and calculated mode distribution associated with the cross-sections.

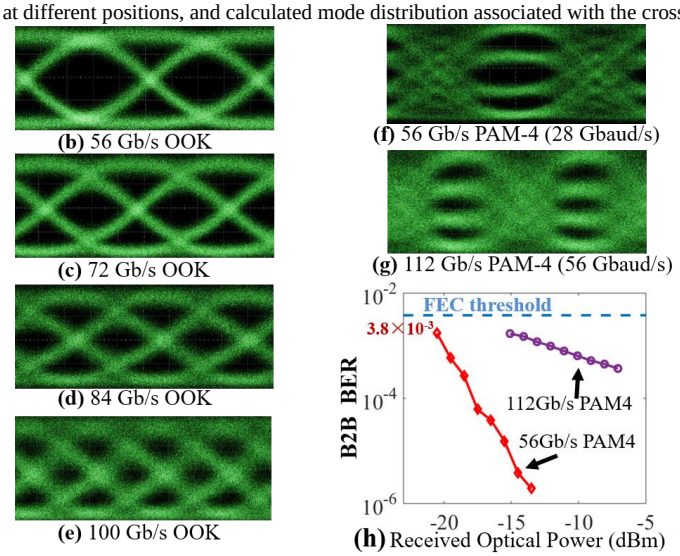

Fig. 2 (b-e) Optical eye diagrams at data rates of 56 GBaud/s, 72 GBaud/s, 84 GBaud/s, and 100 GBaud/s. The dynamic extinction ratios are 11.8 dB, 6.0 dB, 5.5 dB and 5.0 dB, respectively. (f-g) Measured PAM-4 modulation optical eye diagrams at 28 GBaud/s and 56 GBaud/s. (h) Measured curve of BER versus the received optical power for 28 GBaud/s (56 Gb/s) and 56 GBaud/s (112 Gb/s) PAM-4 signal.

High-Density Waveguide Integration and Optical Phased Arrays

Le-Meng Leng[1,2], **Yue Shao**[1,2],**Pei-Yan Zhao**[1,2], **Guang-Fan Tao**[1,2],and **Wei Jiang**[1,2]

1. National Laboratory of Solid State Microstructures, Nanjing University, Nanjing 210093, China

2. College of Engineering and Applied Sciences, Nanjing University, Nanjing 210093, China

Modern optics systems face major challenges as complexity and integration level increase at a fast pace. Integrated photonics has offered a chip-scale platform that can consolidate a large number of devices into a small chip, thereby significantly reducing the system footprint and complexity. However, as the number of on-chip elements increases, integration density limitation is becoming a major bottleneck for further development of integrated photonic systems. Particularly, in many on-chip photonic applications such as space/wavelength division multiplexing, optical interconnects, and optical phased array, waveguides are used profusely as a fundamental bulk for guiding optics signal. High-density waveguide integration is highly desirable, but this is fundamentally limited by strong crosstalk at high density.

Recently, low-crosstalk high-density waveguide integration has been demonstrated by introducing a waveguide superlattice [1]. A waveguide superlattice where the waveguide widths repeat periodically every *n* waveguides is illustrated in Fig. 1(a). The pitch of such a waveguide array can reach half-wavelength, yet the crosstalk remains low. If this structure is considered by the perturbation theory that treats the surrounding waveguides as perturbation to any given waveguide, the perturbation potential will corresponds to a magnitude of dielectric constant. Such a large magnitude will disqualify many approximate theories in modeling such a system, particularly when we are trying to modeling low crosstalk around -20dB, which represents very weak signals. A rigorous coupled mode theory has been developed to model such a system [1,2]. Sidewall roughness plays an important role for understanding the crosstalk in the system as well, as modeled in Fig. 1(c).

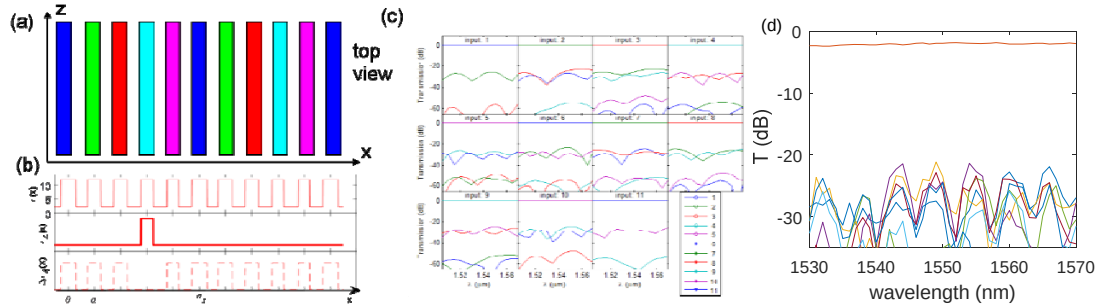

Fig. 1 (a) Schematic of waveguide superlattice (n=5). (b) Dielectric constant profile for the superlattice (top), an isolated waveguide (middle), and the perturbation potential (bottom). (c) Transmission/crosstalk spectra with a random roughness configuration. (d) preliminary experimental results: representative normalized transmission/crosstalk spectra of a recently made waveguide superlattice.

We have recently explored better fabrication routes for making waveguide superlattices and demonstrated the low crosstalk in a SC5 superlattice array as shown in Fig. 1(d). The loss is also lower (propagation loss 3~6dB/cm, coupling loss <2dB per waveguide endface).

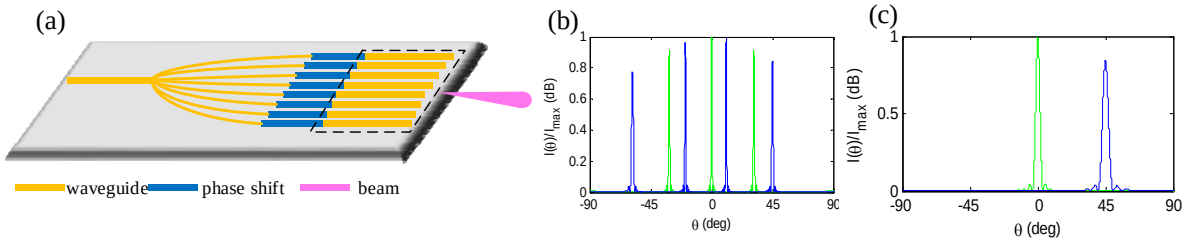

Fig. 2 Optical phased array. (a) schematic; (b) Simulated beam characteristics for a conventional OPA with pitch a~2λ. Green line: intended 0-deg beam with a few secondary beams (called grating lobes); Blue line: 45-deg beam with grating lobes; (c) waveguide superlattice OPA simulation, a=λ/2. Green line : 0-deg beam, Blue line: 45-deg beam. No grating lobes show up.

One of the important applications for such a high-density waveguide superlattice is half-wavelength pitch optical phased array. Traditional optical phased arrays have large pitches of a few wavelengths, which leads to small scanning range and high-level secondary beams as shown in Fig. 2(b). With half-wavelength (λ/2) pitch, low crosstalk waveguide superlattice, one can potentially achieve a λ/2-pitch OPA free of all these issues as shown in Fig. 2(c). As such, it could unlock the potential of OPAs in many applications such as LIDARs for autonomous vehicles and wireless optical communications.

References

[1] Weiwei Song, Robert Gatdula, Siamak Abbaslou, Ming Lu, Aaron Stein, Warren Y-C Lai, J. Provine, R. Fabian W. Pease, Demetrios N. Christodoulides & Wei Jiang, "High-density waveguide superlattices with low crosstalk," *Nature Communications* **6**, 7027 (2015).

[2] Nan Yang, Huashan Yang, Hengrun Hu, Rui Zhu, Shining Chen, Hongguo Zhang, and Wei Jiang, *Photonics Research* **4**, 233-239 (2016).

THz Enhanced EIT resonance based on the coupled electrical dropping effect with undulating meta-surface

Lan Wang[1], **Yaxin Zhang**[1], **Shixiong Liang**[2]

1. University of Electronic Science and Technology of China, Chengdu 610054, China
2. Hebei Semiconductor Research Institute, Shijiazhuangt 050051, China

Electromagnetically induced transparency (EIT) has attracted a lot of research interest in recent years. However, very limited attempts have been made to mimic the EIT phenomena by varying the lateral distance between the resonatorss or breaking the structural symmetry[1-2]. In this letter, a significant amplitude modulation of EIT resonance is demonstrated by undulating meta-surface. A schematic of the proposed EIT is shown in Fig.1(a). The metamaterial unit cell consists of a two-gap outer split ring resonator (SRR) and an inner ring resonator which is thicker than the outer ring.

The undulating meta-surface design shown in Fig.1(a) has been fabricated with photolithography and metallization process steps. We designed 5 sets of samples with inner ring thickness *h* of 0.2um,1um, 2um, 3um, 4um, respectively. In the experiments, a normal incident THz wave is perpendicularly projected onto the surface of the samples with the polarization of the electric fields parallel to the split gaps. Fig.1(b) is experimental transmission spectrum, which shows the EIT transmission peak value gradually increase with h increasing from 0.2um to 4um.

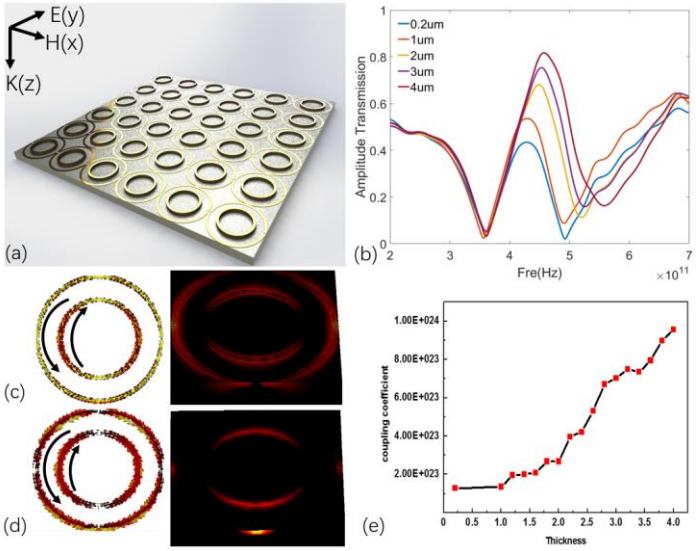

Fig. 1 (a) The schematic of the undulating meta-surface structure; (b) The experimental results with the different thickness of inner ring; (c) and (d) are simulated surface current distribution and electric field distribution with *h*=0.2um and *h*=4um at 0.47 THz; (e) Coupling coefficient of the EIT with varying the value of *h*.

In order to gain insight into the mechanism of the enhanced EIT, simulation based on the finite element method (FEM) are performed by using the frequency-domain solver in CST Microwave Studio for the unit-cell structure. As shown in Fig.1(c) and (d), it is the destructive interference between the two surface currents on the resonators that leads to EIT. However, when the thickness of inner ring *h* increases, the electric field on the ring would drop onto the SRR resulting in a stronger coupling electic field. Thus, there is an enhanced EIT.

We adopt a widely used coupled Lorentz model to reveal the coupling characteristics due to variations of the thickness of inner ring in further detail. The transmission equation can be obtained:

$$t_1(\omega) = \left| 4n_{active}\, e^{i\omega dn_{active}/c} / ((n_{active}+1)(n_{active}+n_{sap}) + (1-n_{active})(n_{active}-n_{sap})\, e^{i2\omega dn_{active}/c}) \right|$$

Therefore, the fitted transmission of different thickness and the relationship between the thickness d and the coupling coefficient κ can be obtained. It can be seen that the coupling coefficient increases with the thickness, indicating that as the thickness of the inner ring increases, the coupling between the two resonators increases, as shown in Fig.1(e).

References

[1]. Gu, J., et al. "Active control of electromagnetically induced transparency analogue in terahertz metamaterials." *Nature Communications*3.4(2012):1151.
[2]. Xu, Q., et al. "Experimental realization of an on-chip all-optical analogue to electromagnetically induced transparency." *Physical Review Letters*96.12(2006):123901.

Hard Evidence Revealing the Cause of Thermally-Induced Luminescence Enhancement in Upconversion Nanocrystals

Yanqing Hu

School of Materials Science and Engineering, Southeast University, Nanjing 211189, People's Republic of China

Luminescent bulk materials generally suffer from the thermal quenching, while upconversion nanocrystals (UCNCs) have recently been found to show the dramatic emission increase at elevated temperatures. A deep understanding of this quite different light-heat interaction at the nanoscale is important both scientifically and technologically. Herein, temperature-dependent upconversion luminescence (UCL) is investigated for UCNCs with various sizes, activators (Ho^{3+}, Tm^{3+}, Er^{3+}) and core/shell structures. An anomalous UCL enhancement with increasing temperature is demonstrated for UCNCs with larger surface/volume ratios (SVRs). Moreover, this heat-favorable UCL shows a pronounced dependence on the SVRs, activators, emitting levels and measuring environments. Substantial evidence confirms that the thermally-induced UCL increase is primarily due to the temperature-dependent quenching effect of surface-adsorbed water molecules (Fig. 1), instead of the previously proposed surface phonon-assisted mechanism[1]. Temperature-dependent spectral investigations also show that the energy-loss process of Yb^{3+}-sensitized UCNCs is largely due to the deactivation of Yb^{3+} ions caused by surface quenchers, rather than the direct quenching to activators. UCNCs with an active-shell (doped with Yb^{3+}) exhibit the similar thermally-induced UCL increase, due to energy migration to the surface over the Yb-Yb internet. It implies that active-core/active-shell UCNCs still are susceptible to surface quenchers and would be unsuitable for specific applications in aqueous environments.

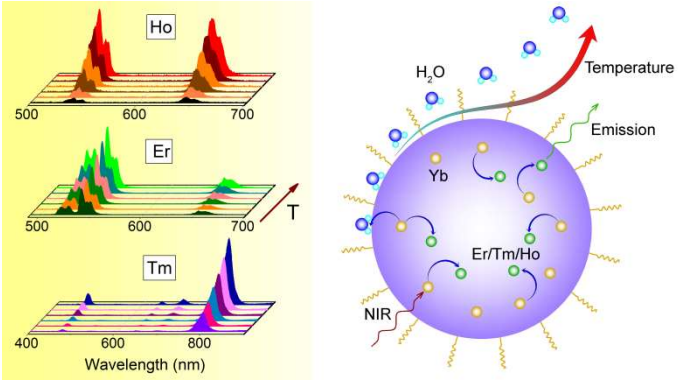

Fig. 1 The thermally-induced emission increase of solid-state upconversion nanocrystals results from a gradually-attenuated quenching effect of surface-adsorbed water molecules at elevated temperature.

[1] J. Zhou, S. Wen, J. Liao, C. Clarke, S. A. Tawfik, W. Ren, C. Mi, F. Wang, D. Jin, Nat. Photonics 2018, 12, 154–158.

Octave spanning supercontinuum generation in air cladding tantalum pentoxide based optical waveguide

Xin-Yu Liao[1], Chung-Lun Wu[1], Chao-Wei Liu[1], Pin-Shuo Hwang[1], Chin-Yu Liu[1], and Chao-Kuei Lee[1,2,3]

[1] *Department of Photonics, National Sun Yat-sen University, Kaohsiung, Taiwan*
[2.] *Department of Physics, National Sun Yat-sen University, Kaohsiung, Taiwan*
[3.] *Research Center for Applied Sciences, Academia Sinica, Taipei, Taiwan*

Tantalum pentoxide (Ta_2O_5) is a large bandgap material, which shows ultralow linear and nolinear absorption loss in visible to infrared region. Such optical property enables it to realize low loss optical waveguide platform [1]. Recently, Ta_2O_5 has been widely utilized to demonstrate nonlinear waveguide applications due to its huge optical nonlinearity. For instance, the four-wave-mixing, third-harmonic generation and self-phase modulation have been realized in Ta_2O_5 waveguide structures [2-4]. However, seldom work reports the supercontinuum generation in Ta_2O_5, especially in the visible region.

In this work, anomalous dispersion Ta2O5 based waveguide was designed for super-continuum generation(SCG) due to its nature of two photon absorption free and high optical nonlinearity. The Ta_2O_5 film is deposited by using RF sputtering technique. After deposition, the e-beam lithography and reactive ion etching are utilized to fabricate the waveguide structure. A 5mm length air cladding Ta2O5 waveguide with dimension of 800nm x 700nm was fabricated for fulfilling anomalous dispersion requirement which is crucial for SCG, as shown in Fig. 1. Fig. 2 shows the spectrum of SCG with various power. By injecting a 100-fs pulse laser at central wavelength of 1-um, the output spectrum of Ta_2O_5 waveguide shows an octave spanning (at -30dB). For excitation laser wavelength of 1056nm, with excitation peak power of around 400W, the 1.5 octave spanning was demonstrated. In addition, the SCG from various dimension Ta_2O_5 waveguide was investigated and discussed. Our primary result shows that Ta_2O_5 has great potential in developing visible to infrared broadband light source, which can be applied in optical coherence tomography and frequency metrology.

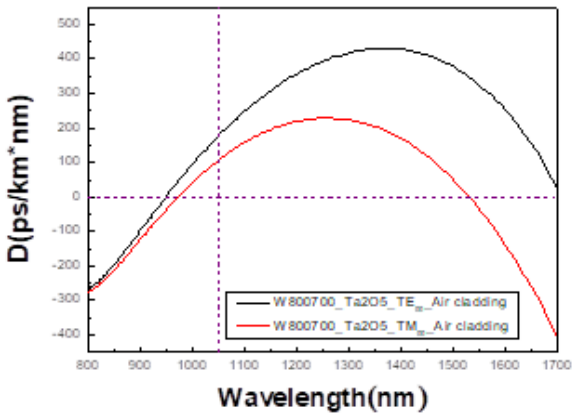

Fig. 1 Dispersion and wavelength relation chart

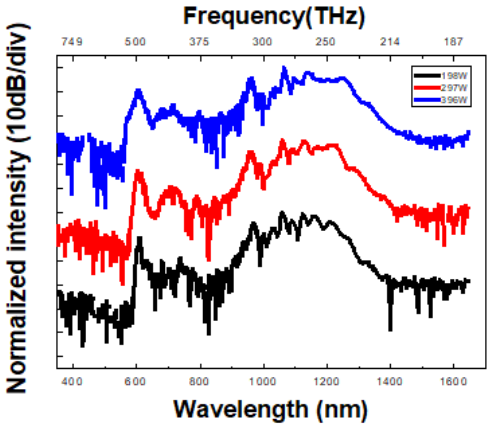

Fig. 2 SCG spectrum of air cladding Ta2O5 waveguide under various excitation power

References

[1] M. Belt, M. L. Davenport, J. E. Bowers, and D. J. Blumenthal, Optica 4, 532 (2017).
[2] C.-Y. Tai, J. Wilkinson, N. Perney, M. Netti, F. Cattaneo, C. Finlayson, and J. Baumberg, Opt. Express 12, 5110 (2004).
[3] R. Y. Chen, M. D. B. Charlton, and P. G. Lagoudakis, Opt. Lett. 34, 1135 (2009).
[4] C.-L Wu, J.-Y Huang, D.-H. Ou, T.-W. Liao, Y.-J. Chiu, M.-H. Shih, Y.-Y. Lin, A.-K. Chu, and C.-K. Lee, Opt. Lett. 42, 4804 (2017).

Rabi splitting in photoluminescence of gold nanorod–WS_2 heterostructure

Yinzhu Jiang[1], **Huanjun Chen**[1]

1. State Key Laboratory of Optoelectronic Materials and Technologies, Guangdong Province Key Lab of Display Material and Technology, School of Electronics and Information Technology, Sun Yat-sen University, Guangzhou 510275, China

Abstract Two-dimensional transition metal dichalcogenides (2D TMDs) have been demonstrated as promising candidates for strong light–matter interactions, due to their large exciton binding energy and exciton transition dipole moment. Here we investigated strong coupling between exciton and plasmonic nanocavity in heterostructure consisting of monolayer WS_2 and an individual gold nanorod. Giant Rabi splitting was observed in the photoluminescence (PL) spectrum, which can be evidenced by the anti-crossing behaviour with Rabi splitting strength of 106 meV on the energy diagram.

Strong light–matter coupling systems with large vacuum Rabi splitting are important for quantum information application, such as quantum manipulation, quantum information storage and processing. To achieve strong coupling, two requirements need to be satisfied: large transitional dipole moment and strong mode confinement [1]. Most recently 2D TMDs have attracted enormous interests in studying strong coupling owing to their large exciton transition dipole moment and exciton binding energy [2]. On the other hand, due to their extremely small mode volumes, simple excitation manner, and facilely tunable resonance frequencies, plasmonic nanostructures are prior to the conventional optical cavities in studying strong coupling [2]. Therefore, hybrid system consisted of 2D TMD and plasmonic nanostructure has been demonstrated to be an excellent platform for studying strong coupling [2]. However, mode splitting, which is an experimental manifestation of strong coupling phenomena, obtained by the common experimental technique, dark field (DF) microscopy, may be confused by other effects such as enhanced absorption, plasmonic quenching, and Fano resonances in the weak coupling regime. These subtle effects may show the similar experimental observations, namely split-like line shape or asymmetry of the spectroscopic signal as strong coupling regime but with different physic origins. Alternative method in revealing strong coupling has been demonstrated by utilizing PL spectroscopy, which can directly interpret the strong coupling phenomena and help us deeply understand physic nature of strong coupling [1]. Although a few studies have demonstrated the strong coupling in PL of hybrid system consisted of excitonic organic dyes and individual plasmonic nanostructure [1, 3], research on strong coupling from PL spectrum of hybrid system consisted of 2D TMD and individual plasmonic nanostructure has not been reported yet.

In this study, we numerically investigate the PL of strongly coupled heterostructure consisted of monolayer WS_2 and an individual gold nanorod by using the finite-difference time-domain method (FDTD). An electric dipole, acting as excitonic emitter, is placed in the gap of the gold nanorod and monolayer WS_2. By selecting a typical gold nanorod (aspect ratio ~ 2.4) of plasmon energy in resonance with the exciton emission of monolayer WS_2, a clear mode splitting can be observed in the PL spectrum. In addition, the strength of the splitting strongly depends on the orientations of the dipole. In particular, the strongest splitting can be observed when the orientation direction of the dipole is parallel with the long axis of the gold nanorod. To further ascertain that the heterostructure enter the strong coupling regime, we measure PL spectrum of the heterostructures with gold nanorods of varied aspect ratio. Finally, an anti-crossing behaviour with Rabi splitting strength of 106 meV is observed on the energy diagram, which fulfils the requirement for the strong coupling to occur.

In conclusion, we have studied the strong coupling in PL of gold nanorod–WS_2 heterostructure. We revealed the anti-crossing behaviour with Rabi splitting strength of 106 meV. Our result offer guidelines for investigating strong coupling in PL of hybrid system consisted of 2D TMD and individual plasmonic nanostructure, paving the way of developing novel light-emitting nanophotonic and optoelectronic devices.

Reference

[1] Wersäll M, Cuadra J, Antosiewicz T J, et al. “Observation of mode splitting in photoluminescence of individual plasmonic nanoparticles strongly coupled to molecular excitons,” Nano Lett. 17(1), 551–558 (2017).

[2] Wen J. X, Wang H, Wang W, et al. “Room-temperature strong light–matter interaction with active control in single plasmonic nanorod coupled with two-dimensional atomic crystals,” Nano Lett. 17(8), 4689–4697 (2017).

[3] Melnikau D, Esteban R, Savateeva D, et al. “Rabi splitting in photoluminescence spectra of hybrid system of gold nanorods and J-aggregates,” J. Phys. Chem. Lett. 7(2),354–362 (2016).

Induce Surface Plasmon on Thin Gold Films Using Dimer-Structure Plasmonic Metadevices

Zhixia Xu[1], **Xiao Cui**[2], **Xiaoxing Yin**[1]

1. State key laboratory of millimeter waves, Southeast University, Sipailou Road 2, Nanjing 210096, China
2. Department of Physics, Imperial College London, South Kensington Campus, London SW7 2AZ, UK

Surface plasmon, as electron oscillations, exists widely at the interference between a metal and a dielectric. The rising field has shown varieties of applications in nano-devices [1], molecular sensors [2], and life sciences [3]. Exciting surface plasmon by photons has to meet the momentum matching condition, which usually requires a prism, or a grating, or a defect on the surface [4]. As shown in Fig. 1(a), a method to excite surface plasmon under normal incident light is investigated. In the method, a plasmonic coupling metadevice is placed 80 nm above a thin gold film whose thickness is 50 nm. The dimer-structure metadevice, consisting of pairs of gold elliptical cylinder nanoparticles, is embedded in a fused silica bulk. The system is excited by a normal incident plane wave, which is a Gaussian pulse with 15 fs duration. Induced plasmonic resonances of gold nanoparticles enhance the electromagnetic field around dramatically and further excite surface plasmon on the thin gold film below. As shown in Fig. 1(b), Fourier spectra of time domain electric fields on the up side of the film are calculated under normal incident lights with different polarization angles. Several peaks exist in every curve, which represents different resonant modes, including plasmonic resonances of nanoparticles and surface plasmon resonances of the film. The sharpest resonance represents surface plasmon, and the broader resonances are plasmonic resonances of nanoparticles. With the orthogonally arranged dimer structure, surface plasmon can be induced insensitive of polarization angles.

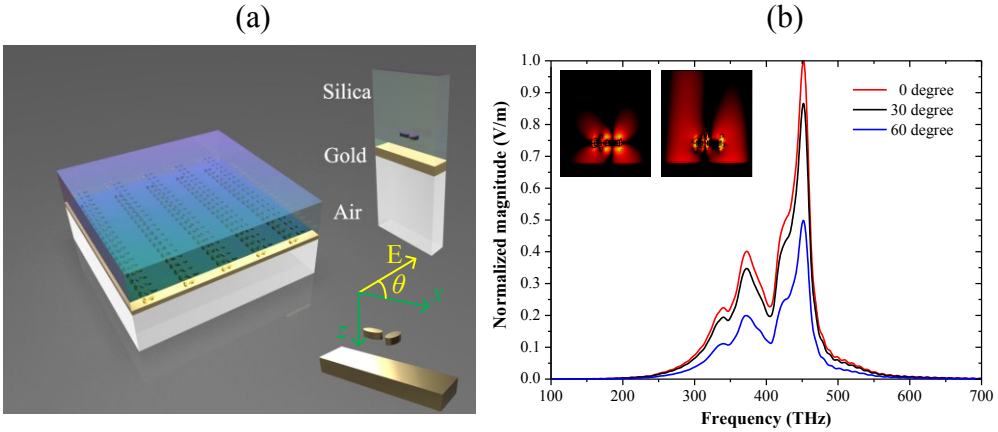

Fig. 1 (a) Schematic of the proposed metadevice where inset pictures show the detailed structure. (b) Fourier spectra of time domain electric fields under incident lights with different polarizations.

This research uses metadevice on one side of the thin metal film to induce surface plasmon, overcoming the momentum mismatch between normal incident light and surface plasmon. Compared to other Silica-Metal-Air sandwich-like systems, such as Otto configuration and Kretschmann configuration, the proposed multi-layer system is insensitive to the polarization of incident light. Moreover, results in the spectra also indicate some important characteristics of resonant modes, such as Q-factors and centre frequencies.

References

[1] M. Chanana, M. A. Correaduarte, and L. M. Lizmarzan, "Insulin‐Coated Gold Nanoparticles: A Plasmonic Device for Studying Metal‐Protein Interactions," Small, **7**, 2650-2660 (2011).
[2] J. Homola, S. S. Yee, and G. Gauglitz, "Surface plasmon resonance sensors: review. Sensors and Actuators B-chemical," **54**, 3-15 (1999).
[3] H. Xin, B. Namgung, and L. P. Lee, "Nanoplasmonic optical antennas for life sciences and medicine," Nat. Rev. Mat., **1** (2018).
[4] S. A. Maier, 1st. ed., *Plasmonics: fundamentals and applications*, (Springer Science & Business Media, 2007).
[5] R. M. Gazoni, M. G. Bellino, M. C. Fuertes, G. Gimenez, G. J. Solerillia, and M. L. Ricci, "Designed nanoparticle–mesoporous multilayer nanocomposites as tunable plasmonic–photonic architectures for electromagnetic field enhancement," J. Mat. Chem. C, **5**, 3445-3455 (2017).

Acknowledgements

This work was supported by National Natural Science Foundation of China (Nos. 61427801, 61771127, U1536123, and U1536124), Scientific Research Foundation of Graduate School of Southeast University (No. YBJJ1814), and Postgraduate Research & Practice Innovation Program of Jiangsu Province (No. KYCX18_0098).

High Extinction Ratio 2×2 Thermo-Optic Switch in Silicon

Qiuyang Jiang[1,2], **Rui Zhu**[1,2],**Guangfan Tao**[1,2], and **Wei Jiang**[1,2]

1. National Laboratory of Solid State Microstructures, Nanjing University, Nanjing 210093, China

2. College of Engineering and Applied Sciences, Nanjing University, Nanjing 210093, China

Silicon photonics has developed rapidly in recent years. As an important type of silicon photonic devices, optical switches [1] are widely used in optical communications, interconnections, quantum photonics, and signal processing. For a normal Mach-Zehnder thermo-optic switch, many of its performance parameters have reached an excellent level. However, the extinction ratios (ERs) of silicon thermo-optic switches are still at a modest level [2], whereas many applications in quantum photonics and signal processing desire high ERs>30dB.

In this work, we design and fabricate a Mach–Zehnder thermo-optic switch on SOI wafer towards the goal of achieving extinction ratios of all paths over 30dB. Through simulation and experiment, we assess the effect of fabrication variability on the extinction ratios of two outputs, and suggests potential solutions.

In the experiment, light from a tunable laser is coupled into one input waveguide, electric signal is applied to the electrode to generate heat to achieve phase shift. We find that at designed operating wavelengths, there are huge differences between extinction ratios of two outputs, with the bar port always having lower ERs (by as much as 20 dB), as shown in Fig. 1(a). To investigate the mechanism behind the huge disparity of ER_{bar} and ER_{cross}, theoretical analysis and simulation are carried out. The theoretical dependence of ERs on the splitting ratios (r_1, r_2) of the two direcitonal couplers (DCs) in a switch are shown in Fig. 1(b),(c). During fabrication, the splitting ratios r_1 and r_2 tend to vary by the similar amount. Interestingly, Fig. 1(c) shows that if r_1 and r_2 vary synchronously, ER_{cross} remains high, but ER_{bar} cannot enjoy such a benefit for r_1=r_2, as shown in Fig. 1(b).

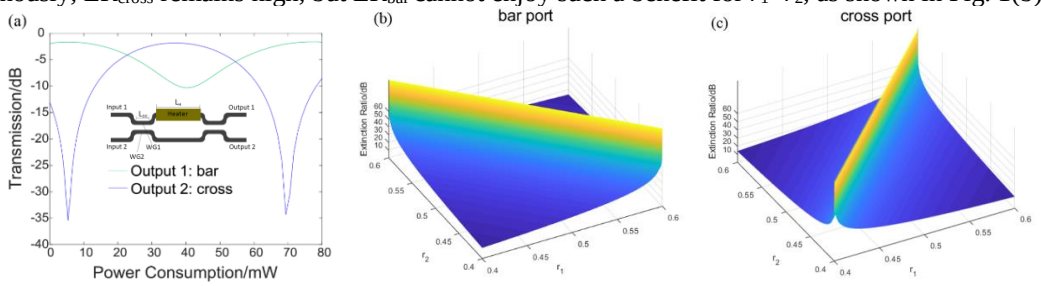

Fig. 1 (a) Measured transmission at 1550nm as a function of heating power, for light injected to Input 1 port; (b) ER simulation for bar port; (c) ER simulation for cross port. r_1 and r_2 are power splitting ratios of the two directional couplers.

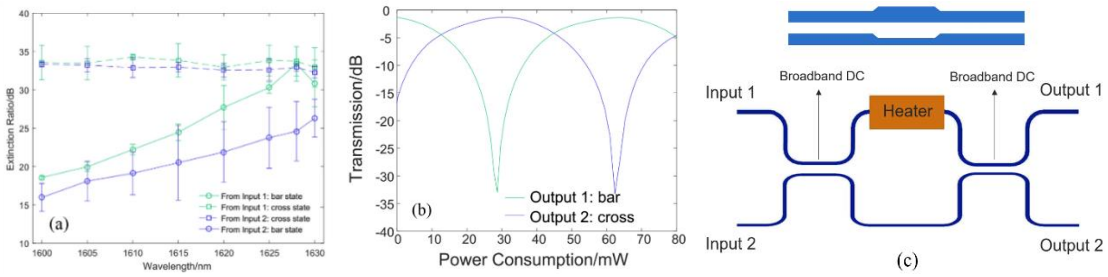

Fig. 2 (a) Variation of the extinction ratios of four paths with wavelength; (b) Measured transmission at 1628nm, light injected to Input 1 port; (c) Schematic drawing of a proposed switch to achieve both high ERs and broadband operation.

Statisticals of the measured extinction ratios of a number of switches fabricated in the same batch are shown in Fig. 2(a). From this figure, we can see always $ER_{bar} < ER_{cross}$. But as the wavelength increases, the difference becomes less. This can be interpretted that r_1 and r_2 approaches the designed value of 0.5 at longer wavelengths, and the wavelength shift may be attributed to fabrication variation [2]. Detailed fabrication variation scenarios for such r_1 and r_2 are simulated and classified in Ref. [2]. At 1628nm, some devices can have ER_{bar} and ER_{cross} both reaching 30dB [Fig.2 (b)]. For some quantum photonics and signal processing applications that require high ER and allow free choice of the working wavelength, the current structure suffices.

In order to reduce the negative effect of wavelength sensitivity, a switch comprising broadband 3dB DCs, as shown in Fig.2 (c), may be used. In combination with proper padding to minimize fabrication variation, this structure may achieve high ER_{bar} and high ER_{cross} over a broad wavelength range with good fabrication tolerance.

References

[1] Xia F., W. M. Green, Y. Vlasov, "High-Throughput Silicon Nanophotonic Deflection Switch for On-Chip Optical Networks," Nature Photonics, 2(4), 1-3(2008).

[2] R. Zhu, X. Zhou, N. Yang, L. Leng and W. Jiang, "Towards High Extinction Ratio in Silicon Thermo-Optic Switches—Unravelling Complexity of Fabrication Variation, " IEEE Photonics Journal 10(4), 1-8 (2018).

Exciting and Shaping the Bloch Surface Wave

Ruxue Wang[1], Douguo Zhang[2], Aimin Wu[1]

[1]*Department of Silicon Optical Integration, Shanghai Institute of Microsystem and information Technology Chinese Academy of Sciences, Shanghai, 200050, China*

[2]*Department of Optics and Optical Engineering, University of Science and Technology of China, Hefei, Anhui, 230026, China*

Bloch surface waves (BSWs) are surface electromagnetic modes which are excited at the interface between a truncated period dielectric multilayer and its surrounding medium [1]. BSWs can be considered as the dielectric analogue of surface plasmon polaritons (SPPs) but with lower losses and longer propagation length because of the lower absorption of dielectrics compared with metals. In this talk, I will present our recent work in this filed. We have demonstrated a diffraction-free BSW that does not diffract after passing through three obstacles [2]. And to overcome the crushing cost of fabrication, we used a single silver nanowire as a flexible coupler to transform a free space beam into a BSW propagating on the dielectric multilayer. The reconfigurable or dynamical BSWs have been obtained with the aid of a spatial light modulator [3]. With the ability to be used in water, the long propagation distance, and the high flexibility, BSW is ideal for certain applications in areas such as the biological sciences, where many measures are made on glass surfaces or for which an aqueous environment is required, and for high-speed interconnections between chips, where low loss is necessary.

Reference

[1] Yeh, P.; Yariv, A.; Hong, C.S.; Electromagnetic propagation in periodic stratified media. I. General theory, *J. Opt. Soc. Am.*, 67, 423–438 (1977).

[2] Wang, R. X.; Wang, Y.; Zhang, D. G; Si, G. Y; Zhu, L. F.; Du, L. P.; Kou, S. S.; Badugu, R.; Rosenfeld, M.; Lin, J.; Wang, P.; Ming, H.; Yuan, X. C.; and Lakowicz, J. R.; Diffraction-Free Bloch Surface Waves, *ACS Nano* 11, 5383–5390 (2017).

[3] Zhang, D. G; Wang, R. X.;, Xiang,Y.F.;, Kuai, Y.; Kuang, C. F.; Badugu, R.; Xu, Y. K.; Wang, P.; Ming, H.; Liu, X.; and Lakowicz, J. R.; Silver Nanowires for Reconfigurable Bloch Surface Waves, *ACS Nano*, 11 (10), 10446–10451 (2017).

Gradient index metamaterials for enhancing local field

Yang Li[1,2], **Philip Camayd-Muñoz**[2], **Peter Saeta**[2], **Eric Mazur**[2]

1. Tsinghua University, 30 Shuangqing Rd, Haidian Qu, Beijing Shi, China
2. Harvard University, Cambridge, MA 02138, USA

Most forms of light-matter interaction are mediated by the electric field. Therefore, these effects can be dramatically amplified by enhancing the applied field locally [1]. Local-field enhancement has applications in sensing, nonlinear optics, photovoltaics, and quantum optics [1]. Such local-field enhancement is typically achieved using free-space optics such as lenses, or at the microscale using dielectric resonators or plasmonics [1]. However, the field enhancement factor of these mechanisms is restricted by the focusing limit of lenses, or large mode volumes of dielectric resonators, or heating and parasitic losses of plasmonics in the optical regime. These drawbacks limit the strength of light-matter interactions and restrict applications.

Here, we present a mechanism to achieve strong local-field enhancement within a gradient index slab, where the refractive index varies from positive to negative value (Fig. 1a). Electromagnetic waves entering this material at oblique angles refract as they propagate through the slab, which can be modeled as a series of interfaces between materials with increasingly negative index. The normal component of the electric displacement field (D_x=ϵE_x) must be continuous across each interface, causing the electric field to increase in proportion to the decrease in permittivity. If the index decreases gradually, the reflections at each interface can be minimized, and the incident wave can be partially transmitted through the metamaterial slab. As the wave penetrates into the slab, the electric field continues to grow until it diverges at the middle of the slab where the index reaches zero [2].

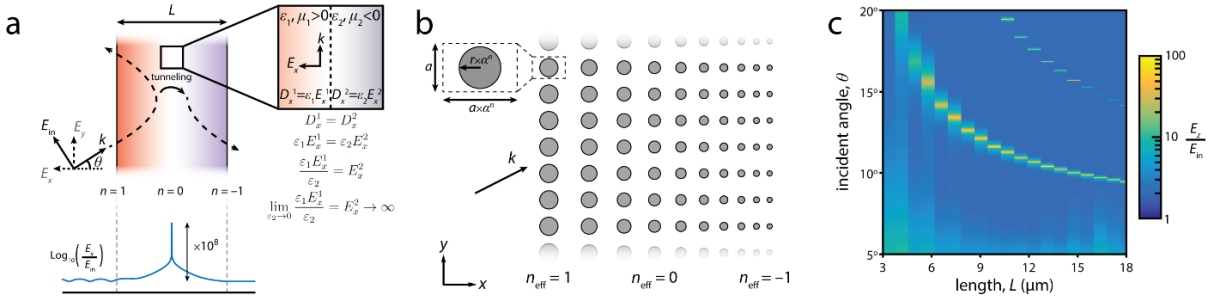

Fig. 1 (a) Schematic of a bulk gradient index metamaterial (GIM). Top left: a transverse-electric (TE) polarized light is obliquely incident onto a GIM with refractive index gradually changing from one to zero to negative one. Top right: constitutive relation at the zero-index transition. The normal component of electric field E_x diverges as the permittivity approaches zero. Bottom: normalized electric field component E_x as a function of the longitudinal coordinate. (b) GIMs consisting of 2D Dirac-cone metamaterials with positive-zero-negative gradient index. The period a and radius r of the centre unit correspond to an effective index of zero. (c) Electric field enhancement as a function of the incidence angle [θ in (a)] and the length of the GIM made of 2D Dirac-cone metamaterial [L in (a)].

We design a GIM based on 2D Dirac-cone metamaterials, consisting of a square array of dielectric pillars [3]. By adjusting the radius and separation of the pillars, we obtain an effective refractive index equal to zero in the optical regime, while maintaining finite impedance. This design is easily extended to positive (negative) index by increasing (decreasing) the separation and radius of the pillars. A GIM can be created by continuously varying the dimensions of the unit cell across the width of the array (Fig. 1b).

To characterize the performance of GIM, we numerically simulate the enhancement of the electric field as a function of the incident angle and slab length (Fig. 1c). Here the Dirac-cone metamaterial consists of silicon pillars, designed for an operating wavelength λ=1550 nm. The field enhancement is maximized for a narrow range of incident angles, which depends on the length of the metamaterial slab. This is caused by a "forbidden" region near the middle of the slab, across which electromagnetic field tunnels as an evanescent wave. Longer slabs require smaller incidence angles to minimize the width of the "forbidden" region near zero index, while thinner slabs can tolerate relatively wider forbidden regions. So, we can control the optimal angle for field enhancement by adjusting the slab length. For optimized incident angle, the tangential component of the electric field E_z is enhanced by a factor of more than 400 due to the zero-index transition (Fig.1c).

References

[1] J. A. Schuller, E. S. Barnard, W. Cai, Y. C. Jun, J. S. White, and M. L. Brongersma, "Plasmonics for extreme light concentration and manipulation," Nature Mater. **9**, 193–204 (2010).
[2] N. M. Litchinitser, A. I. Maimistov, I. R. Gabitov, R. Z. Sagdeev, and V. M. Shalaev, "Metamaterials: electromagnetic enhancement at zero-index transition," Opt. Lett **33**, 2350–2352 (2008).
[3] X. Q. Huang, Y. Lai, Z. H. Hang, H. H. Zheng, and C. T. Chan, "Dirac cones induced by accidental degeneracy in photonic crystals and zero-refractive-index materials," Nature Mater. **10**, 582–586 (2011).

Janus structural color from a 2D photonic crystal hybrid with a Fabry–Perot cavity

Chang Li[1,2], Maoxiong Zhao[3], Xue Zhou[1,2], Huizeng Li[1,2], Yang Wang[1,2], Xiaotian Hu[1,2], Mingzhu Li[1], Lei Shi[3], and Yanlin Song[1]

1. *Institute of Chemistry Chinese Academy of Sciences (ICCAS), Zhongguancun North First Street 2, Beijing 100190, China*
2. *University of Chinese Academy of Sciences, Yuquan Road 19, Shijingshan District Beijing 100049, China*
3. *Fudan University, 220 Handan Road, Shanghai, China 200433*

Structural colors are widely applied for their stability and their sophisticated optical responses. However, these colors always appear washed-out or pale assigning to the defect hardly avoided in the manufacturing procedures. It's still a challenge to bring multifunctional vivid color via a facile method. Here, we construct a composite structure combining 2D photonic crystal and Fabry-Perot cavity by a simple and convenient method. Various metallic colors with tunable hue and high saturation are produced by the composite structure. What's more, an obvious optical Janus effect is created by the composite structure. Iridescent colors can be observed when viewing from the same side of incident light but only pale colors can be seen from the opposite side. The hues and saturation of the colors can be adjusted by the parameters of the composite structure. The experimental results indicate that the color is derived from the synergistic effect of the interference, the diffraction and the Rayleigh scattering of the composite structure. The facile composite photonic structure pioneers a new way for art, architecture and security features in anti-counterfeiting materials.

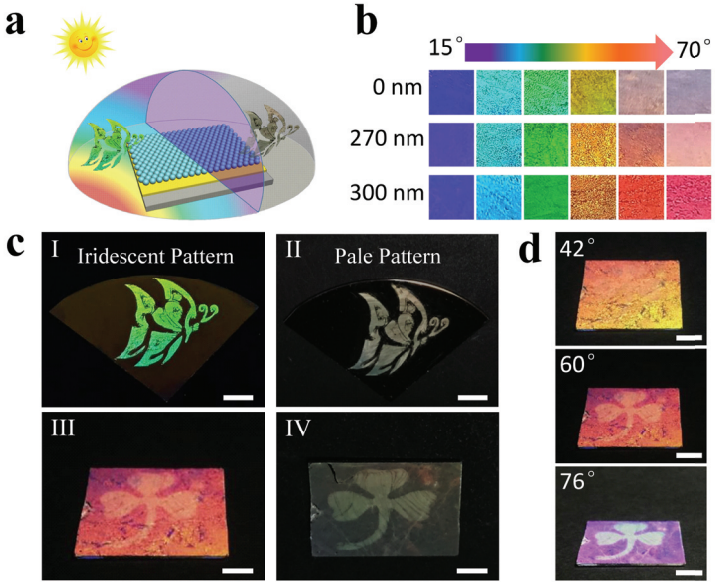

Fig. 1 a) Schematic of optical Janus effect generated by the composite structure; b) A palette obtained by the different composite structures; c) Optical images of the butterfly and the anti-counterfeiting material at iridescent zone and pale zone respectively. Scale bar: I-II: 1 cm, III-IV: 0.5 cm; d) Anti-counterfeiting clover pattern on the composite structure.

References

[1] A. Tikhonov, N. Kornienko, J. T. Zhang, L. L. Wang, S. A. Asher, J. "Reflectivity enhanced two-dimensional dielectric particle array monolayer diffraction," Nanophotonics **6**, 063509 (2012).

[2] D. Ge, L. Yang, G. Wu, S. Yang, "Angle-independent colours from spray coated quasi-amorphous arrays of nanoparticles: combination of constructive interference and Rayleigh scattering," J. Mater. Chem. C **2**, 4395-4400 (2014).

[3] S. A. Asher, J. M. Weissman, A. Tikhonov, R. D. Coalson, R. Kesavamoorthy, "Diffraction in crystalline colloidal-array photonic crystals," Phys. Rev. E **69**, 066619 (2004).

Demonstration of a next generation of satellite laser ranging with superconductor single photon detector array

Qi Chen[1] , Biao Zhang[1] , Labao Zhang[1*], Rui Ge[1], Ruiying Xu[1] , Yang Wu[1] , Lin Kang[1] , Jian Chen[1] , Peiheng Wu[1]

1. Nanjing University, Hankou Road 22, Nanjing 210093, China

*Lzhang@nju.edu.cn

Satellite Laser Ranging (SLR) is a recognized technique with the most precision measurements in determining the orbits of space targets. The developments of SRLs were fired by critical technologies over the past 50 years. At the first period, SLR proposed by Plotkin in 1964 was equipped by a Q-switched ruby laser and photoelectric receiver. In the 80s and 90s of twenty centuries [3], Nd:Yag laser and photomultiplier tube (PMT) were widely adopted. The new technologies increased the accuracy to several cm of SLR, which extended the applications to geodesy, fundamental science and precise orbit determination. Currently, most SLR stations doubled the frequency from 1064 nm of Nd:Yag laser to 532 nm wavelength for the response band of silicon-based single photon detectors. In theory, the 1064 nm system may be featured with no conversion loss and doubled photon number. At the same time, the laser with higher power may be produced for no risk of burning Nonlinear Crystal in for frequency doubling. The main barrier for 1064 nm SLR is lake of high efficiency detector.

In this work, we demonstrated a next generation of satellite laser ranging with NbN-based SNSPD array. The total active area of the superconducting nanowires increases to 80 μm × 80 μm. Compact wiring between the cells ensures a 98.5% filling rate. An equivalent receiving aperture of 300 μm associated with beam compression technology. Experimental results showed a quantum efficiency of 94.5%, and a system efficiency of 46% for photons coupled from 300 μm fiber without optimizing polarization, and a system time resolution of 92 ps. This work demonstrates the feasibility of large SNSPD array based on NbN, and furthermore, paves the new way for developing large pixel photons camera.

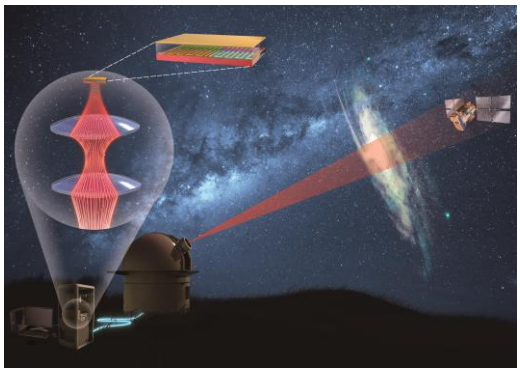

Fig. 1 Schematics of satellite laser ranging with SNSPD array.

The detector also has significant advantages in the field of satellite laser ranging. First of all, the size of the received reflected spot is generally on the order of several tens of micrometers because of long detection distance. However, the size of the active area of traditional array single-photon detectors is only a few ten micrometers. They cannot cover all photons, extremely limit the detection efficiency and ranging accuracy. Our device overcomes this difficulty due to its large active area. Secondly, the previous single photon detectors mostly have single-pixel or small-array structure, so the speed of signal response and the detection efficiency is slow. Our device has a large-array structure. Making it easier to have a fast signal response speed and even can perform well in parallel processing 16 channels which further improves the detection efficiency and ranging accuracy.

Up to now, we have successfully ranged over 200 targets. The analysis indicated that the max. distance is up to 1 million km for typical cooperative targets, and the min. size is 1 cm for non-cooperative targets at a typical distance of space debris. According to our knowledge, both of them updated the records of SLR.

Example References

[1] Gol'tsman, G. N. et al. Picosecond superconducting single-photon optical detector. Appl. Phys. Lett. 79, 705–707 (2001).

[2] Doerner, S. et al. Frequency-multiplexed bias and readout of a 16-pixel superconducting nanowire single-photon detector array. Appl. Phys. Lett. 111, 1–5 (2017).

[3] Jahanmirinejad, S., Frucci, G., Mattioli, F., Sahin, D. & Gaggero, A. Photon-number resolving detector based on a series array of superconducting nanowires Photon-number resolving detector based on a series array of superconducting nanowires. 072602, (2012).

[4] Marsili, F. et al. Detecting single infrared photons with 93% system efficiency. Nat. Photonics 7, 210–214 (2013).

[5] Allmaras, J. P. et al. Large-Area 64-pixel Array of WSi Superconducting Nanowire Single Photon Detectors. Conf. Lasers Electro-Optics JTh3E.7 (2017)

Strong damping of the localized surface plasmon resonance of metal nanoparticles and its applications

Hongliang Hao, Shuai Wang, Huanhuan Li, Qingmeng Wu, Bing Zhang, Jinjun He, Yingcui Fang
Department of Vacuum Science and Devices, School of mechanical Engineering, Hefei University of Technology, Hefei, P. R. China, 230009

Strong localized surface plasmon resonance (LSPR) of metallic nanoparticles has been proved to be able to effectively enhance the Raman scattering, the visible light absorption and the photoluminance emission of organic molecules and has thus got wide applications. Recently, strong damping of LSPR of metallic nanoparticles being demonstrated can produce new effects[1], which is now drawing increasing attention. We fabricate samples whose LSPR is strongly damped [2-3] and we explore the LSPR damping induced improvement of transmittance of dielectric/nanopariticles/dielectric layers [2] and the LSPR damping induced visible light photocatalytic efficiency of nanopariticles[4].

[1] K. Wu, J. Chen, J. R. McBride, T. Lian, “Efficient hot-electron transfer by a plasmon-induced interfacial charge-transfer transition”, Science 349, 632, 2015.
[2] Yingcui Fang, Jinjun He, Kang Zhang et al, “Ar plasma irradiation improved optical and electrical properties of TiO_2/Ag/ TiO_2 multilayer thin film”, Optics Letters 40, 5455(2015).
[3] Qingmeng Wu, Mengting Si, Bing Zhang et al, “Strong damping of the localized surface plasmon resonance of Ag nanoparticles by Ag_2O”, Nanotechnology 29, 295702(2018).
[4] Yingcui Fang, Qingmeng Wu, Huanhuan Li et al, Photocatalytic activity of silver oxide capped Ag nanoparticles constructed by air plasma irradiation, Appl. Phys. Lett. 112, 163101(2018).

A Near-Perfect Chiral Single-Photon Interface: Isolation and Unidirectional Emission

Lei Tang[1], Jangshan Tang[1], Weidong Zhang[2], Guowei Lu[2], Han Zhang[3], Yong Zhang[1*], Keyu Xia[1*], and Min Xiao[1,4]

1.National Laboratory of Solid State Microstructures, College of Engineering and Applied Sciences, and School of Physics, Nanjing University, Nanjing 210093, China

2.State Key Laboratory for Mesoscopic Physics & Collaborative Innovation Center of Quantum Matter, Department of Physics, Peking University, Beijing 100871, China

3.Collaborative Innovation Center of Advanced Microstructures, and School of Physics, Nanjing University, Nanjing 210093, China

4.Department of Physics, University of Arkansas, Fayetteville, Arkansas 72701, USA

Abstract: Chiral quantum systems have received intensive attention in fundamental physics and applications in quantum information processing including optical isolation and photon unidirectional emission. We design an on-chip resonator-emitter system with chiral light-matter interaction. The system includes a microring resonator with near-unity optical chirality along both of the whole outside and inside walls, allowing a strong and chiral coupling of the Whispering-Gallery mode to a quantum emitter. Using this design and initializing a quantum dot in a specific spin ground state, we show a broadband optical isolation at the single-photon level over several GHz. Furthermore, a quantum emitter chirally coupling to the microring resonator can emit single photons unidirectionally. This chiral single-photon interface paves a way to realize optical non-reciprocity in on-chip quantum information processing and quantum networks.

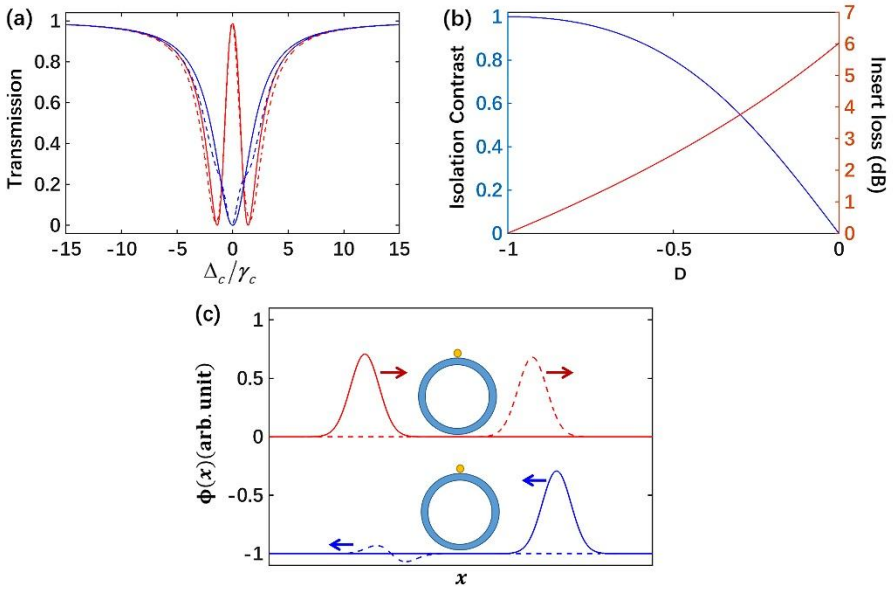

Fig. 3 Single-photon transmission. (a) The steady state transmission for D = -0.99. Red (blue) curves are for the forward transmissions T_+ (T.) in the cases without the backscattering, i.e. h = 0, (solid curves) and with a backscattering of h = γ_c (dashed curves). (b) Isolation contrast (blue curve) and insertion loss (red curve) as a function of the optical chirality D. Δ_c= 0; h = 0. Other parameters for (a) and (b) are given in text. (c) Propagation of single-photon pulses, incident to the ports 1 and 2 simultaneously, through the QD-resonator system. Up (lower) panel shows the propagation of single-photon pulse input to the port 1 (2). Solid curves are the input single-photon wavefunction, and dashed curves for the transmitted wavefunction.

References

[1] P. Lodahl, S. Mahmoodian, S. Stobbe, A. Rauschenbeutel, P. Schneeweiss, J. Volz, H. Pichler, and P. Zoller, Nature (London) 541, 473 (2017).
[2] M. Scheucher, A. Hilico, E. Will, J. Volz, and A. Rauschenbeutel, Science 354, 1577 (2016).
[3] C. Sayrin, C. Junge, R. Mitsch, B. Albrecht, D. O'Shea, P. Schneeweiss, J. Volz, and A. Rauschenbeutel, Phys. Rev. X 5 (2015).
[4] K. Xia, G. Lu, G. Lin, Y. Cheng, Y. Niu, S. Gong, and J. Twamley, Phys. Rev. A 90 (2014).
[5] J.-T. Shen and S. Fan, Phys. Rev. A 79, 023838 (2009).
[6] J.-T. Shen and S. Fan, Opt. Lett. 30, 2001 (2005).

Strong Plasmon–Exciton Coupling in Single Au Nanohole–Monolayer WS_2 Hybrid Nanostructures

Xuexian Chen, Huanjun Chen*

State Key Laboratory of Optoelectronic Materials and Technologies, Guangdong Province Key Laboratory of Display Material and Technology, School of Electronics and Information Technology, Sun Yat-sen University, Guangzhou 510275, China
** corresponding author: chenhj8@mail.sysu.edu.cn*

Abstract Two-dimensional transition metal dichalcogenides (TMDCs) are emerging as promising materials for studying light–matter interactions due to their excellent optical properties. Realizing strong plasmon–exciton coupling in single nanoantenna level is of importance in pursuing of novel nanophotonic devices under ambient conditions. Here, we have proposed a strong plasmon−exciton coupling systems by integrating the monolayer tungsten disulfide (WS_2) with individual plasmonic gold nanohole. Our results demonstrate that Rabi splitting exceeding 162 meV can readily be achieved in planar TMDC/metal nanostructure at room temperature. We strongly believe that such hybrid systems can provide a simple and robust single nanostructure design to manipulate the light−matter interactions at the nanoscale.

In the past five years, strong light–matter interactions have attracted a great deal of attentions because they exhibit fascinating applications in optoelectronics, nanophotonic devices, and quantum optics.[1] Many efforts have been made concerning the strong coupling between surface plasmon and exciton in J-aggregates, dye molecules, and qutantum dots.[2] At the same time, another prominent atomic crystal materials, transition metal dichalcogenides (TMDs), have emerged as a promising light-active material for studying plasmon−exciton coupling under ambient conditions. One of the most remarkable features of TMDs is the bandgap changed from indirect-to-direct when passing from bulk to a monolayer. On the other hand, benefited from the small mode volume of the plasmonic systems, metal nanostructures exhibit exceptional electromagnetic field localizations which can deliver strong optical confinements and enhance light–matter interactions.[3] Although such a strong coupling behavior has been reported in the MoX_2 coupled with metal nanostructure. However, MoX_2 always have relative small Rabi splitting, while WX_2 own sharper and stronger isolated absorption band. In addition, WX_2 exhibit larger exciton binding energy, whose Rabi splitting can exceed the exciton line-width.[4]

In our study, we investigate the coupling effect in hybrid nanostructures consisting of monolayer WS_2 and an individual planar plasmonic gold nanohole. We showed from both experiments and numerical simulations that the strong coupling could be obtained between the WS_2 excitons and gold nanohole plasmons at room temperature. The underlying mechanisms of plasmon–exciton coupling were systematically studied by single particle dark-field scattering spectroscopy, scanning near-field optical microscopy (SNOM) and a coupled harmonic oscillator model. A Rabi splitting of 162 meV was extracted from the anti-crossing curves by measuring dozens of individual nanoholes scattering spectra.

In summary, we have demonstrated that the strong coupling between an individual plasmonic gold nanohole and monolayer WS_2 flake from both experimentally and theoretically. WS_2–gold nanohole hybrid nanostructures were created by transferring monolayer WS_2 onto the Au nanoholes fabricated by focused ion beam technique. Photoluminescence emission enhancement was observed due to the strong near-field localization. Further, by fitting the anti-crossing curve of scattering spectra from the hybrid nanostructures, a Rabi splitting energy of 162 meV was achieved at room temperature owe to the strong optical field confinements of the Au nanoholes and large transition dipole moment of the WS_2 exciton. We strongly believe that such a coupling nanophotonic systems can open new avenues to realize tunable planar plasmonic devices operating at the nanoscale.

References

[1] F. Monticone, A. Alù, "Metamaterial, plasmonic and nanophotonic devices," Rep. Prog. Phys. **80,** 036401 (37pp) (2017).

[2] H. Wang, A. Toma, H. Y. Wang, A. Bozzola, E. Miele, A. Haddadpour, G. Veronis, F. De Angelis, L. Wang, Q. D. Chen, H. L. Xu, H. B. Su and R. P. Zaccaria, "The role of Rabi splitting tuning in the dynamics of strongly coupled J-aggregates and surface plasmon polaritons in nanohole arrays," Nanoscale **8**, 13445–13453, (2016).

[3] Y. Zakharko, A. Graf, J. Zaumseil, "Plasmonic Crystals for Strong Light–Matter Coupling in Carbon Nanotubes," Nano Lett. **16**, 6504–6510, (2016).

[4] S. Wang, S. Li, T. Chervy, A. Shalabney, S. Azzini, E. Orgiu, J. A. Hutchison, C. Genet, P. Samorì and T. W. Ebbesen, "Coherent Coupling of WS_2 Monolayers with Metallic Photonic Nanostructures at Room Temperature," Nano Lett. **16**, 4368–4374, (2016).

Metasurface Realization for Complementary Medium-type Optical Illusion

Yineng Liu

Institute of Electromagnetics and Acoustics and Department of Electronic Science, Xiamen University, Xiamen 361005, China

Metasurface has recently become a practical surface-equivalent route to transformation optical (TO) applications due to its simplicity in fabrication and high resolution in constructing a desired wavefront[1–3]. In this work, we propose an out-of-the ordinary approach in designing metasurface using the concept of complementary media as an intermediate step. The metasurface, effectively storing all the original information in TO media, enables specific TO applications which normally requires complementary media. According to the established design scheme, we numerically demonstrate compact and simple-to-design metasurfaces for transforming, shifting, and splitting an object with very good camouflaging performance. Although such metasurfaces for illusion optics ideally work at designed incident angle like other metasurface devices, they still have angle tolerances about (20 °). Our scheme for metasurface-enabled illusion optics opens a gate for realizing more complicated transformation optic device with a single sheet of surface.

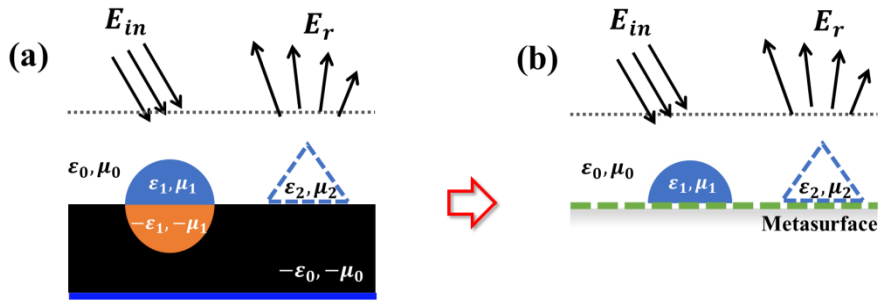

Fig. 1 The schematic diagram of metasurface-enabled illusion optics. (a) The virtual space with complementary media to obtain the design of metasurface. (b) The physical space with the "real" object to turn into the virtual object by the metasurface.

References

[1] X. Ni, Z. J. Wong, M. Mrejen, Y. Wang, X. Zhang, "An ultrathin invisibility skin cloak," Science **349**, 1310-1314 (2015).
[2] B. Orazbayev, E., N. Mohammadi, A. Alù, M. Beruete, "Experimental Demonstration of Metasurface-Based Ultrathin Carpet Cloaks for Millimeter Waves," Adv. Opt. Mater.**5**, 1600606 (2017).
[3] S. Vellucci, A. Monti, A. Toscano, F. Bilotti, "Scattering manipulation and camouflage of electrically small objects through metasurfaces," Phys. Rev. Appled. **7**, 034032 (2017).

Toroidal Response Based on Localized Spoof Plasmons

Pengfei Qin[1], Ran Hao[1], Jianyao Jiao[1], Xiaobin Lin[1], Zheng Zhen[1], Dagarbek Rakhatbek[1], Ibrahim Nasidi[1], Hongsheng Chen[1], Erping Li[1]

1. Zhejiang University, Zheda Road 38, Hangzhou 310027, China

Surface plasmon polaritons (SPPs) are a kind of electromagnetic (EM) surface wave propagating at the interface between noble metals and dielectrics at optical frequencies [1]. With the ability to confine EM waves at a deep sub-wavelength scale, SPPs provide solutions to overcome the diffraction limit and miniaturize the photonic components. At microwave or terahertz frequencies, a concept of spoof SPPs has been proposed by Pendry et al. in 2004, where a special surface wave mode, propagating on a periodically subwavelength structured metal surface, has enhanced energy confinement and a dispersion similar with that of natural SPPs but at much lower frequencies [2]. Recently, a toroidal multipole is another form of multipole which is produced when currents flow on the surface of a torus along its meridian [31]. Because of its unusual EM properties like dynamic non-radiating charge-current configurations, the toroidal multipoles have attracted increasing attentions recently. Currently, most of the studies focus on electric/magnetic localized spoof surface plasmons (LSSPs), where the LSSPs show multipole electric/magnetic dipole moments.

In this work, we propose and experimentally demonstrate compact planar meta-disks based on split ring resonators (SRRs) to support toroidal LSSPs at microwave frequencies. We focus on the localized toroidal modes, which is a new field where very few works have been done. Our proposed structures show the merits of compactness, elegance, and high compatibility with the photonic integrated circuits. Fig. 1(a) show the proposed structure consists of metallic SRRs and FR4 dielectric substrate. Fig. 1(b) show the magnetic field intensity distribution of the SRR disks at 4.16 GHz. The magnetic field distributions exhibit a vortex with the field that threads all the SRRs, which is produced by the surface current oscillating on the SRRs. Also, the magnetic field is in a shape of torus, which is an important signature of the toroidal dipole moment as it provides a toroidal dipole along z direction. In the experimental setup shown in the inset of Fig. 1(c), two dipole antennas connected with VNA are used to measure the transmission. Moreover, around 4.16 GHz the transmission curves experience resonances which are in accordance with our expectation, which agrees well with simulated scattering parameters.

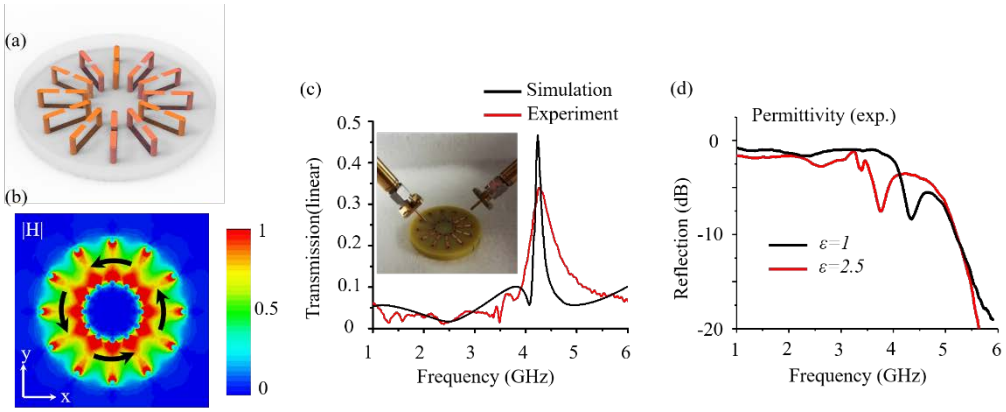

Fig. 1 (a) Top view of the proposed structure consisting of 12 SRRs. (b) Simulated magnetic field intensity distribution in the xy plane of the SRR disks at 4.16 GHz. (c) Simulated and experimental transmission parameters. (d) Measured reflection parameters, where the background is air and oil with the relative permittivity 1 and 2.5, respectively.

We also study the impact of background parameters to the proposed toroidal LSSPs resonator. In the experiment, we change the background medium from air to oil (relative permittivity of 2.5), as shown in Fig. 1(d). The resonance frequency shifts from 4.17 GHz in the air to 3.8 GHz in the oil and the corresponding resonance frequency shift per refractive index is 0.8 GHz/refractive index unit (RIU). Therefore, the toroidal LSSPs resonator can work as a deformation sensor and to detect the refractive index changes of the surrounding medium.

References

[1] W. L. Barnes, A. Dereux, T. W. Ebbesen, "Surface plasmon subwavelength optics," Nature **424**, 824-830 (2003).

[2] J. B. Pendry, L. Martín-Moreno, F. J. Garcia-Vidal, "Mimicking surface plasmons with structured surfaces," Science **305**, 847-848 (2004).

[3] T. Kaelberer, V. A. Fedotov, N. Papasimakis, D. P. Tsai, N. I. Zheludev, "Toroidal dipolar response in a metamaterial," Science 330, 1510-1512 (2010).

Broadband Integrated Polarization Rotator Using Three-Layer Metallic Grating Structures

Hao Jing[1], Ren-Hao Fan[1], Cheng-Yao Li[1], Zheng Wang[1], Dong-Xiang Qi[1], Ru-Wen Peng[1], and Mu Wang[1]

[1]National Laboratory of Solid State Microstructures, School of Physics, and Collaborative Innovation Center of Advanced Microstructures, Nanjing University, Nanjing 210093, China

Here we present our recent work on broadband linear polarization rotator. Firstly, we have experimentally demonstrated a linear polarization rotator that is a three-layer metallic grating structure for manipulating the polarization of broadband terahertz (THz) waves. By mechanical rotations of the composite grating layers, this freely tunable device can rotate the polarization of a linearly polarized THz wave to any desired direction with high conversion efficiency [1]. Then we demonstrate broadband integrated polarization rotator (IPR) with a series of three-layer rotating metallic grating structures in the near-infrared region. This transmissive optical IPR can conveniently rotate the polarization of linearly polarized light to any desired directions at different spatial locations with high conversion efficiency, which is nearly constant for different rotation angles. The linear polarization rotation originates from multi-wave interference in the three-layer grating structure. [2]. We anticipate that this type of linear polarization rotator will find wide applications in analytical chemistry, biology, communication technology, imaging, etc.

References

[1] R. H. Fan, Y. Zhou, X. P. Ren, R. W. Peng, S. C. Jiang, D. H. Xu, X. Xiong, X. R. Huang, and Mu Wang. "Freely tunable broadband polarization rotator for terahertz waves", Adv. Mater. **27**, 1201 (2015).

[2] R. H. Fan, D. Liu, R. W. Peng, W. B. Shi, H. Jing, X. R. Huang, and Mu Wang. "Broadband integrated polarization rotator using three-layer metallic grating structures", Opt. Express **26**, 516 (2018).

Optically controllable superconducting electromechanical oscillator

Yong-Chao Li[1,†], Jiang-Shan Tang[2,3,†], Jun-Liang Jiang[1,†], Jia-Zheng Pan[1], Xin Dai[1], Xin-Yu Wei[1], Ya-Peng Lu[1], Sheng Lu[1],Xue-Cou Tu[1], Hua-Bing Wang[1], Ke-Yu Xia[3,4,*], Guo-Zhu Sun[1,*], and Pei-Heng Wu[1]

[1] Research Institute of Superconductor Electronics, School of Electronic Science and Engineering, Nanjing University, Nanjing 210093, China

[2]School of Physics, Nanjing University, Nanjing 210093, China

[3]National Laboratory of Solid State Microstructures, College of Engineering and Applied Sciences, Nanjing University, Nanjing 210093, China

[4] Collaborative Innovation Center of Advanced Microstructures, Nanjing 210093, China

[†]These authors contribute equally to the work

[*] Corresponding author. E-mail : gzsun@nju.edu.cn, keyu.xia@nju.edu.cn,

Transferring information between the microwave and optical domains is a longstanding goal in quantum information processing as it can link remotely separate superconducting circuits optically, and is still a long way from realization. An opto-electro-mechanical resonator is a very promising candidate to complete this challenging task. We fabricate a microscale electromechanical system, in which a suspended superconducting membrane as a mechanical resonator capacitively couples to a superconducting microwave resonator. As the microwave driving power increases, the resonance frequency of the mechanical resonator can be nonlinear, first increasing and then quickly decreasing to its original value. We also demonstrate the optical switching of the transmitted microwave signal through the microwave resonator. We provide a theoretical model for a qualitative understanding of our experimental observations. Our experiment may pave a way for interfacing the microwave and optical domains.

Investigation of Thermal Evolution in $Ge_xAs_ySe_{1-x-y}$ Thin Films by in-situ measurements

Xueqiong Su [a*], DongWen Gao [a], Shufeng Li [a], Yong Pan [a], Xiaowei Han [a], GuiSheng Wang [a], R. P. Wang [b], Li Wang [a*]

[a] *College of Applied Sciences, Beijing University of Technology, Beijing 100124, China*

[b] *Centre for Ultra-high Bandwidth Devices for Optical Systems, Laser Physics Centre, Australian National University, Canberra, ACT 2600, Australia*

Keywords: Chalcogenide glasses, GexAsySe1-x-y, Conduction mechanisms, Electrical conductivity

Chalcogenide glasses, an important photonics material, are applied to Mid infrared waveguide devices, Supercontinuum optical fiber, Optical recording media and phase change non-volatile memory, due to their unique properties of low phonon energy, ultrafast response time, and high optical nonlinearity [1-2]. The resistance of chalcogenide glass $Ge_xAs_ySe_{1-x-y}$ film material is difficult to be observed due to the electrons pinned near the Fermi level, the large electron binding energy, and the large film resistance. This work is mainly about a series of different components of $Ge_xAs_ySe_{1-x-y}$ chalcogenide glass films. Under the condition of heating, the research is focused on the amorphous semiconductor energy band structure and localized state electron transport mechanism under non-equilibrium conditions by observing the change of resistance. Under non-equilibrium conditions, the electrical properties parameters show three relaxation states. 1） Under heating, the film resistance shows a tendency to be consistent with the bulk with the low value of MCN. The higher the temperature, the lower the resistance. 2） as the MCN increases, the resistance appears wavy. Especially as for the samples of $Ge_{33}As_{12}Se_{55}$ and $Ge_{11.5}As_{24}Se_{64.5}$, the resistance falls instead. Computer simulations show that the Boltzmann fit formula is more suitable for $Ge_xAs_ySe_{1-x-y}$ chalcogenide film, a low-mobility semiconductor with deep Fermi level and hopping conduction, than simplified Boltzmann formula. Through simulation calculations, it is found that the relaxation state of the resistance is proportional to the density of localized states at E_f.

To study the effects of thermal annealing on the structure of $Ge_xAs_ySe_{1-x-y}$ thin films, the thermal evolution of these films was measured by the in-situ X-ray diffraction (XRD) up to temperature (1273K) in vacuum (10^{-1} Pa). Using in-situ XRD, the entire process of crystallization can be observed, which is from appearing crystal structure to melting liquid-state and ultimately to disappearing of amorphous structure. It is worth mentioning that a completely amorphous phase suddenly appears between crystallization temperature Tx and peak temperature Tp and the transition temperature T_l from glassy-state to liquid-state. In the crystallized process, the corresponding state-transition temperatures T_x, T_l, T_p are linear with MCN. Based on the above results, it is accessible to expand the glass phase region and increase the initial crystallization temperature by introducing targeted protective atmospheres or doping inhibitors.

In order to obtain information about changes in the amorphous structural origin of the anneal-induced, the samples were analyzed by in-situ Raman spectroscopy. The broad peaks were appeared in Raman spectra between 150 cm^{-1} and 330 cm^{-1} for amorphous nature of the glasses and the proximity of the elements in the periodic table.With the MCN increasing, the position of the broad peak occurs blue shift. The individual feature peaks show that the Ge–As–Se glass network consists of the basic building units specifically GeSe4/2 tetrahedra, AsSe3/2 pyramids, and Ge-Ge or Se-Se homopolar bonds. There are the vibrations of the homopolar Se－Se bonds at 250cm^{-1}, and the ethane-like Ge－Ge modes have peaks at 175 and 300 cm^{-1}.[3-5] It appears that the formation of the Ge－Ge or As-As homopolar bonds is relatively easier as the temperature increases, but the formation of these bonds cannot be completely suppressed in any case, as one falls and another rises.

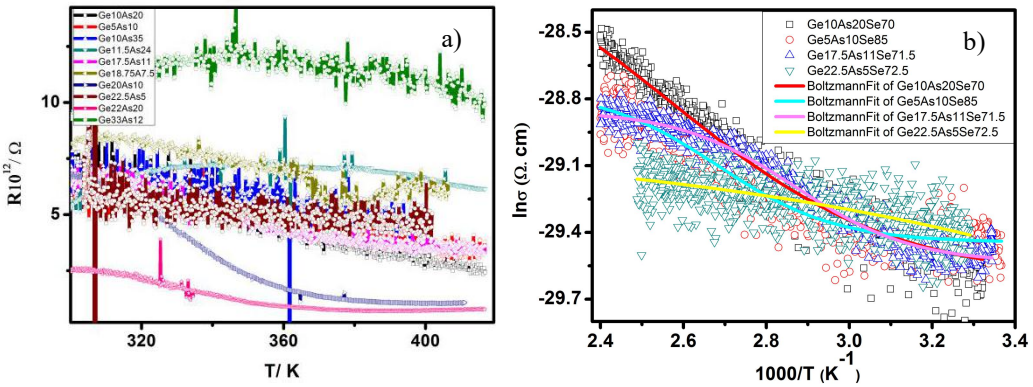

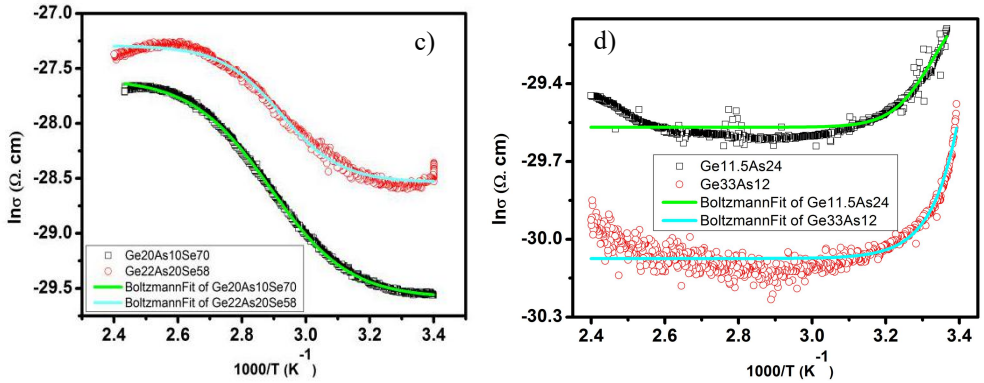

Fig. 1 (a) The relation between resistance and temperature of $Ge_xAs_ySe_{1-x-y}$ thin films. (b)(c)(d) Three kinds of relaxation states of conductivity with of $Ge_xAs_ySe_{1-x-y}$ thin films.

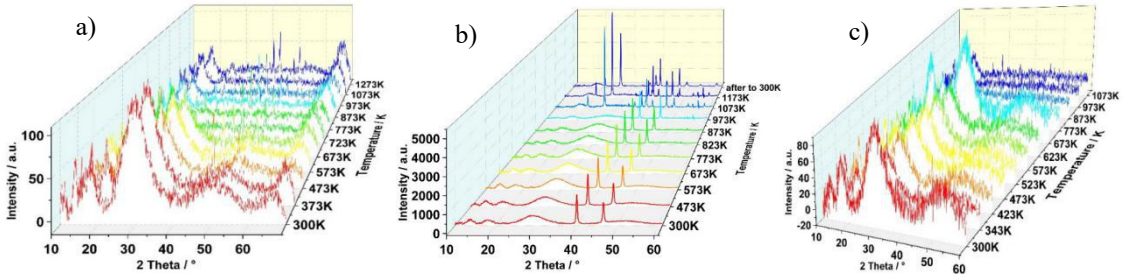

Fig. 2 The in-situ x-ray diffraction patterns of $Ge_xAs_ySe_{1-x-y}$ thin films was measured by the X-ray diffraction (XRD) up to temperature (773K) in vacuum (10^{-1} Pa) measured at room-temperature. (a) $Ge_{17.5}As_{11}Se_{72.5}$ (b) $Ge_{33}As_{12}Se_{55}$ and (c) $Ge_{20}As_{10}Se_{70}$, .

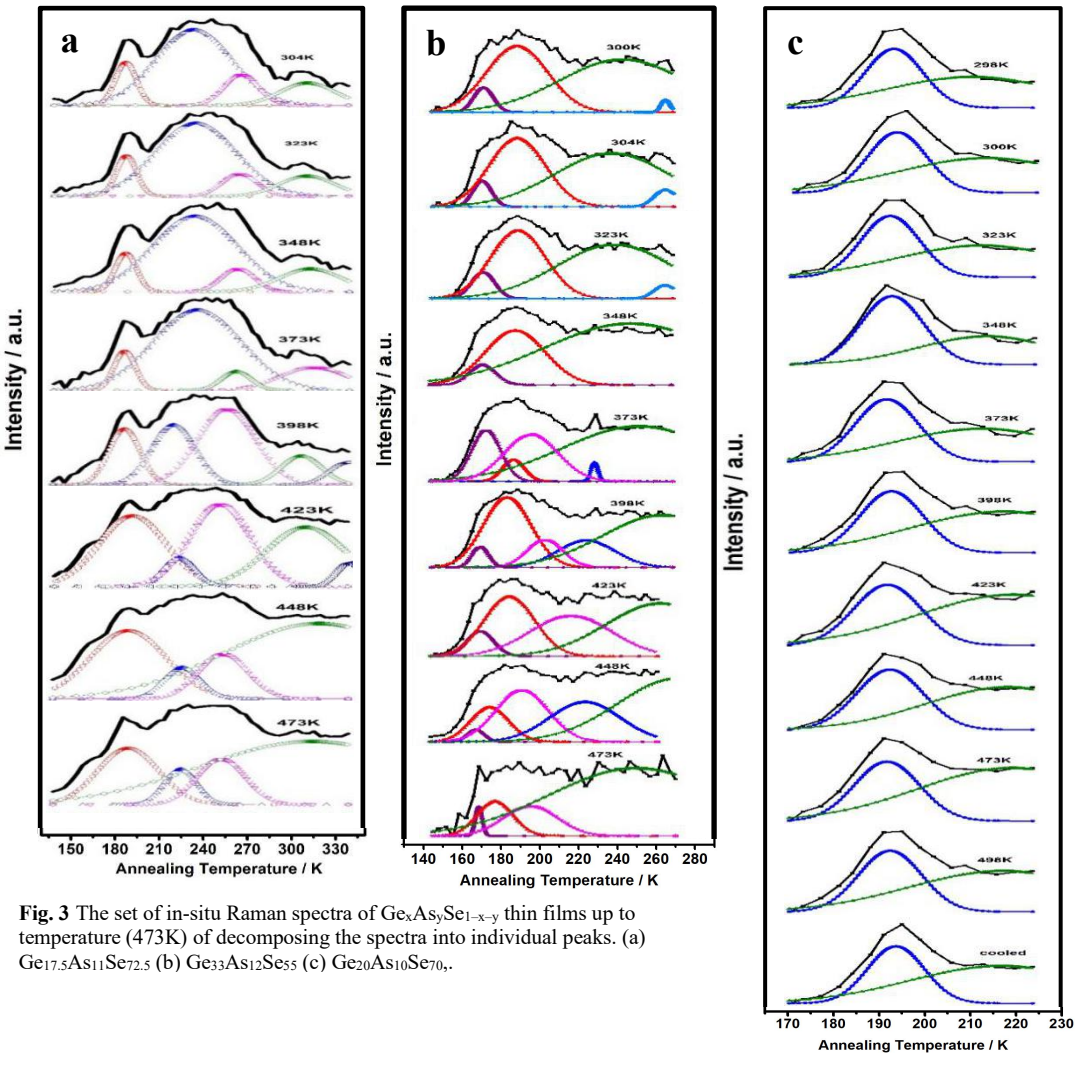

Fig. 3 The set of in-situ Raman spectra of $Ge_xAs_ySe_{1-x-y}$ thin films up to temperature (473K) of decomposing the spectra into individual peaks. (a) $Ge_{17.5}As_{11}Se_{72.5}$ (b) $Ge_{33}As_{12}Se_{55}$ (c) $Ge_{20}As_{10}Se_{70}$,.

References

[1] R. P. Wang, *Amorphous Chalcogenides: Advances and Applications* (Pan Stanford Publishing, Singapore, 2014).
[2] K. Tanaka and K. Shimakawa, *Amorphous Chalcogenide Semiconductors and Related Materials* (Springer, New York, 2011).
[3] P. Tronc, M. Bensoussan, A. Brenac, and C. Sebenne, Phys. Rev. B 8, 5947 (1973).
[4] N. Kumagai, J. Shirafuji, and Y. Inuishi, J. Phys. Soc. Jpn. 42, 1262 (1977).
[5]K. Jackson, A. Briley, S. Grossman, D. V. Porezag, and M. R. Pederson, Phys. Rev. B 60, R14985 (1999).

Plasmon enhanced optical coherence tomography imaging using nanorods of large aspect ratios

Yifan Xu[1], Chao Zhuang[1], Jianhua Zhou[2], Huanjun Chen[1*]

[1]State Key Laboratory of Optoelectronic Materials and Technologies, Guangdong Province Key Laboratory of Display Material and Technology, School of Electronics and Information Technology, Sun Yat-sen University, Guangzhou 510275, China
[2]Key Laboratory of Sensing Technology and Biomedical Instruments of Guangdong Province, School of Engineering, Sun Yat-sen University, Guangzhou 510275, China
** corresponding author: chenhj8@mail.sysu.edu.cn*

Abstract Optical coherence tomography (OCT) imaging is a common used technique in biomedical research. However, such a techinqe is limited by the low light scattering signals from the organic tissues, especially in the near-infrared region, which hinder its application in retriving the informaion of the deep tissues. In our study, we propose to use plasmonic metal nanorods for enhancing the OCT imaging in the near-infrared regions (808 nm and 1310 nm). We successfully synthetized Au@Ag nanorods with large aspect ratios, which exhibit plasmon resonances in the near-infrared region. The nanorods were shown to enhance the light scattering from the organic tissues, which can therefore employed for enhancing the OCT imaging intensity.

OCT imaging is a powerful tool for providing 3D molecular features at the tissue level in real time[1]. However, their applications are limited by the relatively low light scattering intensity from the tissue, especially in the near-infrared region where biological technologies pay much attention to. Noble metal nanostructures exhibit strong plasmon resonances, which can squeeze the free-space light down to the nanoscale and lead to strong electromagnetic field confinements[2]. In addition, their plasmon resonances can be synthetically tuned across the visible to the near-infrared region by modifying their morphologies. These characteristics have made the metal nanostructure potential candidates for enhancing various light–matter interactions. In particular, the strong light scattering properties can make the metal nanostructure excellent contrast agents for the OCT imaging technique[3,4].

In our study, we successfully prepared nanorods (Au@Ag) using a wet-chemical method. The nanorods exhibit strong plasmon resonances from 800 nm~1300 nm, which can be tuned by tailoring their aspect ratios. The nanorods with large aspect ratios were then integrated onto the surface of a piece of pig skin, which acted as a model for the human skins due to the anatomical and physiological similarities between them[1]. The nanorods can greatly enhance the light scattering from the tissue, which enable a OCT imaging with much higher contrast in comparison with the tissue without nanorods. In addition, due to their high photothermal conversion efficiency, the nanorods can further induce efficient heating of the pig skin, which highlights their applications in biological imaging with simultaneous photothermal therapy characteristics.We believed that our results opened new avenues for the plasmonic nanorods in biological imaging and photothermal therepy.

References

[1] X. Q. Jiang, P. J. Tang,“Gold Nanoprobe-Enabled Three-Dimensional Ozone Imaging by Optical Coherence Tomography,”Analytical Chemistry **89**, 9758−9766 (2017).
[2] M. Aioub, S. R. “Platinum-Coated Gold Nanorods Plasmonic Photothermal Therapy,”ACS Nano **11**, 579−586 (2017).
[3] P. J. Tang, X. Q. Jiang, “Plasmonic Nanoprobe of Gold Triangular Nanoprism Core for Real-Time Three-Dimensional pH Imaging of Anterior Chamber” Analytical Chemistry **89**, 2561−2568 (2017).
[4] H. J. Chen, L. Shao, T. Ming, Z. H. Sun, C. Zhao, B. C. Yang, J. F. Wang “Understanding the Photothermal Conversion Efficiency of Gold Nanocrystals,” Small, **20**, 2272–2280 (2010).

Rigorous Analysis and Engineering of Radiation Pattern of Single Emitters in Anisotropic Planar Structure via Coupling to Nanoantenna

Pu Zhang*, Penglong Ren, and Xue-Wen Chen*
School of Physics, Huazhong University of Science and Technology, Wuhan, China
*xuewen_chen@hust.edu.cn

Solid-state single quantum emitters are the key component of several emerging fields, such as quantum nanophotonics, super-resolution imaging, and advanced light emitting devices. The ultimate success of these research fields and applications relies on the emission properties of single emitters, for instance, the emission rate and radiation pattern. Solid-state emitters are necessarily supported in thin film or stratified media, which on one hand provides great opportunies for nanophotonic engineering and on the other hand complicates their emission behavior. While the coupling of single emitters with isotropic nanophotonic structures has been well studied, there are few studies on the emission properties (esp. radiation pattern) of single emitter coupled to anisotropic media. In fact, anisotropic optical environment generally occurs for solid-state quantum emitters [1], such as single organic molecules in single-crystalline matrices (e.g. dibenzoterrylene, DBT, in anthracene) and single defects in hexagnal boron nitride.

In this study, we rigorously examine the influence of anisotropy on the radiation pattern of single emitters and control their emission via coupling to nanoantennas in Anisotropic Planar Structure [2]. To this end, we developed a near-to-far field transformation package for anisotropic and stratified nanophotonic platforms. The stratified system under consideration (Figure 1(a)) consists of multilayers of anisotropic media sandwiched between isotropic cladding and substrate. Quantum emitters and optical antennas are embedded in or situated on the multilayers. The near field from the emitters is first calculated with numerical techniques like finite element method. Then we extract the near field on the boundaries of a box enclosing all the inhomogeneities, and transform them to the far field using a theoretical formulation based on reciprocity theorem [3]. The procedure allows us to predict the influence of anistropy on the far field behavior for a specific DBT in anthracene system as shown in Figure 1(b), where anthracene crystal is biaxially anisotropic [4]. Anthracene has been taken to be either anisotropic or istropic when calculating the back focal plane images (Figure 1(b)). The anisotropy clearly introduces new features in the image, calling for further experimental corroboration.

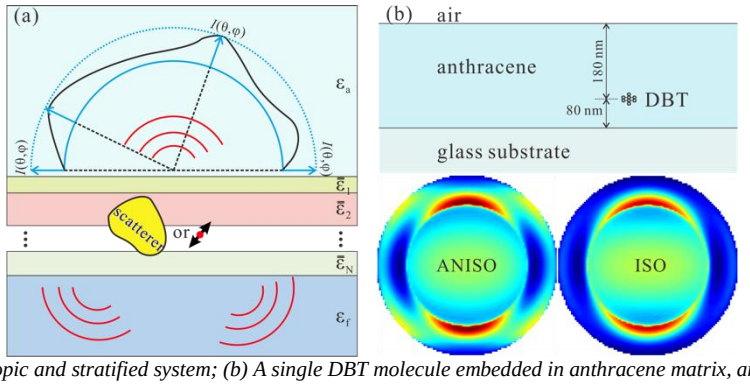

Fig 1. *(a) Anisotropic and stratified system; (b) A single DBT molecule embedded in anthracene matrix, and the back focal plane images calculated when anthracene is taken anisotropic or isotropic.*

Example References

[1] J. A. Schuller, S. Karaveli, T. Schiros, K. He, S. Yang, I. Kymissis, J. Shan, and R. Zia, *Nat. Nanotechnol.* **8**, 271 (2013).
[2] P. Zhang, P. Ren, and X.-W. Chen, manuscript in preparation.
[3] J. Yang, J.-P. Hugonin, and P. Lalanne, *ACS Photonics* **3**, 395 (2016).
[4] M. I. Alonso and M. Garriga, *Thin Solid Films* **455**, 124 (2004).

Suppressing Ohmic loss and enhancing active material absorption in a plasmonic cavity

Jing Zhou, Tao Zhen, Xiaoshuang Chen, Wei Lu

State Key Laboratory of Infrared Physics, Shanghai Institute of Technical Physics, Chinese Academy of Sciences, China

Plasmonic structures are famous for subwavelength light confinement and magnificent field enhancement [1]. Based on that, they have been proposed to enhance light absorption of active materials in small volumes and with low absorptivity [2-3]. Among all the plasmonic structures for this purpose, plasmonic cavities recently received the most attention because of their efficient light coupling, easily tunable resonance, insensitive angle dependence and good compatibility with device structure. However, ohmic loss, as the deadly defect of plasmonic structures, also becomes a big concern in this scenario. In many cases, although the plasmonic structure integrated devices could absorb most of the incident light, a great part is dissipated in the metal instead of the active material [4]. In this work, we propose a photonic approach to reduce the ohmic loss and increase the absorption of the active materials in plasmonic cavities. This approach relies on manipulating the light absorption competition between the metal parts and the active materials, and controlling the light coupling efficiency of the system. Fig. 1 (a) presents a typical plasmonic cavity. At resonance, the system is under the critical coupling condition ($Q_{rad} = Q_{abs}$) so that all the incident power is absorbed either by the active material or by the metal. Although the resonance appears in the mid-IR range, the ohmic loss is still more than 40% of the total power. In order to enhance active material absorption and suppress ohmic loss, increasing the thickness of the active material (h) seems to be a straightforward way, since the ratio of the active material absorption (A_a) to the metal absorption (A_m) is proportional to h [5]. However, simply increasing h could deviate the system from the critical coupling status and results in a decrease of the active material absorption (Fig. 1 (b)). The reason is that Q_{rad} decreases h with while Q_{abs} increases with (Fig. 1 (d)). Therefore, we proposed two practicle methods to compensate the decreasing Q_{rad} during the increase of h: i) switching the resonance from the fundamental order to a higher order; ii) creating abrupt physical boundaries by etching away part of the active materials. By doing these two, the absorption of the active material is enhanced to 80% and the ohmic loss is suppressed to 18% (Fig. 1 (c)). This approach could prominently enhance the performance of a plasmonic cavity integrated quantum well infrared photodetector (QWIP) device (Fig. 1 (e) and (f)). For the conventional configuration, the highest absorption of the QWs is less than 40% of the incident power and the ohmic loss is more than 52% (Fig. 1 (e)). By increasing the layers of the QWs and creating abrupt physical boundaries, the highest absorption of the QWs could be 82% and the ohmic loss lower than 18% (Fig. 1 (f)).

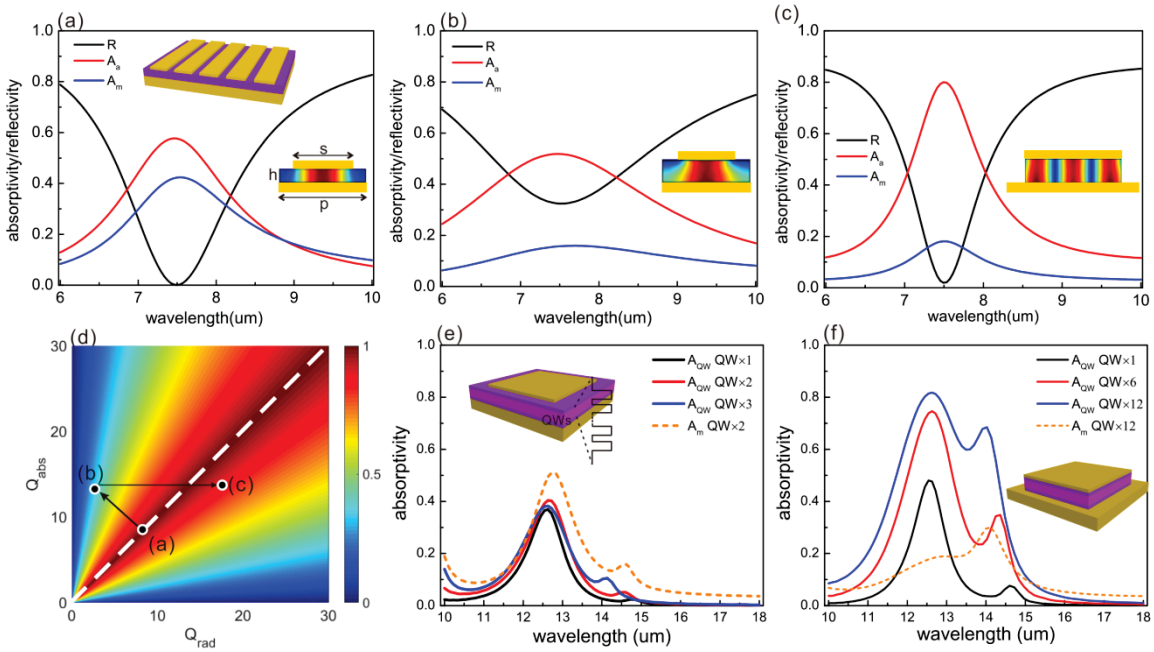

Fig. 1 (a)-(c) Reflection and absorption spectra of the plasmonic cavities with different configurations; the absorption rate of the active material is ~0.2 um^{-1}; the metal is Au. (a) h=0.14 um, p=1.2 um, s=0.8 um, (b) h=0.4 um, p=1.2 um, s=0.53 um, (c) h=0.8 um, p=3.2 um, s=2.78 um; the resonance is switched from the fundamental order to the 3rd order at the same wavelength and abrupt physical boundaries are created. (d) Phase diagram of the on-resonance total absorption versus Q_{rad} and Q_{abs}. (e) Absorption spectra of a conventional plasmonic cavity integrated QWIP. The active material contains 1, 2 or 3 periods of QWs. (f) Absorption spectra of a plasmonic cavity integrated QWIP with abrupt physical boundaries. The active material contains 1, 6 or 12 periods of QWs.

References

[1] W. L. Barnes, et al., Nature **424**, 824–830 (2003).
[2] C.-C. Chang, et al., Nano Lett. **10**, 1704 (2010).
[3] H. Atwater, et al., Nat. Mater. **9**, 205 (2010).
[4] J. Montoya, et al., Opt. Express **25**, 23343 (2017).
[5]J. Khurgin, et al., Nat. Nanotech. **10**, 2 (2015).
[6] C. Qu, et al., Phys. Rev. Lett. **115**, 235503 (2015).

Strong Coupling Between a Quasi-Single Molecule and a Plasmonic Cavity Based on Molecules Trapping in the Blue-detuned Trapping System

Yunfei Zou[1,2], **Qingan Sun**[1,2], **Gang Song**[1,2]

1. *State Key Laboratory of Information Photonics and Optical Communications, Beijing University of Posts and Telecommunications, Xitucheng Road 10, Beijing 100876, China*
2. *Beijing University of Posts and Telecommunications, Xitucheng Road 10,Beijing 100876 ,China.*

We theoretically investigate the strong coupling phenomenon between a quasi-single molecule and a plasmonic cavity based on the blue-detuned trapping system [1]. The trapping system is made up of a metallic nano-hole array, as is shown in Fig.1. Finite-difference time-domain method is employed to simulate the system and the molecule is treated as a dipole in simulations. By calculating the electromagnetic field distributions and the transmission of the proposed structure without and with the molecule, not only can we get the best trapping position in each unit of the trapping system but also can find that there are two splitting peaks in the transmission spectrum in the structure with the molecule and the Rabi splitting is 17 meV [2], while only one peak is observed in the one without the molecule. The working wavelength depends on the lattice constant of blue-detuned trapping system. Hence, we can design blue-detuned trapping system to achieve the strong coupling according to the resonant wavelength of the molecule. We theoretically provide a new way to realize the strong coupling between a single quasi-single molecule and a plasmonic cavity, which has potential applications in quantum information processing.

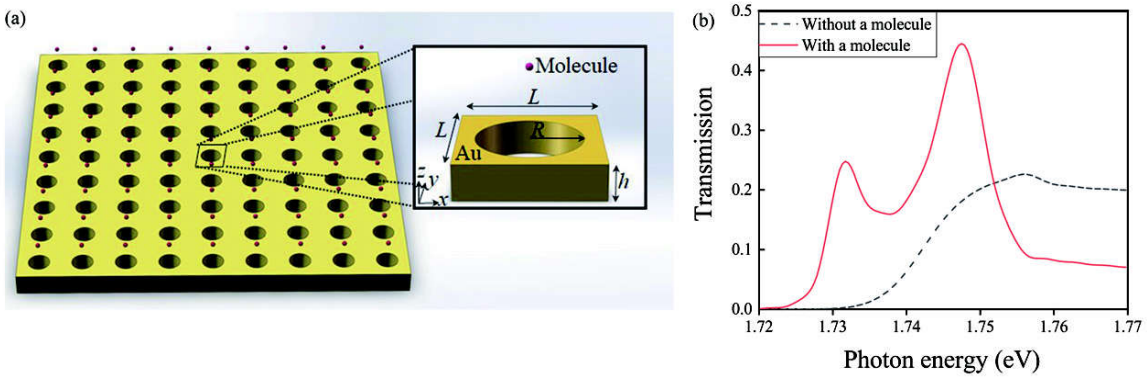

Fig. 1 (a)Schematic diagram of the blue-detuned trapping system (b) Transmission spectra with and without a molecule.

Example References

[1] Grimm, R., Weidemuller, M. and Ovchinnikov, "Optical Dipole Traps For neutral atoms" Adv. At., Mol., Opt. Phys. 42, 95–169 (2000).
[2] Törmö, P. and Barnes, W. L. "Strong coupling between surface plasmon polaritons and emitters: A review. " Reports Prog. Phys. 78, 13901 (2015).

Strain Induced Terahertz Modulation in Nanogap

Bamadev Das[1], Jeeyoon Jeong[1], Bidhek Thusa[1], Hyunwoo Park[2], Om Krishna Suwal[1], Hyeongtag Jeon[2], Dai Sik Kim[1]

1. *Department of Physics and Center for Atom Scale Electromagnetism, Seoul National University, Seoul 08826, Republic of Korea*
2. *Division of Materials Science and Engineering, Hanyang University, Seoul 04763, Republic of Korea*

The technological innovation in the terahertz(THz) frequency range i.e. from 0.1-3 THz is taking place at a rapid speed due to its applications in imaging, medical diagnosis, defense and security, and high bandwidth communication [1]. Moreover, with help of advanced patterning techniques, it is possible to confine THz radiation to subwavelength metallic nanostructures, thereby enabling study of nanoscale [2-5]. Although there are tremendous technological advancements in THz generation and detection, research on modulation, control and tuning of the THz radiation with external stimuli such as mechanical strain, voltage, and/or by using functional material is still lagging behind.

Here, we report modulation and tuning of terahertz radiation in nanogaps by means of mechanical strain. The nanogap arrays of width 12 nm and 60 nm are fabricated by atomic layer lithography technique [5] on flexible substrates i.e. PET (polyethylene terephthalate). Also, a microngap sample is fabricated by using simple photolithography in order to compare the strain effect with nanogap sample. THz-time domain spectroscopy is used to measure THz transmission amplitudes in the nanogaps and the microngap with applied strain of -0.8% (compressive strain) to +0.8% (tensile strain). We observe a strong increase (decrease) in transmission as the tensile (compressive) strain is applied to the 12 nm gap sample, which amounts to a huge modulation depth of 350%. Moreover, a strong 60% change in resonance peak position is observed with respect to tensile strain. But there is no change in transmission amplitude and resonance peak for the microngap with respect to the same amount of strain. The changes in both the transmission amplitude and resonance peak are attributed to the change in the gap width under applied strain.

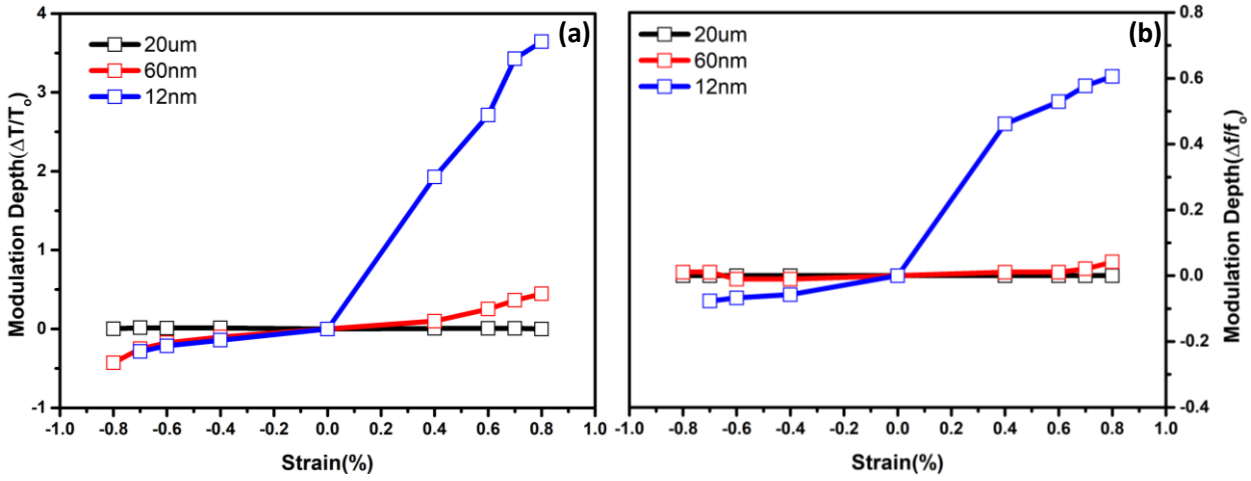

Fig. 1 (a) Measured THz Transmission amplitude modulation depth, (b) measured resonance peak modulation depth with different applied strain.

[1] Editorial, "Terahertz optics taking off," Nat. Photon. **665**, 7 (2013).
[2] J. H. Kang, D. S. Kim, and M. Seo, "Terahertz wave interaction with metallic nanostructures," Nanophotonics **7,** 763-793(2018).
[3] G. C. Choi, Y. M. Bahk, T. Kang, Y. Lee, B. H. Son, Y. H. Ahn, M. Seo, and D. S. Kim, "Terahertz nanoprobling of semiconductor surface dynamincs," Nano Lett. **17,** 6397-6401(2017).
[4] Y. J. Jeong, S. Han, J. Rhie, J. S. Kyoung, J. W. Choi, N. Park, S. Hing, B. J. Kim, H. T. Kim, and D. S. Kim, "A vanadium dioxide metamaterial disengaged from insulator-to-metal transition," Nano lett. **15**, 6318-6323(2015).
[5] X. Chen, H. R. Park, M. Pelton, X. Piao, N. C. Lindquist, H. Im, Y. J. Kim, J. S. Ahn, K. J. Ahn, N. Park, D. S. Kim, and S. H. Oh, "Atomic layer lithography of wafer scale nanogap arrays for extreme confinement of electromagnetic waves," Nat. Commun. **4**, 2361(2013).

Dynamic Plasmonic Color Generation Based on Phase Transition of Vanadium Dioxide

Fang-Zhou Shu[1], Yue Xu[1], Li-Heng Zhang[1], Bo Xiong[1], Ren-Hao Fan[1], Ru-Wen Peng[1], and Mu Wang[1]

[1]National Laboratory of Solid State Microstructures, School of Physics, and Collaborative Innovation Center of Advanced Microstructures, Nanjing University, Nanjing 210093, China

Plasmonic color filtering and color printing have attracted considerable attention in recent years due to their supreme performance in display and imaging technologies. Although various color-related devices are designed, so far very few studies have touched the topic of dynamic color generation. In this article, dynamic color generation is demonstrated by integrating plasmonic nanostructures with vanadium dioxide based on its tunable optical properties through insulator–metal transition [1]. Periodic arrays of silver nanodisks on a vanadium dioxide film are fabricated to realize different colors, relying on the excitation of localized and propagating surface plasmons, and Wood's anomaly. By tuning spatial periodicity of the arrays and diameter of the silver nanodisks, various colors can be achieved across the entire visible spectrum. Further, using insulator–metal transition of vanadium dioxide, the colors can be actively tuned by varying temperature. The approach of dynamic color generation based on the phase transition of vanadium dioxide can easily realize diverse color patterns, which makes it beneficial for display and imaging technology with distinct advantages of multifunctionality, flexibility, and high efficiency.

References

[1] F. Z. Shu, F. F. Yu, R. W. Peng, Y. Y. Zhu, B. Xiong, R. H. Fan, Z. H. Wang, Y. M. Liu, and Mu Wang, "Dynamic plasmonic color generation based on phase transition of vanadium dioxide", Adv. Optical Mater. **6**, 1700939 (2018).

High Efficient Perovskite Photovoltaic Devices through Nanophotonic Light Trapping

Mingzhu Li*, Yang Wang and Yanlin Song
Key Laboratory of Green Printing, Institute of Chemistry, Chinese Academy of Sciences, Beijing 100190, P. R. China.

Perovskite material is a hybrid inorganic-organic direct-bandgap semiconductor. It is of great promise for perovskite solar cells and photodetectors as a light harvester. High-quality perovskite thin films are formed at room temperature, which show great advances for fabricating facile photovoltaic (PV) devices. Achieving light-harvesting is crucial for the efficiency of PV devices. We develop a simple and facile strategy to introduce scalable photonic structure into the perovskite active layer of a PV device by utilizing commercial optical discs (CD-R and DVD-R), robust micro pillar arrays, and highly ordered closed-packed submicrometer spheres. The constructed optical structures on the perovskite active layer realize nanophotonic light trapping by diffraction and effectively suppresses carrier recombination. High photovoltaic performances are achieved. Moreover, the stability of the PSCs is greatly enhanced. It is expected that the photonic-structured perovskite can be an effective approach to improve the photo-electric properties of solar cells, photoelectric detectors, OLED, laser devices and other photoelectric wearable devices.

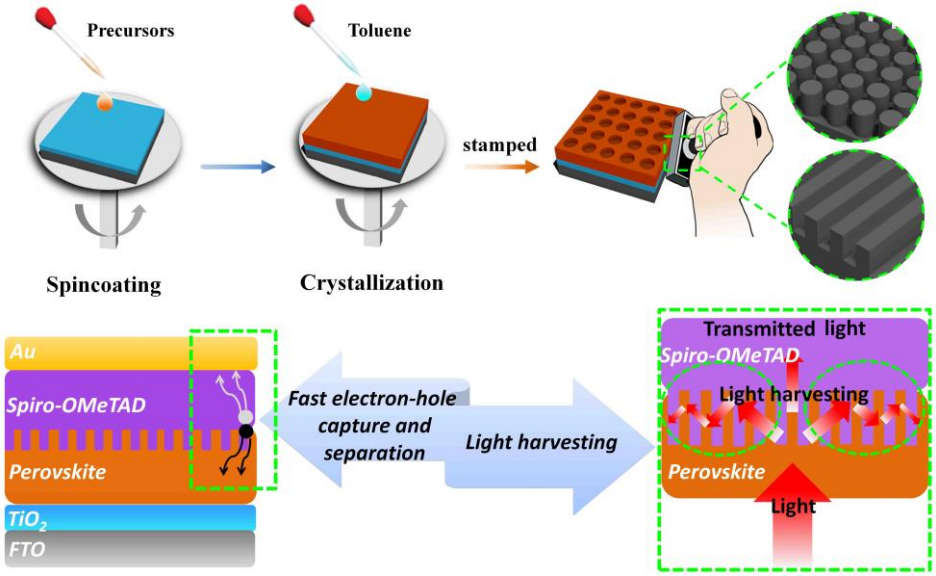

Fig. 1 The imprinted PSCs with light trapping structure to achieve high light-harvesting efficiency.

References

[1] Y. Wang, P. Wang, X. Zhou, C. Li, H. Li, X. Hu, F. Li, X. Liu, M. Li, Y. Song, Diffraction-Grated Perovskite Induced Highly Efficient Solar Cells through Nanophotonic Light Trapping, Adv. Energy Mater., 1702960 (2018).
[2] Y. Wang, M. Li, X. Zhou, P. Li, X. Hu, Y. Song, High efficient perovskite whispering-gallery solar cells, Nano Energy 2018, 51, 556-562 (2018).
[3] M. Li, U. Guler, Y. Li, A. Rea, E. K. Tanyi, Y. Kim, M. A. Noginov, Y. Song, A. Boltasseva, V. M. Shalaev, N. A. Kotov, Plasmonic Biomimetic Nanocomposite with Spontaneous Subwavelength Structuring as Broadband Absorbers, ACS Energy Lett. 3, 1578-1583 (2018).
[4] H. Li, Q. Yang, J. Hou, Y. Li, M. Li, Y. Song, Bioinspired Micropatterned Superhydrophilic Au-Areoles for Surface-Enhanced Raman Scattering (SERS) Trace Detection, Adv. Funct. Mater., 1800448 (2018).
[5] Z. Gu, Z. Huang, C. Li, M. Li, Y. Song, A general printing approach for scalable growth of perovskite single-crystal films, Sci. Adv., 4, eaat2390 (2018).
[6] X. Hu, Z. Huang, X. Zhou, P. Li, Y. Wang, Z. Huang, M. Su, W. Ren, F. Li, M. Li, Y. Chen, Y. Song, Wearable Large-Scale Perovskite Solar-Power Source via Nanocellular Scaffold, Adv. Mater. 29, 1703236 (2017).

Nature Conference on Nanophotonics and Integrated Photonics 2018

Independent linear dual-polarization terahertz focusing at a composite multifunctional metasurface

Wei Kou[1], **Yaxin Zhang**[1]

1. University of Electronic Science and Technology of China, Chengdu 610054, China

Metasurface, a 2D version of metamaterials, enables devising of amplitude, phase, and polarization via a thin layer of unit cells with different shapes and structures, thus opening up new phenomena and ultrathin optical devices. Phase is one of the basic characteristics of an electromagnetic (EM) wave, whose transition is an accumulation effect along the propagation path. With the ability to generate a spatial phase variation, optical wavefronts can be manipulated [1–3].

Conventional lenses based on the phase accumulation along the optical path are often bulky and heavy, imposing a significant challenge on their integration with other optical devices. metasurface-based lenses offer an opportunity to overcome these limitations. To realize the focusing functionality by metasurface, it is crucial to employ a group of unit elements that support phase shift covering a nearly 2 π range. Ultrathin lenses based on metasurface have already been demonstrated using 2D V-shaped or C-shaped antennas to achieve a spot of focus. Aiming at achieving a meta-len in possession of two different focal lengths under a normal incidence of an x-polarized or y-polarized wave, we proposed a composite multifunctional metasurface enabling independent linear dual-polarization terahertz focusing for efficient terahertz wave control. Due to sensitive response of two orthogonal electric dipoles to polarization direction of electromagnetic wave, two layers composite cruciform structures are adopted by each unit cell of the proposed metasurface, which enables efficient terahertz wave control of phase distributions in both vertical and horizontal directions.

The entire schematic is shown in figure 1(a), two different focal lengths can be achieved under a normal incidence wave with different polarization. The one focal length is 1.2 cm under normally incident plane wave with x polarization while another focal length is 4.4 mm under y-polarized component. Numerical simulations of focusing results are illustrated in Figure 1 (b) ~ (d). This design delivers a promising composite multifunctional metasurface for potential applications in optical devices such as focusing, imaging and holography.

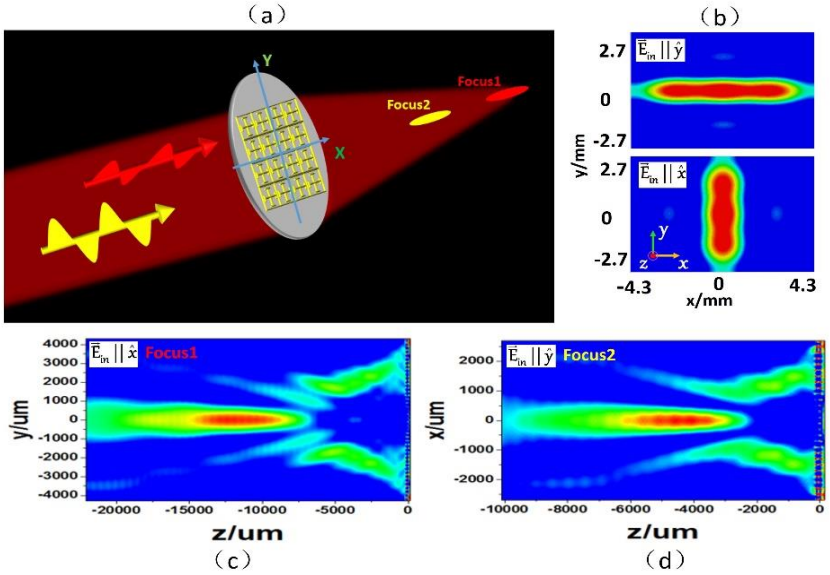

Fig. 1 (a) A schematic of composite multifunctional metasurface. (b) Simulated electric field distributions under a normal incidence wave with different polarization. (c) Simulated 1.2cm focal length under the x-polarized wave. (d) Simulated 4.4mm focal length under the y-polarized wave.

References

[1] N. Yu, P. Genevet, M. A. Kats, F. Aieta, J. P. Tcetienne, F. Capasso, and Z. Gaburro, "Light propagation with phase discontinuities: generalized laws of reflection and refraction," Science 334(6054), 333–337 (2011).

[2] X. Ni, N. K. Emani, A. V. Kildishev, A. Boltasseva, and V. M.Shalaev, "Broadband light bending with plasmonic nanoantennas," Science 335, 427 (2012).

[3] X. Ding, F. Monticone, K. Zhang, L. Zhang, D. Gao, S. N. Burokur, A. de Lustrac, Q. Wu, C. W. Qiu, and A. Alù, "Ultrathin pancharatnam-berry metasurface with maximal cross-polarization efficiency," Adv. Mater. 27(7), 1195–1200 (2015).

Green synthesis and characterization of graphene quantum dots prepared from D-xylose

Xinyu Chai[1, 2], Hanhan Fan[1, 2], Xiheng Kang[1, 2], Hui He[1, 2], Xueping Song[1, 2*]

1. College of Light Industry and Food Engineering, Guangxi University, Nanning, 530004, PR China
2. Guangxi Key Laboratory of Clean Pulp & Papermaking and Pollution Control, Nanning 530004, PR China

Carbon quantum dots (CDs), as a new promising nanophotonics material, have attracted tremendous attentions, compared with traditional quantum dots [1]. CDs perform unique fluorescence properties, such as low cytotoxicity, stability, and excellent biocompatibility. And varieties of potential applications are unfolded for CDs, including photo-catalysis, bio-imaging, fluorenscent probing, and drug delivery [2]. In this research, we reported a green and facile one-pot method for the preparation of blue fluorescence CDs, and investigated their formation mechanism. D-xylose was dissolved in pure water and heated to different temperatures (165 ℃, 170 ℃, 175 ℃, 180 ℃, 185 ℃, 190 ℃) in a reactor. Then the dissolving solution was cooled in an ice water bath, throughout centrifugation and dialysis, and the CDs was obtained and collected for further investigate. The CDs were characterized by Transmission electron microscopy (TEM), UV-Vis, and fluorescence spectrophotometer, and the D-xylose content was measured by high performance liquid chromatography (HPLC). Results were shown in Fig.1 (a), the content of D-xylose was decreased with the increase of temperature, from 13.18 g/L to 10.53 g/L. The TEM images in Fig.1 (b) revealed that the prepared CDs were monodisperse and spherical shape, and the diameter of CDs were less than 10 nm. The results indicated that the CDs had good water solubility. In UV-vis spectrum of Fig.1 (c), a strong absorption peak was existed at 203 nm suggested π-π* transition, and a characteristic peak at 275 nm was determined the n-π*transition, which suggested the existence of poly-aromantic structure. In addition, the photoluminescence spectroscopy (PL) emission of CDs was strongly determined by the excitation wavelength in Fig.1 (d), showing that the maximum emission was red-shifted with the risen of temperature. Moreover, the maximum emission wavelength of CDs were excited at 380 nm when the temperature was below 170 ℃, otherwise the maximum emission wavelength were excited at 450 nm. On the other hand, the UV-vis absorbance peak was invariant whether temperature changed, which suggested that the fluorenscent phenomenon was irrelevant with surface drawback on CDs.

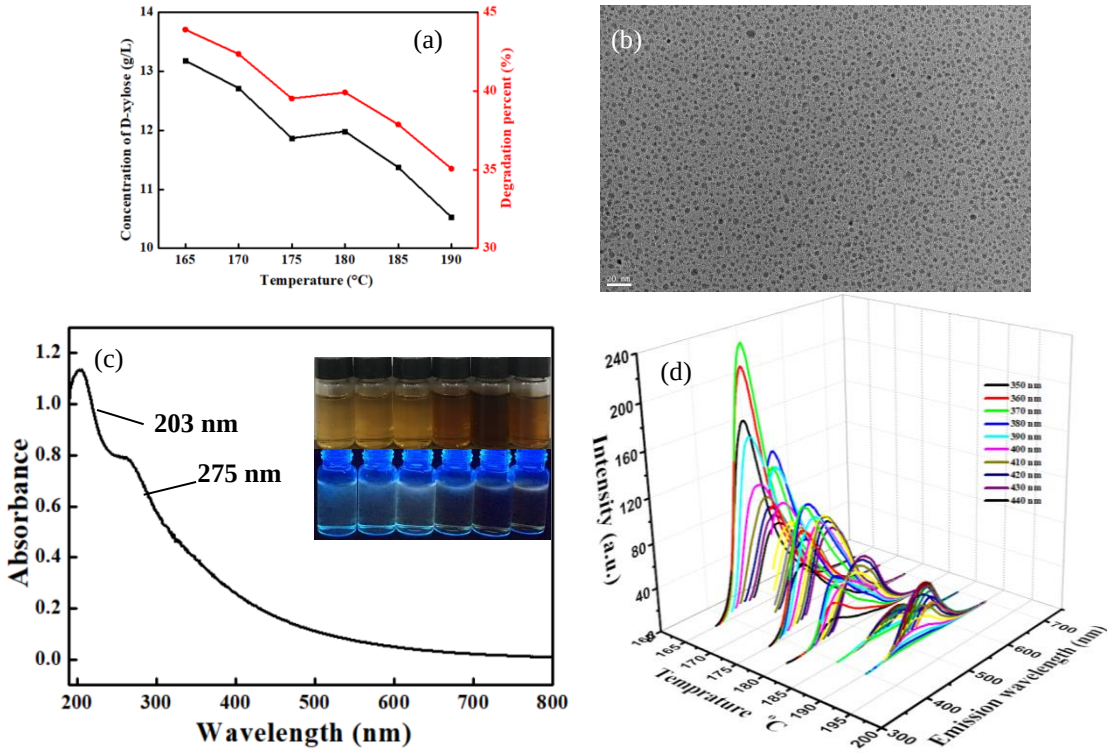

Fig. 1 The residual concentration and the degradation rate of D-xylose during hydrothermal process (a) the TEM image of CDs at 170 ℃ (b), the UV/Vis absorption spectrum at 180 ℃ (c), The PL emission spectra at different temperatures (d).

References

[1] Chen, Wei-Feng, et al. "Green synthesis of graphene quantum dots from natural polymer starch for cell imaging." Green Chem. **20**, 4438-4442(2018).

[2] Liang, Zicheng, et al. "Sustainable carbon quantum dots from forestry and agricultural biomass with amplified photoluminescence by simple NH 4 OH passivation." Journal of Materials Chemistry C **2**,9760-9766(2014).

Precisely Control of Nanoparticles Assembly and Patterning for Three-primary-color Micro-light-emitting Arrays

Zeying Zhang[1], **Yanlin Song**[1]*

1. Institute of Chemistry, Chinese Academy of Sciences, Zhongguancun North First Street 2, Beijing100190, China

Precise assembly of functional nanoparticles is an effective approach to fabricate optoelectronic devices.[1] The conventional methods rely on controlling specific interparticle interaction, the wettability among particles with substrate, external field, template induced liquid shrinking and so on.[2] Here, we report a strategy combining the template tuned liquid confined space and dewettability of droplets to assemble of nanomaterials. First, with evaporation of solvent, the nanoparticles contained in liquid droplet will assemble and deposit following the three-phase contact line pattern. Then, changing the direction of liquid bridge by using same principle can make nano-particles assembled again and form multi-node networks. Moreover, through research the pillar array of the template, concentrate, temperature, surface tension and contact angle, which have influence on rupture and shrink of the liquid membrane during the secondary assembly, achieving precise control of particles assembly and patterning. Finally, three-primary-color fluorescent nanoparticles can also be integrated by successively printed with retention of their individual photoluminance efficiency (5% variances). Yellow, magenta, cyan and white colors with clearly defined interfaces are achieved to reduce the optical cross-talk effect. Therefore, precise control of well-defined assembly patterns can be achieved. This effective and facile approach shows generality for particles assembly of three-primary-color Micro-light-emitting Arrays, indicating promising applications in flexible electronics, waveguide, light modulator, and so on.

Example References

[1]M. Su, Z. Huang, Y. Huang, S. Chen, X. Qian, W. Li, Y. Li, W. Pei, H. Chen, F. Li* and Y. Song*, Swarm intelligence-inspired spontaneous fabrication of optimal interconnect at the micro/nanoscale, Adv. Mater. **29**, 1605223 (2017).
[2] D. Guo, Y. Li, X. Zheng, F. Li, S. Chen, M. Li, Q. Yang, H. Li, Y. Song*, Programmed Coassembly of One-Dimensional Binary Superstructures by Liquid Soft Confinement, J. Am. Chem. Soc. **140**, 18-21 (2018).

Dramatically Enhanced Photoluminescence from Femtosecond Laser Induced Micro/Nano-Structures on $MAPbBr_3$ Single Crystal Surface

Jun Xing
The Guo China-US Photonics Laboratory, State Key Laboratory of Applied Optics,
Changchun Institute of Optics, Fine Mechanics and Physics, Chinese Academy of Sciences, Changchun 130033, P R China

Jun Xing[1], Weili Yu[1], Chunlei Guo[1,2]
1. Changchun Institute of Optics, Fine Mechanics and Physics, Chinese Academy of Sciences, Changchun 130033, P R China
2. University of Rochester NY 14627, USA

Single crystal perovskites have been used in solar cells, photodetectors, and other devices due to their excellent light absorption and carrier transport characteristics [1]. However, for light-emitting applications, photoluminescence (PL) is usually weak for $MAPbBr_3$ ($MA=CH_3NH_3^+$) single crystals (MBSCs) compared with its polycrystalline counterpart. Therefore, developing novel techniques to process MBSCs with different morphologies for PL-related applications is greatly needed. The current strategies for making perovskite crystals are mostly based on bottom-up method (chemical synthesis and assembling). Here, we demonstrate an easy method to achieve top-down fabrication of MBSCs, i.e., femtosecond laser processing MBSCs surface [2].

We have demonstrated that femtosecond laser pulses can be used to produce a variety of surface morphologies, such as nanoparticles, micro/nano-rods, or networks, on MBSC surfaces by changing the peak laser intensity and the scanning speed. In addition, a significant PL enhancement occurred in the processed region with two orders of magnitude greater under ambient conditions and about three times greater than in nitrogen at room temperature. We assume that this is mainly due to the texture based on photon recycling and light out-coupling mechanism [3], and the passivation of surface recombination centers on MBSC [4]. For processed MBSC, under ambient conditions, its PL intensity maintained 75% after nearly 5 months. This indicates that the femtosecond laser-induced micro/nano-structures can not only achieve dramatically PL enhancement but also survive for a long period of time.

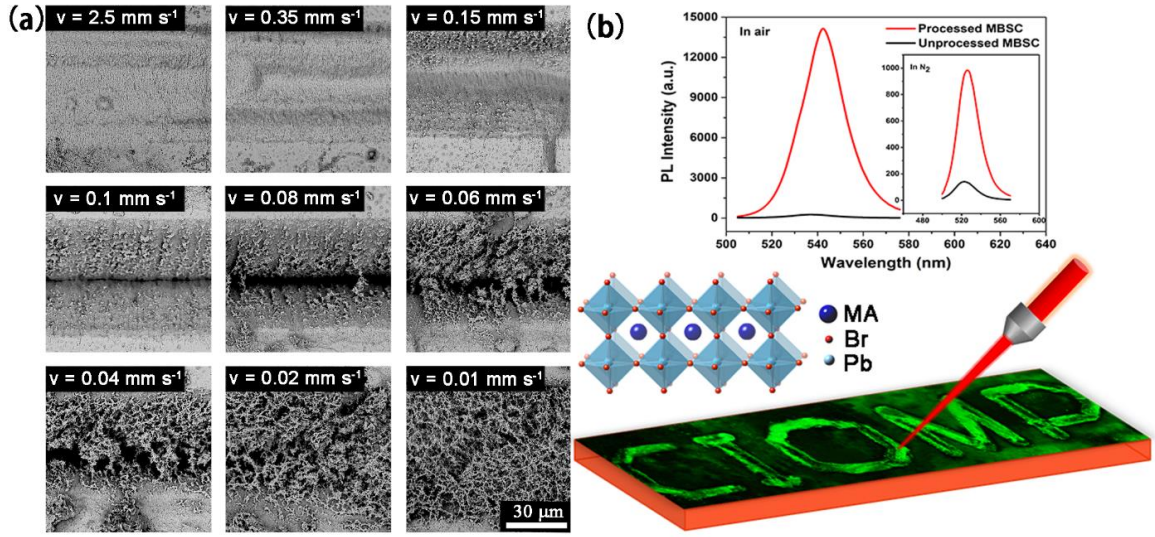

Fig. 1 (a) SEM images of the laser processed regions at different scanning speeds. The peak laser intensity is kept at 2.4 × 10^{12} W cm^{-2} and the scale bar is 30 μm for all images. (b) PL intensity of the MBSC at air and N_2 and the PL image of word "CIOMP". The peak laser intensity is kept at 2.4 × 10^{12} W cm^{-2}, and scanning speed is fixed at 0.2 mm s^{-1}.

This study not only provides a convenient top-down strategy to achieve a range of morphological micro/nano-structures with enhanced PL on MBSC surface, but also paves the way for applications of MBSCs in light emitting or PL imaging devices.

References

[1] Huang J, Shao Y, Dong Q. Organometal Trihalide Perovskite Single Crystals: A Next Wave of Materials for 25% Efficiency Photovoltaics and Applications Beyond?. *J. Phys. Chem. Lett.* ***6***, 3218-3227 (2015).
[2] Vorobyev A Y, Guo C. Direct femtosecond laser surface nano/microstructuring and its applications. *Laser Photonics Rev.* ***7***, 385-407 (2013).
[3] J. M. Richter, M. Abdi-Jalebi, A. Sadhanala, et al. Enhancing photoluminescence yields in lead halide perovskites by photon recycling and light out-coupling. *Nat. Commun.* ***7,*** 13941-13948 (2016).
[4] Fang H H, Adjokatse S, Wei H, et al. Ultrahigh sensitivity of methylammonium lead tribromide perovskite single crystals to environmental gases. *Sci. Adv.* ***2***, e1600534 (2016).

CO_2-Assisted Fabrication of Amorphous Molybdenum Oxide for Enhanced Plasmon Resonances

Wei Liu, Qun Xu, Pengfei Yan

Zhengzhou University, Daxue Road 75, Zhengzhou 450052, China

It is well-known that sufficient free charge carriers can exist in the surface of noble material nanoparticles (e.g., gold and silver) to achieve collective oscillations by light-induced excitations, and this phenomenon is described as surface plasmon resonance (SPR) [1]. It leads to dramatic confinements of optical and electric fields in the vicinity of surface of metallic materials, which is capable of producing various surface effects, such as light-harvesting and surface-enhanced Raman spectroscopy (SERS) [2]. Owing to the nature of noble metals (e.g., electronic structures and free carrier concentrations), their practical applications are limited, especially in applications requiring switching or modulation. Transition-metal oxides (TMOs) are good candidates for SPR, because they have outer-d valence electrons. In research about SPR of TMOs, the used TMOs are crystalline. While amorphous materials are rarely reported owing to limited preparation methods, which impedes comprehensive understanding of their SPR. Therefore, synthesis and fabrication of amorphous TMOs is necessary, although challenging.

Herein, we obtained amorphous molybdenum oxide nanosheets and their quantum dots with assistance of Supercritical CO_2 (sc CO_2). Supercritical CO_2 has been gaining popularity in controlling nanomaterial structure owing to unique characteristics such as the low viscosity, zero surface tension, and high gas-like diffusivity, and it can dissolve materials by adjusting the experimental pressure and temperature. The as-prepared molybdenum oxide nanosheets and the according quantum dots could have sufficient free electrons for tunable plasmon resonances in a wide range of visible and near infrared regions under different illumination time and sc CO_2 pressures, as shown in Fig.1a and b. The stronger interaction of CO_2 and amorphous molybdenum oxide may allow diffusive atomic disordering and achieve stabilization of the amorphous structure. Importantly, compared to the crystal nanosheets, in the biosensing application of these 2D plasmonic nanosheets using bovine serum albumin (BSA) as a model protein, we found the magnitude of plasmon resonance depends on the concentration of BSA (Fig.1c). Moreover, the quantum dots expended remarkable SERS activity with enhancement factor as high as 9.5×10^5 for the detection of methyl blue (MB) at the concentration of 10^{-9} M (Fig.1d). Amorphous molybdenum oxide can supply a platform to quantitative test of cell or organism, and such systems could have a potential for future sensing and optical operation in high precision.

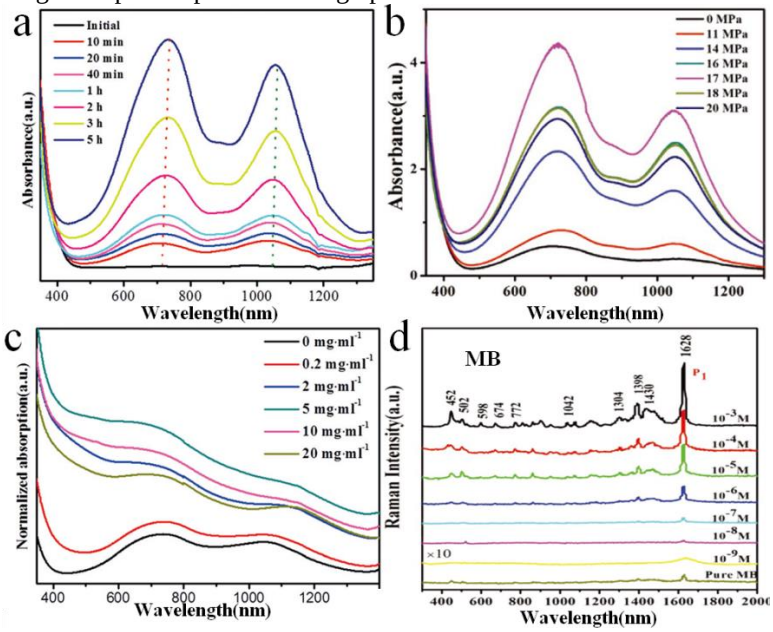

Fig. 1 UV – vis – NIR absorbance spectras of the amorphous nanosheets (a) and quantum dots (b) under different illumination time and sc CO_2 pressures. (c) Normalized absorption spectra of amorphous nanosheets after being incubated with different BSA concentrations for 1 h. (d) Raman spectra of pure MB (10^{-2} M) and quantum dots as an enhancement substrate with different concentrations of MB.

References

[1] J. A. Scholl, A. L. Koh, and J. A. Dionne , "Quantum plasmon resonances of individual metallic nanoparticles," Nature **483**, 421–427 (2012).

[2] S. Linic, U. Aslam, C. Boerigter, and M. Morabito, " Photochemical transformations on plasmonic metal nanoparticles," Nat. Mater. **14**, 567–576 (2015).

THz Ultra-high Q meta-surface based on the tip coupling enhanced FANO resonance

Tianchi Zhou[1], **Bo Zhang**[1]*, **Yaxin Zhang**[1], **Yong Fan**[1]
1. UESTC, No.2006, Xiyuan Ave, West Hi-Tech Zone, Chengdu 611731, China

THz meta-surfaces have great potential for filters, thin-film sensors [1]. To achieve better frequency selectivity, high Q meta-surfaces need to be investigated. FANO surface is always used to reach a relatively higher Q, whose typical value can reach 50 easily [2]. However, it's hard to reach high Q and high resonant intensity at the same time. To solve this problem, we enhanced FANO resonance by strengthen tip coupling in FANO structure and reach a higher Q with high resonant intensity.

The meta-surface applied in this paper is composed of two opposite located crescent-shape arcs. This structure is shaped by elliptical aperture in the center of a circular metallic unit, and split asymmetrically near the middle of the structure.

When the THz wave perpendicularly projects on this meta-surface, the eletrical component of the inicdent wave could induce the FANO and dipolar-like resonances in this strcutre. Different resonance corresponds to various frequency peak in the transmission spectrum. The two arcs work as dipole resonators of different lengths are put together closely and share the same axis, so the transmission characteristic would not only show two independent dipole resonances, but also a high Q FANO resonance. Firstly, the electric field with x-polarization will lead to two different dipolar resonances, one with lower frequency is introduced by the long arc, the other one with higher frequency is introduced by the short one. Secondly, the synergistic effect of the two dipoles would lead to FANO resonance whose frequency lies between the frequencies of the two dipole resonances.

At FANO resonant frequency, charges stack on the tips of dipoles and couple with each other, these unequally stacked charges introduce FANO resonance. To enhance FANO resonance, we make more charges stacking on the tips and strengthened the tip coupling by sharpen the tips. Charges stack at sharp tips, so such structure can get more charges accumulated at the tips, the E field is much stronger and the current is much denser, which caused greater coupling on tips and enhanced FANO resonance. With this enhanced FANO resonance, we can obtain greater Q factor and maintain resonant intensity in an acceptable range.

Simulation results show that we have designed a FANO structure resonate at 420GHz. It reached a Q of 120, doubled compared with classic model whose Q is no more than 50. It's transmission at resonant frequency is less than -20dB, a better value compared other high Q designs whose transmission is more than -10dB [1,2].

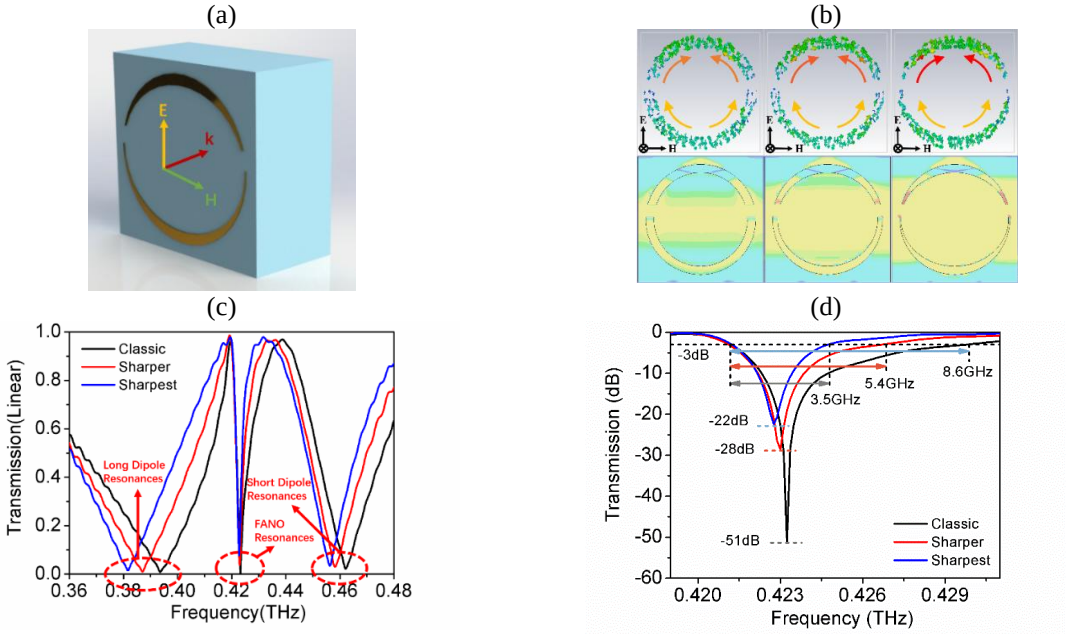

Fig. 1 (a) is the structure of a sharpened FANO design. (b) is the current distribution and E field at resonant frequency of three different tip-sharpness FANO resonators, from left to right are the classic unsharpened model, a tip sharpened model, and the model with sharpest tips. (c) is the S_{21} of the three different tip-sharpness structures (d) is the S21 at FANO resonant frequency of the three different tip-sharpness structures.

References

[1] Christian Jansen, Ibraheem A. I. Al-Naib, Norman Born, and Martin Koch, "Terahertz metasurfaces with high Q-factors," Appl. Phys. Lett. 98, 051109 (2011);

[2] Wei Cao, Ranjan Singh, Ibraheem A. I Al-Naib, Mingxia He, Antoinette J. Taylor, and Weili Zhang, "Low-loss ultra-high-Q dark mode plasmonic Fano metamaterials," OPTICS LETTERS 37, 3366-3368 (2012).

Quantum Teleportation of Surface Plasmon Polariton

Xinhe Jiang, Kaiyi Qian, Peng Chen, Zhaozhong Chen, Xiaosong Ma

School of Physics, National Laboratory of Solid-State Microstructures, Collaborative Innovation Center of Advanced Microstructures, Nanjing University, Nanjing 210093, China

Surface plasmon polaritons (SPPs) are highly confined electromagnetic excitations coupled to electron charge density waves propagating along a metal-dielectric interface. SPP is a promising candidate of integrated photonic devices for both classical [1] and quantum information processing due to their strong subwavelength field confinement [2]. Previously, the quantum nature of surface plasmons has been demonstrated by showing that the entanglement can be preserved during the photon-SPP-photon conversion process [3]. Relevant experiments show that SPPs can be used for manipulating and transmitting the quantum information [4-5]. Today, quantum teleportation has been achieved in laboratories using a variety of different systems, including photonic qubits, nuclear magnetic resonance (NMR), trapped atoms and solid-state systems [6].

Here we experimentally realize the quantum teleportation of surface plasmon. The experimental setup is based on a Sagnac source, which generates polarization-entangled twin photons at a wavelength of 810 nm. One of the photon pairs is sent to Alice for Bell state measurement (BSM) [7]. The other photon is sent to Bob for exciting SPPs. After the SPP is reconverted to photon, the two photons are collected by single-photon counting modules for coincidence measurements. Finally, the quantum state tomography and quantum process tomography are performed. All the results are shown in Fig. 1. We can see that the teleportation fidelity are all above 90% (see Fig. 1d, Insets), exceeding the classical limit of 2/3. The teleportation of the SPP are a quantum process with high fidelity (no sample 91.56±0.02%, with sample 98.59±0.17%).

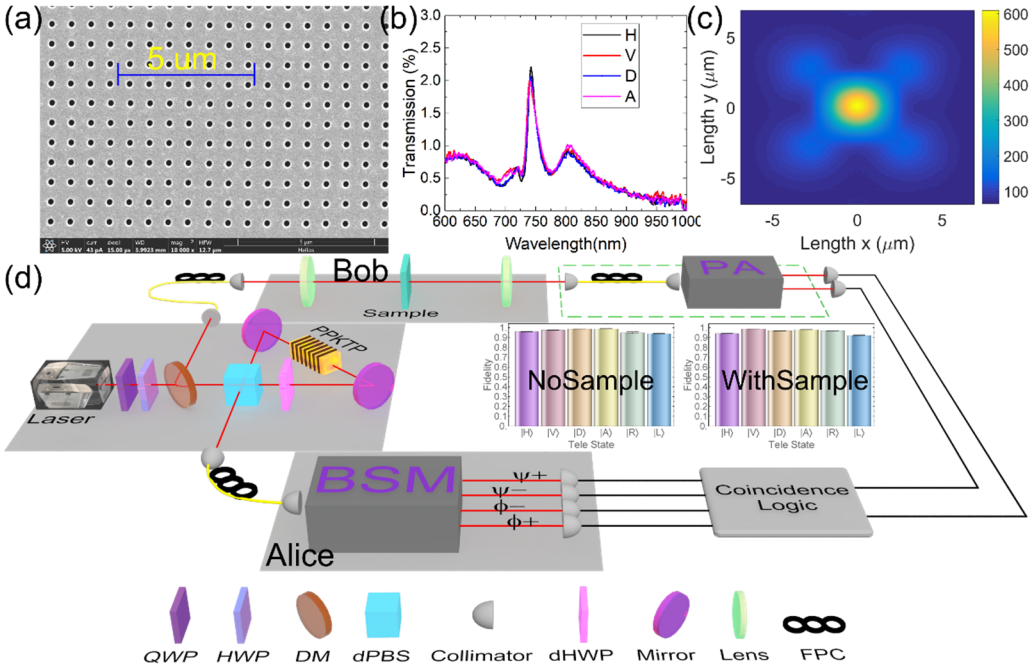

Fig. 1 The sample and experimental setup for quantum teleportation of surface plasmon polaritons. (a) SEM image of the sample. The hole arrays were fabricated with FIB. (b) Transmission spectra of the sample. The peak around 810 nm shows a SPP resonance of (±1, ±1) mode. (c) The SPP mode generated with a horizontal or vertical polarized light. (d) The experimental setup for quantum teleportation of SPPs. Insets are the teleportation fidelity.

Our work shows that hybrid quantum plasmonic-photonic systems is very promising for quantum information processing. Because SPPs have subwavelength confinement, our findings thus pave a new way for them to be utilized in on-chip quantum devices.

References

[1]H. Raether, *Surface Plasmons*, 1rd. ed., (Springer, Berlin, 1988).
[2] M. S. Tame, K. R. McEnery, S. K. Özdemir, J. Lee, S. A. Maier and M. S. Kim, "Quantum plasmonics," Nature Phys. **9**, 329–340 (2013).
[3] E. Altewischer, M. P. van Exter and J. P. Woerdman, "Plasmon-assisted transmission of entangled photons," Nature **418**, 304–306 (2002).
[4] S. Fasel, F. Robin, F. Moreno, D. Erni, N. Gisin and H. Zbinden, "Energy-Time Entanglement Preservation in Plasmon-Assisted Light Transmission," Phys. Rev. Lett. **94**, 110501 (2005).
[5] G. P. Guo, X. F. Ren, Y. F. Huang, C. F. Li, Z. Y. Ou and G. C. Guo, "Observation of two-photon coherence in plasmon-assisted transmission," Phys. Lett. A **361**, 218 (2007).
[6] S. Pirandola, J. Eisert, C. Weedbrook, A. Furusawa and S. L. Braunstein, "Advances in quantum teleportation," Nature Photon. **9**, 641-652 (2015).
[7] D. Boschi, S. Branca, F. De Martini, L. Hardy and S. Popescu, "Experimental Realization of Teleporting an Unknown Pure Quantum State via Dual Classical and Einstein-Podolsky-Rosen Channels," Phys. Rev. Lett. **80**, 1121-1125 (1998).

Gate-tunable Kerr combs in graphene-nitride microresonators

Baicheng Yao[1,2#], Abinav Kuma Vinod[1#], Shu-Wei Huang[1#] Yuan Liu[3,4#], Xiangfeng Duan[3,5], Yunjiang Rao[2], C. W. Wong[1]

1. Mesoscopic Optics and Quantum Electronics Laboratory, University of California, Los Angeles, CA 90095, United States
2. Key Laboratory of Optical Fiber Sensing and Communications (Education Ministry of China), University of Electronic Science and Technology of China, Chengdu 610054, China
3. Department of Materials Science and Engineering, University of California, Los Angeles, CA 90095, United States
4. School of Physics and Electronics, Hunan University, Changsha, China
7Department of Chemistry and Biochemistry, University of California, Los Angeles, CA 90095, United States

Optical frequency combs are cornerstones in modern day frequency metrology, precision spectroscopy and ultrafast optics [1]. The intracavity dispersion – whether in microcavities or fiber cavities – are however hardly amenable to electric-field tunability. Here, combining the cross-disciplinary field of Dirac fermions in two-dimensional graphene, we show for the first time the gated intracavity-tunability of graphene-based optical frequency combs. With the unique linear and massless band structure of graphene [2], we couple the gate-tunable optical conductivity onto a photonic microresonator, modulating its 2nd and 3rd dispersions through the Fermi level. Preserving cavity Q factors up to 10^6 in the graphene-based comb, we implement an ion-gel-gated transistor [3] to tune the electron-hole carrier population for the dynamical and reversible frequency comb control. We uncover the formation of charge-tunable primary comb lines, coherent Kerr frequency combs, controllable Cherenkov radiation, and controllable soliton states – all in a single microcavity. We further demonstrate the voltage-tunable transitions from periodic soliton crystals to crystals with defects, mapped by our ultrafast second-harmonic optical autocorrelation.

Figure 1 shows the major results in our measurements. By using such a graphene-nitride heterogeneous microresonator, we demonstrated optoelectronic control and modulation of Kerr frequency combs via dynamic dispersion tuning. Consequently, both the primary comb lines and the full comb spectra are controllable dynamically, with the on/off switching of the Cherenkov radiation. With control of the graphene Fermi level, we report the first-principle observations of soliton state transition from periodic soliton crystals to crystals with Schottky defects. This first realization of the graphene for ultrafast dynamics and frequency comb formation opens a new architecture at the interface of single atomic layer nanoscience and ultrafast optoelectronics [4].

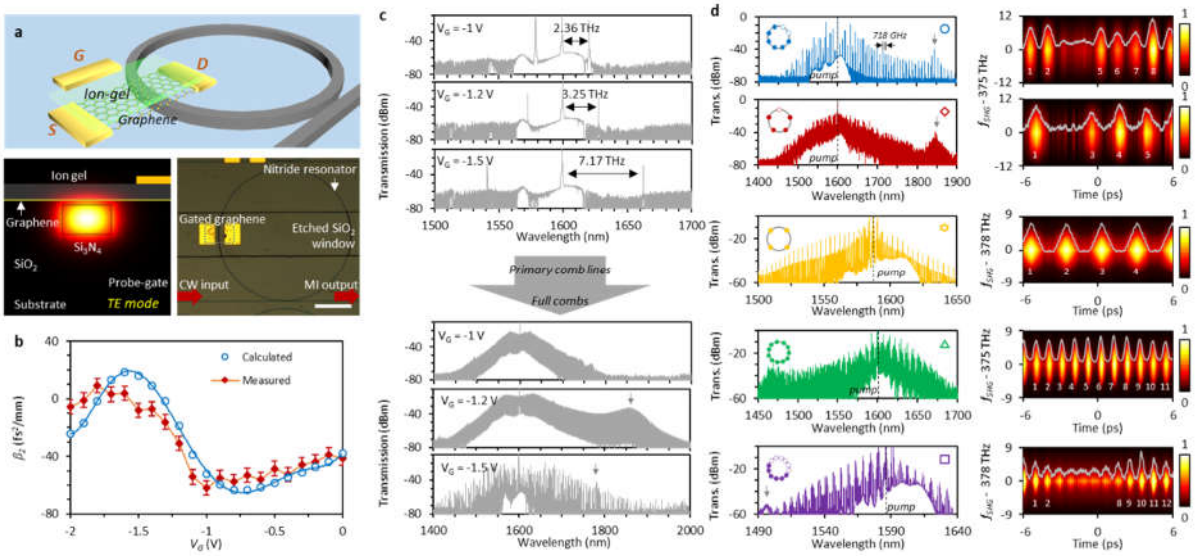

Fig. 1. (a) Device view, scale bar: 50 µm. (b) Measured GVD of graphene based microresonator, ranging from -62 fs^2/mm to 9 fs^2/mm. (c) Gate tuning of the primary and full combs. (c) Corresponding to V_G, observations of the soliton crystals, measured in soliton-steps, spectra, and autocorrelation maps. Pumped by a 2 W continuous-wave laser power, for applied V_G = -1 V, -1.2 V, and -1.5 V, the measured frequency offset between the primary comb line and the pump is observed at 2.36 THz, 3.25 THz, and 7.17 THz respectively. The maximum frequency comb spectra spans over 600 nm at V_G = -1.2 V, with clear Cherenkov radiation. For optimized 2nd and 3rd GVD and TOD via gate tuning, diverse soliton crystal states are achieved. The soliton crystal formation is also akin to harmonic mode-locking where stable high-repetition-rate pulse train can be attained even in longer cavities, and it attracts interests in applications such as high-speed communication and data storage.

References

[1] T. Kippenberg, R. Holzwarth & S. Diddams. "Microresonator-based optical frequency combs." Science **332**, 555 (2011).
[2] F. Bonaccorso, et al. "Graphene photonics and optoelectronics." Nat. Photon. **4,** 611 (2010).
[3] A. Das, et al. "Monitoring dopants by Raman scattering in an electrochemically top-gated graphene transistor." Nat. Nanotech. **3,** 210 (2008).
[4] B. Yao, et al. "Gate-tunable frequency combs in graphene–nitride microresonators" Nature **558,** 410 (2018).

A Silicon-on-Insulator Slab for Topological Valley Transport

Xin-Tao He[1#], **En-Tao Liang**[1], **Jia-Jun Yuan**[1], **Jian-Wen Dong**[1*]

1. Sun Yat-sen University, Xingang Xi Road 135, Guangzhou 510275, China

E-mail: [#]hext9@mail.sysu.edu.cn; [*]dongjwen@mail.sysu.edu.cn

Nanophotonic devices in silicon-on-insulator (SOI) platform can potentially improve the capabilities of modern information-processing systems by replacing some of their electrical counterparts [1]. The discovery of topological photonics provides a new degree of freedom to control the flow of light, enabling novel optoelectronic functionalities and devices [2]. However, the subwavelength strategy at micro-nano scale remains challenge. Recent developments of valley photonic crystals pave an alternative way to achieve SOI topological nanophotonic devices with high performance [3-5]. Last year, we have a theoretical proposal on all-dielectric valley photonic crystals (VPCs) with nonzero valley Chern number by employing valley degree of freedom [5], as well as turn such proposal VPCs into reality by using spoof surface plasmons [6] and all-dielectric rods [7] at microwave region. To retrieve topological valley phase, a general method is to break spatial-inversion (SI) symmetry for accessing opposite Berry curvature profiles near Brillouin zone corners, i.e. K and K' valley. Advanced in nanofabrication techniques, precise manufacture of the SI-symmetry-broken nanophotonic structures is easy to implement nowadays.

In telecommunication wavelength [8], we have realized a VPC in a silicon wafer on the top of silicon dioxide substrate, i.e. silicon-on-insulator slab. Valley-dependent topological edge states operate below the light cone so that the photonic crystal slab can strongly confine the propagating waves in the plane of chip. Benefit from near-quarter-wavelength periodicity, our VPC can develop a high-performance topological photonic device with a compact feature size. We have fabricated flat-, Z- and Ω-shape topological channels. The measured results of these three devices show the flat-top high-transmittance spectra with relatively large bandwidth, even for sharp-bend geometry. Such phenomena give evidences for the observation of topologically robust transport at telecommunication wavelength. Finally, we have experimentally demonstrated on-chip topological photonic routing. Such routing effect is based on the topological chiral channel of VPC. With introducing a subwavelength microdisk to serve as phase vortex generator, the valley-chirality-locked edge state is selectively excited.

The work shows a prototype of on-chip photonic devices, with promising applications for optical isolation, lasing, wavelength division multiplexing, directional antennas, single photon sources, and photonic analog of quantum information processing based on topological nanophotonic modes.

References

[1] H.J. Caulfield and S. Dolev, "Why future supercomputing requires optics," Nat. Photon. 4, 261-263 (2010).
[2] T. Ozawa, H.M. Price, A. Amo, N. Goldman, M. Hafezi, L. Lu, M. Rechtsman, D. Schuster, J. Simon, and O. Zilberberg, "Topological Photonics," arXiv:1802.04173.
[3] T. Ma and G. Shvets, "All-Si valley-Hall photonic topological insulator," New J. Phys. 18, 025012 (2016).
[4] J.-W. Dong, X.-D. Chen, H. Zhu, Y. Wang, and X. Zhang, "Valley photonic crystals for control of spin and topology," Nat. Mater. 16, 298-302 (2017).
[5] X.-D. Chen, F.-L. Zhao, M. Chen, and J.-W. Dong, "Valley-contrasting physics in all-dielectric photonic crystals: Orbital angular momentum and topological propagation," Phys. Rev. B 96, 020202(R) (2017).
[6] Z. Gao, Z. Yang, F. Gao, H. Xue, Y. Yang, J. Dong, and B. Zhang, "Valley surface-wave photonic crystal and its bulk/edge transport," Phys. Rev. B 96, 201402(R) (2017).
[7] X.-D. Chen, F.-L. Shi, H. Liu, J.-C. Lu, W.-M. Deng, J.-Y. Dai, Q. Cheng, and J.-W. Dong, "Tunable light flow control in valley photonic crystal waveguide," arXiv:1805.03404.
[8] X.-T. He, E.-T. Liang, J.-J. Yuan, H.-Y. Qiu, X.-D. Chen, F.-L. Zhao, and J.-W. Dong, "A Silicon-on-Insulator Slab for Topological Valley Transport," arXiv:1805.10962.

Frequency diffraction management through photonic gauge potentials and effective electric-field forces

Chengzhi Qin[1], **Bing Wang**[1], **Peixiang Lu**[1,2]

1. Huazhong University of Science and Technology, Wuhan 430074, China
2. Wuhan Institute of Technology, Wuhan 430205, China

Controlling the spectrum of light is important both in exploring fundamental physics and for practical applications, ranging from high-speed communications, ultrafast spectroscopy to precise metrology. Traditional methods to modify the frequency of light rely on nonlinear optical effects, which, however, are limited by intrinsically low efficiencies and require high pump power. Another possibility to achieve frequency conversion is through temporal modulation, which has raised significant attention recently in the context of non-reciprocal signal propagation [1-3]. Temporal modulation offers the additional advantage of controlling the phase of light through the generation of an effective gauge potential for photons, in direct analogy with how the vector potential changes the phase of electron wavefunction. The gauge potential and associated electric or magnetic fields provide new opportunities to control photons, enabling the realization of photonic Aharonov-Bohm effect [1], photonic quantum Hall effect [2] and non-magnetic optical isolators and circulators [1, 3].

Here in this work, we theoretically and experimentally demonstrate large control over the spectrum of light through photonic gauge potential and effective force in the frequency dimension [4]. We utilize optical phase modulator (PM) to create a discrete frequency dimension through photonic intraband transitions. The phase of index modulation in the PM acts as a photonic gauge potential, leading to the arbitrary control of the central frequency and bandwidth of frequency combs. We experimentally realize 50 GHz spectral shift and three-fold bandwidth expansion, as well as various refraction phenomena, including negative refraction and perfect imaging, both for discrete and continuous incident spectra. As the photonic transition also carries a mismatched wave vector and the phase of modulation exhibits a spatial distribution in the propagation direction, a time-varing gauge potential will emerge, giving rise to a constant and a harmonically oscillating electric-field force in the frequency dimension [5]. Under appropriate combinations of the constant and oscillating forces, we can realize the effects of frequency Bloch oscillations, Super-Bloch oscillations, directional shifting, and dynamic localization. The photonic gauge potential and effective force provide new mechanisms to control the spectrum of light, with potential applications in signal processing and optical communications.

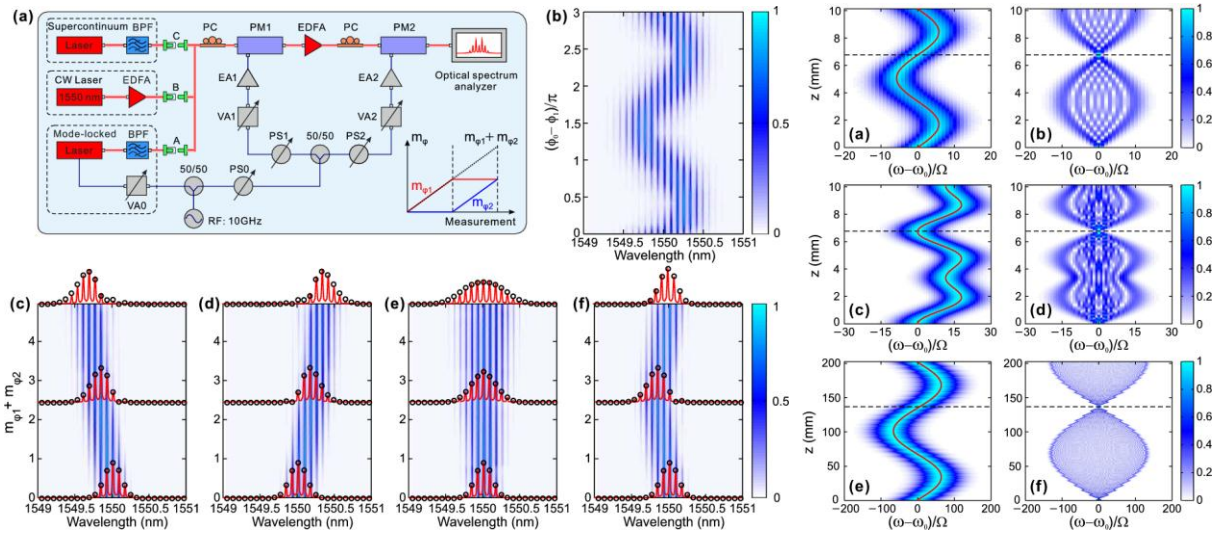

Fig. 1 (1) Experimental setup to realize photonic gauge potentials. (a) Experimental setup. (b) Output spectrum evolution versus the phase difference $\phi_1 - \phi_0$. (c)-(e) Frequency comb evolutions as $\phi_1 - \phi_0 = -\pi/2$, $\pi/2$ and 0. (f) Negative refraction for frequency comb. (2) Spectrum oscillatory motions under the effective electric-field forces. (a)(b) Frequency Bloch oscillations for a frequency comb and a single frequency input. (c)(d) Frequency anharmonic Bloch oscillations under a frequency comb and single frequency input. (e)(f) Frequency Super-Bloch oscillations under a frequency comb and single frequency input.

References

[1] K. Fang, Z. Yu, and S. Fan, Phys. Rev. Lett. **108**, 153901 (2012).
[2] K. Fang, Z. Yu, and S. Fan, Nat. Photonics **6**, 782 (2012).
[3] D. Sounas, A. Alù, Nat. Photonics **11**, 774 (2017).
[4] C. Qin, F. Zhou, Y. Peng, D. Sounas, X. Zhu, B. Wang, J. Dong, X. Zhang, A. Alù, and P. Lu, Phys. Rev. Lett. **120**, 133901 (2018).
[5] C. Qin, L. Yuan, B. Wang, S. Fan, and P. Lu, Phys. Rev. A **97**, 063838 (2018).

Six dimensional light-matter interactions

Yi Xu[1] **Ouyang Xu**[1], **Yaoyu Cao**[2], **Xiangping Li**[2]

1. Department of Electronic Engineering, College of Information Science and Technology, Jinan University, Guangzhou, China
2. Guangdong Provincial Key Laboratory of Optical Fiber Sensing and Communications, Institute of Photonics Technology, Jinan University, Guangzhou, China.

Amplitude, frequency and polarization of light are conventional physical dimensions involved in light-matter interaction[1-4]. Pursuing new physical dimensions that can be synchronously multiplexed with the conventional dimensions for engineering light-matter interaction is of virtue importance for optical information processing [5]. Orbital angular momentum (OAM) of light is regarded as a new dimension of light to twist the light-matter interaction, since the states of an OAM carrying beam are unbounded [5]. The state-of-the-art nanofabrication technologies have enabled the integrated generation [6,7] and transmission multiplexing of twisted light [5,8-10].To date, the multiplexed storage of OAM beam beyond the diffraction limit is a goal not yet achieved.

Herein, we report on the first demonstration of six-dimensional light-matter interaction mediated by structured light and engineered disorder simultaneously [see Fig. 1 (a) for the schematic]. The light-matter interaction between a tightly focus Laguerre-Gauss femtosecond laser pulse and a disorder plasmonic nanoparticle assembly enables the realization of multidimensional optical multiplexing. The plasmonic coupling among metallic nanoparticles mediated by spatial disorder can introduce localization of electromagnetic modes of this system which is manifested as the generation of random distributed hot spots. Such hot spots are sensitive to the topological charge of light which provides the possibility to multiplex utilizing OAM as well as other conventional physical dimensions. At the same time, such OAM sensitive hot spots can also be used to boost up the nonlinear light-matter interaction in such plasmonic system. Our experimental results are shown in Fig. 1 (b), where the colour bars indicate the binary coding. Our results might pave the wave for the manipulation of light-matter interaction in disordered photonic structures.

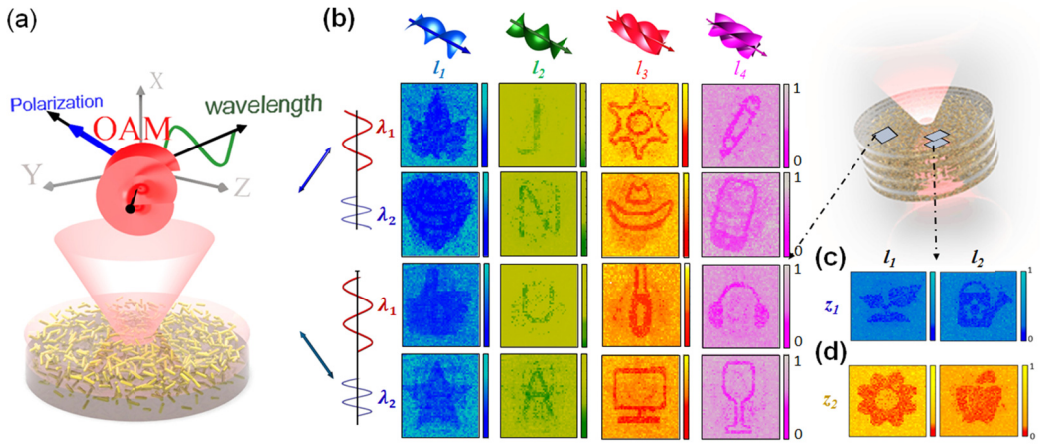

Fig. 1 (a) Schematic of the six dimension light-matter interaction utilizing the OAM, polarization, wavelength of light and three spatial dimensions with disorder nanoparticles. (b) Optical multiplexing of sixteen patterns at the same X-Y location using four OAM states, two wavelengths and two polarizations are used. (c) and (d) are multiplexing using planes with different Z locations. The size of images is 80 x 80 μm^2.

References

[1] M. Gu, X. P. Li, Y. Cao, "Optical storage arrays: a perspective for future big data storage," Light: Sci. Appl., **3**, e117 (2014).
[2] X. Li, T. H. Lan, C. H. Tien and M. Gu, "Three-dimensional orientation-unlimited polarization encryption by a single optically configured vectorial beam," Nat. Commun. **3**, 998 (2012).
[3] J. X. Li, Y. Xu, Q. F. Dai, S. Lan, and S. L. Tie, "Manipulating light-matter interaction in a gold nanorod assembly by plasmonic coupling," Laser Photonics Rev. **10**, 826-834 (2016).
[4] Q. F. Dai, M. Ouyang, W. G. Yuan, J. X. Li, B. H. Guo, S. Lan, S. H. Liu, Q. M. Zhang, G. Lu, S. L. Tie, H. D. Deng, Y. Xu, and M. Gu. "Encoding random hot spots of a volume gold nanorod assembly for ultralow energy memory," Adv. Mater. **29**, 1701918 (2017).
[5] J. Wang, J.-Y. Yang, I. M. Fazal, N. Ahmed, Y. Yan, H. Huang, Y. Ren, Y. Yue, S. Dolinar, M. Tur, A. E.. Willner, "Terabit free-space data transmission employing orbital angular momentum multiplexing," Nat. Photonics **6**, 488-496 (2012).
[6] X. Cai, J. Wang, M. J. Strain, B. Johnson-Morris, J. Zhu, M. Sorel, J. L. O'Brien, M. G. Thompson, S. Yu, "Integrated compact optical vortex beam emitters," Science **338**, 363-366 (2012).
[7] P. Miao, Z. Zhang, J. Sun, W. Walasik, S. Longhi, N. M. Litchinitser, and L. Feng, "Orbital angular momentum microlaser," Science **353**, 464–467 (2016).
[8] N. Bozinovic, Y. Yue, Y. Ren, M. Tur, P. Kristensen, H. Huang, A. E. Willner, S. Ramachandran, "Terabit-scale orbital angular momentum mode division multiplexing in fibers," Science **340**, 1545–1548 (2013).
[9] C. Shi, M. Dubois, Y. Wang, and X. Zhang, "High-speed acoustic communication by multiplexing orbital angular momentum," Proc. Natl. Acad. Sci. **114**, 7250–7253 (2017).
[10] H. Ren, X. Li, Q. Zhang, and M. Gu, "On-chip noninterference angular momentum multiplexing of broadband light," Science 352, 805–809 (2016).

High Numerical Aperture Crystalline Silicon Metalenses and Applications at Visible Wavelengths

Haowen Liang [1,2], Qiaoling Lin [2], Yin Wang[2], Qian Sun[1,2], and Juntao Li [1,2,*].

1 School of Physics, Sun Yat-sen University, No. 135 Xingang-Xi Rd., 510275, Guangzhou, China;

2 State Key Laboratory of Optoelectronic Materials and Technologies, Sun Yat-sen University, No. 135 Xingang-Xi Rd., 510275, Guangzhou, China;

Author e-mail address: lianghw26@mail.sysu.edu.cn, lijt@mail.sysu.edu.cn

Abstract:

Metasurfaces are ultra-thin optical structures relying on the scattering properties of subwavelength scale optical resonators to control the polarization, phase, amplitude and dispersion of light. Among all the metasurface devices, focusing metasurfaces – namely metalenses – are one of the most promising optical elements in terms of applications since the subwavelength nanostructures are able to provide more precise and efficient phase control compared to Fresnel zone plates.

Even though low index materials based on titanium dioxide (TiO_2) and silicon nitride (Si_3N_4) are good candidates to achieve high focusing efficiency and high numerical aperture (NA) metalenses at the visible wavelengths, it hinders the applications of metalenses in different surrounding background due to the small index difference between low index structures and the surrounding materials. Alternatively, high contrast materials, such as amorphous silicon (a-silicon), have been demonstrated to be able to provide high focusing performance in the near infrared range, yet their transmission drops drastically in the visible range due to the high intrinsic losses.

Based on these insights, we now propose and demonstrate a c-Si metalens with high NA and high transmission in the visible range. By using the geometry of nano-bricks in an arrangement determined by the hybrid optimization algorithm (HOA), a very low loss metalens can be realized. As an example, we demonstrate an NA = 0.98 metalens in air with a bandwidth (FWHM) of 274 nm and a focusing efficiency of 67% at 532 nm wavelength, which is close to the transmission performance of a TiO2 metalens. Moreover, and uniquely so, our c-Si metalens can be front-immersed into immersion oil and achieve an ultra-high NA of 1.48 experimentally and 1.73 theoretically, thereby demonstrating the highest NA of any metalens in the visible regime reported to the best of our knowledge.

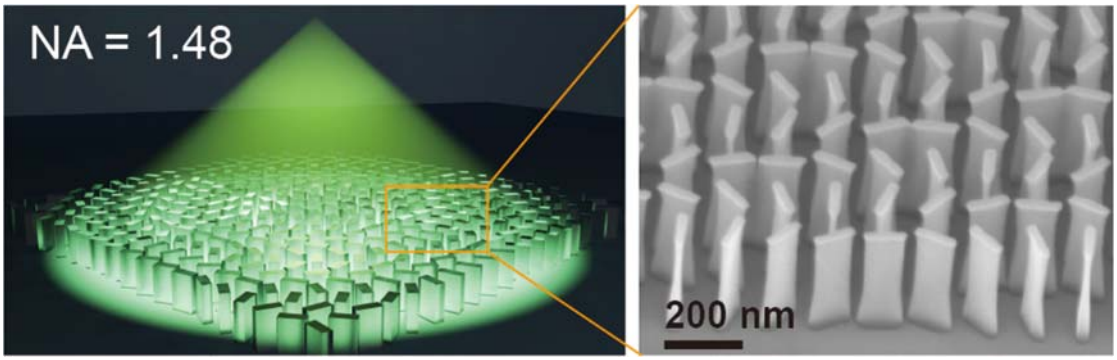

Fig. 1 Schematic show of the metalens and its SEM image.

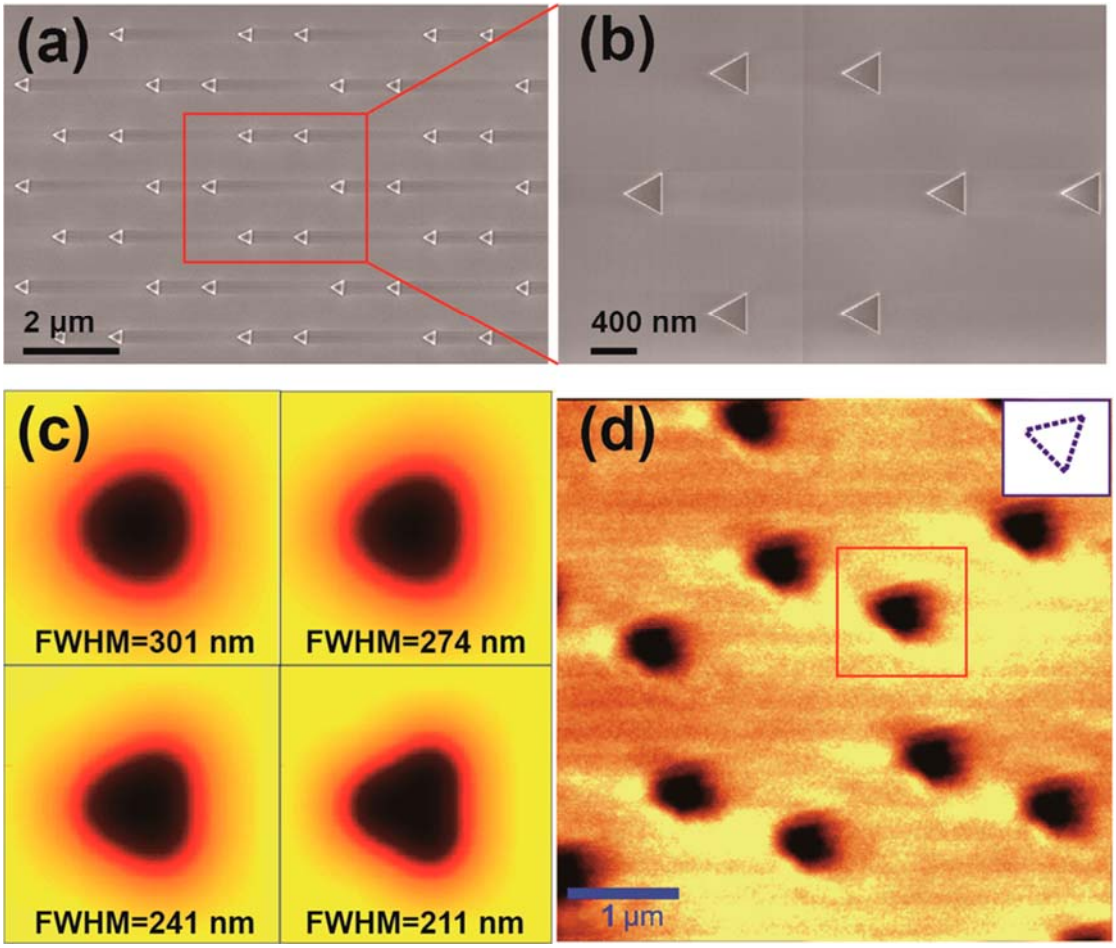

Fig. 2 (a) SEM micrograph of silicon triangles on a sapphire substrate. (b) The magnified image highlights the dimensions, especially the side length of each triangle of 320 nm. (c) The simulation of the same triangle imaged with focal spots of different fwhm. (d) Experimental scanned image using the immersion metalens. The inset shows the orientation of the triangles, and it is possible to determine the orientation. A correlation analysis shows that the experimental image most closely corresponds to the simulation for fwhm = 211 nm.

Reference: Nano Lett. **2018**, 18, 7, 4460-4466.

Dissipative Kerr solitons generation and switching in a thermally controlled micro-ring resonator

Zhizhou Lu
State Key laboratory of Transient Optics and Photonics, Xi'an Institute of Optics and Precision Mechanics (XIOPM), Chinese Academy of Sciences (CAS), Xi'an 710119, China
University of Chinese Academy of Sciences, Beijing 100049, China

Weiqiang Wang[1, 2], Wenfu Zhang[1, 2], Sai T. Chu[3], Brent E. Little[1] Bailing Zhao[1, 2] and Wei Zhao[1, 2]
1. State Key laboratory of Transient Optics and Photonics, Xi'an Institute of Optics and Precision Mechanics (XIOPM), Chinese Academy of Sciences (CAS), Xi'an 710119, China
2. University of Chinese Academy of Sciences, Beijing 100049, China
3. Department of Physics and Materials Science, City University of Hong Kong, Hong Kong, China

Dissipative Kerr solitons (DKSs) generated in a high-Q micro cavities have drawn considerable interests for the possibility of broad bandwidth, chip-scale and low-power consumption operation. Varieties of schemes have been proposed to generate DKSs [1]. Here we apply the auxiliary-lasing-assist method [2], where an auxiliary laser is introduced which is orthogonally polarized and counter-propagating compared with the pump inside the cavity. By simply decreasing and increasing the temperature, generation and switching of DKSs until single soliton state is realized. Using our scheme, single DKS could be deterministically reached from soliton crystal state, which is critical for practical applications.

Figure 1(a) shows the experimental set-up for DKSs generation and switching behaviour. The pump and auxiliary laser are both wavelength-fixed. The micro-ring resonator (MRR) is made of high index doped silica glass with the Q-factor of 2.05×10^6 and radius of ~592.1μm [3], which corresponds to the free spectral range (FSR) of ~49GHz. The power trace possessing couples of steps is shown in Fig. 1(b), each of the steps corresponds to a specific soliton state and the transition of the steps show the soliton switching behaviour. The generated single-soliton spectra is illustrated in Fig. 1(c) where the $sech^2$ fitting (red) suggests obvious Raman induced self-frequency shift (RSFS). It is obvious that the auxiliary comb evolved into secondary comb state. In addition, Cherenkov-radiation induced dispersive waves (DWs) are also observed in our device, which is caused by spatial-mode interaction as shown in Fig. 1(d) where a polarization beam splitter is used to separate the orthogonal-polarized pump and auxiliary comb. The repetition rate of single DKS is ~48.97 GHz.

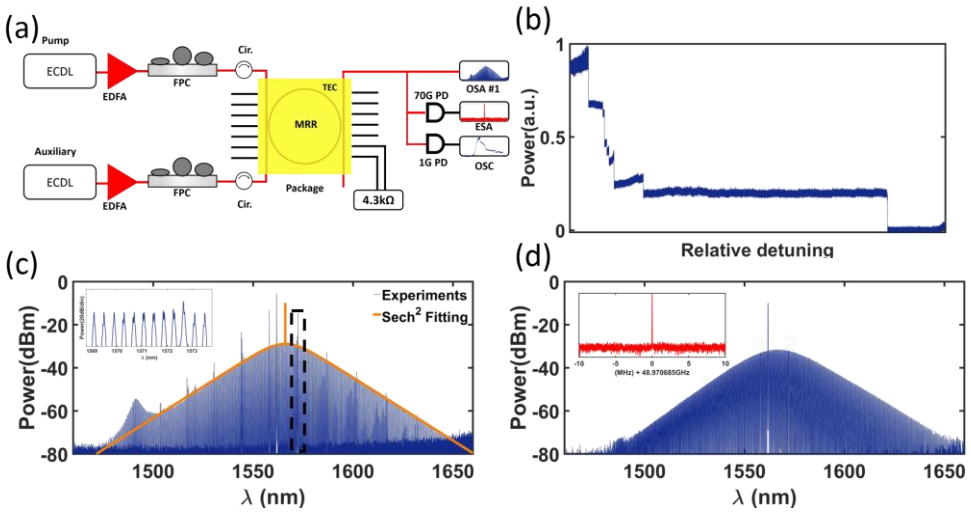

Fig. 1 (a) experimental set up for soliton generation and switching. (b) Power trace inside the MRR, the steps correspond to specific soliton state. (c) Single DKS spectra and $sech^2$ fitting, showing obvious RSFS. The auxiliary laser evolved to secondary comb with sub-comb lines. Inset: zoom-in figure of the comb components. (d) Soliton comb spectra after a PBS. Inset: repetition rate of single DKS.

We believe our work will facilitate the study of soliton interactions inside the MRR, as well as on-chip applications based on this platform.

References

[1] T. J. Kippenberg, A. L. Gaeta, M. Lipson and M. L. Gorodetsky, "Dissipative Kerr solitons in optical microresonators," Science **354**, 567 (2018).
[2] Y. Geng, M. Liao, H. Zhou, B. Wu, and K. Qiu, "Kerr frequency comb dynamics circumventing cavity thermal behavior," in Nonlinear Optics, 2017), NM1A.4..
[3] W. Wang, W. Zhang, Z. Lu, S. T. Chu, B. E. Little, Q. Yang, L. Wang, and W. Zhao, "Self-locked orthogonal polarized dual comb in a microresonator," Photon. Res. **6**, 363-367 (2018).

Integrated quantum memory based on rare-earth ion nanowire

Yu-Bo Xie[1], **Hao Sun**[2], **Ming-Hao Jiang**[1], **Yu-Ping Liu**[1], **Yu-Hui Chen**[3], **Wei Liu**[4], **Xiaomu Wang**[4], **C. Z. Ning**[2], **Xiao-Song Ma**[1]

1. *School of Physics, National Laboratory of Solid-State Microstructures, Collaborative Innovation Center of Advanced Microstructures, Nanjing University, Nanjing 210093, China*
2. *Department of Electronic Engineering, Tsinghua University, Beijing 100084, China.*
3. *School of physics，Beijing institute of technology, Beijing 100081, China.*
4. *School of electronic science and engineering，Nanjing University, Nanjing 210093, China*

Optical quantum memory plays a vital role in quantum networks for long distance quantum communication. Rare-earth ions (REIs) [1-3] doped material is one of the leading candidates for realizing quantum memory. It exhibit excellent coherence properties at low temperature (below 4 K), both for the optical and the spin transitions. Several quantum memory protocols have been implemented, such as electromagnetically induced transparency, Raman interactions, and atomic frequency combs [4]. Moreover, integrated quantum memory can also been made in this REI-doped solids, making it very promising [5].

Here we propose and experimentally demonstrate a novel integrated device for quantum memory based on single-crystal erbium chloride silicate (ECS) [6] nanowire in conjunction with silicon optical waveguide as shown in figure 1 (a). Using a stamping procedure, a 900 nm width ECS nanowire is put on the 25 μm length Si tapper, which adiabatically transform the optical energy between Si waveguide and ECS nanowire. Figure 1 (b) show the electric field of taper region simulated by finite difference time domain method. In figure 1 (c), transmission spectrum measured in 2.4 K and 30mT magnetic field gives a full width at half maxima of 0.536nm and optical depth of 3, corresponding to a large absorption coefficient of 2.1 dB/μm. ECS nanowire also has a short excited-state lifetime of 153 μs measured by TCSPC method as shown in figure 1 (d). It reduces by 2 order of magnitude compared to the lifetime in the low doping crystal, benifitial to quantum initial state preparation. Our work pave the path to the large-scale integrated quantum memory.

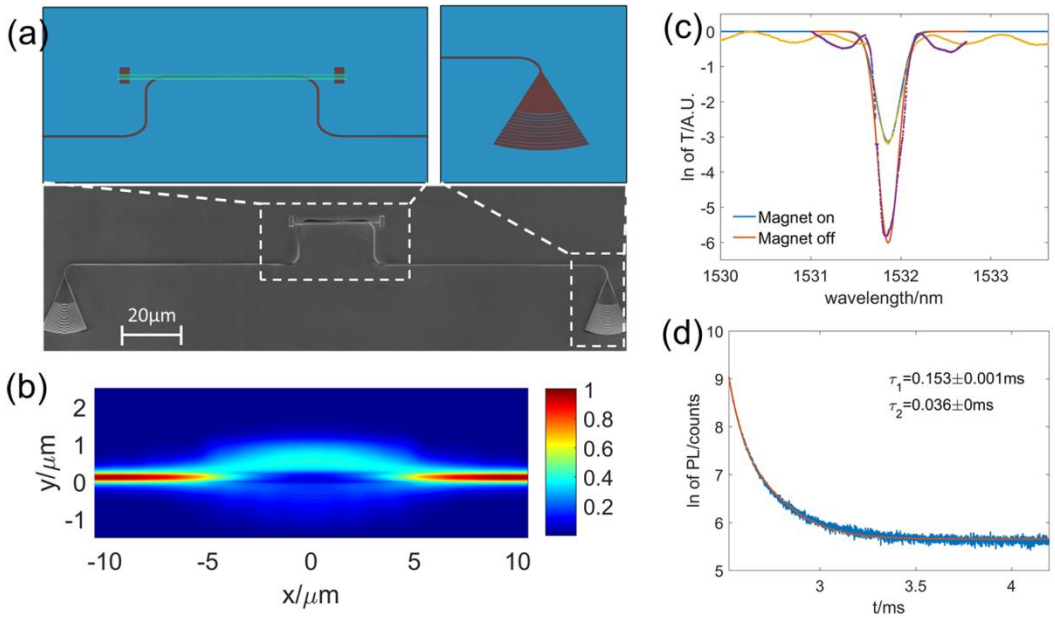

Fig. 1 (a) Scanning electron microscopy image and schematic view of the device. (b) Side view of the mode between ECS nanowire and Si waveguide. (c) Optical spectrum of device with (blue curve) and without (red curve) 30mT magnetic field. (d) Photoluminescence lifetime modelled as $a_1 e^{\frac{\tau_1}{t}} + a_2 e^{\frac{\tau_2}{t}} + b$.

Example References

[1] C. Simon, et al., "Quantum memories-A review based on the European integrated project Qubit Applications (QAP)." Eur. Phys. J. D **58**, 1–22 (2010).
[2] Wolfgang Tittel, Mikael Afzelius, Thierry Chaneli ère, Rufus L. Cone, Stefan Kr öll, Sergey A. Moiseev, Matthew Sellars, "Photon-echo quantum memory in solid state systems." Laser & Photon. Rev. **4**, 244–267 (2010).
[3] Mikael Afzelius, Nicolas Gisin, Hugues de Riedmatten, "Quantum memory for photons." Phys Today **68**, 42-47 (2015).
[4] Hugues de Riedmatten, Mikael Afzelius, Matthias U. Staudt, Christoph Simon and Nicolas Gisin, "A solid-state light–matter interface at the single-photon level," Nature **456**, 773–777 (2008).
[5] A. M. Dibos, M. Raha, C. M. Phenicie, J. D. Thompson, "Atomic Source of Single Photons in the Telecom Band." Phys Rev Lett **120**, 243601(2018).
[6] Hao Sun, Leijun Yin, Zhicheng Liu, Yize Zheng, Fan Fan, Shilong Zhao, Xue Feng, Yongzhuo Li, C. Z. Ning, "Giant optical gain in a single-crystal erbium chloride silicate nanowire." Nat Photonics **11**, 589–593 (2017).

On-chip photonic quantum sources based on silicon waveguides

Lan-Tian Feng,[1, 2] Yang Chen,[1, 2] Zhi-Yuan Zhou,[1, 2] Ming Zhang,[3] Ming Li,[3] Dao-Xin Dai,[3] Guo-Ping Guo,[1, 2] Guang-Can Guo,[1, 2] Mark Tame,[4, 5] and Xi-Feng Ren[*1, 2]

1. Key Laboratory of Quantum Information, University of Science and Technology of China, CAS, Hefei, 230026, People's Republic of China.

2. Synergetic Innovation Center of Quantum Information & Quantum Physics, University of Science and Technology of China, Hefei, Anhui 230026, China.

3. State Key Laboratory for Modern Optical Instrumentation, Centre for Optical and Electromagnetic Research, Zhejiang Provincial Key Laboratory for Sensing Technologies, Zhejiang University, Zijingang Campus, Hangzhou 310058, China.

4. School of Chemistry and Physics, University of KwaZulu-Natal, Durban 4001, South Africa.

5. National Institute for Theoretical Physics (NITheP), KwaZulu-Natal, South Africa.

** Email: renxf@ustc.edu.cn*

Integrated quantum photonics has attracted intensive attention due to the compactness, scalability, and stability. An on-chip photonic quantum source, especially an on-chip entangled photon source, is a basic device for realizing quantum photonic integrated circuits (QPICs) [1].

We first demonstrate that a silicon-on-insulator nanowire can be used to generate frequency-nondegenerate bi- and multiphoton polarization entangled qubits, and directly compatible with the (100 GHz) dense wave division multiplexing communication system [2]. Multiphoton interference and quantum state tomography were used to characterize the quality of the entangled states. Four-photon entanglement states among two frequency channels were ascertained with a fidelity of 0.78. The emission spectral brightness of the four-photon entanglement source reached 340 kHz at the pump power 600 μW. Our work realizes the integrated multiphoton source in a relatively simple pattern and paves a way for the revolution of multiphoton quantum science.

We also experimentally demonstrate frequency-degenerate quantum state generation using two pico-second pulsed lasers in a silicon nanophotonic waveguide. By using a dual-pump SFWM process with a low pump power (several hundred μW), we prepare a series of degenerate quantum states – a product state of two photons, a Fock state of four photons, and multi-photon entangled states of two and four photons. The generation methods we use could be extended to produce more complex states with a higher number of photons, and thus potentially used in on-chip operations for realizing quantum algorithms within integrated photonic circuitry.

Then we report an on-chip transverse-mode entangled photon source via the spontaneous four-wave mixing processes in a multimode silicon waveguide [3]. Transverse-mode entanglement is verified over multiple frequency channels within a bandwidth of 2 THz, and a maximally entangled Bell state is also produced with a fidelity of 0.92. Our entangled photon source is the key element for quantum photonics based on transverse-mode, and enables on-chip quantum information processing within high-dimensional Hilbert space. Furthermore, the transverse-mode entanglement can be converted coherently to path and polarization entanglements, which paves the way to realize highly complex quantum photonic circuits with multiple degrees of freedom.

Example References

[1] Caspani, L. et al. "Integrated sources of photon quantum states based on nonlinear optics" Light Sci. Appl. 6, e17100 (2017).
[2] M. Zhang, et al. "Generation of multiphoton entangled quantum states with a single silicon nanowire" arXiv:1803.01641.
[3] L. T. Feng, et al. "On-chip transverse-mode entangled photon source" arXiv:1802.09847.

Topologically Protected Edge States for Robust Integrated Photonic Devices

Wange Song[1], **Wenzhao Sun**[2], **Shumin Xiao**[2], **Shining Zhu**[1] **and Tao Li**[1*]

[1] *College of Engineering and Applied Sciences, Nanjing University, Nanjing, 210093, China*
[2] *State Key Laboratory on Tunable Laser Technology, Ministry of Industry and Information Technology, Key Lab of Micro-Nano Optoelectronic Information System, Shenzhen Graduate School, Harbin Institute of Technology, Shenzhen, 518055, China*
** Corresponding author: taoli@nju.edu.cn*

Integrated photonic devices usually suffer from structure-sensitive performance, which requires severely very high manufacturing accuracy and strongly prevents the practical applications [1]. Although there have been several approaches proposed to overcome this difficulty, they usually have to sacrifice in other important aspects [2,3]. Fortunately, recent topological photonics provides some robust designs for photon behaviours, e.g., topologically protected edge state (TES) for one-way propagation [4]. It would quite possibly offer us a solution to other optical routings.

In this work, we proposed and demonstrated that robust optical routing (e.g. directional coupler (DC) and splitter) can be achieved utilizing the TES in a Su-Schriffer-Heeger (SSH) [5] modelled optical waveguide array [6]. The robust DC and splitter structures consist of arrays of straight silicon waveguides on alumina chip, as depicted in Figs. 1(a) and 1(b), respectively. Figures 1(c) and 1(d) show the simulated field evolutions in ideal and imperfect DC and splitter with different fluctuation strength *R* (varying from 0 to the 1). The immunity against the structural discrepancies can be clearly seen. The functionality of directional coupling and splitting preserved perfectly with almost unaffected coupling distance. In experiments, we fabricated the corresponding silicon waveguide arrays on sapphire substrate and measured their optical routing properties. The results of DC and splitter are shown in Figs. 1(e) and 1(f), respectively. As have demonstrated that the intentionally introduced discrepancies almost have nothing to do with the routing function, showing the robustness. We additionally analysed another set of samples in conventional DC and splitter design, which behave quite large discrepancy in output signals, indicating the degraded performance of optical routing.

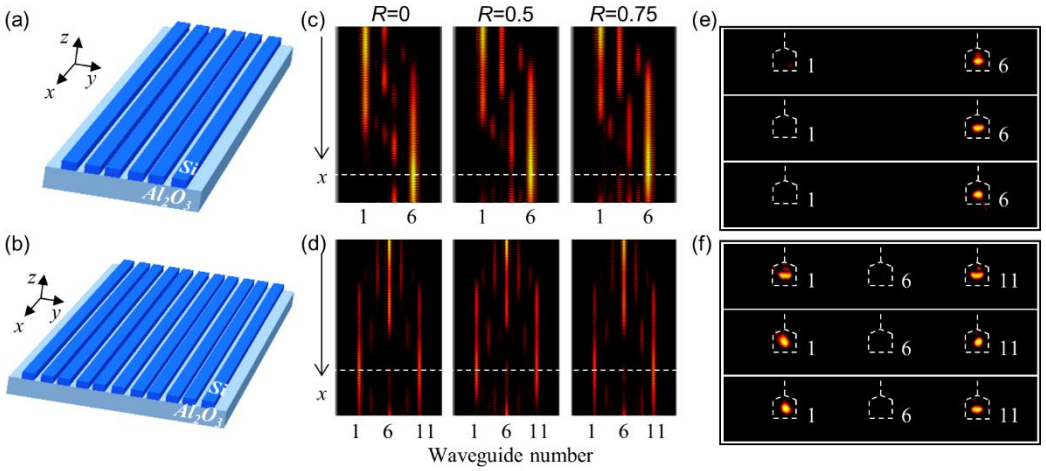

Fig. 1 Schematics of the structures of (a) robust DC and (b) robust splitter. Simulated field intensity in the structures of (c) robust DC and (d) robust splitter with fluctuation strength of R=0, 0.5, and 0.75. Output intensities of (e) robust DC samples and (f) robust splitter samples with structural discrepancy Δd =0nm, 20nm and 40nm (from top to bottom).

On the basis of our topological design, the topological protection leads to more efficient optical routing than for the conventional devices, even in the presence of structural disorders. This work paves the way for integrated photonic devices with stable performances against nanofabrication discrepancy, which could lead to new families of optical structures and devices by exploiting robust optical propagation.

References

[1] D. Dai, Z. Wang, and J. E. Bowers, "Ultrashort broadband polarization beam splitter based on an asymmetrical directional coupler," Opt. Lett. **36**, 2590–2592 (2011).
[2] M. Born, and E. Wolf, *Principles of Optics*, 7th. ed., (Cambridge Univ. Press, Cambridge, UK, 1999).
[3] X. Chen, et.al, "Towards an optical FPGA-Programmable silicon photonic circuits," Preprint at https://arxiv.org/abs/1807.01656 (2018).
[4] T. Ozawa, et al, "Topological photonics," Preprint at http://arXiv.org/abs/1802.04173 (2018).
[5] W. P. Su, J. R. Schrieffer, and A. J. Heeger, "Solitons in Polyaeetylene," Phys. Rev. Lett. **42**, 1698 (1979).
[6] W. Song, et al, "Topological edge states in waveguide array for robust optical routing," unpublished.

Engineered graphene/GaAs van der Waals heterostructures and InAs quantum dots for mode-locked laser

Xu Wang[1], Xiaohui Li[2], Jiqiang Ning[1], Kai Zhang[3], and Ziyang Zhang[1]

1. Key Laboratory of Nanodevices and Applications, Suzhou Institute of Nano-Tech and Nano-Bionics, CAS, Suzhou 215123, China.

2. School of Physics and Information Technology, Shaanxi Normal University, Xi'an 710062, China.

3. i-Lab, Suzhou Institute of Nano-Tech and Nano-Bionics, CAS, Suzhou 215123, China

Van der Waals (vdW) heterostructures formed by graphene and III-V semiconductors hold great promise for high performance optoelectronic devices such as solar cells, photodetectors, and light emitting diodes because of the outstanding light harvesting enhancement and an efficient rectifying behavior [1]. However, the work utilizing the graphene/III-V semiconductor vdW heterostructures as saturable absorber (SA) to improve the mode-locked characteristic for ultrafast photonic applications is still lacked. Although graphene has been successfully used as an effective SA for ultrashort pulse generation due to its ultrafast carrier dynamics and remarkable nonlinear optical properties, its low damage threshold dramatically hamper the applications.

Self-assembled InAs/GaAs quantum dots (QDs), as a mature technique, has been successfully employed in high performance laser diodes, photodetectors, and superluminescent light emitting diodes due to precisely customized parameters and great reproducibility [2]. InAs/GaAs QDs-based semiconductor saturable absorber mirrors (SESAMs) offer many potential advantages for ultrashort pulse laser because of extremely broad gain bandwidths and fast carrier dynamics in comparison with commercial quantum well-based SESAMs. However, the operating wavelength of the InAs/GaAs QD-based SESAMs is in the range of ~1-1.3 μm, while it is still a huge challenge to fabricate a high performance SESAMs working at the wavelength of 1.55 μm. Following the introduction of a strained InGaAs cap layer to reach 1.3 μm, the even higher In content in QD cap layer are logically merely required. However, high In content in the QDs and the surrounding matrix very readily leads to non-radiative recombination centers which rapidly degrade the crystal and optical quality of the QDs, making this QD device unsuitable for application.

In this paper, for the first time, we describe the development of a SA comprised of graphene/short-period superlattice (SSL)/QD vdW heterostructure fabricated by graphene layer coating onto the SSL capped InAs/GaAs QD SA as shown in Fig. 1(a). In comparison with general InGaAs strain reducing layer, the $(In_xGa_{1-x}As/\ In_yGa_{1-y}As)_n$ SSL layer provides a uniform In distribution and lower In content. Significant improvements in pulse width, threshold, average power and stability are all exhibited in a mode-locked Er doped fiber laser based on the above engineered SA. Fig. 1(b) presents the autocorrelation trace of the optical pulse for the mode locking with the hybrid SA. Both theoretical calculations and experimental results demonstrate that in graphene/SSL/QD vdW heterostructure, graphene acts as an light funnel to enhance photon carrier generation, SSL serves as a carrier distributer and reservoir, and QD plays a role as the final absorption, enabling a strong interlayer coupling effect in comparison with separated InAs/GaAs QD SA, graphene, or graphene/QD vdW heterostructure as shown in Fig. 1(c). This graphene/low dimensional III-V semiconductor vdW heterostructure may thus represent a pathway towards the application of all-optical clocking recovery, optical frequency, and coherent optical communication systems.

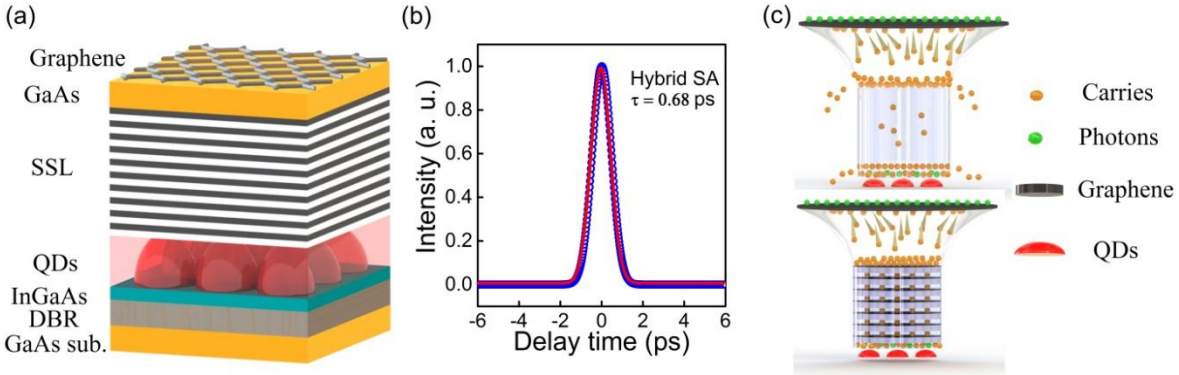

Fig. 1(a) Schematic illustration of graphene capped SSL/QD vdW heterostructure SAs. (b) autocorrelation trace of the optical pulse for the mode locking with the single layer graphene capped SSL/QD vdW heterostructure SA. (c) Schematic diagram showing photo-generated transitions in graphene capped QD vdW heterostructure.

References

[1] S. Wang, D. Scarabelli, L. Du, Y. Y. Kuznetsova, L. N. Pfeiffer, K. W. West, G. C. Gardner, M. J. Manfra, V. Pellegrini, S. J. Wind, and A. Pinczuk, "Observation of Dirac bands in artificial graphene in small-period nanopatterned GaAs quantum wells," Nature Nanotech. **13**, 29-33 (2018).

[2] Z. Y. Zhang, R. A. Hogg, X. Q. Lv, Z. G. Wang, "Self-assembled quantum-dot superluminescent light-emitting diodes," Adv. Opt. Photonics **2**, 201-208 (2010).

Entangled qutrits on a silicon chip

Lijun Xia[1], Zhiyu Chen[1], Tonghua Yu[1], Leizhen Chen[1], Yin Pan[2], Liangliang Lu[1], Xinlun Cai[2], XiaoSong Ma[1]

[1]*School of Physics, National Laboratory of Solid-state Microstructures,Collaborative Innovation Center of Advanced Microstructures, Nanjing University, Nanjing 210093, China*

[2]*State Key Laboratory of Optoelectronic Materials and Technologies, School of Electronics and Information Technology, Sun Yat-sen University, Guangzhou 510275, China*

High-dimensional quantum states, i.e., qudits, have unique quantum features and offer advantages in particular quantum information tasks. Integrated photonics offers high-efficiency single-photon generation as well as multi-mode, high-precision and reconfigurable quantum controls, which are particularly suited for generating, manipulating qudits [1-3].

Here, we experimentally realize the generation and manipulation of a pair entangled qutrits on a silicon chip. This is realized by integrating three dual Mach-Zehnder interferometers (DMZI) micro-ring photon-pair sources which allows us to independently tune the coupling conditions of pump, signal and idler photons. This configuration greatly enhances generation and extraction efficiency of the photon pairs. In addition, it also relaxes the amount of off-chip filtering for the pump [4].

Figure 1a presents the layout of our photonic chip. The chip consists of 3 DMZI micro-ring sources, 15 multi-mode interferometer beam splitters and 28 simultaneously running thermo-optic phase shifters. We generate an entangled state of three-path encoded qutrits by creating a photon pair in a superposition between three sources, then separating the generated photons of each part. Non-degenerate signal and idler photons are generated by the spontaneous four-wave mixing in the DMZI micro-ring sources, and further separated by on-chip resonator-based wavelength devision multiplexers (WDMs). Path entanglement requires indistinguishable photons. We achieved that by performing reverse Hong-Ou-Mandel (HOM) interference. The results are shown in Fig. 1b, with an raw/accidental-subtracted visibility of 94.7%/97.1% and 85.3%/86.1% for sources1,3 and sources 2,3, respectively. This high-visibility indicates that the three sources are spectrally well overlapped. With good sources interference established, we setup the qutrit entanglement state via the WDM resonators, the coincidence results are plotted in Fig. 1c. Although the state is not a maximally entangled state, a series of on-chip states can be produced by using different configurations of sources and built-in WDM tuning.

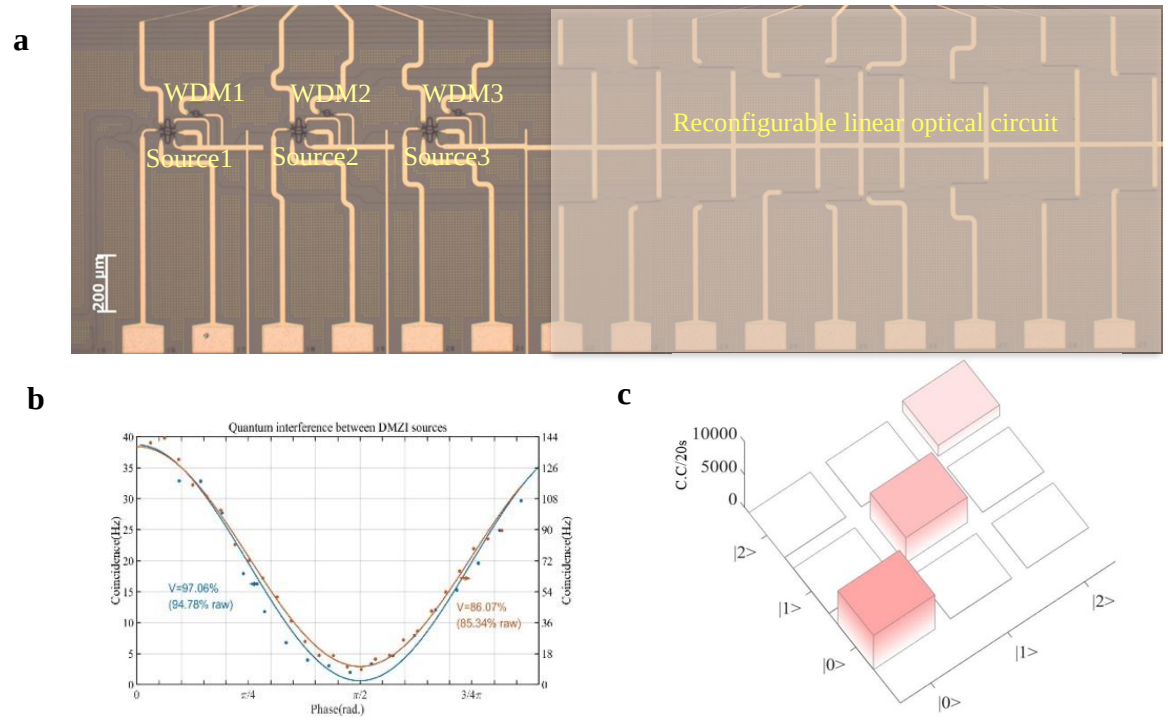

Fig. 1. a) Optical micrograph of the device. A 200- μ m scale bar is shown. b) Anti-HOM interference fringes between sources. c) Two-fold Coincidences from three DMZI micro-ring sources.

These results represent a new application in functionally integrated quantum photonics, demonstrating the high potential of this platform for the progress of quantum information processing.

References

[1] C. Schaeff *et al*. "Experimental access to higher-dimensional entangled quantum systems using integrated optics," Optica **6**, 523 (2015).

[2] J. Wang *et al*. "Multidimensional quantum entanglement with large-scale integrated optics," Science **360**, 285 (2018).

[3] X. Qiang *et al*, "Large-scale silicon quantum photonics implementing arbitrary two-qubit processing," Nat. Photon. **12**, 534 (2018).

[4] C. Tiso*n et al.* "Path to increasing the coincidence efficiency of integrated resonant photon sources," Opt. Express **26**, 33088 (2017).

Second-order Photonic Topological Insulator with Corner States

Bi-Ye Xie[1], Hong-Fei Wang[1], Hai-Xiao Wang[2], Xue-Yi Zhu[1], Jian-Hua Jiang[2], Ming-Hui Lu[1], Yan-Feng Chen[1]

1. National Laboratory of Solid State Microstructures and Department of Materials Science and Engineering, Nanjing University, Hankou Road 22, Nanjing 210093, China

2. School of Physical Science and Technology, and Collaborative Innovation Center of Suzhou Nano Science and Technology, Soochow University, 1 Shizi Street, Suzhou 215006, China

Higher-order topological insulators (HOTIs) which go beyond the description of conventional bulk-boundary correspondence, broaden the understanding of topological insulating phases [1-3]. Being mainly focused on electronic materials, HOTIs have not been found in photonic crystals (PCs) yet. Here, we propose a type of two-dimensional second-order photonic crystal (PC) which is the photonic analog of 2D the Su-Schrieffer-Heeger (SSH) model [4] with zero-dimensional corner states and one-dimensional boundary states for optical frequencies. All of these states are topologically nontrivial and can be understood based on the theory of topological polarization. Moreover, by tuning the easily-fabricated structure of the photonic crystals, different topological phases can be realized straightforwardly. Our study can be generalized to higher dimensions and provides a platform for higher-order photonic topological insulators and semimetals [5].

The structure of the combined PC and the unit cell of the inner PC and outer PC are depicted in Fig. 1(a). For both PCs, the lattice constants, the radius of the rods and the relative dielectric constant are $a = 1.5\mu m$ $r = 0.12a$ and $\varepsilon = 12$ respectively. The outer (inner) PC is achieved by shrinking (extending) the dielectric rods symmetrically with respect to the center of unit cell comparing to 2D square lattice as depicted in Fig. 1(a). By numerical calculation of the eigenmodes in this combined PC, we find four degenerate 0D mid-gap states as the corner states which are strongly localized at four corners as shown in Fig. 1(a). These corner states are topologically protected by the bulk 2D Zak phase and robust against perturbations which does not close the bandgaps.

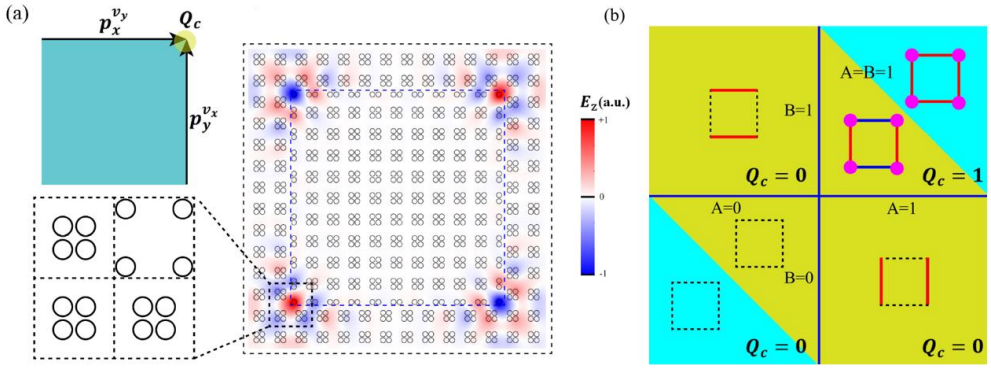

Fig. 1 (a). Schematic of the combined photonic crystal which has corner states. (b). Classification of all kinds of generalized 2D photonic SSH model with different configurations in x-and y-directions.

Besides, we also find that there are 1D edge states which are protected by 1D bulk polarization. Moreover, the existence of these topologically protected 1D edge states can be easily controlled by changing the lattice structures. We then classify all the topological edge states with respect to the bulk polarizations in x- and y-directions as depicted in Fig. 1(b). A(B) = 1 means 2D PC is in topologically nontrivial phase along x-(y-) directions. A(B) = 0 means 2D PC is in topologically trivial phase along x-(y-) direction. The blue area represents isotropic cases (symmetric in x- and y- directions) and yellow area represents anisotropic cases (PC is different in x- and y- directions). The dashed lines represent there are no 1D edge states and solid lines represent the existence of 1D edge states. The solid circles mean there are corner states. The edge (or corner) states of the same color have the same frequency, whereas the states with different colors have different frequencies. The result is concise and may provide instructions on future exploration on HOTIs without negative hopping in photonic systems.

References

[1] W. A. Benalcazar, B. A. Bernevig, and T. L. Hughes, Science **357**, 61-66 (2017).
[2] W. A. Benalcazar, B. A. Bernevig, and T. L. Hughes, Phys. Rev. B **96**, 245115 (2017).
[3] M. Ezawa. Phys. Rev. Lett. **120** 026801 (2018).
[4] F. Liu, H. Y. Deng, and K. Wakabayashi. Phys. Rev. B **97**, 035442 (2018).
[5] M. Lin and T. L. Hughes, arXiv preprint, arXiv:1708.08457 (2018).

Self-assembling of Nanomaterials via Droplet Manipulation for Multifunctional Optoelectronics Devices

Meng Su[1], **Yanlin Song**[1]

1. Institute of Chemistry, Chinese Academy of Sciences, Zhongguancun North First Street 2, Beijing100190, China

The ability to rapidly and precisely construct multifunctional electronic and optic devices would enable myriad applications, including displays, solid-state lighting, wearable electronics and biomedical devices with embedded circuitry. Here, **the droplet manipulation strategy** is demonstrated for **rapidly patterning materials** over a broad range of **compositions** and accurately achieving the **correct position at the micro- and nanoscale**. Firstly, 0D microdots are connected by 1D microwires through regulating the Rayleigh-Taylor instability of materials solution or suspension, which display bright **dichromatic photoluminescense**. [1] Secondly, a **3D liquid self-shaping strategy** is developed for rapidly patterning materials over a series of compositions and accurately achieving micro- and nanoscale structures. The 3D architectures achieved by two different quantum dots show **non-interfering optical properties** with feature resolution below 3 μm. [2] Thirdly, **three-primary-color fluorescent nanoparticles** can also be integrated by successively printed with retention of their individual photoluminance efficiency (5% variances). Yellow, magenta, cyan and white colors with clearly defined interfaces are achieved to reduce the optical cross-talk effect. Finally, nanoparticle-based curves are assembled through pillar-patterned silicon template-induced printing, and integrated as **flexible sensors** to perform complex recognition of human facial expression. [3] **Optimal interconnect** are spontaneously patterned between certain nodes on diverse substrates, as natural systems spontaneously figuring out the shortest path. The optimal interconnect leads to a 65.9 percent decrease in the electromagnetic interference. [4] Therefore, self-assembling of nanomaterials via droplet manipulation are achieved in **all dimensions for multifunctional optoelectronics**.

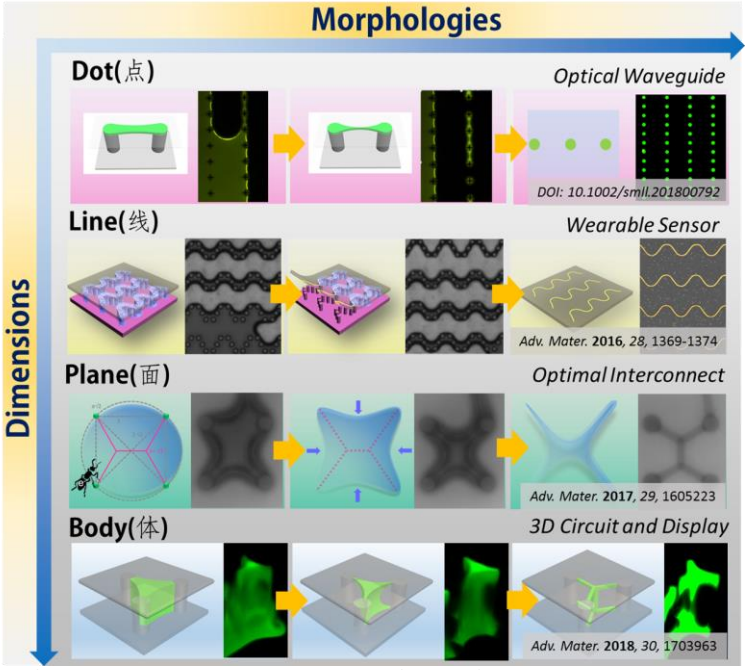

Fig. 1 Self-assembling of Nanomaterials via Droplet Manipulation for Multifunctional Optoelectronics Devices

Example References

[1] Y. Li, M. Su*, Z. Huang, F. Li, Q. Pan, W. Ren, X. Hu and Y. Song*, "Patterned arrays of functional lateral heterostructures via sequential template-directed printing" Small **14**, 1800792 (2018).

[2] M. Su, Z. Huang, Y. Li, X. Qian, Z. Li, X. Hu, Q. Pan, F. Li*, L. Li and Y. Song*, "A 3D self‐shaping strategy for nanoresolution multicomponent architectures" Adv. Mater. **30**, 1703963 (2018)

[3] M. Su, F. Li*, S. Chen, Z. Huang, M. Qin, W. Li, X. Zhang and Y. Song*, "Nanoparticle based curve arrays for multirecognition flexible electronics" Adv. Mater. **28**, 1369-1374 (2016).

[4] M. Su, Z. Huang, Y. Huang, S. Chen, X. Qian, W. Li, Y. Li, W. Pei, H. Chen, F. Li* and Y. Song*, "Swarm intelligence-inspired spontaneous fabrication of optimal interconnect at the micro/nanoscale" Adv. Mater. **29**, 1605223 (2017).

Efficient Conversion between Plasmonic Waves and Spin Optical Waves Enabled by Nanopatch Antenna Array

Yuan-Song Zeng[1], Shi-Wei Qu[1]

1.University of Electronic Science and Technology of China, Xiyuan Avenue 2006, Chengdu 611731, China

The use of circularly polarized light for information transmission and processing, i.e., spintronics, has drawn great interest in the past decade because it holds promise for future energy-efficient communication system free from Joule heating [1]. Circularly polarized light is unique because it carries spin angular momentum with two different signs determined by the helicity. Utilization of the spin-controlled helicity has enabled a lot of applications in light-matter interaction [2] and quantum communications.

Plasmonics, with an unprecedented ability to concentrate light into deep sub-wavelength scale, have emerged as a solution to future optical chips with simultaneous high operating speed and compact sizes. It has thus become an ideal on-chip platform for the researches of spintronics. For practical implementations of spin waves, a device that is capable of transmitting/receiving spin information to/from another device is necessary. However, it is challenging to generate spin optical waves from a plasmonic circuit. Recently, based on the concept of spoof surface plasmons, a microstrip antenna array with the capability of bridging the gap between circularly polarized microwave radiation and spoof surface plasmons has been reported in microwave regime [3].

Inspired by the work in [3], in this paper, a plasmonic nanopatch antenna array capable of converting the plasmonic waves in the plasmonic nanoslot waveguide into free space spin optical waves is proposed. Figure 1a shows the structure of the proposed nanopatch array. The nanopatch array is located above the plasmonic nanoslot waveguide with a SU-8 spacer between them. By properly designing the sizes and the inclined angle of the nanopatch, two orthogonal modes with equal amplitude and 90-degree phase difference can be excited. The superposition of these two modes results in a spin light emission. Figure 1b gives the E_z distributions on the lower surface of the nanopatch with a = 350 nm and b = 250 nm at four different phases. It can be seen that the nanopatch exhibits a right-hand circular polarization. The corresponding far-field directivity and axial ratio (AR) of an 8-element nanopatch array are plotted in Fig. 1c. As seen from Fig. 1c, the 3-dB axial ratio bandwidth is around 6.11% (207 ~ 219 THz). Within the 3-dB AR bandwidth, the directivity is all above 10.5 dBic with a peak directivity of 11.5 dBic. A high directivity is beneficial to transmit the spin waves over a long distance. The simple structure, compact size, high directivity and ease of fabrication make the proposed nanopatch array a useful building block for future spin-optoelectronic circuits and integrated quantum communications.

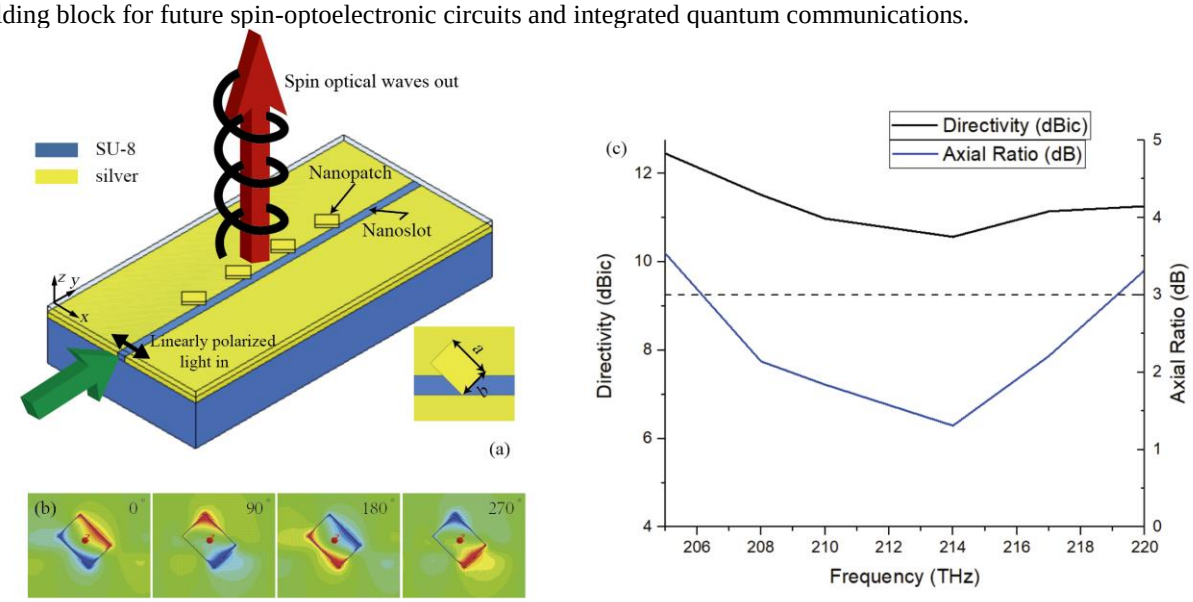

Fig. 1 (a) A schematic showing the structure and the function of the proposed design. The SU-8 layer between the nanopatches and the nanoslot is set to be transparent for clear illustration. (b) E_z distributions on the lower surface of the nanopatch at four phase states. The inclined angle of the nanopatch is 45° and the nanopatch has an offset of 60 nm with respect to the nanoslot central line. (c) Directivity and AR versus frequency.

References

[1] Bliokh K Y, Rodríguez-Fortuño F J, Nori F and A. V. Zayats, "Spin–orbit interactions of light," Nature Photonics **9**, 796–808 (2015).

[2] Liu C, Chen J, Liu T, et al, "Long-distance propagation of short-wavelength spin waves", Nature communications **9**, 738 (2018).

[3] Bai X, Qu S W and Yi H, "Applications of spoof planar plasmonic waveguide to frequency-scanning circularly polarized patch array", Journal of Physics D: Applied Physics, **47**, 325101 (2014).

The study on plasmonics imaging to single nanoparticle

Xinchao Lu[1], **Hongyao Liu**[1], **Xuqing Sun**[1], **Liwen Jiang**[1], **Ruxue Wei**[1,2], **Chengjun Huang**[1]
1 Institute of Microelectronics of Chinese Academy of Sciences, Beijing, China
2 University of Chinese Academy of Sciences, Beijing, China

Nanoparticles are applicable widely and exist everywhere. As the unique properties distinguished with bulk materials, synthetic nanoparticles are playing a key role in applications of disease diagnosis, cancer treatment, and drug delivery. Adversely, growing concerns over the potential toxic effects of nanoparticles on human health have arisen, with the nanoparticles released from industrial products increasingly. Meanwhile, nanoparticles occurring naturally, such as virus and nano-pollutants, might also introduce severe diseases and environmental deterioration. The label-free single nanoparticle imaging is crucial for in-situ tracking to nano-pollutants and virus in environmental monitoring and biological sciences.

Surface plasmon polaritons (SPPs) is a good candidate for label-free single nanoparticle detection [1-3]. In this study, the imaging to single polystyrene nanoparticle with particle size down to 39nm (~ deep subwavelength with λ/16) is demonstrated (shown in Figure 1(a)), which is characteristic of localized surface plasmon (LSP) enhancement induced by nanoparticle polarization and interference fringes relative to the plasmonic in-plane scattering (see Figure 1(b)). The directionality of the imaging is found which transforms the spatial imaging to spatial frequency via Fourior transform, which is due to the interaction between the electric and magnetic dipole modes from nanoparticle polarization, e.g. the Kerker scattering [4] (see Figure 2(a)). Finally, the connection between LSP enhancement and optical properties of single nanoparticle is illustrated (shown in Figure 2(b)). Our study provides experimental access and theoretical understanding of the plasmonic imaging to the single nanoparticle. Both the scattering directionality and LSP enhancement retrieved from the plasmonic imaging connect to the size and refractive index of single nanoparticle, which paves the way for in-situ and fast detection and identifying the nano materials in the environment.

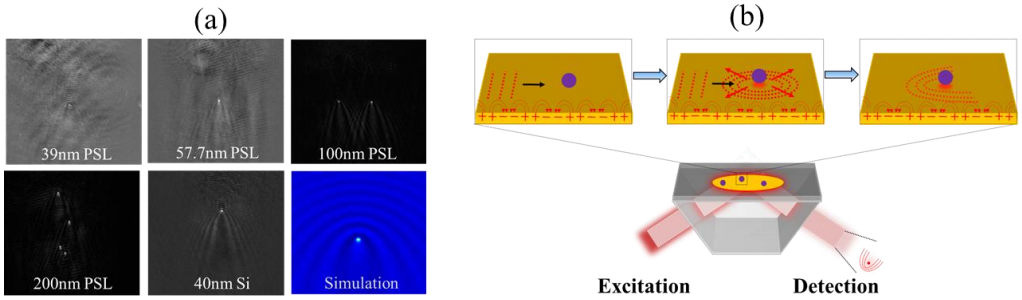

Fig. 1 (a) The imaging to single polystyrene and Si nanoparticle with size down to 39nm. (b) The mechanism of the characteristic of single nanoparticle imaging.

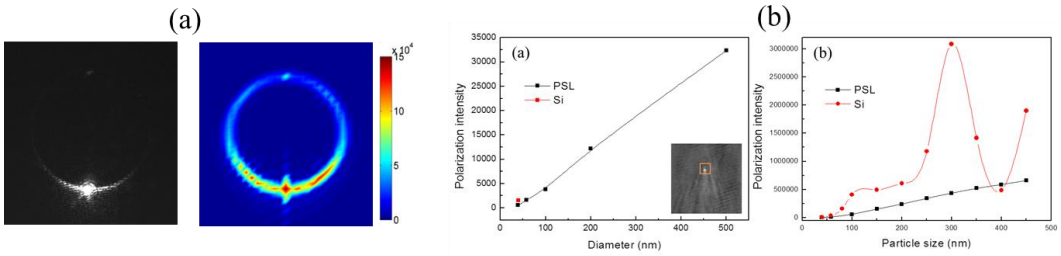

Fig. 1 (a) The directionality of the single nanoparticle imaging in spatial frequency domian. (b) The connection between LSP enhancement and optical properties of single nanoparticle.

References

[1] A. Zybin, Y. Kuritsyn, E. Gurevich, V. Temchura, K. Überla, and K. Niemax, "Real-time detection of single immobilized nanoparticles by surface plasmon resonance imaging," Plasmonics **5**, 31-35 (2010).
[2] S. Wang, X. Shan, U. Patel, X. Huang, J. Lu, J. Li, and N. Tao, "Label-free imaging, detection, and mass measurement of single viruses by surface plasmon resonance," P NAS **107**, 16028-16032 (2011).
[3] X. Sun, H. Liu, Y. Yang, W. Xiong, Y. Chen, L. Jiang, N. Li, X. Lu, H. Tang, and Y. Xia, "Imaging to Single Virus by Using Surface Plasmon Polariton Scattering," Proc. SPIE **10244**, 1024425. (2017).
[4] M. Kerker, D. S. Wang, and C. L. Giles, "Electromagnetic scattering by magnetic spheres," Journal of the Optical Society of America **73**, 765-767 (1983).

Bio-inspired chiral photonic crystals

Jiawei Lv, Zhiyong Tang

National Center for Nanoscience and Technology, Beiyitiao 11, Zhongguancun, Beijing 100190, China

Colors are essential for the survival of animals and plants in nature [1]. After millions of years of evolution and selection, the biological systems have developed very efficient ways to make and modulate colors with relative few building blocks available [1]. Structural colors, which originate from the scattering, interference and diffraction of light with structured dielectric materials with a feature size comparable to the visible light wavelength, are prevalent in the biological world [2]. This library of structural colors offers tremendous inspirations for humans to design advanced optics. Among the various structural colors developed in nature, one particularly intriguing phenomenon is the circular dichroism. The exocuticles of many scarabaeid beetles selectively reflect left circularly polarized light, showing distinct appearances (Fig. 1a) when viewed under left and right circular polarizers [3]. Detailed structural investigations reveal that this is because the exoskeleton consists of helicoidally assembled chitin fiber layers, with a structure analogous to a cholesterol liquid crystal (Fig. 1b,c).

Inspired by nature, we have developed a Langmuir-Blodgett assembly based method to fabricate bio-mimicry chiral photonic crystals (Fig. 1d-e). Our method combines the nano-scale resolution of bottom-up self-assembly and the precise structural control of top-down approaches, giving rise to unprecedentedly diversified chiral photonic crystal structures. Making use of the intimate structure-property relationship, we have proposed and demonstrated barcode applications with giant coding capacity based on the programmed circular dichroism spectra through structure design.

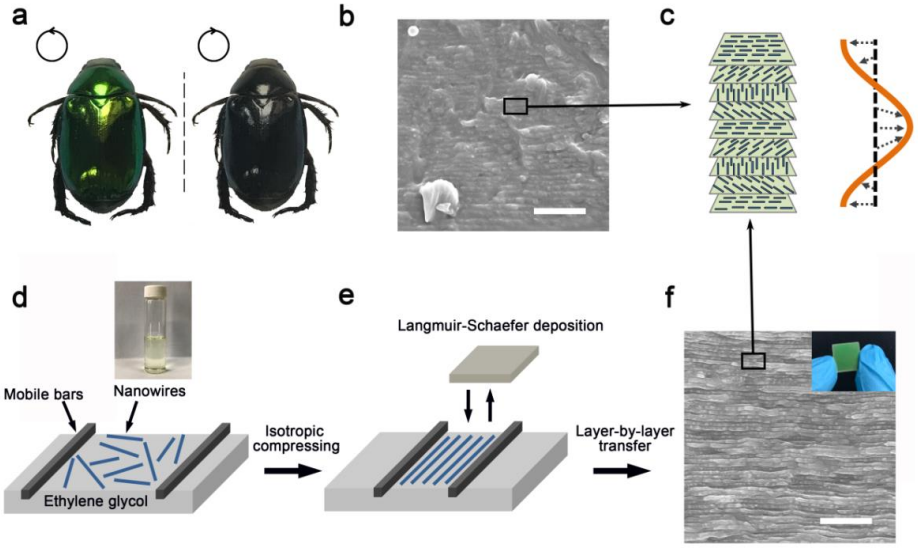

Fig.1 A biomimetic route to chiral photonic crystals. a) Photographs of the beetle Anomala corpulenta Motschulsky (a kind of scarabaeid beetle) taken through a left (left) and right (right) circular polarizer, respectively. b) SEM image of the cross section of cuticle of the beetle Anomala corpulenta Motschulsky, showing layered structures, typical of cholesterol liquid crystals. c) Schematic representation of the helical arrangement of aligned layers to constitute chiral photonic crystals. d) Dispersing nanowires on the air-liquid interface in the Langmuir trough, on top is the photograph of $NiMoO_4 \cdot xH_2O$ nanowire cyclo-hexane solution. e) Compressing the barriers to obtain aligned nanowire films. Afterwards, the aligned layer is transferred onto a substrate via a horizontal lifting method with a twist. f) SEM image of the cross section of one chiral photonic crystal film through layer-by-layer transfer with a predesigned twisting angle. Inset is the corresponding photograph of the sample. Scale bars: b and f, 2 μm.

References

[1] A. G. Dumanli, T. Savin. "Recent advances in the biomimicry of structural colours, " Chem. Soc. Rev., **45**, 6698-6724 (2016).

[2] S. Tadepalli, J. M. Slocik, M. K. Gupta, R. R. Naik, S. Singamaneni. "Bio-Optics and Bio-Inspired Optical Materials, " Chem. Rev.**, 117**, 12705-12763 (2017).

[3] V. Sharma, M. Crne, J. O. Park and M. Srinivasarao. "Structural Origin of Circularly Polarized Iridescence in Jeweled Beetles," Science **325**, 449-451 (2009).

Bright and tunable single-photon sources for quantum optics

Thomas Lettner[1], **Katharina D. Zeuner**[1], **Huiying Huang**[2], **Selim Scharmer**[1], **Saimon Filipe Covre da Silva**[2], **Eva Schöll**[1], **Lucas Schweickert**[1], **Armando Rastelli**[2], **Klaus D. Jöns**[1] **and Val Zwiller**[1,3]

1. Quantum Nano Photonics, Department of Applied Physics, KTH Royal Institute of Technology, Albanova University Centre, Roslagstullsbacken 21, 106 91 Stockholm, Sweden
2. Institute of Semiconductor and Solid State Physics, Johannes Kepler University Linz, Altenbergerstr. 69, 4040 Linz, Austria
3. Kavli Institute of Nanoscience Delft, Delft University of Technology, 2628 CJ Delft, The Netherlands

Optically active semiconductor quantum dots (QDs) are nanostructures with zero-dimensional confinement potential leading to discrete electron and hole energy levels. These so-called "artificial atoms" are excellent single-photon sources [1] with tailorable optical properties [2] and applications in quantum communication [3], quantum sensing [4], and quantum simulations [5].
We work with highly symmetric QDs of gallium arsenide (GaAs) infilled holes obtained by aluminium (Al) droplet etching in $Al_{0.4}Ga_{0.6}As$ [6]. In order to utilize those QDs we develop new structures to efficiently couple the single photons out of the semiconductor material and into the collection optics of our micro-photoluminescence (μ-PL) experiment. For this, we employ a low-Q microcavity with a metallic gold backside mirror, which we fabricate by a combination of dry reactive ion etching in an inductively coupled plasma and selective wet chemical etching. Precise control of the etch sidewall curvature allows us to achieve a parabolic backside mirror shape and enhanced μ-PL intensity (Fig. 1) with an estimated extraction efficiency of 12.5%.
Furthermore, we integrate our QD microcavity structures onto 200 μm thick lead magnesium niobate-lead titanate (PMN-PT) piezoelectric substrates using a polymer-based bonding process. The piezo allows us to induce a large in-plane biaxial strain into the semiconductor material at low temperature. With our devices, we tune the emission of the QDs with planar (parabolic) metallic backside mirror by 1 meV (0.4 meV) for 400V of applied voltage, in a dynamic, reversible and linear way.

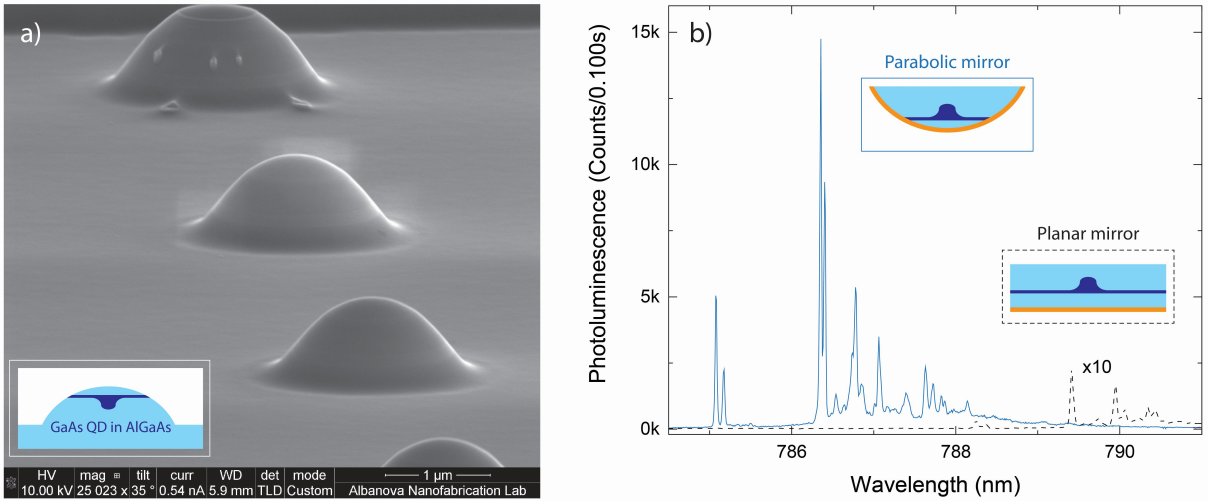

Fig.1 Parabolic mirror microcavity for enhanced photoluminescence extraction efficiency: a) Scanning electron microscope image of circular paraboloids obtained by dry reactive ion etching in an inductively coupled plasma. The sample is mounted on a 45° tilted sample holder and tilted 35° more for imaging. b) μ-PL measurements under continuous-wave above-band excitation of a sample with single quantum dots in parabolic (solid line) and planar metallic backside mirror (dashed line) microcavity structures. Schematics: A dark blue drop represents the quantum dot and an orange line corresponds to the gold backside mirror.

[1] P. Senellart, G. Solomon, and A. White, "High-performance semiconductor quantum-dot single-photon sources", Nat. Nanotech. **12**, 1026-1039 (2017).
[2] A. Rastelli et al., "Controlling quantum dot emission by integration of semiconductor nanomembranes onto piezoelectric actuators", Phys. Status Solidi B **249**, 687-696 (2012).
[3] P. M. Intallura, M. B. Ward, O. Z. Karimov, Z. L. Yuan, P. See, A. J. Shields, P. Atkinson, and D. A. Ritchie, "Quantum key distribution using a triggered quantum dot source emitting near 1.3μm", Appl. Phys. Lett. **91**, 161103 (2007).
[4] M. Müller, H. Vural, C. Schneider, A. Rastelli, O. G. Schmidt, S. Höfling, and P. Michler, "Quantum-Dot Single-Photon Sources for Entanglement Enhanced Interferometry", Phys. Rev. Lett. **118**, 257402 (2017).
[5] Hui Wang et al., "High-efficiency multiphoton boson sampling", Nat. Photon. **11**, 361-365 (2017).
[6] Y. H. Huo, A. Rastelli, and O. G. Schmidt, "Ultra-small excitonic fine structure splitting in highly symmetric quantum dots on GaAs (001) substrate" Appl. Phys. Lett. **102**, 152105 (2013).

Length-relaxed nanocavity for large spontaneous emission enabled by epsilon-near-zero substrate

Xueke Duan[1], **Fan Zhang**[1], **He Hao**[1], **Lingxiao Shan**[1], **Qihuang Gong**[1,2], **and Ying Gu**[1,2*]

1. State Key Laboratory for Mesoscopic Physics, Collaborative Innovation Center of Quantum Matter, Department of Physics, Peking University, Beijing 100871, People's Republic of China
2. Collaborative Innovation Center of Extreme Optics, Shanxi University, Taiyuan, Shanxi 030006, People's Republic of China

Epsilon near zero (ENZ) material, whose permittivity is near zero, has been the research hotspot because of its distinctive features, and is widely used in photonic researches [1]. Previous study has shown that the red shift of the resonance wavelength of longer nanoantennas can be slowed down when they are placed on the ENZ film, and get a resonance "pinning" at ENZ wavelength [2]. In addition, the enhancement of spontaneous emission (SE) by plasmonic nanostructures, which has important applications in quantum information and integrated photonic circuit, is sensitive to the size of the metallic nanocavity, i.e., enhancement factor will decrease rapidly if the nanocavity deviates from the resonant size [3].

Combining the "pinning" effect and the ultrasmall mode volume of the metallic nanocavity placed on the ENZ substrate, we demonstrate the relaxed length restriction of the nanocavity for large SE enhancement in the ENZ substrate-Ag nanorod system [4]. As shown in Fig. 1 (a), we put the Ag nanorod on the substrate whose permittivity decreases linearly with the increment of the wavelength and crosses zero at 657 nm (i.e., the ENZ wavelength of the film is 657 nm). Originate from the resonance "pinning" effect, when the working wavelength of the dipole nearby is equal to the ENZ wavelength of the substrate, large SE enhancement of the dipole can be achieved in wider size of the Ag nanorod. Displayed in Fig. 1(b), when the working wavelength λ of the dipole is 500 nm, the linewidth of the curve of SE enhancement factor γ/γ_0 and the length of the Ag nanorod is only 4 nm, but the linewidth increases to 13 nm when $\lambda = 657\text{nm}$. In other words, ENZ substrate can relieve the strict demand on the size of the nanocavity for enormously enhancing the SE of the dipole working at the same wavelength. This kind of size-relaxed nanocavity for large SE enabled by ENZ substrate has potential applications in the preparation of single photon sources, plasmon-based nanolasers and on-chip nanodevices, promotes the development of quantum information and integrated photonic circuit.

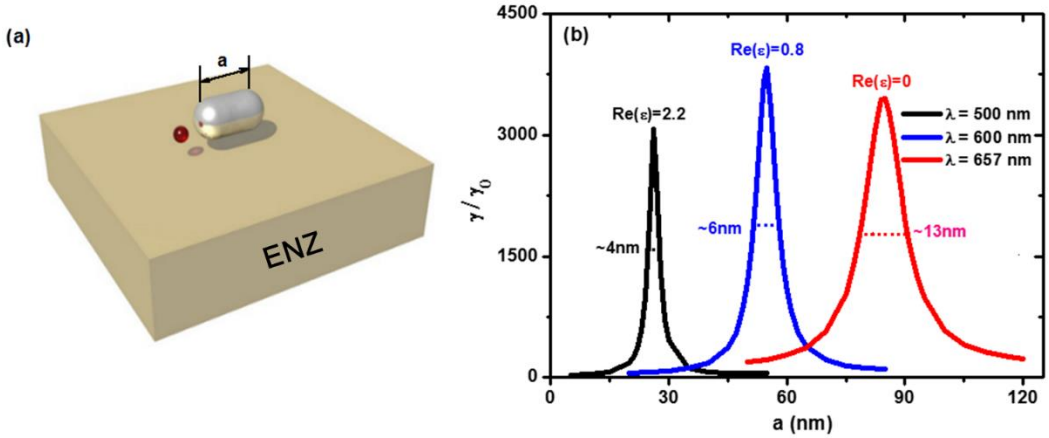

Fig. 1 (a) Schematic diagram of the proposed Ag nanorod-ENZ substrate system. The dipole emitter is placed near the Ag nanorod with length of a. The permittivity of the substrate decreases linearly with the increment of the wavelength and crosses zero at 657 nm. (b) Length-relaxed nanocavity when the working wavelength of the dipole is equal to the ENZ wavelength.

[1] Iñigo Liberal and Nader Engheta, "Near-zero refractive index photonics," Nat. Photonics **11**, 149–158 (2017).
[2] J. Kim et al, "Role of epsilon-near-zero substrates in the optical response of plasmonic antennas," Optica **3(3)**, 339–346 (2016).
[3] Xueke Duan et al, "Large Purcell enhancement with efficient one-dimensional collection via coupled nanowire–nanorod system," Nanotechnology **29,** 045203 (2018).
[4] Xueke Duan et al, "Length-relaxed nanocavity for large spontaneous emission enabled by epsilon-near-zero substrate," in preparation.

Mid-infrared biaxial hyperbolic phonon polaritons in a van der Waals crystal

Zebo Zheng, **Huanjun Chen**

State Key Laboratory of Optoelectronic Materials and Technologies, Guangdong Province Key Lab of Display Material and Technology, School of Electronics and Information Technology, Sun Yat-sen University, Guangzhou 510275, China

Abstract We report the study on thin flakes of a van der Waals crystal, α-MoO_3, which can support in-plane hyperbolic polariton guided modes in mid-infrared frequencies, without the need for structural patterning. This is possible because α-MoO_3 is a biaxial hyperbolic crystal with three different Restrahlen bands, each corresponding to a different crystalline axis. These findings can pave the way towards new paradigm to manipulate and confine light in planar photonic devices.

Hyperbolic materials refer to those media exhibit permittivty tensor having one principal component with opposite sign with respect to the other two axes. They have been extensively studied for their exotic optical properties, particularly the highly confined electromagnetic fields with arbitrarily high momenta *(1)*. This concept can be directly generalized to 2D media, where surface waves or guided waves are considered, and implemented using hyperbolic metasurfaces (HMSs) *(2)*. These are flat photonic nanopatterned structures that support guided waves with in-plane hyperbolicity and can control the two-dimensional light propagation in unconventional way, giving rise to a variety of intriguing optical phenomena such as all-angle negative refraction, greatly enhanced photonic density of states, and wavefronts with concave curvatures *(3)*. The necessity of patterning, however, typically leads to strong optical losses, and limits the actual confinement that can be reached. Furthermore, the electromagnetic responses of the HMSs are governed by the permittivity tensors that are derived from the effective medium theory, which is only valid in the long-wavelength limit where the structural periodicity is much smaller than the incidence wavelength. Consequently, the hyperbolic dispersion is constrained to a very small region in the reciprocal space, leading to rather limited electromagnetic wavevectors. Such an issue can in principle be alleviated by reducing the structural periodicities of the metasurfaces down to sub-10 nm scale. However, this should happen without bringing in additional surface roughness or defects, which is a great challenge for nano-fabrication techniques. Thus, the quest for a natural medium that can be used to achieve in-plane hyperbolicity without nanopatterning is a very important open problem in nano-photonics.

In a recent work we have demonstrated highly confined hyperbolic phonon polaritons (PhPs) in a new type of vdW semiconducting crystal, the alpha-phase molybdenum trioxide (α-MoO_3), grown by thermal physical deposition method. Now, we show that the vdW α-MoO_3 is actually a type of natural biaxial hyperbolic crystals with pristine in-plane hyperbolic dispersion in the mid-infrared regime. We use high-resolution optical scanning probe nano-imaging techniques to investigate phonon polariton modes launched, guided, and manipulated within the α-MoO_3 thin flakes in the different hyperbolicity bands of the crystal. In particular, the concave wavefront of a polaritonic mode originated from the in-plane hyperbolicity of the flake is shown as an unmistakable signature of the preserved three-dimensional hyperbolicity of this 2D material.

The homogenous biaxial hyperbolic vdW α-MoO_3 crystal investigated here offers the prospect of planar photonics without the need for complex nanopatterning, which is unavoidable in 2D artificial counterparts. In principle, the wavevectors of the guided electromagnetic waves that can be attained within α-MoO_3 are only limited by the atomic crystalline periodicity; thus, very strong electromagnetic confinement can be reached. In addition, the confinement and manipulation of electromagnetic fields at the nanoscale can be further enriched by introducing sophisticated nanostructures

Reference

[1] Poddubny. A, Iorsh. I, Belov. P, Kivshar. Y. “Hyperbolic metamaterials”. Nat. Photonics 7, 958–967 (2013).

[2] Yu. N, Capasso. F, “Flat optics with designer metasurfaces”. Nat. Mater. 13, 139–150 (2014).

[3] Kildishev. A. V, Boltasseva. A, Shalaev. V. M., “Planar photonics with metasurfaces”. Science 339, 1232009 (2013).

Hexagonal Packed Tungsten Nanocylinder Array as Efficient Selective Solar Absorber for Concentrating Solar Thermoelectrical Generator

Zhubing He[1], Yudong Zhu[1,2], Xusheng Zhang[1]

1. Department of Materials Science and Engineering, Shenzhen Key Laboratory of Full Spectral Solar Electricity Generation (FSSEG), Southern University of Science and Technology, No. 1088, Xueyuan Rd., Shenzhen, 518055, Guangdong, China.
2. Hong Kong University of Science and Technology, Clear Water Bay, Hong Kong SAR, P. R. China

Clean and abundant solar energy has been intensively explored as an alternative to traditional fossil fuels to alleviate the energy crisis and reduce the pollution of greenhouse gases over the past decades. Solar absorber, a key component to convert solar radiation into thermal energy, plays a significant role in various solar thermal applications [1,2]. The challenge for a solar selective absorber should be simultaneously with a broad absorptance in the solar spectrum covering ultraviolet (UV), visible and near infrared (NIR) to convert most solar radiation into heat and along with low emittance in the mid-IR regime to prevent energy loss from blackbody radiation [3].

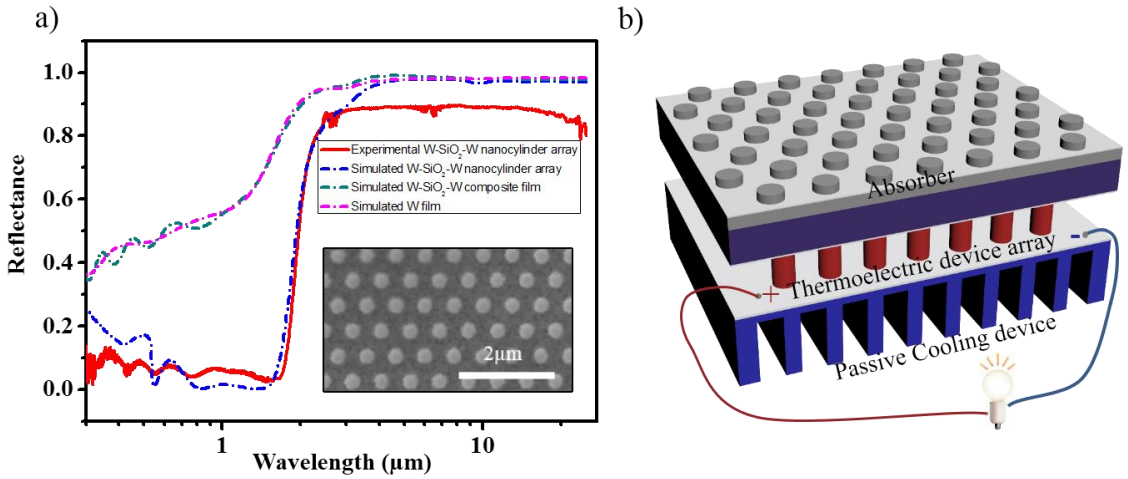

Fig. 1 (a) The reflective spectrum with the wavelength from 0.3 to 25 μm of the optimal W-SiO_2-W nanocylinder array in experimental (red solid) and simulation (blue dash) along with the non-microstructure W-SiO_2-W composite film (magenta dash) and the pure W film (pink dash). (b) The schematic of solar thermoelectrical system, consist of absorber, thermoelectric device array and passive cooling device.

In this work, we designed and realized an effective and robust selective solar absorber (SSA) in a structure of W/SiO_2/W, where a thin layer of SiO_2 is sandwiched between a layer of hexagonal packed tungsten nanocylinders array at the surface and a thicker tungsten film at the bottom on a silicon wafer. As the red solid line shows in Fig. 1, the optimal absorption was characterized to be higher than 0.9 over the wavelength from 300 nm to 1500 nm while its reflectance in the region from near infrared (NIR) to mid infrared (MIR) is also over 0.9, which is well matched with the simulation results of that identical structure (the blue dash line). The transition edge turns around 1.5μm. At a designed working temperature of 150˚C, the energy conversion efficiency of the full spectral solar light reaches 84.5% from photon to thermal at irradiance of one standard sun (100mW/cm^2), which is successfully applied to a typical solar thermoelectric generator (STEG) consisting of a commercial thermoelectric device, Through varying the concentration ratio of solar illumination, the working temperature and open-circuit voltage of the whole STEG can be modulated accordingly. The high performance SSA and its derived STEG system in this work pave a promising and alternative way for solar thermal energy harvesting at the low-mid temperature.

References:

[1] Zhou, L., Tan, Y., Wang, J., Xu, W., Yuan, Y., Cai, W., Zhu S. & Zhu, J., "3D self-assembly of aluminium nanoparticles for plasmon-enhanced solar desalination, " Nature Photonics, **10(6)**, 393 (2016).
[2] Kraemer, D., Poudel, B., Feng, H. P., Caylor, J. C., Yu, B., Yan, X., Ma. Y., Wang, X., Wang, D., Muto, A., Mcenaney, K., Chiesa, M., Ren, Z. & Chen, G., "High-performance flat-panel solar thermoelectric generators with high thermal concentration, " Nature materials, **10(7)**, 532 (2011).
[3] Cao, F., McEnaney, K., Chen, G., & Ren, Z., "A review of cermet-based spectrally selective solar absorbers," Energy & Environmental Science, **7(5)**, 1615-1627 (2014).

Weak-measurement-enhanced Metrology in the Presence of CCD Noise and Saturation

Liang Xu[1], **Zexuan Liu**[1], **Lijian Zhang**[1]

1. National Laboratory of Solid State Microstructures and Colloge of Engineering and Applied Sciences, Nanjing University, Nanjing 210093 China

Weak value and measurement[1] have been used as a metrological protocol for amplifying the minute physical effect, also known as weak value amplification(WVA). Unfortunately, the amplified outcomes tend to occur with highly suppressed probabilities due to the post-selection. Whether the overall measurement precision of WVA is improved in comparison to that of conventional measurement (CM) is under heated debate. Many works show that both WVA and CM have respective advantages under the different theoretical assumption or experimental conditions[2,3]. In this paper, we experimentally investigate the measurement precision of WVA and CM in an optical system with a generic scientific CCD. The reported experiment demonstrates that WVA offers metrological advantages over the CM in the presence of classical noise and detector saturation which are ubiquitous in scientific CCDs.

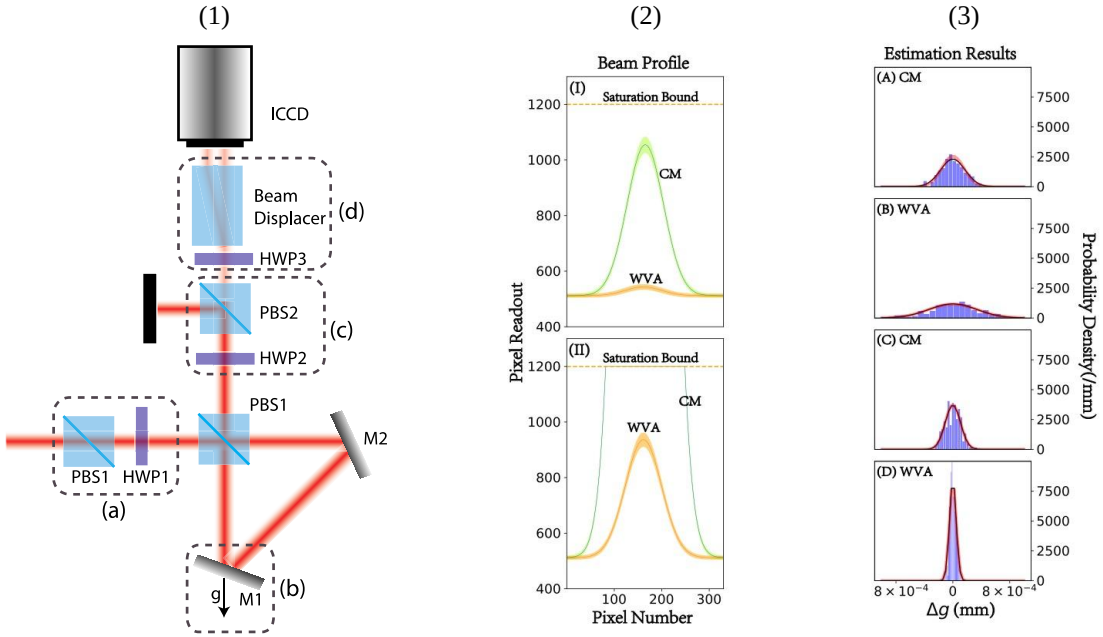

Fig. 1 (1). Experimental Setup (2).Beam Profiles (3).Histograms of Estimation Results

To demonstrate the superiority of WVA over CM in comfonting saturation of CCD, two typical cases are illuestrated in Fig.1(2). In the former case, neither WVA nor CM saturate the CCD; in the latter case, saturation happens in the CM scheme. The green and orange regions represents the fluctuations of pixel readouts caused by the shot noise of light and the classical noise of CCD. Maximum Likelihood estimation of the coupling parameter g is performed using 300 frames selected at random in 6000 frames which is repeated for 200 times for each cases.

The blue bars in the Fig.1(3) show the histogram of estimation results for both CM and WVA. The black lines give the Gaussian fitting of the distribution, while the red lines refer to theoretical calculation. Our experiment results agree well with the theoretical prediction implying that the Cram'er-Rao bound is catched. We can see from Fig.1(3)(A) and (B) that CM behaves better than WVA in precision when the incident photon number is small, since stronger signals of CM help suppress the dark noise.

By contrast, with much more incident photons, WVA turns out to be an effective method to circumvent the saturation and preserve the metrological information, thus outperforming CM, as is shown in Fig.1(3)(C) and (D).

We have experimentally demonstrated that WVA could offer improved metrological performance than CM in the presence of the noise and saturation of photodetectors, extending greatly the dynamic range of the system. In addition, our results shed new light on the applications of weak measurement in practical quantum metrology.

References

[1]*Y. Aharonov, D. Z. Albert, and L. Vaidman, Phys. Rev. Lett.* ***60****, 1351 (1988).*
[2]*L. Zhang, A. Datta, and I. A. Walmsley, Phys. Rev. Lett.* ***114****, 210801 (2015).*
[3]*J. Harris, R. W. Boyd, and J. S. Lundeen, Phys. Rev. Lett.* ***118****, 070802 (2017).*

Dynamic Color Displays Using All-Dielectric Metasurfaces

Shumin Xiao1,2,#

1. State Key Laboratory on Tunable laser Technology, Ministry of Industry and Information Technology Key Lab of Micro-Nano Optoelectronic Information System, Shenzhen Graduate School, Harbin Institute of Technology, Shenzhen, 518055, P. R. China.
2. Collaborative Innovation Center of Extreme Optics, Shanxi University, Taiyuan, 030006, Shanxi, P. R. China.
Email: # shumin.xiao@hit.edu.cn

Structural colors arising from all-dielectric nanostructures are very promising for high-resolution color nanoprinting and high-density optical storage. However, once the all-dielectric nanostructures are fabricated, their optical performances are usually static or change slowly, significantly limiting the practical applications in advanced displays. Herein, we experimentally demonstrate the real-time tunable colors with microfluidic reconfigurable all-dielectric metasurfaces. The metasurface is composed of an array of TiO2 nanoblocks, which are embedded in a polymeric microfluidic channel. By injecting solutions with a different refractive index into the channel, the narrow band reflection peak and the corresponding distinct colors of a TiO2 metasurface can be precisely controlled. The transition time is as small as 16 ms, which is orders of magnitude faster than the current techniques. By varying the lattice size of TiO2 metasurfaces, the real-time tunable colors are able to span the entire visible spectrum. Meanwhile, the injection and ejection of solvent have also shown the capability of the erasion and the restoration of information encoded in TiO2 metasurfaces. The combination of all-dielectric nanostructures with microfluidic channels shall boost their applications in functional color display, banknote security, anticounterfeiting, and point-of-care devices.

References

[1] Y. Gao, C. Huang, S. Sun, L. Zhang, C. Zhang, Z. Duan, K. Wang, Z. Jin, N. Zhang, A. Kildishev, C. Qiu*, Q. Song*, S. Xiao*, Lead Halide Perovskite Nanostructures for Dynamic Color Display, ACS Nano, In Press.
[2] S. Sun, W. Yang, C. Zhang, J. Jing, Y. Gao, X. Yu, Q. Song*, S. Xiao*, Real-Time Tunable Colors from Microfluidic Reconfigurable All-Dielectric Metasurfaces, ACS Nano, 12, 3 2151-2159(2018).
[3] S. Sun, Z. Zhou, C. Zhang, Y. Gao, Z. Duan, S. Xiao*, Q. Song*, All-Dielectric Full-Color Printing with TiO2 Metasurfaces, ACS Nano, 11, 5, 4445-4452(2017).

High-harmonic Generation in an Epsilon-near-zero Material

Yuanmu Yang,[1] Jian Lu[2], Alejandro Manjavacas[3], Ting S. Luk,[4,5] Hanzhe Liu[2], Kyle Kelley,[6] Jon-Paul Maria,[6] Michael B. Sinclair,[4] David A. Reis[2], Shambhu Ghimire[2], Igal Brener[4,5*]

[1] State Key Laboratory for Precision Measurement Technology and Instruments, Department of Precision Instrument, Tsinghua University, Beijing 100084, China

[2]Stanford PULSE Institute, SLAC National Accelerator Laboratory, Menlo Park, California, 94025, USA

[3]Department of Physics and Astronomy, University of New Mexico, Albuquerque, New Mexico 87131, USA

[4]Sandia National Laboratories, Albuquerque, New Mexico 87185, USA

[5]Center for Integrated Nanotechnologies, Sandia National Laboratories, Albuquerque, New Mexico 87185, USA

[6]Department of Materials Science and Engineering, North Carolina State University, Raleigh, North Carolina 27695, USA

High-harmonic generation (HHG) plays an essential role in applications such as coherent attosecond pulse generation[1] and extreme ultra-violet (EUV) spectroscopy[2], yet the typically weak conversion of pump light to HHG could largely hinder its applications. While traditionally occurs in rare-gas atoms, HHG has also recently been reported in solids with reduced threshold pump field and the additional advantage to produce stable EUV waveform in a compact setup[3-5]. Nevertheless, due to the above-band-gap absorption and the short coherent length, only a small fraction (typically tens of nanometers in thickness) of the solid phase material can be truly exploited for HHG, significantly limiting the generation efficiency.

In this work, we report HHG up to the 9th order directly from an ENZ material, indium-doped cadmium oxide (CdO). The structure is a Berreman-type plasmonic cavity formed from a 75-nm-thick In-doped CdO layer and 200-nm-thick gold capping layer, sequentially deposited on a magnesium oxide (MgO) substrate. The In-doped CdO film has a measured carrier density of 2.8×10^{20} cm^{-3} and an electron mobility of 300 cm^{2}V^{-1}s^{-1}, respectively. According to the Drude formula, its real part of permittivity crosses zero at a wavelength of 2.1 μm. The thickness of the CdO film is deep sub-wavelength, and comparable to its absorption length for high-harmonic radiation in the ultraviolet spectral range. With *p*-polarized light illumination at an incident angle of 50 °, the sample exhibits resonant near-perfect absorption at 2.08 μm[6].

High harmonic radiation is generated using a linearly polarized laser with 1 kHz repetition rate and 60 fs pulse duration. The laser illuminates the sample at an angle of incidence θ. The emitted harmonic signal propagates along the specular reflection direction, collinear with the pump beam. With pump wavelength centered at 2.08 μm and θ of 50 °, for *p*-polarized illumination, odd-order harmonics are observed from the 3rd to the 9th order. In contrast, for *s*-polarized illumination, a configuration that does not lead to field enhancements, no harmonic signal above 3rd order is observed.

With a careful examination of the harmonic spectra, we find that the harmonic peaks all exhibit substantial, excitation intensity-dependent redshifts away from the expected harmonic photon energy $N\hbar\omega_0$, the product of the fundamental photon energy $\hbar\omega_0$ and the harmonic order N. The measured N^{th} harmonic peak appears approximately at $N\times0.93\hbar\omega_0$ for all harmonic orders. We attribute the peculiar behavior of harmonic spectral red-shift and broadening to the sub-picosecond hot electron dynamics in the CdO film.

References

[1]F. Krausz and M. Ivanov, "Attosecond physics," *Reviews of Modern Physics*, vol. 81, no. 1, pp. 163-234, 02/02/ 2009.
[2]T. T. Luu, M. Garg, S. Y. Kruchinin, A. Moulet, M. T. Hassan, and E. Goulielmakis, "Extreme ultraviolet high-harmonic spectroscopy of solids," *Nature*, vol. 521, p. 498, 05/27/online 2015.
[3]S. Ghimire, A. D. DiChiara, E. Sistrunk, P. Agostini, L. F. DiMauro, and D. A. Reis, "Observation of high-order harmonic generation in a bulk crystal," *Nature Physics*, vol. 7, p. 138, 12/05/online 2010.
[4]M. Sivis *et al.*, "Tailored semiconductors for high-harmonic optoelectronics," *Science*, 10.1126/science.aan2395 vol. 357, no. 6348, p. 303, 2017.
[5]G. Vampa *et al.*, "Plasmon-enhanced high-harmonic generation from silicon," *Nature Physics*, vol. 13, p. 659, 04/03/online 2017.
[6]Y. Yang *et al.*, "Femtosecond optical polarization switching using a cadmium oxide-based perfect absorber," *Nature Photonics*, vol. 11, pp. 390-395, 2017.

Enhancing Graphene Photoresponse by an Optical Patch Antenna

Jing Zhou, Changlong Liu, Donghai Zhang, Lin Wang, Xiaoshuang Chen, Wei Lu

State Key Laboratory of Infrared Physics, Shanghai Institute of Technical Physics, Chinese Academy of Sciences, China

Graphene has attracted significant attention as a promising candidate for high-performance infrared photodetection material because of its broadband absorption, ultrafast carrier dynamics, and good controllability through electrostatic doping [1]. However, the photoresponse of those graphene based photodetectors is limited by the poor absorption since graphene has only one atomic layer. Micro photonic structures, such as waveguides and micro cavities, could effectively enhance the absorption of graphene [2,3], but suffer from the bulky pixel sizes and the difficulty to integrate with the device structure of photodetectors. Nanophotonic structures, such as plasmonic resonantors and nano antennas, offer a more compact and compatible solution [4-6].

Among nanophotonic structures for this purpose, the optical patch antenna structure received a lot of attention due to their high in-coupling efficiency, insensitive angle dependence and good compatibility to device configuration [7,8]. But there are few experimental studies in this direction. In this work, we investigated the possibility to integrate an optical patch antenna with a graphene infrared photodetector. The device was designed and fabricated (Fig. 1 (a)-(c)). We found an 18 times increase of graphene's photoresponse (Fig. 1 (d)) due to a resonantly enhanced localized mode (Fig. 1 (b)). The photocurrent was collected with zero bias between source and drain in a short circuit scheme. The resonance behaviour is evidenced by the photoresponse spectra measurement. By increasing the patch width, the photoresoponse peak is red-shifted. The significant increase in photoresponse is attributed to the impedance matching design of the patch antenna, as proved by the measured reflection spectrum with a dip that approaches zero. The anisotropic configuration of the patch antenna provides a 11:1 polarization extinction ratio. By integrating the patch antenna with on contact and thus breaking the symmetry, the device shows photoresponse under flood illumination. It shows that other than making dissimilar metal contacts, creating an asymmetric optical field distribution by nanophotonic structures is a new way for graphene photodetectors at zero bias to have photoresponse under flood illumination. Based on the photocurrent characterization versus gating voltage, the photoresponse mechanism is attributed mainly to the photothermoelectric effect.

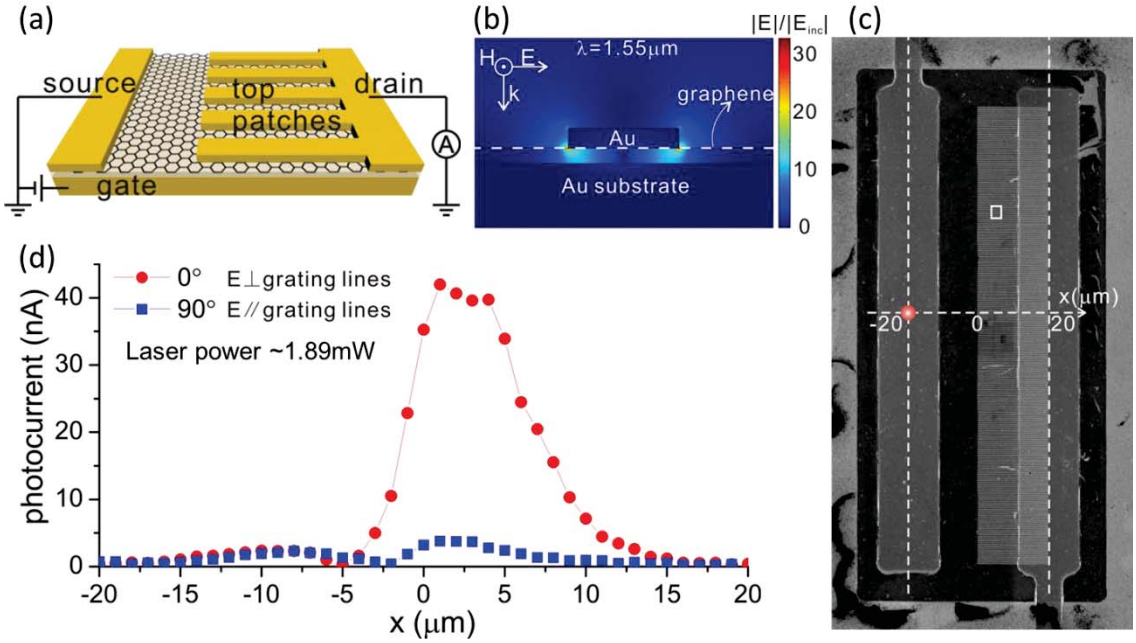

Fig. 1 (a) Sketch of the patch antenna integrated graphene photodetector. (b) Electric field distribution on the cross-sectional plane of the patch antenna integrated with graphene. (c) SEM image of the device; the dark area is covered by graphene. (d) Photocurrent as a function of laser scanning position; the red line and the blue line correspond to the incident polarizations perpendicular and parallel to the metal stripes, respectively.

References

[1] F. Koppens, et al., Nat. Nanotechnol. **9**, 780 (2014).
[2] M. Furchi, et al., Nano Lett. **12**, 2773 (2012).
[3] X. Gan, et al., Nature Photon. **7**, 883 (2013).
[4] Y. Liu, et al., Nat. Commun. **2**, 579 (2011).
[5] T. Echtermeyer, et al., Nat. Commun. **2**, 458 (2011).
[6] Z. Fang, et al., Nano Lett. **12**, 3808 (2012).
[7] S. Song, et al., Nanoscale 5, 9615 (2013).
[8] J. Zhu, et al., Appl. Phys. Lett. 105, 021102 (2014).

Tunable Whispering Gallery Mode Lasing from the Printed High-Q Microdisk

Kaixuan Li[1,2], **Mingzhu Li**[1,*], **Yanlin Song**[1,*]

1. Key Laboratory of Green Printing, Institute of Chemistry, Chinese Academy of Sciences, Beijing 100190, China

2. Department of Chemistry, University of Chinese Academy of Sciences, Beijing 100049, China

High quality (Q) factor microdisks are fundamental building blocks of on-chip integrated photonic circuits and biological sensors. The resonant modes in microdisks are circulating near their boundaries, making their performances strongly upon the surface roughness. Surface-tension-induced microdisks are superior to other structures when comparing Q factors. However, the versatile fabrication of desired photonic performance structure remains a big challenge [1-3]. Here, we propose the idea of printing the polymer droplet on the super-hydrophilic substrate to fabricate the high-Q microdisks. By printing the polymer droplet on the super-hydrophilic substrate, the droplet would spread on the substrate, which induces the construct of high quality factor microdisk. By mixing the polymer with the gain medium, optically pumped lasing with selective wavelengths in a range of about 100 nm can be achieved. Furthermore, the size of micro-disk can be adjusted easily. We hope that these results will pave an avenue for the construction of new types of flexible WGM-based components for photonic integration.

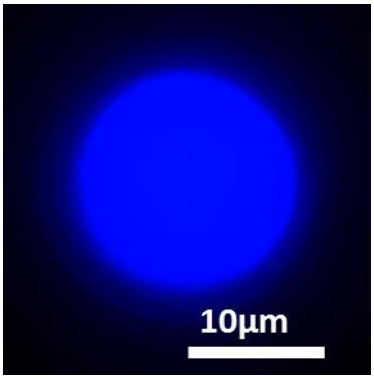

Fig. 1 the fluorescence microscopic observation images of the printed microdisk.

References

[1] Zhu, Y. et al. On-Chip Single-Mode Distributed Feedback Colloidal Quantum Dot Laser under Nanosecond Pumping. ACS Photonics 4, 2446-2452, (2017).

[2] Lin, C. H. et al. Large-Scale Robust Quantum Dot Microdisk Lasers with Controlled High Quality Cavity Modes. Advanced Optical Materials 5, 1700011, (2017).

[3] Wei, C. et al. Controlled self-assembly of organic composite microdisks for efficient output coupling of whispering-gallery-mode lasers. Journal of the American Chemical Society 137, 62-65, (2015).

Green Printing Technology for Colloidal Photonic Crystals

Yanlin Song[1]

1. Institute of Chemistry, Chinese Academy of Sciences, Zhongguancun North First Street 2, Beijing100190, China

Highly precise self-assembly of nanomaterials in the ink droplets along the vapor-solid-liquid three phase contact lines could be accurately achieved. [1] Significantly, the basic units (dot, line, plane and stereo structures) via the printing technology can be precisely controlled. Based on the manufacturing of functional nanomaterials and controllable spreading and transferring of liquid droplets, we fabricated the superoleophilic patterns on the hierarchically structured superhydrophilic plate by ink-jet printing. Thus the image area and non-image area can be achieved on the plate, which can be directly used as the printing-plate. Our further work on assemble metal nanomaterials or colloidal nanoparticles via feasible printed process, patterned the various linear or curves 1D/2D morphologies and optimal interconnects on diverse substrates. [2] Patterned colloidal PC contributes a novel approach to constructing high-performance photonic crystal (PC) devices with unique structures and specific functions. Based on droplet manipulation green printing technology, we fabricated various patterned PC devices. For example, the detection sensitivity and response speed of sensors can be improved; cross-reactive molecules can be recognized through array patterned microchip; the display devices with tunable pattern, well-arranged RGB unit, and wide viewing-angle can be fabricated; and several anti-counterfeiting devices with different security strategies can be fabricated. [3] These achievements on functional printing are derived and benefited from the fundamental researches on solid/liquid interfacial wettability manipulation, morphology control of dried ink droplets, as well as functional nanomaterial fabrication, which develop the research system of Green Printing Technology.

References

[1] a) Tian, D.; Song, Y. Jiang, L; et al, Chem. Soc. Rev. **42**, 5184-5209 (2013). b) Huang, Y.; Song, Y.; et al., J. Am. Chem. Soc. **134**, 17053-17058 (2012). c) Guo, D.; Song, Y.; et al., J. Am. Chem. Soc. **140**,18-21 (2018).
[2] a) Kuang, M.; Song, Y. Adv. Mater. **26**, 6950-6958 (2014); b) Wu, L.; Song, Y.; et al, Adv. Funct. Mater., **15**, 2237-2242 (2015); 3) Hou, J.; Song, Y.; et al., Angew. Chem. Int. Ed. **57**, 2544-2553 (2018).
[3] a) Huang, Y.; Song, Y.; et al., Angew. Chem. Int. Ed., **52**, 7296 (2013); b) Hou, J.; Song, Y.; et al., Angew. Chem. Int. Ed., **53**, 5791 (2014); c) Qin, M.; Song, Y.; et al., Angew. Chem. Int. Ed. **55**, 7025 (2016).

Topological Properties of Comb-like Waveguide Systems

Weiwei Zhu

Tongji University, Shanghai 200092, China

The comb-like waveguide systems has attracted a lot attention for the existence of the locally resonant bandgap besides Bragg band gap and the potential to realize slow wave. Here we study the topological properties of two types of comb-like waveguide systems. The first one is dimerized comb-like waveguide system, whose unit cell contains two side-branch waveguides and has mirror symmetry as shown in Fig.1(a), the other one is Aubry-Andr é-Harper(AAH) comb-like waveguide system, whose unit cell contains three side-branch waveguides and the distance between the n^{th} and $(n+1)^{th}$ side-branches is modulated as $d_n = d\{1 + \delta\cos[2\pi b(n-1) + \phi]\}$ as shown in Fig.1(b).

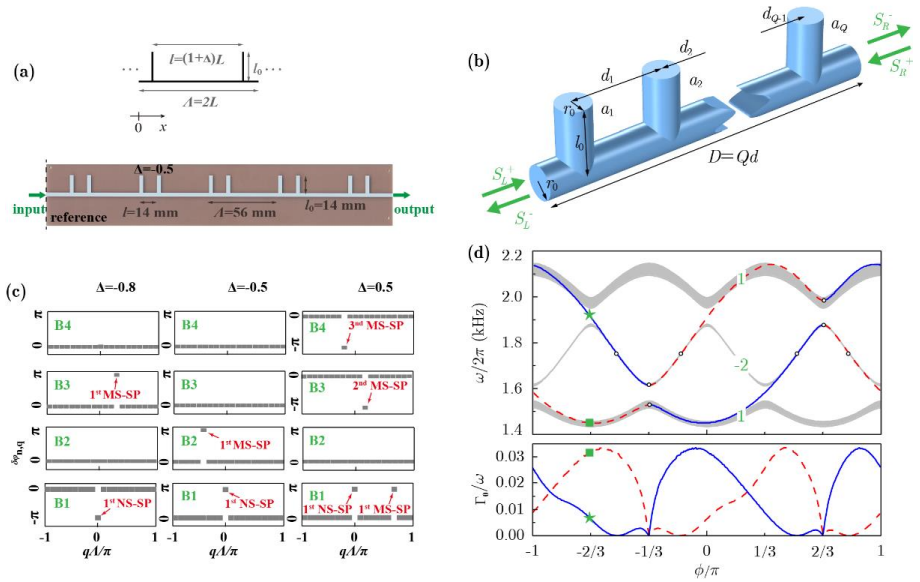

Fig. 1 (a) The unit cell of the dimerized comb-like waveguide system and an experimental sample. (b) The unit cell of the AAH comb-like waveguide system. (c) The contribution of each Bloch mode to the Zak phase. (d) The topological edge state.

Dimerized Comb-like Waveguide System~ The topological properties of one-dimensional periodic system which has mirror symmetry can be described by the Zak phase. The Zak phase in dimerized comb-like waveguide system is investigated. It is found that there are some singular points in the bulk band across which the Bloch states contribute π to the Zak phase, whereas in the rest of the band the contribution is nearly zero [shown in Fig.1(c)]. **It is demonstrated that the dimerized comb-like waveguide system contains two types of singular points**[1]**.** By tuning the dimerization parameter, the first band could contain one or two singular points, which is impossible for simple comb-like waveguide system and one-dimensional photonic systems. **So the topological properties of the first band gap which is located in the subwavelength region can be tuned**.

AAH Comb-like Waveguide System~ AAH model is one-dimensional tight-binding model whose on-site potential or the nearest neighbour couplings are modulated by the Harper equation. Recent studies show that it has topological nontrivial edge state. The AAH comb-like waveguide system is composed of a main waveguide and Q side-branch waveguides. The side-branch waveguides have same resonant frequency and are coupled with each other by the far-field couplings. When the distance between the nearest neighbour side-branch waveguides is modulated as $d_n = d\{1 + \delta\cos[2\pi b(n-1) + \phi]\}$, the system has topological nontrivial edge state. **Different from the tight-binding AAH model, the eigen frequencies of the topological nontrivial edge state in AAH comb-like waveguide system are complex[Fig.1(d)], the real part of which is the frequency of the topological edge state and the imaginary part is the intrinsic loss rate**. We then use the topological edge state to obtain exceptional point by tailoring the loss of the system.

References

[1] W.W. Zhu, Y.Q. Ding, J. Ren, Y. Sun, Y.H. Li, H.T. Jiang, and H. Chen, "Zak phase and band inversion in dimerized one-dimensional locally resonant metamaterials," Physical Review B **97**, 195307 (2018).

[2] W.W. Zhu, X.S. Fang, D.T. Li, Y. Sun, Y. Li, Y. Jing, and H. Chen, "Simultaneous Observation of a Topological Edge State and Exceptional point in an Open and Non-Hermitian Acoustic system," Physical Review Letters **121**, 124501 (2018).

On-demand generation and depth control of shallow silicon vacancy in silicon carbide

Qiang Li[1,2], Jun Feng Wang[1,2], Fei Fei Yan[1,2], Jin Shi Xu[1,2], Chuan Feng Li[1,2] and Guang Can Guo[1,2]

[1]*CAS Key Laboratory of Quantum Information, University of Science and Technology of China, Hefei, Anhui 230026, People's Republic of China*

[2] *CAS Center for Excellence in Quantum Information and Quantum Physics, University of Science and Technology of China, Hefeii, Anhui 230026, People's Republic of China*

Defects in silicon carbide have been explored as promising spin systems in quantum technologies. However, for practical quantum metrology and quantum communication, it is critical to achieve the on-demand shallow spin-defect generation [1]. In this work, it is presented that the generation and characterization of shallow silicon vacancies in SiC by using different implanted ions and annealing conditions. The conversion efficiency of silicon vacancy of helium ions is shown to be higher than that by carbon and hydrogen ions in a wide implanted fluence range. Furthermore, after optimizing annealing conditions, the conversion efficiency can be increased more than 2 times. Due to the high density of the generated ensemble defects, the sensitivity to sense a static magnetic field can be researched as high as $\eta_B \approx 11.9\mu T/\sqrt{Hz}$, which is about 15 times higher than previous results [2]. By carefully optimizing implanted conditions, it is further showed that a single silicon vacancy array can be generated with about 80 % conversion efficiency, which reaches the highest conversion yield in solid state systems. Besides, a method is also presented, describing how to precisely control the depth of the ion implanted generated shallow silicon vacancy defects in SiC using the reactive ion etching. By successive nanoscale plasma etching, the shallow defects are brought close to the SiC surface step by step. The results pave the way for using on-demand generated shallow silicon vacancy for quantum information processing and quantum photonics and investigating the surface spins properties in SiC and the applications in nanoscale sensing [3].

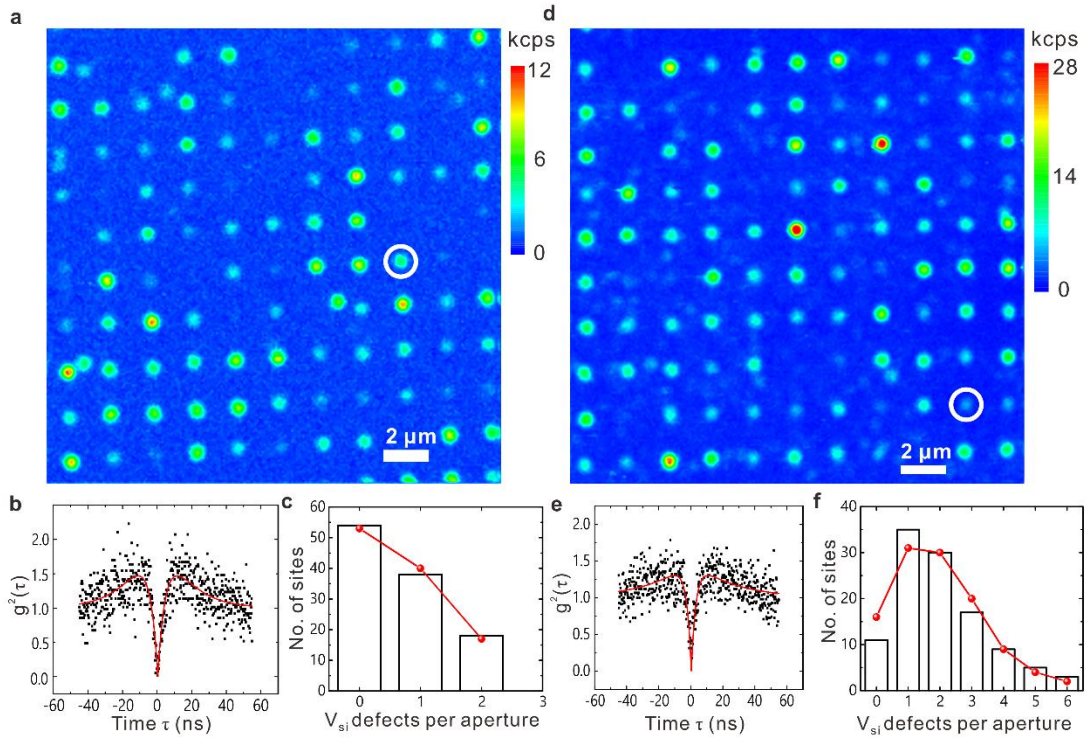

Fig. 1 Character of the carbon implanted shallow single V_{Si} defect arrays. (a) and (d) are two representative confocal fluorescence images (20×20 μm^2) of the implanted shallow single V_{Si} defect arrays before and after annealing (600 ℃ for 1 h) with an excitation power of 0.5 mW, respectively. The scale bars are 2 μm. (b) and (e) are the second-order correlation function measurement of the single V_{Si} defects (correspond to the circled single V_{Si} defects in (a) and (b), respectively), respectively. The red lines are the fits of the data. (c) and (f) are the statistics of the number of V_{Si} defects per implanted aperture. The data are fitted with the Poisson distribution (red curves).

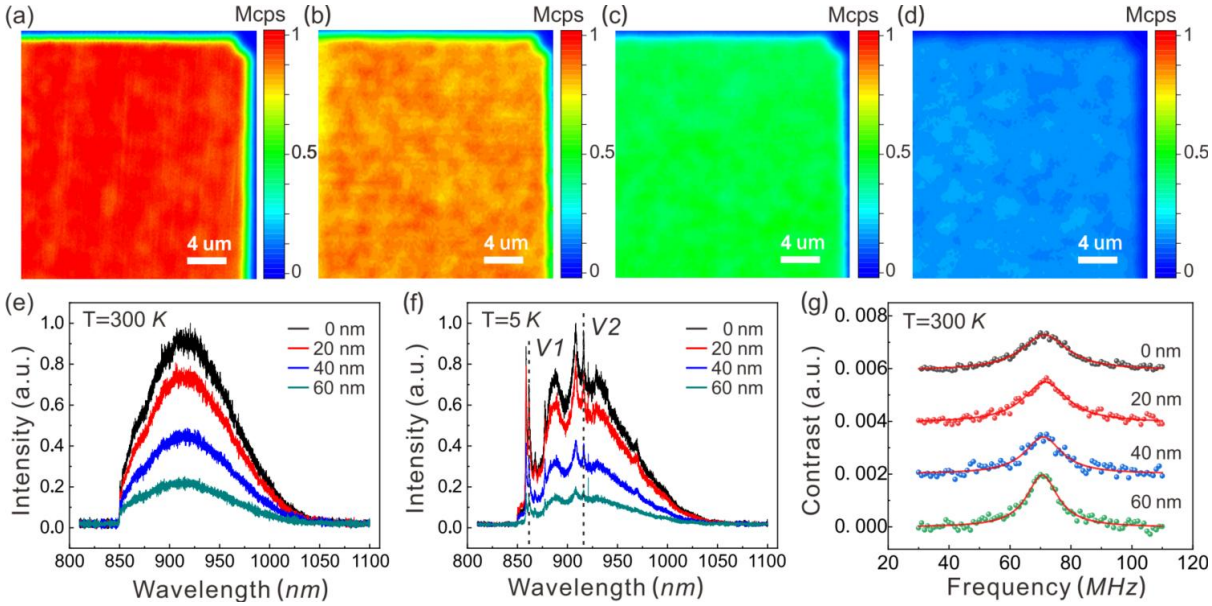

Fig. 2 Four respectively depth dependence of the counts, PL spectrum and ODMR of V_{Si} defects generated by 20 keV C^+ ions with dose of 10*13 cm^{-2}. (a)-(d) Fluorescence images at the same position after different etched depths of 0 nm, 20 nm, 40 nm and 60 nm, respectively. All the scale bars and the color bars in (a), (b), (c) and (d) are 4 um and 1 Mcps, respectively. (e) The RT PL spectrum of the V Si defects after different etched depths. (f) The LT PL spectrum of the V_{Si} defects after different etched depths at low temperature of 5 K. Two characterized peaks labeled as V1 (861 nm) and V2 (915 nm), denoted by vertical black dashed lines, are corresponding to the ZPL of two types of V_{Si} defects in SiC. (g) The ODMR signals of the V_{Si} after different etched depths at room temperature. The red solid lines are the Lorentz fitting to the data.

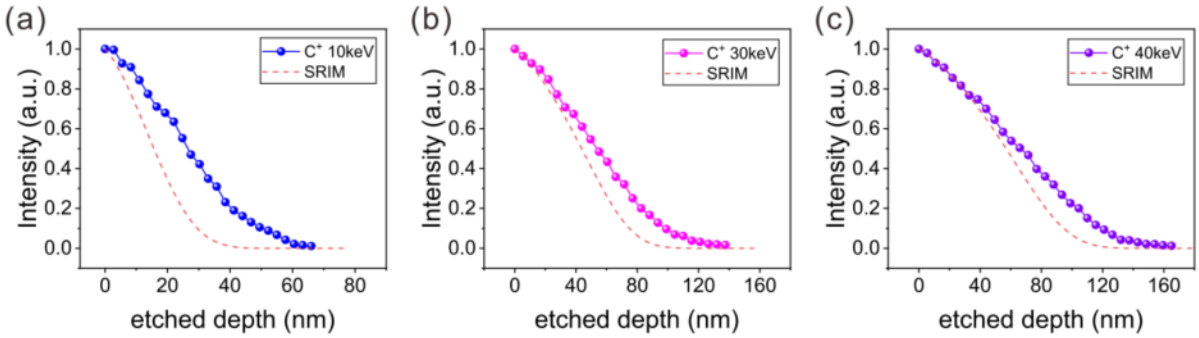

Fig. 3 Normalized mean PL intensity of the shallow V Si defects generated by C^+ ions implantation for various energy with the same dose of 10*13 cm^{-2} after different etched depth. The energy of C^+ is 10 keV (a), 30 keV (b), 40 keV (c),respectively. The blue dots in (a), pink dots in (b) and purple dots in (c) represent the experimental results of the mean PL intensity with the etched depth and the red dashed line in each figure represents the SRIM simulation result under the corresponding ion implantation conditions. The difference between the experiment and SRIM simulation is due to the effect of ion channel.

Example References

[1] J. F. Wang, Y. Zhou, X. M. Zhang, F. C. Liu, Y. Li, K. Li, Z. Liu, G. Z. Wang, W. B. Gao, "Efficient Generation of an Array of Single Silicon-Vacancy Defects in Silicon Carbide," Phys. Rev. Appl, **7**, 064021. (2017).

[2] M. Widmann, S.-Y. Lee, T. Rendler, N. T. Son, H. Fedder, S. Paik, L.-P. Yang, N. Zhao, S. Yang, I. Booker, A. Denisenko, M. Jamali, S. A. Momenzadeh, I. Gerhardt, T. Ohshima, A. Gali, E. Janzén, J. Wrachtrup, " Coherent control of single spins in silicon carbide at room temperature," *Nature Materials*, **14**, 164-168 (2014).

[3] F.-Z. Shi, Q. Zhang, P.-F. Wang, H.-B. Sun, J.-R. Wang, X. Rong, M. Chen, C.-Y. Ju, F. Reinhard, H.-W.Chen, et al. " Single-protein spin resonance spectroscopy under ambient conditions," *Science*, **347**, 1135–1138 (2015).

Deterministic phase estimation in standard quantum limit with real-time feedback control

Kaimin Zheng[1*], Huichao Xu[1], Aonan Zhang[1], and Lijian Zhang[1]
[1] College of Engineering and Applied Sciences, and School of Physics, Nanjing University, Nanjing 210093, China

*kaiminzheng@smail. nju.edu.cn

Abstract : An ab initio phase estimation protocol based on zero-photon measurement and a feedback control is proposed in this paper. Compared to the no-feedback case, we can eliminate the ambiguity when the estimated phases are inferred from the conditional probability distribution. After 100 times measurement, we can saturate the Cramér-Rao bound. By using the feedback control, the ultimate measurement precisions are independent on the true phases. In addition, we employ the rejection filtering Bayesian inference algorithm to realize the Bayesian phase estimation.

In this paper, we have realized the ab initio phase estimation at the SQL independent on the true phase. In our adaptive Bayesian phase estimation, the other phase θ is adjusted with an online approach. The experiment apparatus is described in Fig.1

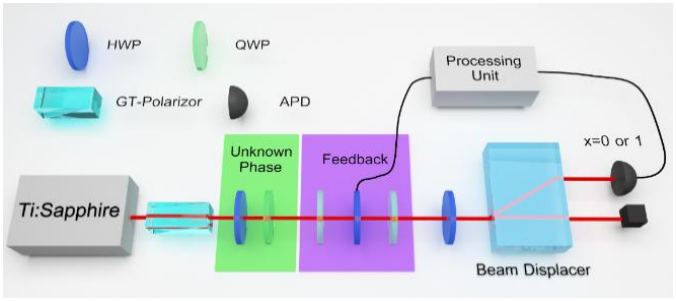

Fig. 1 The abbreviation "Fig." (for figure) should appear first, followed by the figure number, a space, and then the figure caption. Use the same sequence for table but do not abbreviate "Table."

In our experiment， all the input photons are prepared in $|\psi\rangle=\left(|H\rangle+|V\rangle\right)/\sqrt{2}$, after the insert phase ϕ and feedback phase θ， we can obtain the measurement result x_k from the APD in each step detection. Then the result is sent to the processing unit, which contain a MATLAB program perform the Bayesian algorithm to update the conditional probability distribution $p\left(\phi|\vec{x}_k,\vec{\theta}_k\right)$. We can obtain the estimated phase ϕ_{est} and Holevo variance from the last conditional probability distribution. After 100 times measurement, we can saturate the Cramér-Rao bound, which is described in Fig.2. At last, we can saturate the Cramér-Rao bound after 100 times measurement.

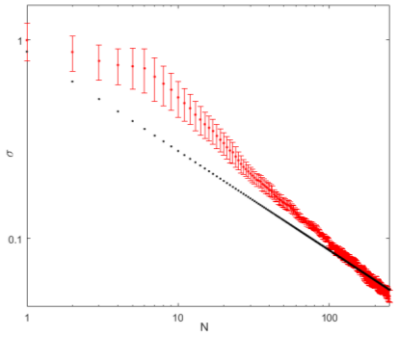

Fig. 2 :The evolution of σ during the 150 steps .Black dotted line is SQL; Red dotted line is Holevo variance.

References

[1] V. Giovannetti, S. Lloyd, and L. Maccone, "Advances in quantum metrology," Nat. Photonics 5(4), 222 (2011).
[2] S. L. Braunstein and C. M. Caves, "Statistical distance and the geometry of quantum states," Phys. Rev. Lett. 72(22), 3439–3443 (1994)

Repetition rate tuning of soliton in microrod resonators

Rui Niu[1], Shuai Wan[1], Shu-Man Sun[1], Tai-Gao Ma[1], Hao-Jing Chen[1], Wei-Qiang Wang[2], Zhizhou Lu[2], Wen-Fu Zhang[2], Guang-Can Guo[1], Chang-Ling Zou[1], Chunhua Dong[1]

1. Key Laboratory of Quantum Information, CAS, University of Science and Technology of China, Hefei, Anhui 230026, P. R. China

2. State Key Laboratory of Transient Optics and Photonics, Xi'an Institute of Optics and Precision Mechanics (XIOPM), Chinese Academy of Sciences (CAS), Xi'an 710119, China

Benefiting from the strongly enhanced nonlinear optics effects in high-quality (Q) factor whispering gallery (WG) microresonators, frequency combs have been observed in various experimental platforms via cascaded nonlinear processes [1-5]. In 2014, it was demonstrated that the coherent frequency comb, which is called temporal soliton state, can be generated spontaneously by the competition of Kerr nonlinearity, continuous laser driving and dissipation in a crystalline WG microresonator [6-7]. The dissipative Kerr soliton (DKS) offers broadband low-noise frequency comb in frequency domain, or the femotsecond pulse train in the time-domain. The DKS in microphotonic cavities has the merits of scalability, stability, portability and low power consumption, thus it holds great potentials for applications in ultrahigh data rate communication, high precision optical ranging, dual-comb spectroscopy, low-noise microwave source, optical clock and astronomical spectrometer calibration.

Here, we experimentally demonstrate the effective tuning of the repetition rate of DKS in a microrod cavity. By introducing an auxiliary laser to excite the mode that is excluded from soliton micro-comb generations, the cavity thermal response is effectively adjusted and the switching to the DKS can be stably achieved. Based on such a controlling approach, we realized the DKS in the microrod under different external bias stress, and successfully tuned the repetition rate f_{rep} of the soliton microcomb over 30 MHz. Our platform allows the stabilization of the device temperature by the auxiliary laser, precise and fast tuning of the f_{rep}, thus making it potential for locking soliton microcomb.

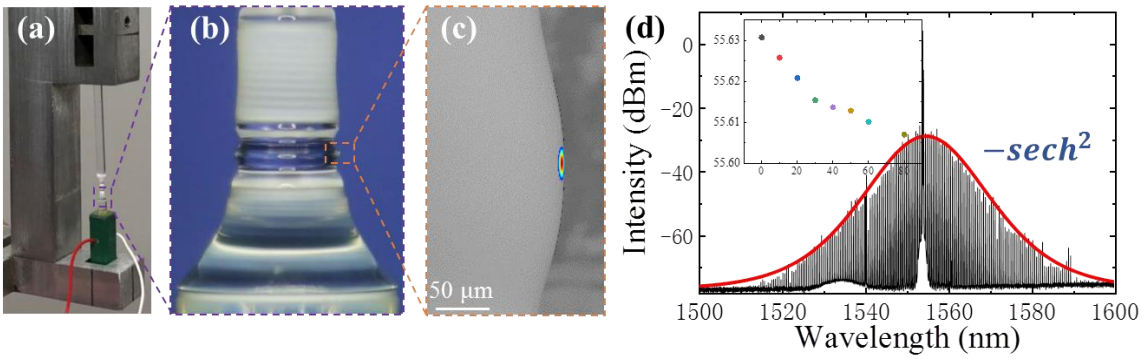

Fig. 1 (a) The setup for the mechanical tuning of microrod, where a PZT (green block) is used to compress the microrod. (b) The photo of the microrod cavity, with a diameter of about 1.2 mm. (c) The optical microscopy picture of microrod cavity and the corresponding optical mode profile of the whispering gallery modes by numerical simulation. (d) Typical optical spectrum of single DKS, the red line shows the spectral $sech^2$ envelope. Inset: The dependence of RF beat note frequency with the different applied PZT voltage.

Example References

[1] T. J. Kippenberg, R. Holzwarth, and S. a. Diddams, "Microresonatorbased optical frequency combs," Science **332**, 555–9 (2011).
[2] P. Del'Haye, A. Schliesser, O. Arcizet, T. Wilken, R. Holzwarth, and T. J. Kippenberg, "Optical frequency comb generation from a monolithic microresonator," Nature **450**, 1214–1217 (2007).
[3] Y. K. Chembo, "Kerr optical frequency combs: theory, applications and perspectives," Nanophotonics **5**, 214–230 (2016).
[4] X. Guo, C.-L. Zou, H. Jung, Z. Gong, A. Bruch, L. Jiang, and H. X. Tang, "Efficient Generation of a Near-visible Frequency Comb via Cherenkovlike Radiation from a Kerr Microcomb," Phys. Rev. Appl. **10**, 014012 (2018).
[5] A. Pasquazi, M. Peccianti, L. Razzari, D. J. Moss, S. Coen, M. Erkintalo, Y. K. Chembo, T. Hansson, S. Wabnitz, P. Del'Haye, X. Xue, A. M. Weiner, and R. Morandotti, "Micro-combs: A novel generation of optical sources," Phys. Rep. **729**, 1–81 (2018).
[6] S. B. Papp, P. Del'Haye, and S. A. Diddams, "Mechanical control of a microrod-resonator optical frequency comb," Phys. Rev. X **3**, 031003 (2013).
[7] T. J. Kippenberg, A. L. Gaeta, M. Lipson, and M. L. Gorodetsky, "Dissipative Kerr solitons in optical microresonators," Science **361**, eaan8083 (2018).

Optical Frequency Comb Generation Based on High Order Mode in a Thin Micro-ring Resonator

Yanjing Zhao, Liao Chen, Xinliang Zhang*

Wuhan National Laboratory for Optoelectronics & School of Optical and Electronic Information, Huazhong University of Science and Technology, Wuhan 430074, China

High-Q Si_3N_4 micro-resonators with anomalous group velocity dispersion has enabled broadband optical frequency comb generation [1]. However the intrinsically high film stress of Si_3N_4 has limited the layer thickness, suppressing the realization of anomalous dispersion. Intensive efforts have been made to overcome the problem, such as photonic Damascene process [2] and introducing mechanical trenches [3], which has either complicated the fabrication process or made it difficult for subsequent processing. Here we present a novel method enabling the generation of frequency comb in Si_3N_4 thin waveguide based on higher order mode, bypassing the challenge of high film stress.

The dispersion of our micro-ring is calculated by full-vector mode solver. Fig. 1(a) shows the dispersion of multiple modes (TE0 TE1 TE2 TM0) for Si_3N_4 waveguide with a height of 400nm and width of 2000nm. As higher modes have bigger dispersion parameter than the fundamental mode at shorter wavelength, they suffer greater loss. Considering the tradeoff between dispersion and loss, we choose TE1 mode. By properly designing the structural parameters, the anomalous dispersion region can be tuned from C band to visible band with height of waveguide smaller than 450nm, as illustrated in Fig. 1(b). The coupling coefficient of the micro-ring for TE0 and TE1mode varies with the width of straight waveguide. As shown in Fig. 1(c)-1(d), TE1 mode can be excited efficiently with the width of straight waveguide being 1100nm. Kerr comb generation based on TE1 mode in the modified structure is simulated by the Lugiato-Lefever equation, as exhibited in Fig. 2.

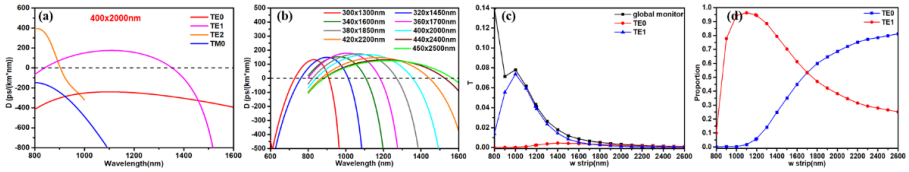

Fig. 1 (a) Dispersion of multiple modes for Si_3N_4 waveguide with a height of 400nm and width of 2000nm. (b) Dispersion for Si_3N_4 waveguides with modified cross sections. (c)- (d) Coupling coefficient of TE0 and TE1 mode between micro-ring and the straight waveguide.

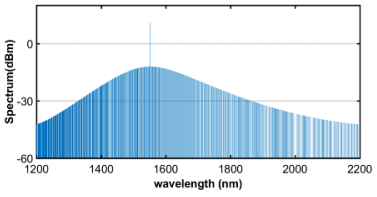

Fig. 2 The frequency comb generation based on TE1 mode in a micro-ring with the radius 100μm and cross section 450x2000nm when the pump power is 1.5W and pump wavelength is 1550nm.

References

[1] Okawachi, Yoshitomo, "Octave-spanning frequency comb generation in a silicon nitride chip." Optics letters **36**, 3398-3400(2011).

[2] Pfeiffer, Martin HP, "Ultra-smooth silicon nitride waveguides based on the Damascene reflow process: fabrication and loss origins." Optica **5**, 884-892(2018).

[3] Luke, Kevin, "Overcoming Si_3N_4 film stress limitations for high quality factor ring resonators." Optics express **21**, 22829-22833(2013).

High speed silicon Mach-Zehnder modulator via a pilot run

Peiyan Zhao[1,2], **Zhaobang Zeng**[1,2], **Nan Yang**[1,2], and **Wei Jiang**[1,2]

1. National Laboratory of Solid State Microstructures, Nanjing University, Nanjing 210093, China

2. College of Engineering and Applied Sciences, Nanjing University, Nanjing 210093, China

Recently, silicon photonics has developed rapidly and showed great potential for next generation high speed data processing and transmission[1], due to its inherent compatibility with CMOS technologies. Silicon modulators constitute a key building block[2] in silicon photonics considering its broad applications in short-reach optical interconnects for data centers and supercomputers.

We design an asymmetric MZM with a length difference of 20 μm between two arms, which results in a free spectral range (FSR) of about 30nm. Considering the complex fabrication of MOS capacitor and vertical PN junction, we finally use the lateral PN junction. Its length is 2mm due to the tradeoff between the modulation efficiency and the insertion loss. Two 1×2 MMI structures are utilized for input/output 3-dB couplers. The electrode is designed to be the coplanar waveguide (CPW) electrode, the matched resistances are integrated on chip to reduce the reflection of the RF signal. The device was fabricated in a CMOS foundry with no experience in active photonic devices (process development for this pilot run will be reported elsewhere).. Figure 1(a) shows the schematic view of the MZM and figure 1(b) shows the experimental setup of the measurement system.

In the experiment, The input and output chip coupling is achieved via grating couplers and the insertion loss of the fiber to the chip is about 4.8 dB. Then, we apply various reverse DC voltages for one arm through a bias tee and measure the optical transmission spectrum of the MZM as shown in the figure 1(c). After subtracting the grating coupler losses, the insertion loss of the MZM is about 8.6 dB, including the loss of doped phase shifters and two MMIs. The observed static extinction ratio is more than 30 dB, which indicates a good balance of the optical power between the two arms of the MZM. The FSR is about 30 nm, which is consistent with theory. And at the bias voltage of -1.9 V, the calculated $V_\pi L_\pi$ is 0.75 V·cm. Then, the wavelength of the laser is fixed at 1556 nm, and we record the data of the output optical power versus continuous bias voltages.

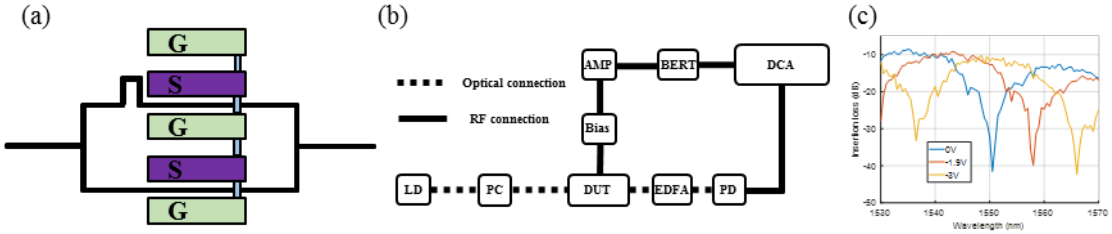

Fig. 1 (a) the schematic view of the MZM; (b) the experimental setup of the measurement system; (c) the optical transmission spectrum of the MZM.

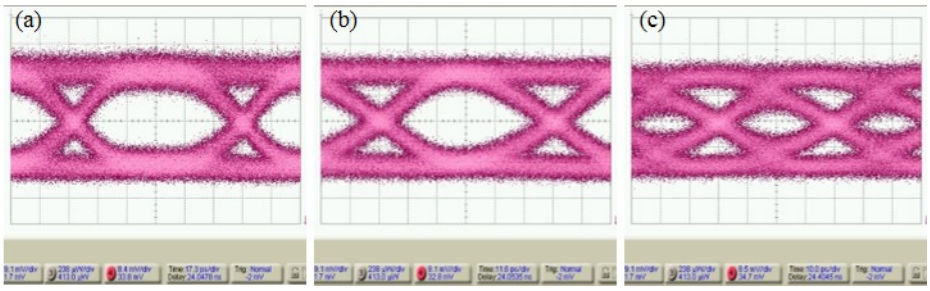

Fig. 2 The eye diagrams at different transmission rate of (a) 10Gb/s (b) 14Gb/s and (c) 25Gb/s.

Optical eye diagrams are measured to show the high speed modulation performance of the MZM. A pseudorandom binary sequence (PRBS) signal with a pattern length of 2^{31}-1 is generated by a bit error rate tester. Then the electrical signal is passed through power amplifier and bias tee to obtain a 3.2 Vpp driving signal with 1.9 V reverse bias voltage. The signal is applied to the MZM using a 40 GHz GSG probe fabricated by GGB industries incorporation. The power of the input laser is 10dBm. The output optical signal is amplified using the erbium doped fiber amplifier (EDFA) and fed into the Agilent wide band oscilloscope by means of commercial 50GHz photodetector. Figure 2 shows single-arm-drive eye diagrams at different transmission rate of (a) 10Gb/s (b) 14Gb/s and (c) 25Gb/s when the wavelength is 1556nm, set at the quadrature point of the MZM.

References

[1] Soref, R., "The Past, Present, and Future of Silicon Photonics," IEEE Journal of Selected Topics in Quantum Electronics, 12(6), 1678-1687 (2007).

[2] Reed, G. T., Mashanovich, G. Z., Gardes, F. Y., and Thomson, D. J., "Silicon optical modulators," Nature Photonics, 4(8), 518-526(2010).

High-contrast and Low-power All-optical Switch Using Fano Resonance Based on A Silicon Nanobeam Cavity

Gaoneng Dong, Yilun Wang, Xinliang Zhang*

Wuhan National Laboratory for Optoelectronics & School of Optical and Electronic Information, Huazhong University of Science and Technology, Wuhan 430074, China

All-optical switch is a basic building block for all-optical signal processing, which is expected to meet the increasing demands on communication networks for higher and higher information processing rates [1]. Thanks to the small mode volume (V) and high quality factor (Q), photonic crystal (PhC) nanocavity, which can effectively enhance the interaction between light and matter, has been used to demonstrate all-optical switch with relatively high speed and low switching energy [2, 3]. However, as most of these schemes are based on Lorentzian resonance, which consists of a gradual change in the tailing, there is a trade-off between the switching contrast and the switching energy. In contrast, a Fano resonance [4], which originates from an interference effect between a discrete state and a continuous background, can realize high-contrast and low-power all-optical switch, simultaneously [5].

Here, we experimentally demonstrate an ultra-compact all-optical switch involving Fano resonance based on a side-coupled Fabry-Perot (F-P) resonator and a silicon PhC nanobeam cavity, with an area of only 11 μm^2, as illustrated in Fig. 1(a)-(b). By adding a central-taper section with ten holes in the nanocavity to increase its intrinsic Q, we achieve a sharp asymmetric transmission spectrum, with an extinction ratio (ER) as high as 40 dB and a peak loss as low as 0.6 dB, as shown in Fig. 1(c). As far as we know, this is the highest measured ER in PhC-based Fano resonance. These excellent properties enable us to realize an all-optical switch with faster switching recovery time, lower power consumption and higher contrast, comparing to that involving Lorentzian resonance, as shown in Fig. 1(d)-(e). Figure 1(f) shows that the switching recovery time (90%-10%) for Fano resonance is 200 ps, which is about one third of that for Lorentzian resonance (580 ps). Besides, under a signal rate of 2.5 Gb/s, the switching contrast for Fano resonance (10 dB) is 6-dB smaller than that for Lorentzian resonance (4 dB), while the switching energy of the former (226 fJ) is 7-dB smaller than that of the later (1.12 pJ), as illustrated in Fig. 1(g).

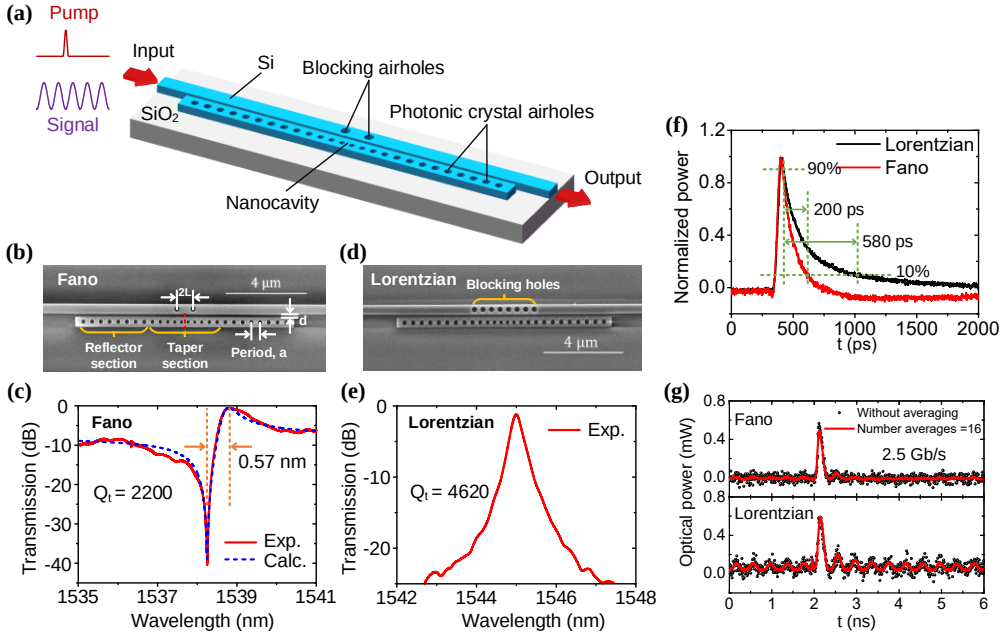

Fig. 1 (a) Schematic of the all-optical switch involving Fano resonance. (b)-(e) SEM images and experimental transmission spectra of fano and Lorentzain structures. (f)-(g) Switching dynamic characteristics of fano and Lorentzain structures.

References

[1]. A. E. Willner, S. Khaleghi, M. R. Chitgarha, and O. F. Yilmaz, "All-Optical Signal Processing," J. Lightwave Technol. **32**, 660-680 (2014).

[2]. K. Nozaki, T. Tanabe, A. Shinya, S. Matsuo, T. Sato, H. Taniyama, and M. Notomi, "Sub-femtojoule all-optical switching using a photonic-crystal nanocavity," Nat. Photon. **4**, 477-483 (2010).

[3]. T. Tanabe, M. Notomi, S. Mitsugi, A. Shinya, and E. Kuramochi, "All-optical switches on a silicon chip realized using photonic crystal nanocavities," Appl. Phys. Lett. **87**, 151112 (2005).

[4]. U. Fano, "Effects of Configuration Interaction on Intensities and Phase Shifts," Phys. Rev. **124**, 1866-1878 (1961).

[5]. K. Nozaki, A. Shinya, S. Matsuo, T. Sato, E. Kuramochi, and M. Notomi, "Ultralow-energy and high-contrast all-optical switch involving Fano resonance based on coupled photonic crystal nanocavities," Opt. Express **21**, 11877-11888 (2013).

Plasmonic Photothermoelectric Generator

Chao Zhuang[1], **Huanjun Chen**[1]

1. State Key Laboratory of Optoelectronic Materials and Technologies, Sun Yat-Sen University, Guangzhou, 510275

Localized surface plasmon resonance (LSPR) occurs when free electrons in metal nanoparticle oscillate resonantly with incident electromagnetic waves [1]. Robust and versatile as it is, there has been numerous efforts utilizing this phenomenon for various applications, among which, photothermal effect stands out for its excellent conversion efficiency [2], and it has been heavily investigated in the research of photothermal therapy [3]. By varying the size and shape of Au nanorod (AuNRs), its resonance wavelength can be readily tailored across visible to infrared, that is to say, this characteristics grant us the ability to intensely absorb the large portion of solar radiation and turn it efficiently into heat. Having this material at hand, solar cells' flaw of incapability of utilizing full spectrum of solar radiation occurs to us that the photothermal effect might be an alternative to improve solar cell efficiency.

In this work, we utilized polyvinyl alcohol-made film to encapsulate gold nanorods mixture, which consist of various AuNRs with different aspect ratios. The content of the film was so diverse that a large portion of the solar spectrum was easily covered, as shown in Fig.1 (a). Further, we integrated the film with commercial Peltier cooler, also known as thermoelectric cooler, which uses electrical input to generate heat flux between the junction of two different types of materials, or it can be used the other way around, that is, by applying a temperature difference on two sides of the cooler, a voltage will be generated. By combining the plasmonic polymer film and Peltier cooler, this integrated device can now convert light into heat and into electricity.

To examine the integrated device's conversion efficiency, we placed it under a solar simulator where the junction between the film and the cooler would be heated up while the other side of the cooler was in contact with a big metal substrate, causing temperature difference in the two side of the cooler. By controlling the shutter turned on and off with 1 min period, the voltage output of the Peltier cooler is shown in Fig.1 (b). The red and black curves represent the output of mere Peltier cooler and the integrated device, respectively, confirming the existence of photothermal effect, indicated by Fig.1 (c). According to the results, the overall conversion efficiency of the integrated device is 0.04%.

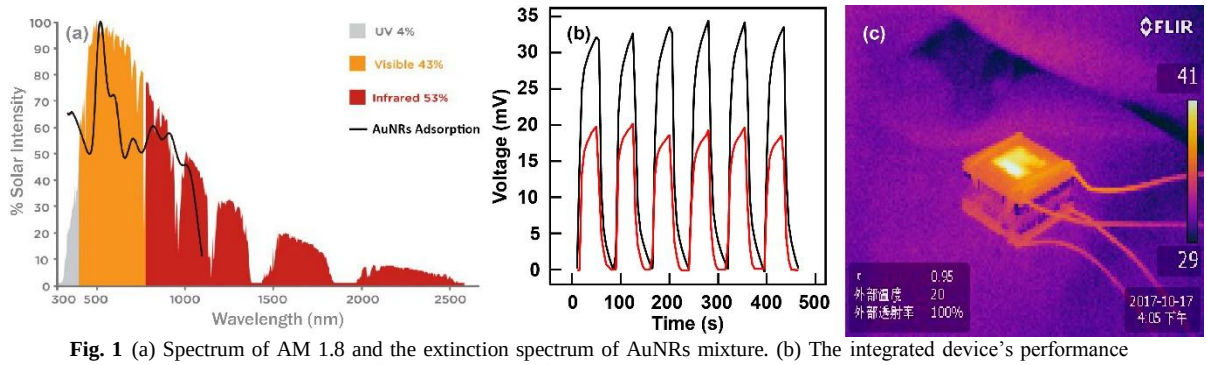

Fig. 1 (a) Spectrum of AM 1.8 and the extinction spectrum of AuNRs mixture. (b) The integrated device's performance under solar simulator. (c) Digital infrared photograph of integrated device at work. Bright yellow area is the place where the plasmonic polymer film locates.

In summary, we have here demonstrated a proof-of-concept of a novel device, consisting of a polymeric film containing various AuNRs and a Peltier cooler, which converts visible and near infrared portion of solar radiation into electricity in an indirect fashion. In addition, if further integrate this device with solar cell, waste heat generated by which can also be utilized to produce extra electricity. Thus we believe this device could be useful and complementary for solar cell studies.

Example References

[1] H. Chen, L. Shao, Q. Li, and J. Wang, "Gold nanorods and their plasmonic properties," Chem. Soc. Rev **42**, 2679-2724 (2013).
[2] H. Chen, L. Shao, T. Ming, Z. Sun, C. Zhao, B. Yang, et al., "Understanding the Photothermal Conversion Efficiency of Gold Nanocrystals," Small **6,** 2272-2280 (2010).
[3] X.H. Huang, I.H. El-Sayed, W. Qian and M.A. El-Sayed, "Cancer cell imaging and photothermal therapy in the near-infrared region by using gold nanorods," J. Am. Chem. Soc **128,** 2115-2120 (2006).

Device-independent Characterization of Quantum Measurements

Aonan Zhang,[1] Jie Xie,[1] Michele Dall'Arno,[2] Francesco Buscemi,[3] Vlatko Vedral,[4] Lijian Zhang[1,*]

[1] *College of Engineering and Applied Sciences and School of Physics, Nanjing University, Nanjing 210093, China*

[2] *Centre for Quantum Technologies, National University of Singapore, 3 Science Drive 2, 117543, Singapore*

[3] *Graduate School of Informatics, Nagoya University, Chikusa-ku, Nagoya, 464-8601, Japan*

[4] *Atomic and Laser Physics, Clarendon Laboratory, University of Oxford, Parks Road, Oxford OX13PU, United Kingdom*

The accurate and reliable description of quantum measurements is of both fundamental and practical importance in quantum information science. To date quantum tomography is the common tool to conduct the characterization of quantum detectors. However, such a characterization relies on credible and known probe systems, rendering reliability of the characterization lost in circular argument. This means characterizing a quantum measurement demands extra assumptions on the state-generating device and thus the accuracy of such characterization is in relative sense. Notably, device-independent (DI) way of testing quantum measurements has been proposed to certify the theoretical hypothesis for quantum measurements without any assumptions on the preparation apparatus [1]. In this work, we develop and demonstrate characterization of quantum measurements motivated by the device-independent test, with only measurement statistics.

The characterization protocol is motivated by the device-independent test of a hypothetical quantum measurement. That is, for a qubit positive operator-valued measure (POVM) $\pi \coloneqq \{\pi_y\}$, any output distribution $p \coloneqq \{p_y\}$ belongs to the set of distributions generated by $\pi \coloneqq \{\pi_y\}$ if and only if

$$\begin{cases} (I - QQ^{+})(p - t) = 0, \\ (p - t)^{T} Q^{+} (p - t) \leq 1, \end{cases}$$

where I is the identity matrix, t is the vector $t_y \coloneqq \frac{1}{2}\mathrm{Tr}[\pi_y]$, Q is the matrix $Q_{i,j} = \frac{1}{2}\mathrm{Tr}[\pi_i \pi_j] - \frac{1}{4}\mathrm{Tr}[\pi_i]\mathrm{Tr}[\pi_j]$, and $(.)^{+}$ represents the Moore-Penrose pseudoinverse. Based on this idea, one can optimize Q, t of a quantum measurement from only the measurement statistics, without the information of probe states. Here we demonstrate device-independent characterization of two representative measurements for tomography purpose: mutually unbiased basis (MUB) and symmetric informationally-complete (SIC) measurement.

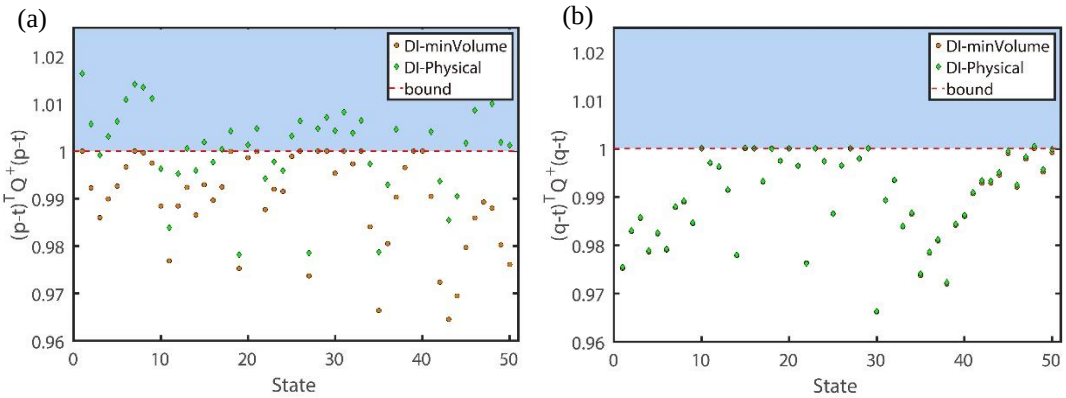

Fig. 1 Experimental results for device-independent characterization of quantum measurements: (a) MUB, (b) SIC. The results given by MVEE (dot, yellow) are further optimized to satisfy the physical constraint (diamond, green).

The characterization perform the minimum volume enclosing ellipsoid (MVEE) algorithm to find Q, t compatible with the DI test. In addition, due to the statistical fluctuations on the measurement results, physical constraint is applied to give a result from a valid quantum measurement. The experimental results for the tests of DI characterization are shown in Fig. 1. The reconstructed results Q and t are very close to the reconstruction given by usual quantum detector tomography.

References

[1] M. Dall'Arno, S. Brandsen, F. Buscemi, and V. Vedral, Device-independent tests of quantum measurements, Phys. Rev. Lett. 118, 250501 (2017).

Novel Cubic Tin Sulfide (π-SnS) chalcogenide as a potential candidate for optoelectronic and energy storage devices

Sajid Ur Rehman[1,2], Zeeshan Tariq[1,2], Faheem K. Butt[3], Bakhtiar Ul Haq[4], Chuanbo Li[5]*

1. State Key Laboratory on Integrated Optoelectronics, Institute of Semiconductors, Chinese Academy of Sciences, 100083, Beijing, China.
2. University of Chinese Academy of Sciences, Beijing 100049, P.R. China.
3. Department of Physics, Division of Science and Technology, University of Education, College Road, Township, Lahore.
4. Advanced Functional Materials & Optoelectronics Laboratory (AFMOL), Department of Physics, Faculty of Science, King Khalid University, P.O. Box 9004, Abha, Saudi Arabia.
5. Minzu University of China, Beijing 100081, China.

The lead-based chalcogenides have been extensively investigated in photovoltaic devices. The concerns over the toxicity of lead have motivated the exploration of less toxic materials. This motivation has led to the exploration of π-SnS (cubic structure). Due to moderate band gap and novel electronic properties π-SnS have received significant consideration for future energy related applications. Here we performed first-principles calculations to investigate the structural, electronic, optical, and elastic properties of π-SnS. Analysis of electronic band structure with hybrid potential (HSE03) reveals that it is indirect semiconductor in nature and its value is ~1.5 eV. We measured the optical phonons dispersion and density of states in the Brillouin zone which proved that cubic SnS is electronically stable. As per our knowledge its elastic constants are calculated for first time which satisfy the criteria of Born stability. Bulk, Young's, shear moduli, Lame's coefficients, Poisson's ratio, Debye temperature and average sound velocity are determined based on Voigt-Reuss approximation. Bulk modulus is estimated as 55.32/20.98 (GPa) for LDA/GGA and calculated values are well consisted with Birch-Murnaghan equation of state (EOS) results. The surface visualization of bulk, Young's, shear moduli in 2D and 3D graphs reveal the elastic anisotropic nature of π-SnS. Debye temperature (θ_D) is found as 314.86/214.88 K for LDA/GGA. Due to high Debye temperature the thermal conductivity of π-SnS could be high as compared to α-SnS (θ_D ~270 K). Also, longitudinal and transversal wave velocities along [100], [110] and [111] directions are calculated for the first time. Current study about π-SnS revealed that it could be potential material for exploitation in energy storage, thermoelectric and optoelectronic devices.

Scattering-immune Surface-wave Open Resonator for Arbitrary Disorders

Jian-Bin Liu[1,2], Su Xu[1]

[1]*State Key Lab of Integrated Optoelectronic, College of Electronic Science and Engineering, Jilin University, 2699 Qianjin Street, Changchun, China.*

[2]*College of physics, Jilin University, 2699 Qianjin Street, Changchun, China.*

The surface electromagnetic wave open resonator played as an extremely important role for providing feedback in the ultra-fast laser systems [1,2]. To overcome scattering loss induced by the optical momentum mismatch at the disorders with sharp corners, topological photonics [3] and transformation optics [4] have been adopted in the design of open resonators. However, the transformation optics-based solution could only work for a specific disorder, while the nontrivial open cavities need redundant photonic-crystal surrounding areas. Therefore, it is still a challenge to obtain a flexible open resonator design that could be integrated into the laser systems without additional space requirement. **Here, we propose a generalized methodology to solve the aforementioned obstacle on common industrial photonic integration of laser systems. By involving the electromagnetic canalization effect by the infinitely anisotropic medium, the photonic momentum could keep matched for arbitrary disorders.** To prove this concept, Ag/dielectric layered structures with deep subwavelength periodicity was adopted to suppress the scattering waves at disorders. As shown in Fig. 1, the scattering-immune guiding effect is observed numerically for the cases of quadrilateral and hexagonal open resonators in different terahertz frequencies. **This flexible integration solution is experimentally feasible at Terahertz and infrared frequencies** with a mixed employment of femtosecond laser direct writing and physical vapor deposition. Our work could find a wide range of applications in laser system and integrated circuits.

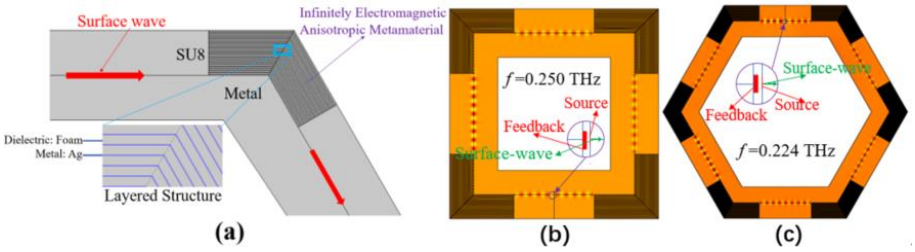

Fig. 1 (a) The schematic of scattering-immune surface-wave guidance with the infinite anisotropic medium. The magnetic field distributions of (b) Quadrilateral open resonator at 0.250 THz and (c) Hexagonal open resonator at 0.224 THz.

References

[1] A. Yariv, Y. Xu, R. K. Lee, and A. Scherer, "Coupled-resonator optical waveguide: a proposal and analysis," Opt. Lett. **24**, 711-713 (1999).

[2] R. W. P. Drever, J. L. Hall, F. V. Kowalski, J. Hough, G. M. Ford, A. J. Munley, and H. Ward, "Laser Phase and Frequency Stabilization Using an Optical Resonator," Appl. Phys. B **31**, 97-105 (1983).

[3] B. Bahari, A. Ndao, F. Vallini, A. E. Amili, Y. Fainman, and B. Kanté, "Nonreciprocal lasing in topological cavities of arbitrary geometries," Science **358**, 636-640 (2017).

[4] S.Xu, H. Y. Xu, H. H. Gao, Y. Y. Jiang, F. X. Yu, J. D. Joannopoulos, M. Soljacic, H. S. Chen, H. D. Sun, and B. L. Zhang, "Broadband surface-wave transformation cloak," PNAS **112**, 7635-7638 (2015).

Terahertz-Induced Resist Polymerization in Nanoantennas

Woongkyu Park[1], **Youjin Lee**[1], **Taehee Kang**[1], **Jeeyoon Jeong**[1], **and Dai-Sik Kim**[1]

[1]*Department of Physics and Astronomy and Center for Atom Scale Electromagnetism, Seoul National University, Seoul 151-747, South Korea*

Plasmon-induced photopolymerization has been intensively studied for various applications including nanolithography [1], near-field mapping [2], and selective functionalization [3]. However, the studies have been limited from the near-infrared to the ultraviolet regime, since the photon energy required for the photopolymerization is in the ultraviolet region. In the visible and near-infrared ranges where the photon energy is relatively smaller than the activation energy, polymerization is induced by multiphoton absorption. This multiphoton polymerization can be realized by an intense light source such as femtosecond laser or high field enhancement of the plasmonic structures. However, in the longer wavelength region, such as mid-infrared, there has been no report of the resist polymerization. It is because the number of the photons required to resist polymerization increases as the wavelength becomes longer, therefore the probability of the polymerization decreases drastically. Then is it impossible to cross-link the resist using longer wavelength light?

Here, we report a resist polymerization phenomena using nano-slot antenna structures or bowtie nanoantennas with intense terahertz pulses [4]. The resist is polymerized when the terahertz light is illuminated. (Fig. 1) The resist is polymerized only in the nanoantennas, where huge local field enhancement occurs. By measuring the electric current between the two poles of the bowtie antennas, we show that terahertz field-driven photoemission is the key mechanism for the resist polymerization. Finite element method simulation and theoretical calculations are well-matched with experimental results. Our work extends nano-photochemistry into the field of terahertz optics.

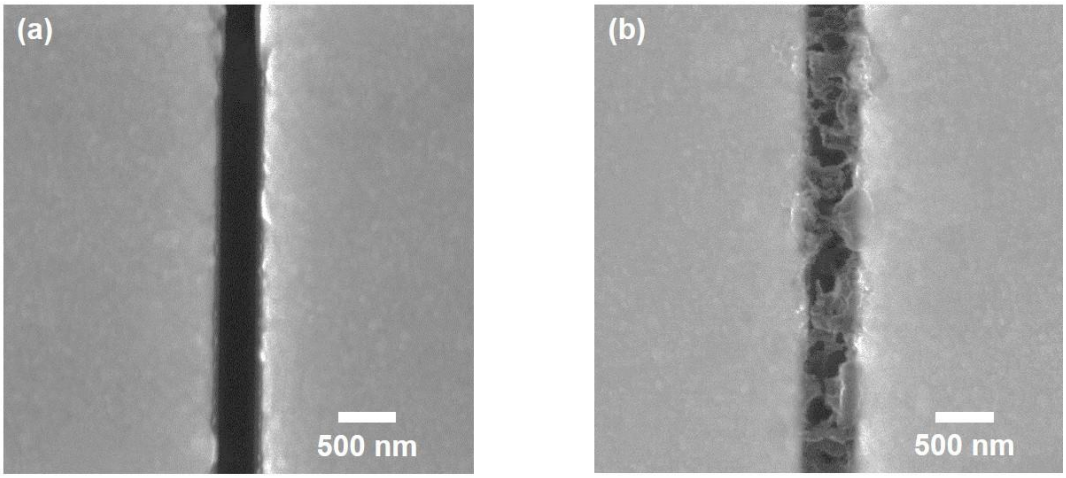

Fig. 1 (a) Scanning electron microscope image of the terahertz nano-slot antenna. (b) Scanning electron microscope image of the terahertz nano-slot antenna after resist coating, terahertz light illumination, and resist development.

References

[1] Srituravanich W., Fang N., Sun C., Luo Q. and Zhang X. "Plasmonic nanolithography", *Nano Lett.* **4**, 1085-1088 (2004).
[2] Gruber C., Hirzer A., Schmidt V., Trügler A., Hohenester U., Ditlbacher H., Hohenau A. and Krenn J. R. "Imaging nanowire plasmon modes with two-photon polymerization", *Appl. Phys. Lett.* **106**, 081101 (2015).
[3] Zhou X., Deeb C., Kostcheev S., Wiederrecht G. P., Adam P.-M., Béal J., Plain J., Gosztola D. J., Grand J., Félidj N., Wang H., Vial A. and Bachelot R. "Selective Functionalization of the Nanogap of a Plasmonic Dimer", *ACS Photonics* **2**, 121-129 (2015).
[4] Park W., Lee Y., Kang T., Jeong J. and Kim D.-S. "Terahertz-driven polymerization of resists in nanoantennas", *Scientific Reports* **8**, 7762 (2018).

Nature Conference on Nanophotonics and Integrated Photonics 2018

Mid-infrared edge plasmon modes of chemically-doped graphene

Ximiao Wang, Zebo Zheng, and Huanjun Chen*

State Key Laboratory of Optoelectronic Materials and Technologies, Guangdong Province Key Laboratory of Display Material and Technology, School of Electronics and Information Technology, Sun Yat-sen University, Guangzhou 510275

**E-mail: chenhj8@mail.sysu.edu.cn*

Abstract Graphene plasmons (GPs) possess excellent performance of ultrahigh electromagnetic field confinement, low-loss, broad band response, which have many potential applications in nanophotonics and optoelectronics such as room temperature mid-infrared photodetectors, sensors and modulators. In particular, the GPs at the edge of graphene have been demonstrated to exhibit superior field confinement compared with sheet plasmons. Here, we report on study of the plasmon modes at different chiral edges of the graphene upon chemical doping. By using scattering-type scanning near-field optical microscopy (s-SNOM), we present detailed insight that edge plasmon behaviors strongly dependent on the chirality, where the electromagnetic confinements of the zigzag edge is better than the armchair edge exhibits. The edge plasmons can be modified by utilizing chemical doping. Due to the discrepancy of charge absorption ability of the two chirality edge, the zigzag edges have a larger tunable range. This presents an encouraging step towards ultrahigh confined graphene plasmonic devices.

GPs are the collective oscillation of Dirac electrons, which exhibits unprecedent high light confinements, substantially low loss and broad band response range from near-infrared to terahertz frequency [1,2]. These outstanding characteristics make the GPs have great potentials in optical communication, sensing, detection and imaging. GPs have been directly observed in graphene nanoribbons and nanostructures by near-field optical microscopy [3,4]. One of the most interesting breakthroughs of the GPs is the edge plasmon modes along the graphene edge. These types of ultra-confined resonating edge modes can realize mush smaller mode volumes [4,5]. However, as far as we know, plasmon at edge of different charities (that is, zigzag edges and armchair) of monolayer graphene have not been studied.

Here we used near field infrared nano-imaging to unravel the edge plasmon characteristics of the zigzag and armchair edges in the graphene. We have presented the strong dependence of the localized electromagnetic fields on the graphene chirality. In order to further investigate the tailoring of the light field by the zigzag ang armchair edges, we adopted chemical doping to the graphene monolayer. The discrepancy in the abilities of charge absorption of the two chiral edges were observed. We further provided a theoretical understanding of the dispersion and modes of the both edges.

In conclusion, we have studied the edge plasmon modes along the zigzag and armchair edges of the monolayer graphene. The results from near field infrared nano-imaging showed that both of the two edge modes could realize electromagnetics confinements, while zigzag edges have stronger light field localizations. We further found that the armchair edges with smaller absorption energy, were not sensitive to the chemical doping. On the contrary, the zigzag edges had higher adsorption energy and were more susceptible upon the chemical doping. Therefore, the zigzag edge has a larger plasmon modulation range. Moreover, the Drude-type conductivity is still applicable to the edge plasmon dispersion of zigzag and armchair edge. We believe our results can provide important reference for the future research and integration of graphene plasmonic devices.

References

[1] Geim, A. K., and K. S. Novoselov, “The rise of graphene.” Nature Materials 6.3:183-91(2007).
[2] Novoselov, K. S., et al, "A roadmap for graphene. " Nature 490.7419:192-200(2012).
[3] Zheng, Ze-Bo, et al. "Tailoring of electromagnetic field localizations by two-dimensional graphene nanostructures." Light: Science & Applications 6.10: e17057(2017).
[4] Fei, Z., et al, "Edge and surface plasmons in graphene nanoribbons." Nano letters 15.12: 8271-8276(2015).
[5] Nikitin, A. Y., et al. "Real-space mapping of tailored sheet and edge plasmons in graphene nanoresonators." Nature Photonics 10.4: 239(2016).

Piezoelectric Effect Tuning on ZnO Microwire WGM Lasing

Junfeng Lu, Caofeng Pan, Zhonglin Wang
Beijing Institute of Nanoenergy and Nanosystems, Chinese Academy of Sciences, Beijing 100083, P. R. China
College of Nanoscience and Technology, University of Chinese Academy of Sciences, Beijing 100049, P. R. China

Chunxiang Xu
State Key Laboratory of Bioelectronics, School of Biological Science and Medical Engineering, Southeast University, Nanjing 210096, P. R. China

Laser has huge applications in science and technology, from medical to manufacture and to defense. An important characteristic of a laser is its wavelength and width of wavelengths. Wavelength tunable nanolasers are promising for multifunctional applications in all-optical integrated nanodevices, optical communication, optical sensing technology and spectroscopy analysis. However, most of the methods for tuning the lasing modes are lack of a dynamical tenability, that is, the ability to reversibly modulate the stimulated emission in a pre-prepared single micro&nanodevice.

In this work, a novel method for a dynamic tuning on coherent light emission wavelengths of single ZnO microcavity has been proposed. Owing to the dominant role occupied by the piezoelectric polarization effect in the wurtzite-structure ZnO microwire, the effective dielectric constant (or refraction index) of the gain media [1, 2] is modulated towards an increasing trend by applying a tensile strain, resulting in a shift of the strain-mediated whispering-gallery mode (WGM) lasing at room temperature. Due to the narrow linewidth in the lasing mode, the strain-dependent spectral resolution is improved by an order of magnitude, making it feasible for achieving high-precision, ultra-sensitive and non-contact stress sensing. Our results have an important impact on laser modulation, optical communication and optical sensing technology.

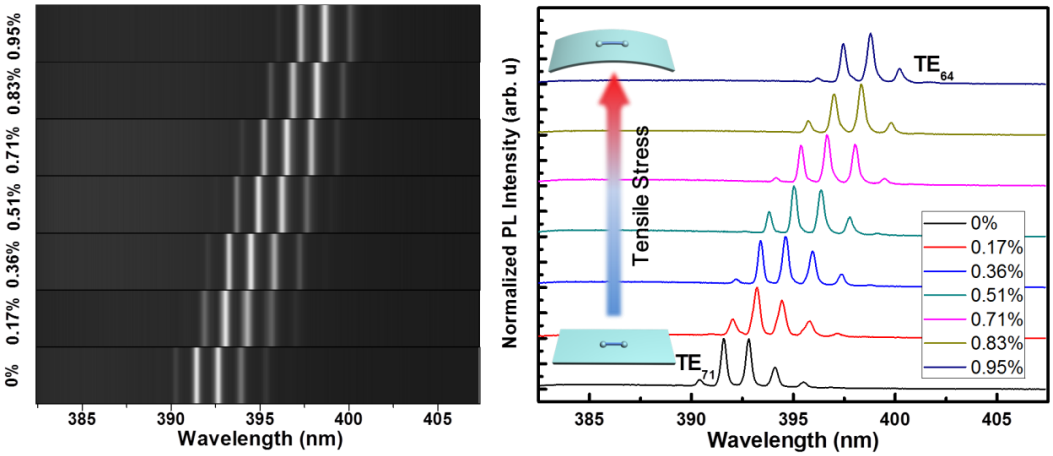

Fig. 1 Dynamical tuning on ZnO lasing mode by strain-induced piezoelectric polarization effect

References

[1] K. Vedam, T. A. Davis. *Phys. Rev.* **1969**, *181*, 1196-1201.
[2] W. Langer. *J. Appl. Phys.* **1966**, *37*, 3530-3532.

Generation of optical frequency comb in a $\chi^{(2)}$ sheet micro optical parametric oscillator via cavity phase matching

Xinjie Lv, Xin Ni, Zhenda Xie*, Huaying Liu, Nicol ò Sernicola, Gang Zhao, Zhenlin Wang, and Shi-Ning Zhu*

1.National Laboratory of Solid State Microstructures, School of Physics, College of Engineering and Applied Sciences, and School of Electronic Science and Engineering, Nanjing University, Nanjing 210093, China

*Corresponding author E-mail: xiezhenda@ nju.edu.cn, zhusn@nju.edu.cn

Optical frequency combs (OFC) are important for high precision spectroscopy[1,2,3], navigation [4], telecommunication [5] and astronomy [6]. These applications benefit from miniaturized comb sources for portable devices with high beat note frequencies, which are not offered with the conventional mode-locked laser [7] sources. So far, the vast majority of studies have focused on micro-ring μOPO with third order nonlinearity $\chi^{(3)}$, but high Q also makes the phase matching condition strict. On the other hand, the parametric oscillation can also be generated using second order nonlinearity $\chi^{(2)}$, which is much stronger than $\chi^{(3)}$ and reveals a new approach for μOPO comb.

Here we report a $\chi^{(2)}$ sheet micro optical parametric oscillator for generation of optical frequency comb via cavity phase matching. In the doubly-resonant SOPO, pumped by pulse, despite the normal dispersion of 275.4 fs^2/mm, comb lines are measured to be equidistant within the accuracy of a high-performance wavelength meter. Broad comb centered at 1064nm are achieved from these SOPOs, whose span exceeds 21.2 THz with comb line spacings of about 133.0 GHz. The slope efficiency and peak output power exceed 22.6 % and 14.9 kW. This new $\chi^{(2)}$ SOPO platform is a promising candidate for portable integrated optical frequency comb generation and the oscillation threshold is possible solved with higher-Q and especially in waveguide devices.

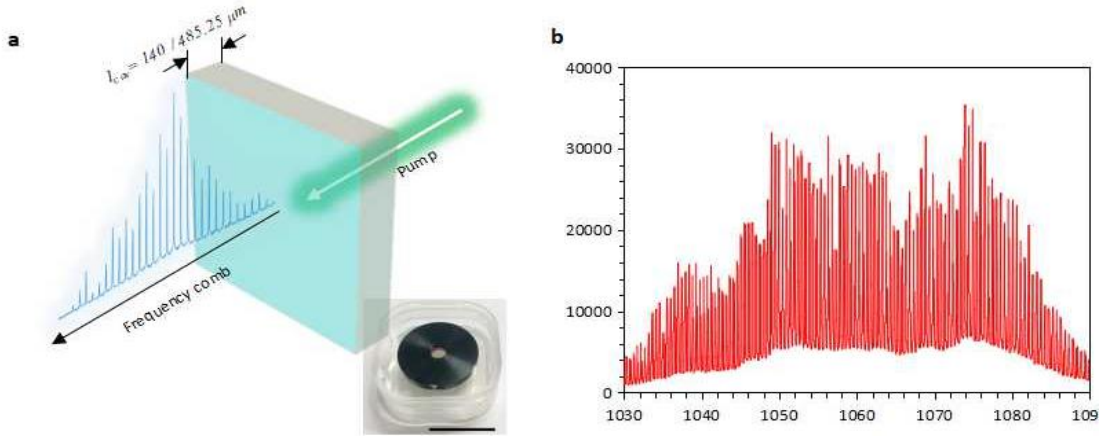

FIG. 1 a. The SOPOs for the comb generation with cavity lengths of 140 μm and 485.25 μm, respectively. Inset shows the picture of our SOPO sample with aluminum mount. **b.** The spectrum of 485.25 μm SOPO at 830μJ pump.

References

[1] S. A. Diddams, L. Hollberg, and V. Mbele, Nature 445, 627 (2007).

[2] J. Mandon, G. Guelachvili, and N. Picque, Nat. Photon. 3, 99 (2009).

[3] Austin G. Griffith, Ryan K.W. Lau, Jaime Cardenas, Yoshitomo Okawachi, Aseema Mohanty, Romy Fain, Yoon Ho Daniel Lee, Mengjie Yu, Christopher T. Phare, Carl B. Poitras, Alexander L. Gaeta and Michal Lipson, Nat. Commun. 6, 6299 (2015).

[4] I. Coddington, W. C. Swann, L. Nenadovic, and N. R. Newbury, Nat. Photon. 3, 351 (2009).

[5] D. Hillerkuss et al., Nat. Photon. 5, 364 (2011).

[6] C. H. Li, A. J. Benedick, P. Fendel, A. G. Glenday, F. X. Kärtner, D. F. Phillips, D. Sasselov, A. Szentgyorgyi, and R. L. Walsworth, Nature 452, 610 (2008).

[7] T. Herr, V. Brasch, J. D. Jost, C. Y. Wang, N. M. Kondratiev, M. L. Gorodetsky and T. J. Kippenberg,, Nat. Photon 8, 145 (2014).

Optical focusing based on the planar metasurface reflector with application to trapping cold molecules

Weiyang Cai[1], Haiyu Yu[1], Tao Li[2], Yaling Yin[1], Yong Xia[1], Jianping Yin[1]

[1]*State Key Laboratory of Precision Spectroscopy, Department of Physics, East China Normal University, Shanghai 200062, China*

[2]*National Laboratory of Solid State Microstructures, College of Engineering and Applied Sciences, Nanjing University, Nanjing 210093, China*

We demonstrate theoretically a 2D sub-wavelength silicon-grating reflector with strong focusing capability, and the potential application to an optical dipole trap of cold molecules such as MgF. We study the dependence of the focusing properties of this reflector on its structural parameters, numerical aperture, and fabrication-error tolerant. Our study shows that the reflector delivers high reflectivity and strong focusing performances with the maximum intensity at the focal point over 200 times of the incident one. Such a focusing field on the reflector can provide a deep potential to trap cold MgF molecules from a standard magneto-optical trap.

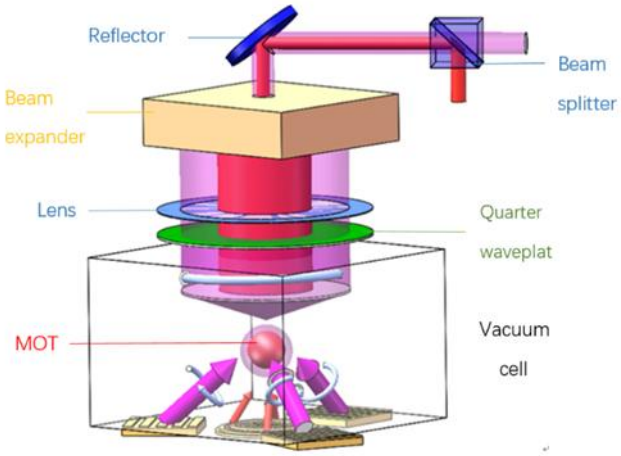

Figure.1 Schematic of grating MOT and surface optical trapping of MgF molecules

Reference

[1] D. Fattal, et al, Flat dielectric grating reflectors with focusing abilities, Nat. Photonics 4, 466 (2010).

[2] C. C. Nshii, et al, A surface-patterned chip as a strong source of ultracold atoms for quantum technologies, Nat. Nanotechnology 8, 321 (2013).

[3] E. Imhof, et al, Two-dimensional grating magneto-optical trap, Phys. Rev. A. 96, 033636 (2017).

Hybridized plasmon – phonon modes supported in graphene/MoO_3 stacked hybrid structures

Fengsheng Sun, Zebo Zheng, Huanjun Chen*

State Key Laboratory of Optoelectronic Materials and Technologies, Guangdong Province Key Laboratory of Display Material and Technology, School of Electronics and Information Technology, Sun Yat-sen University, Guangzhou 510275

**E-mail: chenhj8@mail.sysu.edu.cn*

Abstract At mid-infrared frequencies, graphene supports surface plasmon polaritons (SPPs), whereas van der Waals MoO_3 crystal is found to support surface phonon polaritons (SPhPs). In graphene/MoO_3 stacked hybrid structures, coherent oscillations of the electron density in graphene and the atomic vibrations in MoO_3 can produce hybridized plasmon – phonon modes, which are of hyperbolic nature originated from the highly anisotropic dielectric responses of the MoO_3. The hyperbolic plasmon–phonon polaritons possess the combined features of surface plasmon polaritons in graphene and hyperbolic phonon polaritons in MoO_3. The peculiar electrodynamic responsed of graphene/MoO_3 is illustrated via the calculated dispersion relation of the hybridized plasmon-phonon modes, which clearly indicate that the isotropic SPPs in graphene will be greatly affected by the anisotropic hyperbolic response of the MoO_3crystal.

Polaritons are electromagnetic waves coupled to charged dipoles in solid-state materials. Graphene plasmons are the collective oscillation of Dirac electrons and exhibit unprecedent broad band spectral response covering near-infrared to terahertz frequency. Graphene plasmons possess excellent performance of ultrahigh electromagnetic field confinements, low-loss and broad band responses[1-4]. Phonon polaritons induced by coupling of electromagnetic fields with optical phonons in polar crystals are another type of polaritons which can strongly confine the free-space light field deeply below the subwavelength region. [5]. In comparion with the surface plasmons, the phonon polaritons are able to achieve improved light confinements, reduced optical losses, and much higher quality factors. MoO_3 has been demonstrated as a natural materials supporting anisotropic hyperbolic phonon polaritons due to its crystalline structures [5]. It is forseen that combining the plasmon and phonon polaritons can lead to novle polaritonic modes that may enable a wealth of potential applications.

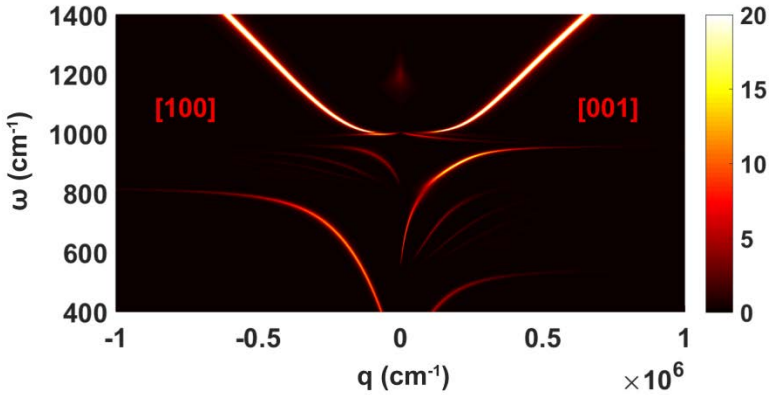

Fig. 1 Dispersion of the hyperbolic plasmon–phonon polaritons in the graphene/MoO_3 structures. The false color image delegates the imaginary part of the complex reflectivity, $Im r_p(q, \omega)$, in different directions of the graphene/MoO_3/SiO_2 multilayer structure.

In our recent study, we investigated the polaritonic responses of a stack hybrid structure, the MoO_3 flake covered with monolayer graphene. We have calculated the polaritonic dispersion relation of the hybrid structure. As shown in Fig. 1, multi-mode hyperbolic plasmon–phonon polaritons waves can be guided by the graphene/MoO_3/SiO_2 multilayer structure. In addition, due to the anisotropic responses of the MoO_3, the hybrid polaritonic modes exhibit distinctly different dispersion along the two in-plane principal crystalline axes, i.e., the [100] and [001] crystalline directions of the MoO_3. We have also conducted three-dimensional finite-difference time-domain (3D-FDTD) simulations to verify the theoretical calculations. Our results can can enrich the research of polaritonics of two-dimensional materials.

References

[1] Ju, L. et al. *Graphene plasmonics for tunable terahertz metamaterials*. Nat. Nanotech. 6, 630–634 (2011) .
[2] Chen, J. et al. *Optical nano-imaging of gate-tunable graphene plasmons*. Nature 487, 77–81 (2012).
[3] Fei, Z. et al. *Gate-tuning of graphene plasmons revealed by infrared nano-imaging.* Nature 487, 82–85 (2012).
[4] Fang, Z. et al. *Active tunable absorption enhancement with grapheme nanodisk arrays.* Nano Lett. 14, 299–304 (2014).
[5] Zheng, Zebo. et al. *Highly Confined and Tunable Hyperbolic Phonon Polaritons in Van Der Waals Semiconducting Transition Metal Oxides.* Adv. Meter. 30,1705318 (2018).
[6] Dai, S. et al. *Graphene on hexagonal boron nitride as a tunable hyperbolic metamaterial.* Nat. Nanotech. 10, 682–686 (2015).

Generation Of Visible Kerr Comb And Platicon Via Raman Assisted Four Wave mixing In Microresonator

Shunyu Yao[1], **Changxi Yang**[1]

1. *State Key Laboratory of Precision Measurement Technology and Instruments, Department of Precision Instruments, Tsinghua University, Beijing 100084, China*

Visible Kerr frequency comb generation is always a challenging subject since modulation instability is hard to occur due to the strong normal material dispersion in visible band. Here we demonstrate that visible Kerr frequency comb can be generated via Raman assisted four wave mixing (RFWM) process when Raman laser is stimulated in the cavity [1, 2]. We theoretically investigate the emergence of the RFWM comb lines by considering the Raman laser as another pump. Our analysis indicate that the spectrum of the parametric gain can be shifted by changing the pump detuning, leading the RFWM process more likely to occur. Thus the dispersion requirement for RFWM is not strict, easing the design and fabricate process significantly. To show the validity of our analysis, an AlN microresonator is demonstrared, a stable platicon and coherent Kerr frequency comb is generated with 780 nm pump.

We consider the condition where the Raman laser and the pump are equilibrated by loss and gain and remain undepleted during the emergence of the RFWM comb. The calculated four wave mixing gain between the pump and Raman laser is given by : $g = -\alpha + \sqrt{4\gamma^2 L^2 P_1 P_2 - \theta^2/4}$, where α is roundtrip loss, γ is nonlinearity coefficient, L is roundtrip length of the microresonator, P_1, P_2 is the intensity of the pump and Raman laser respectively. $\theta = \Delta kL - \delta_1 + \gamma L(2P_1 + 3P_2)$, δ_1 denotes the pump-cavity detuning, the phase mismatching $\Delta k = \sum_{n=1}^{\infty} 2\beta_{2n} L(\omega^{2n} - \Omega^{2n})/(2n)!$, where ω denotes the angular frequency offset from the central frequency between the pump and Raman laser. β_n is nth order dispersion at the central frequency. Our analysis indicates that the spectral location of the RFWM gain changes with different pump detunings. To verify the analysis, we perform simulations of LLE with Raman effect, the parameters used in the equation are from a typical AlN microresonator [2, 3]. Fig. 1(a) and Fig. 1(b) show the evolution of the simulated spectra of RFWM with different detuning, the spacing of the RFWM comb lines are also different. The frequency spacing of the strongest RFWM comb line predicted by our theory is compared with the simulation result, as is shown in Fig 1(c). The deviation may be attribute to the neglect of the Raman effect during the FWM process in the analysis.

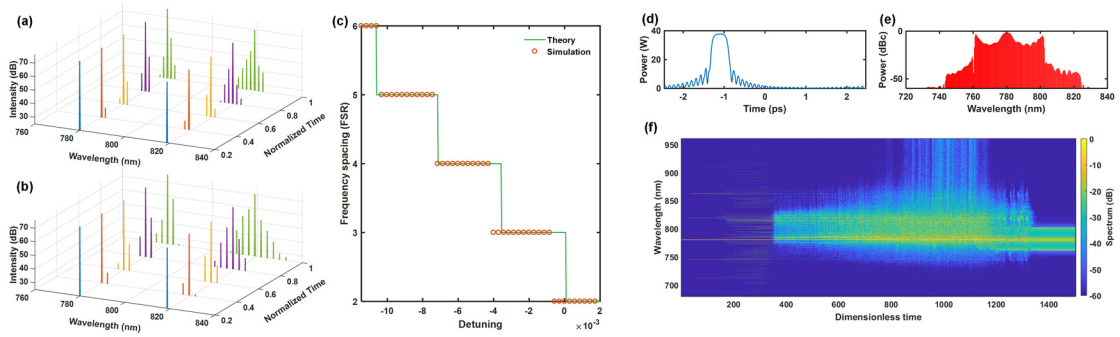

Fig. 1 (a). Evolution of the simulated spectrum of RFWM with $\delta_0 = 0$, the comb spacing is 2 FSRs. (b). Evolution of the simulated spectrum of RFWM with $\delta_0 = 0.006$, the comb spacing is 4 FSRs. (c). The frequency spacing of the strongest RFWM comb line under different detunings, the solid green line is calculated by our theory. (d) Temporal waveform of the platicon. (e) Spectrum of the platicon. (f) Spectral evolution of the platicon formation.

We also investigate the platicon generation via RFWM in a AlN microresonator with LLE. The waveguide is composed of a AlN film over sapphire, the width and the height of the waveguide is 1400 nm and 800 nm. The dispersion is calculated with a finited-element mode solver. The pump is set at 780 nm. After RFWM is generated, the pump is boosted to 433 mW, and is tuned further into the resonance. The comb first turn to a nonstationary state then become stable, and temporal platicon state is finally generated. The spectral evolution of the comb is shown in Fig. 1(f). Fig. 1(d) and Fig. 1(e) show the temporal waveform and the spectrum of the platicon. Our simulation result show that coherent visible Kerr comb can be generated via RFWM process.

References

[1] Y. K. Chembo, I. S. Grudinin, and N. Yu, "Spatiotemporal dynamics of Kerr-Raman optical frequency combs," Physical Review A **92**, 043818 (2015).

[2] X. Liu, C. Sun, B. Xiong, L. Wang, J. Wang, Y. Han, Z. Hao, H. Li, Y. Luo, and J. Yan, "Integrated High-Q Crystalline AlN Microresonators for Broadband Kerr and Raman Frequency Combs," ACS Photonics **5**, 1943-1950 (2018).

[3] X. Liu, C. Sun, B. Xiong, L. Wang, J. Wang, Y. Han, Z. Hao, H. Li, Y. Luo, and J. Yan, "Integrated continuous-wave aluminum nitride Raman laser," Optica **4**, 893-896 (2017).

Excitonic Quantum States in Cu_2O Microcrystals Grown on Silicon Substrates

Stephan Steinhauer[1], **Marijn A. M. Versteegh**[1], **Val Zwiller**[1]

1. Department of Applied Physics, Royal Institute of Technology (KTH), SE-106 91 Stockholm, Sweden

The optical properties of cuprous oxide (Cu_2O) - a p-type semiconductor exhibiting a direct dipole-forbidden band gap of 2.17 eV - have been comprehensively studied for decades, both from a fundamental perspective and for applications in photovoltaics and solar water splitting [1]. In particular, excitons in Cu_2O show large binding energies up to 150 meV, rendering this material a highly promising candidate for excitonic Bose-Einstein condensation [2]. Furthermore, giant Rydberg excitons in analogy to atomic systems have been demonstrated in Cu_2O with principal quantum numbers as large as $n=25$ and spatial extensions of more than 2 µm; these Rydberg excitons are characterized by a blockade effect due to strong dipole-dipole interactions [3], signatures of quantum chaos, and breaking of all anti-unitary symmetries [4]. However, state-of-the-art quantum optics experiments employing Cu_2O rely on natural bulk crystals due to their excellent quality [2–4]. Evidently, the development of optimized methods for the growth of synthetic Cu_2O micro- and nanostructures is required for studies on confinement effects and to deploy the full potential of this material for integrated quantum photonic technologies in the future.

Here, we present the growth of Cu_2O microcrystals on silicon substrates covered with 150 nm silicon dioxide by a facile thermal oxidation process. In Fig. 1 a), a representative example of the resulting structures is shown, which are characterized by faceted grain morphologies and dimensions considerably exceeding 1 µm. Photoluminescence experiments using continuous-wave green laser excitation at cryogenic temperatures in the mK range revealed pronounced emission from *1s* orthoexcitons, both via a direct and a phonon-assisted process. The results were compared with those obtained from a natural bulk single crystal, as can be seen in Fig. 1 b). The synthetic Cu_2O microcrystals exhibit remarkably low emission from oxygen point defects around 1.7 eV compared to the excitonic emission lines, validating the excellent material quality. The kinetic energies of *1s* orthoexcitons were assessed by analysing the lineshape of a phonon-assisted transition and were found to follow quantum-degenerate statistics of a Bose-Einstein distribution. The dependence of the *1s* orthoexciton energy distribution on the incident laser excitation power will be discussed. Furthermore, the synthetic Cu_2O microcrystals were found to host excited *np* Rydberg excitons up to principal quantum numbers n=6, as evidenced from luminescence spectra depicted in Fig. 1 c). The Rydberg exciton energies show excellent agreement with an n^{-2} relation. The power dependence of Rydberg exciton emission will be analysed and compared to reference measurements that were performed using a natural bulk crystal. Eventually, future prospects for site-controlled growth of Cu_2O microcrystals and for on-chip integration with photonic circuits will be discussed.

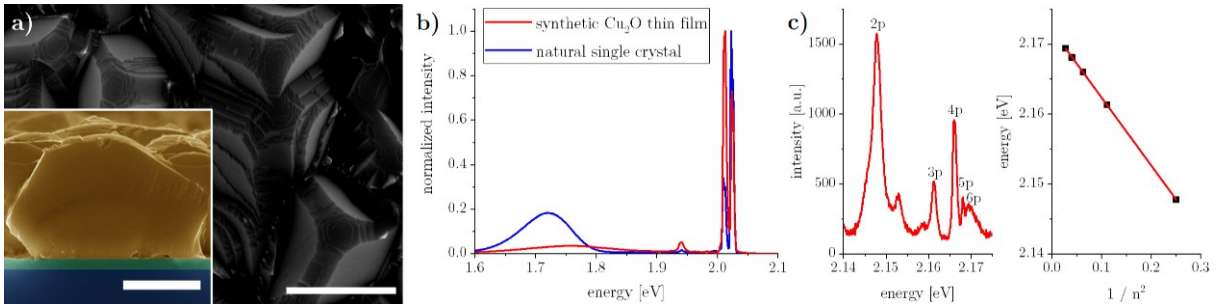

Fig. 1 a) Cu_2O microcrystals grown on SiO_2/Si substrates using a thermal oxidation process (scale bars 1 µm). b) Photoluminescence spectroscopy at cryogenic temperatures shows pronounced emission of *1s* orthoexcitons (around 2.0 eV) and considerably reduced defect luminescence (around 1.7 eV) compared to natural bulk single crystals. c) Photoluminescence of *np* Rydberg excitons up to principal quantum numbers n=6 in Cu_2O microcrystals exhibiting excellent agreement with an n^{-2} relation.

References

[1] L. Pan et al., "Boosting the performance of Cu_2O photocathodes for unassisted solar water splitting devices," Nature Catalysis **1**, 412–420 (2018).

[2] D. Snoke and G. M. Kavoulakis, "Bose–Einstein condensation of excitons in Cu_2O: progress over 30 years," Reports on Progress in Physics **77**, 116501 (2014).

[3] T. Kazimierczuk, D. Fröhlich, S. Scheel, H. Stolz, and M. Bayer, "Giant Rydberg excitons in the copper oxide Cu_2O," Nature **514**, 343–347 (2014).

[4] M. Aßmann, J. Thewes, D. Fröhlich, and M. Bayer, "Quantum chaos and breaking of all anti-unitary symmetries in Rydberg excitons", Nature Materials **15**, 741–746 (2016).

Turbidimetric Inhibition Immunoassay Revisited to Enhance Its Sensitivity by Optofluidic Laser

Xi Yang[1], Wenxiong Shu[1], Yuan Gong[1,*], Chaoyang Gong[1], Qiushu Chen[2], Xiaotian Tan[2], Xudong Fan[2], Yun-Jiang Rao[1]

1. Key Laboratory of Optical Fiber Sensing and Communications (Ministry of Education of China), University of Electronic Science and Technology of China, Chengdu, Sichuan 611731, China

2. Department of Biomedical Engineering, University of Michigan, Ann Arbor, Michigan 48109, USA

** Email : ygong@uestc.edu.cn*

Turbidimetric inhibition immunoassay (TIIA) is a classical immunodiagnostic method that has been extensively exploited for biomarker detection, however, its low sensitivity hinders the application in early diagnosis of diseases [1]. Here a new concept of optofluidic laser TIIA (OFL-TIIA) is proposed and demonstrated for sensitive protein detection. Different from detection of the one-pass laser loss in traditional TIIA, this method puts the immunoreaction into a laser cavity thus considerably multiplies the antigen-antibody complexes (AAC) induced loss by the enhancement of light-matter interaction through both the Fabry-Perot (FP) resonator and amplification effect of gain [2] (Fig. 1a).

Commercial IgG TIIA kit was selected as a demonstrative model to characterize the performance of OFL-TIIA. The immunoreaction between antibody and antigen is a reversible process that results in the formation of AAC. In TIIA, the concentration of the hybrid complexes vary with the ratio of antigen to antibody. As there are sufficient antibody molecules for the immunoreaction, both the size and concentration of AAC would increase with an increasing antigen molecules [3]. Moreover, we use polyethylene glycol (PEG) to reduce the solubility of AAC by exclusion of water and further enhance the turbidity as well as the sensitivity (Fig. 1b). A dynamic range of 5 orders of magnitude with an exceptional lower limit of detection (LOD) (1.8×10^{-10} g/L) was achieved (Fig. 1c).

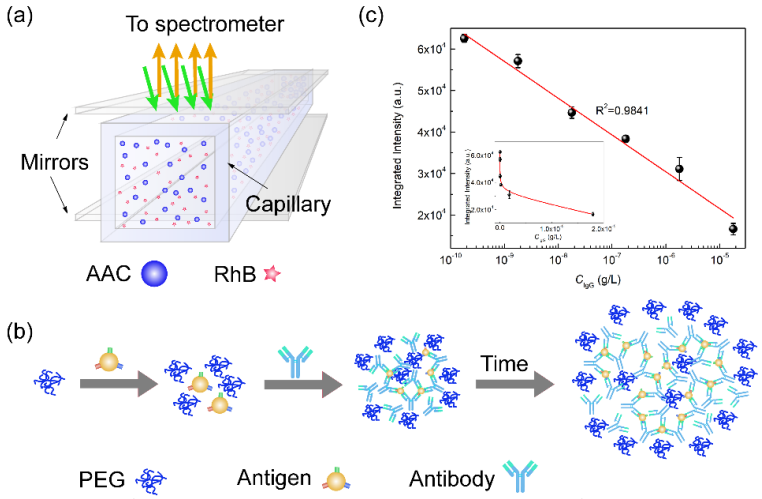

Fig. 1 (a) Schematic diagram of the OFL-TIIA. (b)The experimental procedure to form the AAC. (c) The standard curve for the OFL-TIIA. The error bar was based on triplicate tests.

The unprecedented sensitivity of OFL-TIIA would enable the biomarker detection for early diagnostics of diseases that was impossible by the traditional TIIA. This made up the fatal weakness of TIIA, which may refresh the extension of wide application of TIIA. Besides the high sensitivity, this technology also minimizes the sample volume by almost 1000-fold and thus lowers the cost for each test. The TIIA kits are more cost-effective since the immunoreaction process is very simple compared with ELISA methods. Homogeneous reaction, with short molecule-molecule distance for diffusion, allows the molecules attach to others in a short time and enables the rapid assay. With all these advantages, the OFL-TIIA provides a powerful technological platform for immunoassay in serum. Considering the abundance of commercial TIIA kits available and many under development, further expansion of TIIA applications is highly expected.

References

[1] R.L. Libby, "A new and rapid quantitative technic for the determination of the potency of types I and II antipneumococcal serum," J. Immunol. **34**, 269-279 (1938).

[2] X. Fan and S.H. Yun, "The potential of optofluidic biolasers," Nat. Methods **11**, 141-147 (2014).

[3] J.T. Whicher, C.P. Price, and K. Spencer, "Immunonephelometric and immunoturbidimetric assays for proteins," Crit. Rev. Cl. Lab. Sci. **18**, 213-260 (1982).

High Performance Single Crystalline Perovskite Thin Film Photodetector

Zhenqian Yang[1‡], Yuhao Deng[1‡], Xiaowei Zhang[1‡], Suo Wang[1], Huazhou Chen[1], Sui Yang[2], Jacob Khurgin[3], Nicholas X. Fang[4], Xiang Zhang[2], and Renmin Ma[1*]

1 State Key Lab for Mesoscopic Physics and School of Physics, Peking University, Beijing 100871, China

2 Department of Mechanical Engineering, University of California, Berkeley, California 94720, USA

3 Department of Electrical and Computer Engineering, Johns Hopkins University, Baltimore, Maryland 21218, USA

4 Department of Mechanical Engineering, Massachusetts Institute of Technology, Cambridge, Massachusetts 02139, USA

**Corresponding Author Renmin Ma: renminma@pku.edu.cn*

‡These authors contributed equally.

Single crystal thin film (SC-TF) materials are the cornerstone of modern electronic and photonic devices due to their distinct properties including low trap density, high mobility and well defined thickness. Nowadays, epitaxial growth technology can control the thickness of SC-TF down to monolayer level with high material purity. However, epitaxial growth requires lattice constant and expansion coefficient matches with substrates as well as high vacuum and temperature growth conditions.

Recently, halide perovskites that can be grown by low-cost solution based methods have emerged as a new class of semiconductor for high performance optoelectronic devices, such as solar cells, light emitting diodes and lasers, laser cooling, and photodetectors. In 2015, inverse temperature crystallization method has been developed to grow macroscale single crystalline halide perovskites. To improve the suitability of perovskites in most optoelectronic devices, including solar cells, photodetectors, light-emitting diodes and lasers etc., achieving simultaneously good crystallinity and proper thickness are essential. However, the aspect ratios of these macroscale single crystals have been limited to about unity depending on the isotropous growth rate in solution. Most recently, spatially limited condition has been introduced to grow perovskite crystals with improved aspect ratio. Compared to the bulk crystals, these perovskite crystals with reduced thickness show significantly improved performance in solar cells as well as in photodetectors.

However, to date, single crystalline perovskite based devices including solar cells and photodetectors all have the active layers thicker than several micrometers. Due to its high absorption coefficient, perovskite materials can absorb the incident light completely in hundreds of nanometers. Compared to the optimized film thickness in this range in devices based on polycrystalline films, the unnecessarily thick active layer in single crystalline perovskite based devices leads to a longer transit time and a larger recombination probability for the photon-excited carries, which degrades the device performance. Notwithstanding the growing body of work on perovskite devices, it is still very challenge to achieve simultaneously good crystallinity and proper thickness of perovskites in optoelectronic devices.

Here, we report a photodetector based on SC-TF perovskite active layer with an optimized thickness down to hundreds of nanometers. The device achieves a record photoconductive gain of 50 million and a gain-bandwidth product of 70 GHz. The superior performance of our SC-TF perovskite photodetectors is also been confirmed by their ultrahigh sensitivity with record detection limit down to 100 photons level at 180 Hz modulation bandwidth, which is over 50 times lower than all previously reported perovskite photodetectors. The dynamic range and specific detectivity of the SC-TF perovskite photodetector are about 83 dB and 1.3×1013 cm Hz0.5 W-1, respectively. The superior performance of our devices originates from replacing polycrystalline thin-film with the thickness optimized SC-TF. To further illustrate the crucial role of SC-TF thickness, we have systematically investigated the thickness dependent performance of SC-TF perovskite photodetectors. With the SC-TF thickness decreasing from about 10 m to hundreds of nanometers, the lowest detectable power and internal gain improve 2 and 4 orders of magnitude respectively.

Ultra-High Reflectivity All-dielectric Metasurface at Ultra-Violet Wavelength

Tanchao Pu[1,2], **Ziwei Liu**[1,2], **Jiebin Niu**[1], **Lina Shi**[1], **Changqing Xie**[1]

1. Institute of Microelectronics of Chinese Academy of Sciences, No.3 BeiTuCheng West Road, Beijing 100029, China
2. 2University of Chinese Academy of Sciences, No.19 YuQuan Road, Beijing 100049, China

Metasurface has gained sustaining interest over the past decadesince its ability to manipulate the amplitude, phase and polarization of the light in nanoscale [1]. These manipulations give rise to large optical properties that are applied in sensing, imaging, metalens, photovoltaic device and nonlinear optics, to name a few. Recently, the building block of metasurface based on all-dielectric nanostructures are replacing the metallic counterpart, that are inherently ohmic damping at optical frequencies, in some application, since they are lossless and possess strong Mie resonance with simple geometry [2,3]. The ultra-violet (UV) which are widely used in human's life, such as anti-fake, but will also threaten human's health, especially the UVA (from 320-400 nm) and UVB (280-320 nm). Therefore, a UV reflector is necessary to protect human free from the UV. Although the Bragg reflector and photonics band gap material can achieve high reflection, the necessary multilayers to improve the reflectivity increase its fabrication difficulty. Very recently, perfect reflector based on silicon has been demonstrated in near-infrared range [4,5], but the inherent absorption impedes its application in the UV range. Here, **we proposed a ultra-high reflectivity (UHR, >99%) metasurface reflector based on silicon nitride in UV range**. **The numerical results show a UHR reflection band under carefully design of the building block geometry. Since the response of the metasurface is a function of geometry, here is the diameter and height of the cylinder, the high reflectivity band can be tuned to the desired wavelength range.**

As shown in Fig. 1(a), a cylinder geometry is used to achieve due to its two design degree of freedom and easy fabrication process. Silicon nitride is chosen as the material of the building block since its large band gap which results in its transparent in UV to visible and CMOS compatibility. Using the Finite Difference Time Domain (FDTD) simulation method, we numerically investigate the optical response, reflectance, of the metasurface in air. The optical constant of silicon nitride was from Palik [6]. The response of our metasurface is a function of aspect ratio (AR), defined as AR=H/D, where H is the height and D is the diameter of the cylinder. Fig.1(b) shows the reflection spectrum of the metasurface with AR=0.6. A flat UHR band near 290nm is observed. As demonstrated in [4], the flat UHR band will emerges in the single negative lossless metamaterial. The single negative was observed with seperately electric resonance and magnetic resonance. The electronics field distribution shows a circular displacement current, as shown in the inset of Fig.1(b), which represents a magnetic dipole resonance dominates near the UHR range.

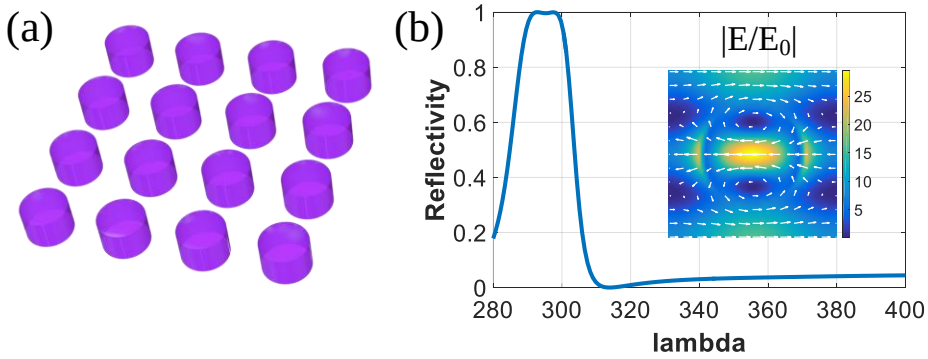

Fig. 1 (a) The schematic image of the all-dielectric metasurface. (b) The reflection spectrum of the carefully designed metasurface based on the building block with an AR=0.6. Inset: the normalized electric field distribution at 291nm.

In summary, **we numerically demonstrated an all-dielectric metasuraface to achieve the UHR in UV range with over 8 nm band width and two perfect reflection peak (>99.99%).** The perfect reflector may also find application in improvement of the laser damage-threshold, bio-imaging and molecule detection and enhancement of the throughput efficiency in the laser cavity.

References

[1] N. Yu and F. Capasso, "Flat optics with designer metasurfaces", Nat. Mater. **13**, 139–150 (2014).
[2] I. Staude, J. Schilling, "Metamaterial-Inspired Silicon Nanophotonics". Nat. Photonics, 11 (5), 274–284 (2017).
[3] A. I. Kuznetsov, A. E. Miroshnichenko, M. L. Brongersma, Y. S. Kivshar, B. Luk'yanchuk, "Optically Resonant Dielectric Nanostructures," Science **354**, 6314 (2016).
[4] B. Slovick, Z. G. Yu, M. Berding, S. Krishnamurthy, "Perfect Dielectric-Metamaterial Reflector", Phys. Rev. B, **88** (16), 165116 (2013).
[5] P. Moitra, B. A. Slovick, W. Li, I. I. Kravchencko, D. P. Briggs, S. Krishnamurthy and J. Valentine, "Large-Scale All-Dielectric Metamaterial Perfect Reflectors", ACS Photonics **2**, 692– 698 (2015).
[6] E. D. Palik, *Handbook of optical constants of solids*, Academic Press: San Diego (1998).

A large-scale synthetic methods for tuning the morphology and chiroptical properties of discrete chiral gold nanorods

Guangchao Zheng[1*], Zhiyong Bao[2], Jorge Pérez Juste[3], Ruolan Du[1], Wei Liu[1], Jiyan Dai[2], Wei Zhang[4], Lawrence Yoon Suk Lee[1], Kwok-Yin Wong[1]

1 Department of Applied Biology and Chemical Technology and the State Key Laboratory of Chirosciences, The Hong Kong Polytechnic University, Hung Hom, Kowloon, Hong Kong, China
2 Department of Applied physics, The Hong Kong Polytechnic University, Hung Hom, Kowloon, Hong Kong, China
3 Departamento de Química Física y Centro Singular de Investigaciones Biomédicas (CINBIO), Universidad de Vigo, Vigo, Spain
4 Institute of Applied Physics and ComputationalMathematics, P. O. Box 8009(28), Beijing 100088, P. R. China
Email: zhengguangchao2008@gmail.com

Plasmonic circular dichroism (PCD) is currently a hot topic due to its great potential in different fields, such as, bio/chemical sensing, photocatalysis, or cancer therapy. However, the synthesis of discrete nanostructures that exhibit consistent and stable PCD signal still is a challenging task. To address this challenge, we have developed a seed-mediated growth approach to obtain chiral Au nanorods (c-Au NRs) with high and stable chiroptical responses, being the final morphologies governed by the concentration of chiral molecules (L-Cysteine or D-Cysteine). Experimental and theoretical studies reveal that chiral molecules within the discrete nanostructure would enhance their PCD signal. The enhancement of PCD is attributed to the coupling of chiral dipoles of molecules with the near-field induced optical activity at the hot spots. Moreover, the stability of PCD signal and biocompatibility of c-Au NRs could be further improved by their encapsulation within either silica or protein corona. In particular, single c-Au NR@SiO_2 with Janus or core-shell configurations are reported with their PCD still retained even in organic solvents. More interestingly, a side-by-side assembly of c-Au NRs induced by chiral molecules give rise to an improvement of the PCD signal, with anisotropic g factors as high as 0.048.[1] This study is substantially important because it will not only simply tune the PCD profiles but also improve the stability and biocompatibility of discrete PCD reporter, which will provide an important technique for the PCD applications.

Figure1 CD spectroscopy of chiral nanostructures (The inset in (a), (b), (c), (d) are the c-Au NRs, c-Au NRs@Silica, side-by-side assembly of c-Au NRs dimers, silica coating on c-Au NRs dimers, respectively)

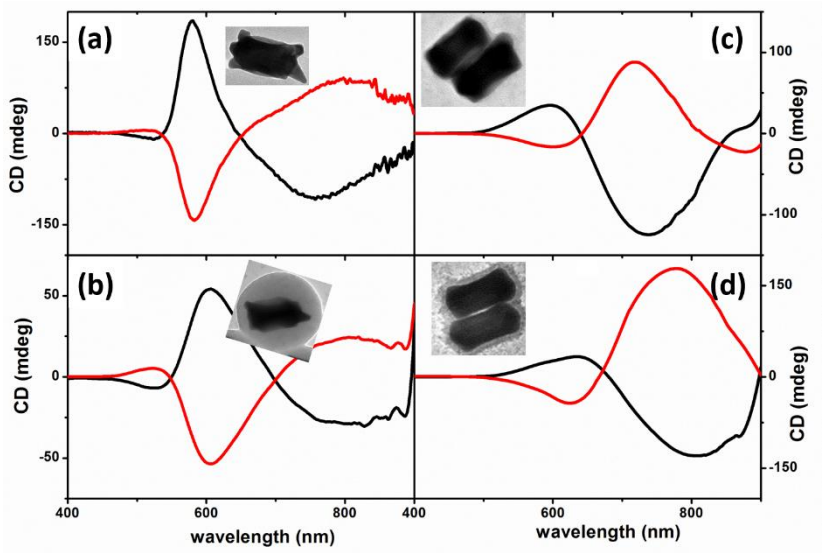

Reference

[1] G. Zheng, Z. Bao, J. Pérez-Juste, R. Du, W. Liu, J. Dai, W. Zhang, L.Y. Suk Lee, K.-Y. Wong, Tuning the morphology and chiroptical properties of discrete gold nanorods with amino acids. Angewandte chemie, DOI: 10.1002/anie.201810693 (2018)

High precision fabrication of sapphire micro-optical elements by femtosecond laser and dry etching

Xue-Qing Liu[1,2]

1. State Key Laboratory of Precision Measurement Technology and Instruments, Department of Precision Instrument, Tsinghua University, Haidian, Beijing 100084, China;

2. State Key Laboratory of Integrated Optoelectronics, College of Electronic Science and Engineering, Jilin University, 2699 Qianjin Street, Changchun, 130012, China

Due to high transparency in the wavelength range from the visible to the mid-infrared, high hardness, and high thermal and chemical stabilities, sapphire is considered as a promising material for optics operating under harsh conditions. Well-defined diffractive and refractive micro-optical elements have been written by scanning the focal spot of a femtosecond laser beam according to three-dimensional (3D) patterns. However, the low efficiency of the pinpoint laser ablation severely hinders its practical application. Here, we propose a dry-etching-assisted femtosecond laser machining (DE-FsLM) technology for sapphire micro-optics manufacturing, with which the fabrication efficiency can be improved, e.g., by over two orders of magnitude for a 15-μm-diameter and 1-μm-depth microlens. The fundamental idea is to generate a laser-damaged seed for the ensuing dry etching via single-burst laser irradiation. The required number of laser pulses for a single lens definition is reduced from typically 10^6 to approximately 50, and the fabrication duration of a cm^2-size array containing approximately 4×10^5 microlenses is improved from 1390 hours to 3.2 hours (including 3 hours for the dry etching). High-quality imaging and wide-band light beam homogenization from ultraviolet to near-infrared are demonstrated for both the original sapphire elements and the cast replicated glass lenses.

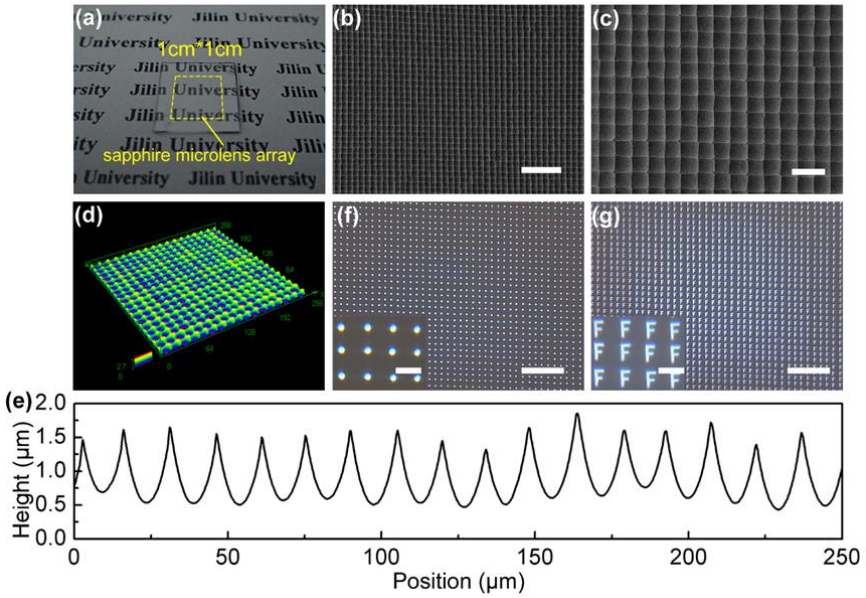

Fig. 1 Characterization of the large-scale SCMA. (a) Photo image of a 1 cm * 1 cm large-scale SCMA. (b) SEM image of the large-scale SCMA. Scale bar = 100 μm. (c) Amplified SEM image of the large-scale SCMA. Scale bar = 30 μm. (d) 3D morphology of the large-scale SCMA. (e) Cross-section profiles of the large-scale SCMA. (f) Focusing and (g) imaging properties of the large-scale SCMA. Scale bar = 100 μm. The insert images are magnified versions of the focusing and imaging photos. Scale bar = 15 μm.

References

[1] 1. Xue-Qing Liu, Qi-Dai Chen, Kai-Min Guan, Zhuo-Chen Ma, Yan-Hao Yu, Qian-Kun Li, Zhen-Nan Tian and Hong-Bo Sun, Dry-etching-assisted femtosecond laser direct writing, Laser Photon. Rev. **11**, 1600115(2017).

[2] Xue-Qing Liu, Lei Yu, Qi-Dai Chen and Hong-Bo Sun, Mask-free construction of three-dimensional silicon structures by dry etching assisted gray-scale femtosecond laser direct writing, Appl. Phys. Lett. **110**, 091602 (2017).

Radio Surface Plasmons on Metamaterial Textiles for Efficient and Secure Body Networks

John S. Ho
1. National University of Singapore, 21 Lower Kent Ridge Road, Singapore 119077, Singapore

Wireless networks of sensors, displays, and smart devices on the body offer powerful capabilities for health monitoring, human-machine interfaces, and other emerging technological applications [1]. Existing approaches for wireless interconnection, however, are limited by challenges in radiative loss, interference, and data vulnerability inherent to the radiation of radio-waves into the surrounding space [2]. In this presentation, we describe an efficient and secure approach to interconnect wireless sensor networks by confining radio-waves on clothing patterned with conductive textiles. We demonstrate how these textile patterns, termed metamaterial textiles, can enhance wireless transmission (including Bluetooth and Wi-Fi) from commercial devices (smartphones) by many orders of magnitude and enable wireless power transfer to sensors on the body.

To efficiently interconnect body networks, we reasoned that clothing structured with conductive textiles could support surface plasmon-like modes at radio communication frequencies that can mold the propagation of radio-waves around the body. In contrast with conventional wireless communication systems, networks based on metamaterial textiles are interconnected by radio surface plasmons that propagate along structures patterned on clothing [Fig. 1(a)]. These networks are not subject to inverse square law losses and require physical proximity to the body in order to transmit and receive signals through interactions mediated by an evanescent field. Fig. 1(b) shows the structure of the metamaterial textile (2.5 cm width, 8 mm unit cell length). The top layer, facing outward from the body, is comprised of a planar comb-shaped pattern that supports surface plasmon-like modes that are conformal to sharp bends and creases [Fig. 1(c)] [3], while the bottom layer is an unpatterned conductor that enhances field confinement and suppresses unwanted interactions with the body.

We show how these metamaterial textiles can enable the translation of concepts from photonic circuits onto a textile platform for capabilities in wireless sensing, signal processing, and energy transfer. Endowing athletic wear, medical clothing, and other apparel with such advanced electromagnetic capabilities should enhance our ability to perceive and interact with the world around us.

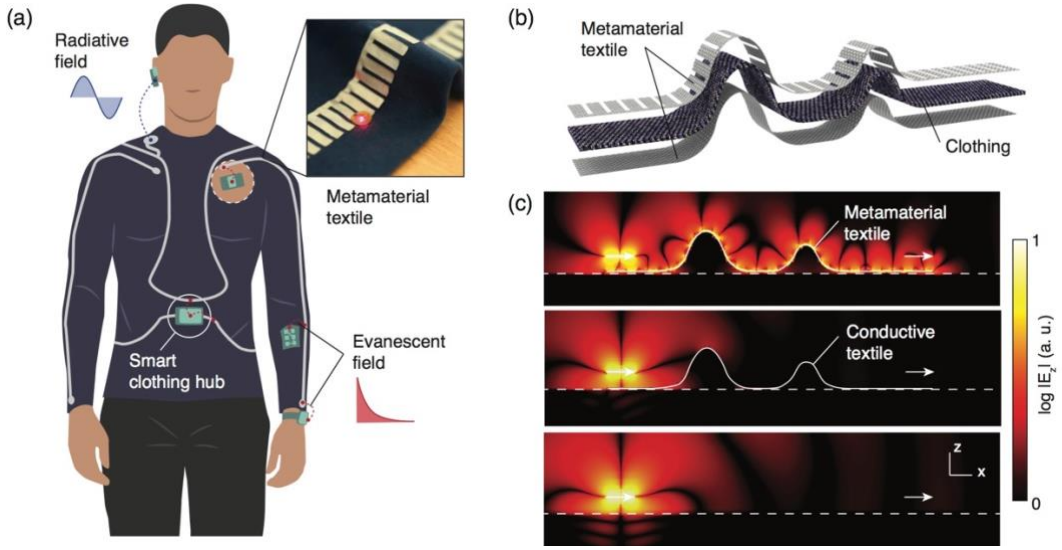

Fig. 1 Radio surface plasmons on metamaterial textiles. (a) Illustration of a sensor network interconnected by radio-waves confined on clothing. Devices in the network exchange energy and information through the evanescent field of surface waves rather than radiation into the surrounding space. (b) Structure of the metamaterial textile. (c) Simulation of the electric field distribution emitted by a dipole above a (top) metamaterial textile, (center) unpatterned conductive textile, and (bottom) nonconductive textile. The textile is placed on the body modeled by air-tissue half-space.

Example References

[1] B. Chu, W. Burnett, J. W. Chung, and Z. Bao, "Bring on the bodyNET," Nature 549, 328–330 (2017).
[2] M. Li, W. Lou, and K. Ren, "Data security and privacy in wireless body area networks," IEEE Wireless Communications 17, 51–58 (2010).
[3] X. Shen, T. J. Cui, D. Martin-Cano, and F. J. Garcia-Vidal, "Conformal surface plasmons propagating on ultrathin and flexible films," Proc. Natl. Acad. Sci., USA 110, 40–45 (2013).

Electromagnetic engineered mechanical trapping potential and the conversion in optomechanical system

Yang Sun[1], **Yong-Pan Gao**[1], **Xiao-Fei Liu**[1], **Tie-Jun Wang**[1], **Chuan Wang**[1]

1. Beijing University of Posts and Telecommunications, Xitucheng Road 10, Beijing 100876, China

The manipulation of the mechanical response in optomechanical system allows the observation of the quantum behaviour by cooling a mechanical resonance to its quantum mechanical ground state [1,2,3], and it relies on the effective tuning of the trapping potentials. In this work, **we investigate the conversion process between the radiation pressure and the mechanical trapping potential**, which is engineered by the optical field in an optomechanical system. **A set of trapping potentials could be achieved** by tuning the system, such as the detuning, pumping power and the decay rates. Specifically, **the speed of conversion between different potential state is studied which approaches the megahertz level**.

[1] Y.-C. Liu, Y.-F. Xiao, X.-S. Luan, and C. W. Wong, "Dynamic dissipative cooling of a mechanical resonator in strong coupling optomechanics," Phys. Rev. Lett. **110**, 153606 (2013).
[2] W.-J. Gu and G.-X. Li, "Quantum interference effects on ground-state optomechanical cooling," Phys. Rev. A **87**, 025804 (2013)
[3] F. Marquardt, J. P. Chen, A. Clerk, and S. Girvin, "Quantum theory of cavity-assisted sideband cooling of mechanical motion," Phys. Rev. Lett. **99**, 093902 (2007).

High performance plasmonic nanolasers with external quantum efficiency exceed 10%

Suo Wang[1], Hua-Zhou Chen [1], Ren-Min Ma[1,2]

[1] *State Key Lab for Mesoscopic Physics and School of Physics, Peking University, Beijing 100871, China.*

[2] *Collaborative Innovation Center of Quantum Matter, Beijing 100871, China*

ABSTRACT:

Plasmonic nanolasers break the diffraction limit for an optical amplifier, which brings new capabilities for various applications, ranging from on-chip optical interconnector to biomedical sensing and imaging. However, the inevitably accompanied metallic absorption loss could convert the input power to heat rather than radiations leading to undesired low external quantum efficiency and device degradation. To date, direct characterization of quantum efficiency of plasmonic nanolasers is still a forbidden task due to its near-field surface plasmon emissions, divergent emission profile and the limited emission power. Here, we develop a method to characterize the external quantum efficiency of plasmonic nanolasers by synergizing experimental measurement and theoretical calculation. With systematical device optimization, we demonstrate high performance plasmonic nanolasers with external quantum efficiency exceed 10% at room temperature [1]. This work fills in a missing yet essential piece of key metrics of plasmonic nanolasers. The demonstrated high external quantum efficiency of plasmonic nanolasers not only clarifies the long-standing debate but also endorses the exploration of them in various practical applications such as near-field spectroscopy and sensing, integrated optical interconnects, solid-state lighting and free-space optical communication.

REFERENCES:

[1] Suo Wang, Hua-Zhou Chen, Ren-Min Ma, Plasmonic nanolasers with high external quantum efficiency. Submitted.

Wideband slowlight in grating waveguide

Ran Hao[1], **Jianyao Jiao**[1], **Xiaobin Lin**[1], **Zheng Zhen**[1], **Dagarbek Rakhatbek**[1], **Ibrahim Nasidi**[1]
1.Zhejiang University, Zheda Road 38, Hangzhou 310058, China

Slow light, a solution to control the optical signal by reducing the group velocity, has been widely studied to obtain enhanced nonlinearities and increased phase shifts owing to its promoting light-matter interaction ability [1-5]. We achieved a wide band slow light in a simple one-dimensional fishbone waveguide. A flat band indicating **slow light with group index of 13 and bandwidth over 10 nm is obtained** by plane wave expansion calculation and measured through the experiment.

The experiment setup for the test of the performance of the grating waveguide is shown in Fig. 1 (a). The input light is generated from a tunable laser source. Its polarization is controlled by a polarization controller to obtain the TE mode light which injects into the chip through a grating coupler with coupling angle of 80 degrees. The output temporal spectrum response is recorded and analyzed by an oscilloscope. Using the Fabry-Perot effect, the output signal is controlled by the phase change at two sides of slow light grating waveguide [6]. From signal "1" to "0", the phase change is $\pi/2$. λ_{max} and λ_{min} are the wavelengths corresponding to the signal "1" and signal "0" in the transmission spectrum, respectively. The spectral dependence of the group index in the grating waveguide can then be deduced from positions of the adjacent peak and valley of the oscillations as:

$$n_g(\lambda) = \lambda_{max}\lambda_{min} / 4L(\lambda_{max} - \lambda_{min}).$$

Where L is the length of the waveguide, n_g is the group index of 1-D grating waveguide. The transmission spectrum was measured and shown in Fig. 1(b), the oscillation period decreases with the increase of wavelength. The group index then can be calculated from the Equation (1), and the group indices are drawn in the same diagram (red plots), where we find group index from 5 to over 60, as the wavelength increases from 1550nm to 1610nm. Fig. 1(c) shows the group index of simulation and experiment as a function of wavelength in one picture. A bandwidth over 10nm with high group index around 12 can be clearly observed. The deviation between the measured and the calculated group indices mainly attributes to fabrication inaccuracies.

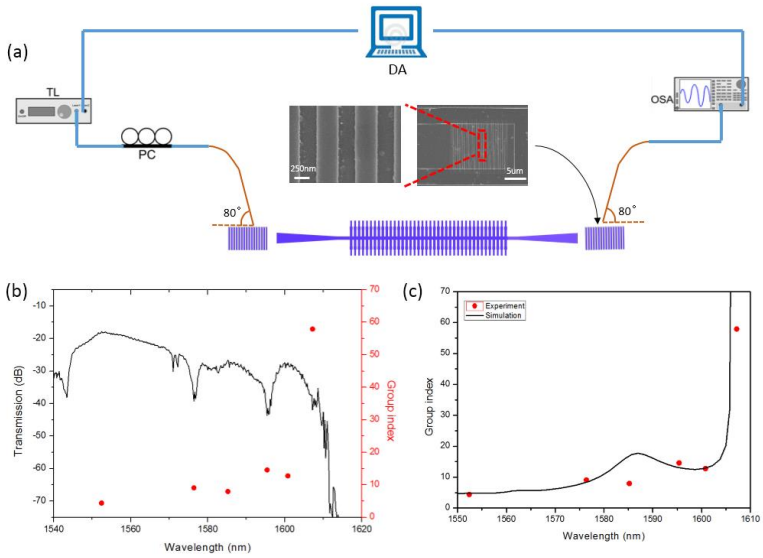

Fig. 1 (a) Schematic of the experimental setup. Insert pictures are SEM images of grating coupler. In addition, we utilize a tunable laser (TL) source, a polarized controller (PC), a data analyzer (DA) and an optical spectrum analyzer (OSA); (b) Measured transmission and group index as a function of wavelength; (c) group index (from both simulation and experiment) as a function of wavelength.

References

[1] T. Baba, "Slow light in photonic crystals, " Nat. Photonics 2, 465-473 (2008).
[2] Y. A. Vlasov, M. O'Boyle, H .F. Hamann, and S. J. Mcnab, "Active control of slow light on a chip with photonic crystal waveguides, " Nature **438**, 65-69 (2005).
[3] R. Hao, E. Cassan, X. Le Roux, D. Gao, L. Vivien, D. Marris-Morini, and X. L. Zhang, "Improvement of delay-bandwidth product in photonic crystal slow-light waveguide, " Optics Express **18**, 16309 (2010).
[4] R. Hao, E. Cassan, H. Kurt, X. Le Roux, D. Marris-Morini, L. Vivien, H. M. Wu, Z. P. Zhou, and X. L. Zhang, "Novel slow light waveguide with controllable delay-bandwidth product and ultra-low dispersion, " Optics Express **18**, 5942-5950 (2010).
[5] R. Hao, X. L. Peng, E. P. Li, Y. Xu, J. M. Jin, and X. M. Zhang, "Improved slow light capacity in graphene-based waveguide, " Scientific Reports **5**, 15335 (2015).
[6] Z. Zou, L. Zhou, X. Li, and J. Chen, "60-nm-thick basic photonic components and Bragg gratings on the silicon-on-insulator platform, " Opt. Express **23**, 20784-20795 (2015).

Low Refractive Index Coating Induced Resonant Kerker Effect

Ziwei Liu[1,2], **Tanchao Pu**[1,2], **Jiebin Niu**[1], **Lina Shi**[1], **Changqing Xie**[1]

1. Institute of Microelectronics of Chinese Academy of Sciences, No.3 BeiTuCheng West Road, Beijing 100029, China
2. University of Chinese Academy of Sciences, No.19 YuQuan Road, Beijing 100049, China

Light interact matter in nanoscale is of fundamental significance in different branches of physics, such as sensing, optical nonlinear enhancement and solar cell, to name a few [1,2]. All-dielectric nanostructures emerge as a promising alternative to noble metal based plasmonic nanostructures in manipulating the Mie resonance since its non-radiative loss is low and electric and magnetic response can be simultaneously excited in a simple geometry. Directional scattering, also named Kerker effect, is one of the basic physics based on the overlapping of the electric dipole (ED) and magnetic dipole (ED) resonance to achieve the suppression of the backward scattering and enhancement of the forward scattering [3,4]. The basic demand is to control ED and MD separately by tuning the geometry of the nanostructure [5] or lattice resonance [6]. **Here, we propose a new scheme to manipulate ED and MD by coating a low index dielectric layer outside the silicon nanostructure, resembling the core-shell structure but with a two-dimensional structure.**

As shown in Fig.1(a), the manipulation factor in our work is the thickness(*t*) and index of the coating. The effect of SiO2 coated Si nanostructure has been discussed in some work [4] origins from the natural oxidation layer outside the Si nanostructures. **But they don't have further discussion on utilizing the low index coating to realize Kerker effect.** Here, the scattering cross section's dependence on the thickness of the coating is shown in Fig.1(b). A distinct overlapping emerges at lambda λ~ 705nm when t ~ 80nm which shows an evidence of the Kerker effect [3-6]. Fig.1(c) shows the forward to backward scattering ratio (F/B) spectrum show a maximum up to 43.

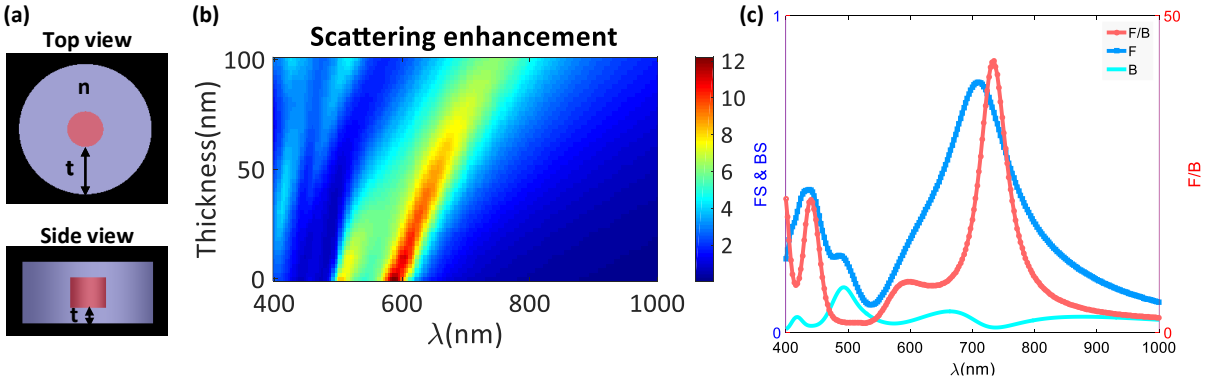

Fig. 1 (a) structure schemetic image(b) the dependence of the scattering enhancement (scatCS divided by geometry CS) on the thickness of the coating. (c) the forward, backward scattering and their ratio F/B with t~ 80nm.

In conclusion, we numerically demonstrate that a low index coating will contribute to an overlap of ED and MD to achieve directional scattering. The realization is easier than the core-shell structure since its 2D structure can be fabricated by the mature CMOS process. These findings make the all-dielectric coating nanostructure a promising candidate for photonics applications in nanoantennas, and optical switches.

References

[1] A. I. Kuznetsov, A. E. Miroshnichenko, M. L. Brongersma, Y. S. Kivshar, B. Luk'yanchuk, "Optically Resonant Dielectric Nanostructures," Science **354**, 6314 (2016).
[2] A. Krasnok, M. Caldarola, N. Bonod, A. Alú, "Spectroscopy and Biosensing with Optically Resonant Dielectric Nanostructures", Adv. Opt. Mater. **6**, 1701094 (2018).
[3] M. Kerker, D. Wang, G. Giles, "Electromagnetic Scattering by Magnetic Spheres", J. Opt. Soc. Am. **73**, 765–767 (1983).
[4] Y. H. Fu, A. I. Kuznetsov, A. E. Miroshnichenko, Y. F. Yu, B. Luk'yanchuk, "Directional Visible Light Scattering by Silicon Nanoparticles", Nat. Commun. **4**, 1527 (2013).
[5] I. Staude, A.E. Miroshnichenko, M. Decker, et al. "Tailoring Directional Scattering through Magnetic and Electric Resonances in Subwavelength Silicon Nanodisks", ACS Nano **7**, 7824–32 (2013).
[6] V. E. Babicheva, A. B. Evlyukhin, "Resonant Lattice Kerker Effect in Metasurfaces With Electric and Magnetic Optical Responses", Laser Photonics Rev., 11, 1700132 (2017).

Refractometric Sensing Using Gradient Plasmonic Nanostructures: Mapping Spectral Information to Spatial Patterns

Siyi Min[1,2], Shijie Li[1], Zhouyang Zhu[1], Chuwei Liang[1], Jingxuan Cai[1], Xing Cheng[2], Wen-Di Li[1]

[1]*Department of Mechanical Engineering and Shenzhen Institute of Research and Innovation, The University of Hong Kong, Hong Kong, China*

[2]*Department of Materials Science and Engineering, Southern University of Science and Technology, Shenzhen, China*

We report a spectrometer-free, pattern-based refractometric sensing scheme. This new detection scheme uses gradient plasmonic nanostructures to map spectral information to spatial locations and then use commercial imaging sensors, rather then spectrometers, to detect pattern change induced by local refractive index change due to adsorbed analyte molecules. Our preliminary results show the sensitivity performance of this new method can be comparable to conventional spectrometer-based methods, but with much more compact and cost-effective setup.

Gradient plasmonic nanostructures in our work are fabricated using interference lithography (IL) (Fig. 1). Conventional IL emphasizes pattern uniformity; therefore, uniform exposure intensity over the patterning area is desired. To fabricate spatially varying structures, we intentionally utilize the non-uniform Gaussian-shaped intensity distribution of the two coherent beams to realize spatially varying patterns with circular symmetry. Exposed patterns on the positive-tone photoresist show pillars at the center, where the Gaussian beam has the maximum intensity. The diameter of pillars increases with the distance from the center. Nearby pillars start to merge and the overall pattern evolves into a hole array with the diameter of holes reducing when the distance from the center is further increased. We also use the IL system to make nanoimprint templates with the gradient structures and then, use NIL and other nanofabrication processing, including reactive ion etching and e-beam evaporation, to fabricate different types of gradient plasmonic structures for various sensing demonstrations.

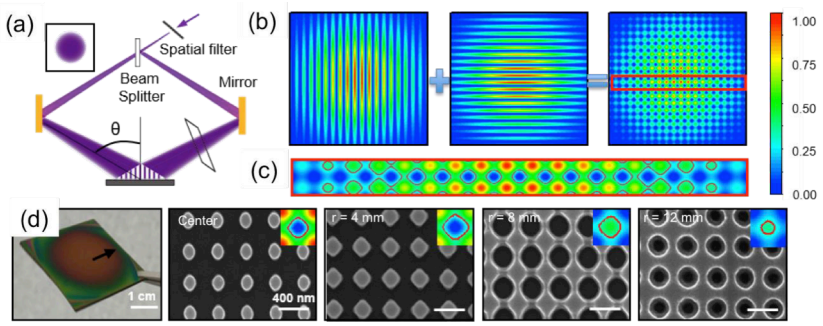

Fig. 1. Interference lithography fabrication process for spatially varying gradient nanostructures. (a) Schematic representation; (b) numerical simulation of double exposure for two-dimensional dots and holes with gradient sizes; (c) zoomed-in view of the numerical simulation of the red box region in (b); and (d) preliminary fabrication results showing the gradient feature sizes on 370-nm-period two-dimensional structures.

We carry out a series of experimental demonstrations and compare the performance of our new sensing scheme with existing spectrometer-based refractometric sensing methods. In our new sensing scheme, a camera is used to record the transmitted intensity pattern on the gradient plasmonic sensing chip. Before and after exposing the sensing chip to analyte substances, two transmitted images are taken and compared. An image processing algorithm is developed to retrieve the change in the patterns to detect the existence of analyte substances. We have performed preliminary experiment on hydrogen gas sensing by using a silver gradient plasmonic structure with 20-nm-thick palladium deposited as the hydrogen-responsive layer [1, 2]. Our preliminary testing result shows that hydrogen gas with 1% and 4% concentrations can induce clearly resolvable intensity pattern changes, which is comparable to many published plasmonic refractometric hydrogen sensing results [1, 3, 4]. We believe that there is considerable room for improvement of the sensing performance of our gradient plasmonic sensors and will explore its ultimate limitations in the subsequent investigation.

References

1. Liu, N., et al., *Nanoantenna-enhanced gas sensing in a single tailored nanofocus.* Nature Materials, 2011. **10**(8): p. 631-636.
2. Sutapun, B., M. Tabib-Azar, and A. Kazemi, *Pd-coated elastooptic fiber optic Bragg grating sensors for multiplexed hydrogen sensing.* Sensors and Actuators B-Chemical, 1999. **60**(1): p. 27-34.
3. Tittl, A., et al., *Palladium-Based Plasmonic Perfect Absorber in the Visible Wavelength Range and Its Application to Hydrogen Sensing.* Nano Letters, 2011. **11**(10): p. 4366-4369.
4. Wadell, C., S. Syrenova, and C. Langhammer, *Plasmonic Hydrogen Sensing with Nanostructured Metal Hydridese.* ACS Nano, 2014. **8**(12): p. 11925-11940.

NJU NIP
NOV 9-11, 2018
Nanjing, China

a nature conference
on Nanophotonics and
Integrated Photonics 2018